The 3-Wave Resonant Interaction Model: Spectra and Instabilities of Plane Waves

Marzia Romano

PhD

Northumbria University
NEWCASTLE

March 2019

The 3-Wave Resonant Interaction Model: Spectra and Instabilities of Plane Waves

Marzia Romano

Submitted in accordance with the requirements of the University of Northumbria at Newcastle for the degree of PhD in Mathematics

Research undertaken in the Department of Mathematics, Physics and Electrical Engineering

Under the Supervision of Dr Matteo Sommacal.

Northumbria University

Department of Mathematics, Physics and Electrical Engineering

October 12, 2019

Abstract

The aim of this thesis is the analysis of the spectral stability of plane wave solutions of the 3-wave resonant interaction (3WRI) model, when such solutions undergo localised perturbations.

For the first time, we provide a comprehensive topological classification of the spatial stability spectra with respect to the parameters space and the gain functions associated to any stability spectrum. We find that all the stability spectra of the coupled nonlinear Schrödinger (CNLS) system are enclosed in those of the 3WRI system. The topological features of the CNLS stability spectra are gaps on the real axis (solutions not bounded in space), and branches and loops off the real axis (solutions bounded in space which can be linearly unstable in time). New topological components exist in the stability spectra of the 3WRI model: we name such components twisted loops. They are associated with explosive instability (the corresponding solutions blow up in a finite time) and their gain function is non-zero in a whole neighbourhood of the origin. We observe that the gain function associated to the branches is non-zero at low wave numbers, symmetrically located with respect tto the zero-value of the wave number, but it is zero at the origin of the plot (linear instability of baseband-type). The gain function associated to the loops is non-zero only away from the origin (linear instability of passband-type).

We show that the plane wave solutions of the 3WRI model are linearly unstable in time for any choice of the physical parameters, including those ones associated to the solutions that are explosive. Thus, there is linear instability of the plane wave for any choice of the physical parameters corresponding to a positive gain-function.

Finally, we conjecture that the existence of branches in the stability spectra is a necessary condition for the onset of rogue waves ascribable to rational or semi-rational solutions obtained by Darboux Dressing Transformation. Indeed, we observe numerically linear instability of plane waves with the subsequent generation of localised structures whose onset, as a result of the perturbation of plane waves, must be investigated further due to the dispersionless nature of the 3WRI system.

Contents

List of Tables

List of Figures

List of Abbreviations

Topological components of the stability spectrum:

B	Branch
G	Gap
L	Loop
SG	Split Gap
TL	Twisted Loop
nA	$n \in \mathbb{N}$ number of a topological component $A \in \{B, G, L, SG, TL\}$

Acknowledgements

Firstly, I would like to express my sincere gratitude to my supervisor Dr Matteo Sommacal for his inspiring guidance, friendly advice during the project work, for his patience and for the huge time dedicated to the research together. He has been an extraordinary mentor and a wise guide. I am thankful to him for giving me the opportunity to participate and meet a wider scientific community during the workshops that he organised: *LMS Norther Regional Society Meeting and Workshop* and *The Onset of Rogue Waves* both at Northumbria University.

I would like to thank Professor Sara Lombardo, for giving me this wonderful opportunity to undertake my PhD at Northumbria University and for introducing me to the fascinating subject of Nonlinear and Integrable Systems. I would like to express my gratitude for helping me in all the time of the PhD project and during the writing of this thesis. I am grateful for her advices both as a friendly woman and as a professional guide.

I want to thank Dr Benoit Huard for the scientific support and proof reading of the thesis. I am also thankful to Professor Antonio Degasperis for his comments and feedback; my PhD project is based on his, Professor Sara Lombardo's and Dr Matteo Sommacal's research work, and without it the accomplishment of this thesis would be impossible.

I want to express my profound gratitude to my parents for the financial support during the extension period and for the encouragement especially during the maternity leave and the difficult period of the childcare while I was undertaking the research.

The biggest thank-you is to my husband, Matteo, who has always encouraged and believed in me; our discussions on physics and mathematics have powered the willing to work ever harder.

Finally, to my daughter Lucrezia: I hope this thesis will inspire you to be determined to follow your dreams.

Declaration

I declare that the work contained in this thesis has not been submitted for any other award and that it is all my own work. I also confirm that this work fully acknowledges opinions, ideas and contributions from the work of others. Any ethical clearance for the research presented in this thesis has been approved. Approval has been sought and granted by the Faculty Ethics Committee on 11 May 2015.

The Word Count of this Thesis is 47213.

Name: Marzia Romano

Signature:

Date: 11 April 2019

Chapter 1

Introduction

1.1 Background and Current Research

1.1.1 Modulation Instability for Scalar Dispersive Equations

Many phenomena in nature can be explained via instabilities. Hydrodynamic instabilities can occur if the initial physical features (velocity, pressure and density) of a fluid flow are exposed to small disturbances. Between all hydrodynamic instabilities *Kelvin-Helmholtz Instability* (KHI) [1, 2] is well-known. It takes place between the interface of two fluids flowing with different velocities. The most famous examples of the manifestation of KHI in nature are the red giant vortex in the Jupiter's atmosphere and the generation of clouds that are "ocean wave-like" in the Earth's atmosphere. If the two fluids flow with different density *Rayleigh-Taylor Instability* (RTI) [3] can occur: it is the explanation of the generation of "mushroom clouds" in the volcanic eruption or atomic explosion. It can be also seen as the limit of another fascinating phenomenon that is the *Richtmyer-Meshkov Instability* (RMI) [4, 5, 6]. In general, it is when a shock wave interacts with the perturbed interface of two fluids with different physical properties. At the beginning of the interaction just a row of vortices with different signs are created, but then the perturbation grows in time and "mushroom" structures arise. Plasmas exhibit a huge number of magnetohydrodynamics instabilities, for example "sausage instability" and "kink instability" are observed in solar corona [7, 8].

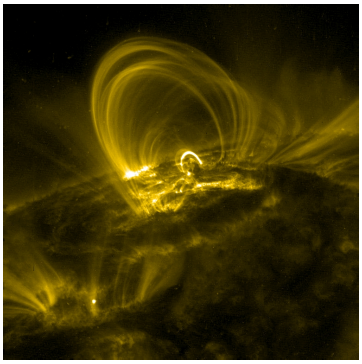

Modulational Instability (MI) is ubiquitous in nature and it was observed in several nonlinear wave phenomena [9], such as in radio waves in transmission lines [10], in light waves in dielectric materials [11] and in plasma waves during the nonlinear coupling of plasma cyclotron waves and magnetohydrodynamic modes [12]. In the context of water waves, MI is referred to as *Benjamin-Feir Instability*, so named because Benjamin and Feir first observed it in nonlinear Stokes waves on deep water surface [13, 14].

MI may arise if a plane wave of a scalar nonlinear dispersive equation is perturbed with a long wave perturbation such that the original waveform is deformed and the wave amplitude is said to be modulated [15, 16, 17]. Perturbing the amplitude of the plane wave $u(x,t) = ae^{i(kx-\omega t)}$ with real amplitude a, wave number k and frequency ω, by means of the plane waves $b(x,t) = b_{01}e^{i(Kx-\Omega t)} + b_{02}e^{-i(Kx-\Omega t)}$, one gets the perturbed solution

$$\bar{u}(x,t) = (a+b(x,t))e^{i(kx-\omega t)} = ae^{i(kx-\omega t)} + b_{01}e^{i((k+K)x-(\omega+\Omega))t} + b_{02}e^{i((k-K)x-(\omega-\Omega))t}, \tag{1.1}$$

where x is space, t is time, b_{0j} are real amplitudes of the perturbations and $b_{0j} << a$, the modulation frequency is $\Omega << \omega$ and the wave number of the perturbation is $K << k$.

After perturbing, the amplitude of the resulting plane wave is not anymore a constant, being instead a function of space and time. The perturbed solution reads $u(x,t) + \delta u_1(x,t) + \delta u_2(x,t)$, where $\delta u_1(x,t) = b_{01} e^{i((k+K)x-(\omega+\Omega))t}$ and $\delta u_2(x,t) = b_{02} e^{i((k-K)x-(\omega-\Omega))t}$ are the so-called sidebands and $u(x,t)$ is known as the carrier wave.

MI has two stages: a linear and a nonlinear stage. [9]. The linear stage is the mechanism responsible for the amplification of the perturbation when the approximation $\delta u_j << u$ remains valid in time. In this limit, the equation for the perturbation is linear, and nonlinear terms in the perturbation are meant as higher order corrections to the linear dispersive equation. This approximated linear dispersive equation is named the *linearised equation*. When this approximation is no longer valid because the perturbations δu_j are such that $\delta u_j \approx u$, and the order of magnitude of the nonlinear terms becomes comparable to the order of magnitude of the linear dispersive equation, then the nonlinear stage comes into play. After the amplitude of the perturbed plane wave reaches its maximum value, it may vanish by causing the formation of localised energy solutions, and solitons may occur as a result of the balance between dispersion and nonlinearity [18].

Since the linear stage of MI is a linear instability, it can be studied via the linearisation of the nonlinear equation around the perturbation. By substituting the explicit expression of $u(x,t)+\delta u_1(x,t)+\delta u_2(x,t)$ into the nonlinear equation, and keeping only the terms at the first order in the perturbation, the linearised equation can be written as a matrix equation (see, for instance, [19])

$$A\,\mathrm{b}_0 = 0_{2\times 2}, \tag{1.2}$$

where [1] A is a 2×2 matrix, $0_{2\times 2}$ is the 2×2 zero matrix and the solution is the vector $\mathrm{b}_0 = \begin{pmatrix} \mathrm{b}_{01} e^{i(Kx-\Omega t)} & \mathrm{b}_{02} e^{-i(Kx-\Omega t)} \end{pmatrix}^T$. The condition such that b_0 is solution of (1.2) is the vanishing of the determinant of the matrix A, i.e. $\det(A) = 0$, which gives the dispersion relation for the perturbations.

In 1965 Lighthill [21] obtained the so called *Benjamin-Feir-Lighthill (BFL) criterion* to determine if a scalar system can be linearly unstable or not. Specifically, he considered a weakly nonlinear Stokes wave (i.e. weakly nonlinear periodic progressive wave, see [22]) on deep water and he found that, if the linearised PDE is a hyperbolic equation, then the Stokes wave is neutrally stable, instead, when the linearised PDE is an elliptic equation, then MI may occur [17]. However, this result is obtained by considering negligible dispersion

[1] The explicit expression of the matrix A depends on the equation in study.

effect and, for this reason, the BFL criterion is not a sufficient condition for the existence of MI. Indeed, when dispersion is negligble, the dispersion relation for the perturbation is independent of the wave number K; on the contrary, when dispersion is present, we can define a domain for the wave number K of the perturbation such that MI can occur. Thus, also in the case in which we have elliptic PDEs, the argument of the square root can be negative only for certain values of K. Moreover, for $\frac{\partial |Im(K)|}{\partial K} = 0$, we obtain the critical value $K_{critic} = K(a, P, Q)$ corresponding to the largest growth rate of $|\mathrm{Im}(\Omega(K))|$. The value K_{critic} depends on the amplitude a of the plane wave solution, but not on its frequency ω and its wave number k, whereas the module $|\mathrm{Im}(\Omega(K))|$ is known as the *gain function*. Thus, MI occurs for values of the physical parameters for which $|\mathrm{Im}(\Omega(K))|$ is not zero [2]. For instance, the NLS equation can be written[3] [15]

$$u_t - iPu_{xx} + iQ|u|^2 u = 0, \tag{1.3}$$

when $PQ > 0$, by the BFL criterion, we have an hyperbolic equation and there is no possibility to have MI; whereas if $PQ < 0$, we have an elliptic equation and we can have MI. Thus, the necessary condition to observe MI is $PQ < 0$ and we need also to compute for which values K the gain function $|\mathrm{Im}(\Omega(K))|$ takes real values different from zero. In this particular case, the physical parameters are related one with each other by the formula

$$(\Omega - 2PkK)^2 = P^2K^2\left(K^2 + 2\frac{Q}{P}a^2\right)^2, \tag{1.4}$$

such that, if $PQ > 0$, the imaginary part of Ω, that is the gain function $|\mathrm{Im}(\Omega(K))|$, does not exist. Instead, if $PQ < 0$, the explicit expression of the gain function is

$$|\mathrm{Im}(\Omega(K))| = 2PkK \pm |PK|\sqrt{K^2 + 2\frac{Q}{P}a^2} \tag{1.5}$$

and the domain of the wave number K, at which the gain function is non-zero, reads

$$K^2 \leq -2\frac{Q}{P}a^2. \tag{1.6}$$

The maximum value of the function $|\mathrm{Im}(\Omega(K))|$ is reached at the wave number [15] $K_{critic} = \pm\sqrt{-\frac{Q}{P}a^2}$.

[2] That is true also for multicomponent models.

[3] In the Chapter 2, we will write the NLS equation in a different manner.

Looking at the expression of the perturbed solution (1.1), the existence of complex modulation frequency Ω entails that, as time goes on, a perturbation grows with the effect of amplifying the amplitude of (1.1). Nevertheless, in general, the amplitude might not grow up indefinitely because, at a certain time, the neglected nonlinear terms come into play to possibly bound such a growth. From the physical point of view, the BFL criterion corresponds to a necessary condition for the occurrence of the localisation of the energy due to a balance between dispersion and nonlinearity. This fact is reflected in the frequency spectrum of the waves interacting during MI. Indeed, MI can be also explained as a four-wave resonant interaction between two infinitesimal sidebands at frequencies $\omega_{1,2} = \omega \pm \Omega$ with a strong carrier wave at frequency ω [23]. A wave at frequency ω interacts twice with a sideband at frequency ω_1 to produce another sideband with a different frequency $\omega_2 = 2\omega - \omega_1$. Similarly, this last sideband interacts with the carrier wave and reinforces the first sideband. In other words, they interact under resonance conditions for the frequencies $\omega_1 + \omega_2 = 2\omega$ and also for the wave numbers $k_1 + k_2 = 2k$, with $k_{1,2} = k \pm K$. Indeed, if we consider the perturbed plane wave (1.1) as solution of the NLS equation, the nonlinearity term becomes proportional to

$$|\bar{u}|^2\bar{u} = a^3 e^{i(kx-\omega t)} + a^2 b_{01} e^{i((2k-(k+K))x-(2\omega-(\omega+\Omega))t)} + \tag{1.7}$$

$$+a^2 b_{02} e^{i((2k-(k-K))x-(2\omega-(\omega-\Omega))t)} + c.c. + o(a^2 b_{0j}), \quad \mathrm{j} = 1, 2,$$

where $c.c.$ stands for complex conjugate of the correcting terms and we have neglected all the terms whose order of magnitude is smaller than the terms multiplied by $a^2 b_{0j}$. Here, the correcting terms to the plane waves have as arguments of the exponentials $2k - (k + K) = 2k - k_1$, $2k - (k - K) = 2k - k_2$ and $2\omega - (\omega + \Omega) = 2\omega - \omega_1$, $2\omega - (\omega - \Omega) = 2\omega - \omega_2$. Thus, $2k - k_2 = k_1$, $2k - k_1 = k_2$ and $2\omega - \omega_2 = \omega_1$, $2\omega - \omega_1 = \omega_2$

If only dispersion was present, the resonance conditions would not be satisfied because, in the linear dispersion relation, frequency would depend only on the wave number. Therefore, even if the waves would interact with different frequencies, in general, they do not match the resonant conditions. The interacting waves would propagate with different phase velocities and, as a result, the dispersion effect pulls apart the resulting wave. On the other hand, if also the nonlinearity is present, then the perturbation satisfies a linearised equation whose dispersion relation involves both the wave number and the amplitude of the carrier

wave. Although with different phase velocities, they propagate on the background of the carrier wave and the wave numbers, as well as the frequencies, match the resonant conditions. Indeed, because of the self-interaction term, the sideband, say, with frequency ω_1 satisfies a linearised equation plus a forcing correction term proportional to the sideband at frequency ω_2 and to the squared carrier wave, (see, for instance, the second corrective term in the expression (1.7)). If this forcing term oscillates with the same frequency of the other sideband, then they resonate [4]. If nonlinearity and dispersion compensate, the sidebands grow linearly as time goes on and drive the carrier wave to oscillate around the resonant frequency ω with greater amplitude. In this case, we say that nonlinearity contrasts dispersion by compressing the plane wave, namely, MI causes the localisation of the energy. As already mentioned above, since when nonlinearity and dispersion balance one each other, we say that the nonlinear stage of MI comes into play and the occurrence of solitons was observed in this stage [24, 25]. From here it is clear the importance of studying the linear stability of physical systems undergoing small perturbations and searching for the existence conditions of localised solutions. In this respect, the interest in mathematical methods to treat MI has witnessed an explosion during the '70s, after the powerful Inverse Scattering Transform (IST) method to find solutions of nonlinear PDEs was developed [26, 27, 28]. It was applied first to the Nonlinear Schrödinger (NLS) equation [29], and then, after the development of the Ablowitz, Kaup, Newell and Segur (AKNS) scheme [30], it was applied to the Kortweg de Vries (KdV) equation [31] and to other physical models. The key idea is that IST is suitable for the investigation of the asymptotic behaviour of solutions of nonlinear equations. A pioneering research in this sense was conducted by Kuznetsov and Mikhailov [32]. Using the Shabat-scheme [33], they studied the stability of periodic stationary waves of the KdV equation as time goes on. The asymptotic stability of the system is explained by the vanishing of the continuous spectrum, while the discrete spectrum survives in time, that is the existence of a set of stable solitons as asymptotic state. Later, several other works were conducted using the Shabat-scheme. For instance, the NLS equation, whose solution goes to the amplitude of the Langmuir wave as $|x| \to \infty$ was used for the investigation of the parametric instability of solitons in a homogeneous plasma [34] and the KP equation, whose solution goes to the cnoidal wave as $|x| \to \infty$ was used

[4] In the case of the NLS equation, we have chosen the frequency and the wave number of the perturbations so that they resonate with the carrier wave.

for the analysis of the stability of periodic waves in a weakly dispersive medium [35].
In the framework of the IST method, particular boundary conditions are required, for example by imposing that the solution and its first derivative are in the class of potentials vanishing sufficiently fast asymptotically. Indeed, it is difficult to deal technically with the IST when solutions have more complicated asymptotic behaviour. Nevertheless, some research works have been conducted to reformulate the IST such that one can work with more sophisticated asymptotic solutions, for instance, solitons with nonzero boundary conditions as solutions of the focusing Nonlinear Schrödinger equation [36, 37], and it has been shown that combinations of the growing exponential solutions of the inverse problem saturate the MI leading, then, to the formation of solitons in the nonlinear stage. In recent times, this subsequent nonlinear stage of MI for the scalar NLS equation has been the subject of intensive investigation and, using numerical and analytical techniques, the stability of plane wave solutions with respect to localised and random perturbations has been studied [38, 39]. Similarly, the stability of plane wave solutions of the scalar NLS equation with respect to periodic perturbations has attracted much attention, and has been investigated in [40, 41, 42, 43] using the theory of finite-gaps and matched asymptotics.
In 1974, Ablowitz developed an alternative and powerful spectral method to lead stability analysis [44]. The method is based on the fact that the solutions of the linearised equation can be written in terms of the so called squared eigenfunctions (SE) (see for example [44], [45, 46] for an introduction to squared eigenfunctions as solutions of the linearised NLS equation), which in turn can be written in terms of the Lax operators [47]. Once a solution of a nonlinear equation is perturbed, the problem to investigate the linear stability of the system is equivalent to investigate the behaviour in time of the SE solutions of the linearised equation (see, for example, [48]). Indeed, via the construction of the SE, one is able to compute the corresponding eigenfrequency whose imaginary part, i.e. the gain function, provides information about the linear stability.

1.1.2 Modulational Instability and Other Linear Instabilities for Multi-Component Systems

As mentioned above, MI for scalar equations is the deformation of the form of the amplitude of a plane wave as a result of the balancing of dispersion and nonlinearity. When these

effects are balanced, solitons may appear in the nonlinear stage. In this case, MI arises when two sidebands are added on the background of the carrier wave with which they interact. MI is the result of the self-interaction of the perturbed solution, such that there exists a nonlinear interaction between plane waves linearly superimposed.

When dispersive nonlinear multi-component systems are taken into account, the single component of a system may exhibit MI, but the entire system can be linearly unstable or not. In this regard, the MI of two-component system of counter-propagating waves has been analysed in the research work [49]. The authors considered two-component solutions of two coupled sine-Gordon equations, which are travelling with different group velocities and each component is composed by two counter-propagating waves linearly superimposed. Then, they used a multiple scale approach to obtain three asymptotic models at different length scales and different timescales, which are systems of four evolution equations, one for each wave. By considering the models so obtained, first, they took into account the two components composed by only one plane wave. At the super-long length scales, the leading order in the dispersion relations is represented by a dispersion term, such that dispersion is considered responsible for the MI. As soon as one considers the long-length scales, a term coming from the self-interaction is added to the linear dispersion relation, so, dispersion and nonlinearity compete with one another as described in the previous subsection. However, without any restriction on the wave number of the perturbation, it has been observed that, besides the linear instability of the single plane wave arising from the competition between the terms of dispersion and self-interaction, any wave can be affected by the coupling between the components. Indeed, such coupling can suppress or enhance this linear instability as a result of the addition of a term coming from the self-interaction. In this way, the effect of nonlinearity becomes stronger or weaker compared to when coupling is absent. The plane wave can gain or lose energy due to the sharing and the exchange of energy occurring when the components overlap, and so, finally, leading to the linear stability or instability of the system [49, 50]. For these two-component systems, dispersion plays a key-role in the occurrence of MI, and it has also been shown that coupled dispersionless nonlinear systems are, indeed, stable with respect to the MI [51]. The linear instability can occur if the dispersive term is taken into account also if it is a higher order correction to the transport and nonlinear terms [49, 50]. Furthermore, the presence of an additional counter-propagating mode in any component can *completely* inhibit or enable the linear

instability because of the exchange of energy between the counter-propagating plane waves in each component and between two coupled components as well. Indeed, because of these couplings, nonlinearity competes with dispersion in a stronger or weaker manner [49, 50]. The classification of the linear instabilities in the parameters [5] space was carried out in the research works for two coupled focusing or for two coupled defocusing NLS equations [71] and for mixed coupled NLS equations, that is a focusing and a defocusing scalar NLS equations are coupled [52]. Taking into account the coupling between two plane waves considered as the two modes of a wave packet and whose perturbations are two Fourier modes, the classification of the linear instabilities is performed on the basis of the energy exchange between plane waves undergoing linear perturbations. These works confirm the existence of instabilities also in defocusing regime (besides the long-wave instability) when there is a coupling of two propagating modes. Several scenarios can occur. For instance, when two focusing NLS equations are coupled, there can be cross-phase instability if one unstable mode, or both unstable modes, of the perturbation excite each plane wave and the energy is shared by the two co-propagating plane waves; or there can be self-phase instability if one mode of the perturbation excites a plane wave more than the other one, there is less shared energy between the two plane waves, and, so, there is linear instability of just one plane wave.

Besides to dispersive nonlinear multi-component systems mentioned above, there is a non-dispersive nonlinear multi-component system which can exhibit linear instability, that is the 3-wave resonant interaction (3WRI) system [53]. The solitons of the 3WRI system interact in a different manner from the solitons of dispersive nonlinear systems, thus one can expect that the mechanism leading to the linear instability (and then to the possible formation of solitons) is different for the two kinds of systems. For this reason, we refer to this phenomenon as linear instability rather than as MI. Indeed, differently from the solitons of dispersive multi-component systems with quadratic coupling, originating from the balance between dispersion and nonlinearity [54], the solitons of the 3WRI system originate from the mismatch of the group velocities of the interacting wave packets, once provided the resonant conditions (see formulas (3.1) in Chapter 3) [53]. In order to highlight how special the 3WRI system is, we remind the reader about the research work [55] where the generation of dispersive shock waves was observed in absence of dispersion and whose behaviour

[5] These parameters are the wave numbers of the two component plane waves and of the disturbance.

resembles the generation of shock waves in dispersive equations, such as the NLS and the KdV equation. Moreover, the role of the dispersion in the system was investigated in [56]. The authors studied the linear stability in space of a triplet of dark solitons and showed that the introduction of a quasi-negligible second order dispersion reduces the instability allowing the three dark solitons propagation.

It is worth pointing out that there is no galilean transformation for which all the three waves have zero group velocity and the velocities mismatch allows the envelopes to overlap when the nonlinearity becomes important. Moreover, due to the fact that the 3WRI system is non-dispersive, in the asymptotic limits $t \to \pm\infty$, the envelopes are well separated and do not overlap; however, during the interaction, the envelopes can exchange both solitons and radiation. Thus, "*the solitons and radiation (continuos spectrum) are on an equal footing*" [57, 58]. This feature of the 3WRI system makes its soliton solutions remarkably different from those ones of other dispersive systems for which radiation decays as time goes on [44, 59]. In fact, solitons and radiation interact nonlinearly and radiation never decays asymptotically [57, 58]. Kaup and collaborators carried out the linear stability analysis of the 3WRI system when its solutions have a vanishing background, and gave necessary and sufficient conditions for linear instabilities to occur [57]. The carrier wave and the two sidebands have finite and infinitesimal amplitudes, respectively, and they interact under the three-wave resonant conditions, $\omega_1+\omega_2+\omega_3 = 0$ and $k_1+k_2+k_3 = 0$, where the frequencies ω_i and the wave numbers k_i can take any value, not necessarily infinitesimally close with one another. These resonant conditions do not originate as a result of selfinteraction, but they must be written together with the 3WRI system [6] [58]. Under particular conditions, the carrier wave can exhibit explosive and the decay instability [60, 61], but only if the carrier wave travels with intermediate group velocity with respect to the group velocities of the two sidebands and if it possesses solitons. We stress that the solitons in question move on a vanishing background and can be obtained, in principle, via IST. In this case, we say that the carrier wave is linearly unstable [57]. Nevertheless, thanks to the lack of the dispersion, all we need to know is the linear behaviour at time $t \to -\infty$, and then "*we can completely determine how this system evolves, even in nonlinear regime*" [57], looking only at the time evolution of the scattering data. This allows to turn around the matter of solving the inverse problem in order to see if an envelope possesses solitons in the nonlinear

[6] We will clarify this concept in Chapter 3.

regime. Some works on the scalar NLS [36, 37, 29] were carried out via this procedure. However, obtaining N-soliton solutions, especially for multi-component systems, can be rather difficult task to achieve.

Hence, the necessity to develop mathematical tools to investigate the linear stability of multi-component systems. The application of perturbation theory to the IST can be extended, in principle, to investigate the linear stability of any integrable system, also those ones which are multi-component [62, 63]. The starting point is still the Lax Pair. Once the scattering data are given by the *direct problem*, one can construct the associated potential by the *inverse problem*. Perturbing the direct and inverse problems, the linear perturbations of the potential are written in terms of the variations of the scattering data (and vice versa) by squared combinations of components of eigenfunctions and its adjoints: the so called *squared eigenfunctions* (SEs) and the *adjoint squared eigenfunctions* (ASEs) [62, 63]. Although, the research works by Kaup and collaborators were carried out both on scalar and multicomponent systems, one needs to use the IST machinery to get a representation of the perturbation in terms of the SEs, and thus their expression in terms of the eigenmodes. It is clear that in the framework of the IST method, the stability analysis is cumbersome to apply to multicomponent systems, in particular for soliton solutions with a non vanishing background. However, the property of the SEs to be solutions of the linearised equation is local and it follows directly from the Lax pair without the need to apply the IST machinery (see Chapters 2 and 3). In this respect, recently a new spectral approach has been developed in [64]. In this research work, the authors investigate the linear stability of continuous waves in all regimes in the framework of the integrability and their method can be applied to other more complicated solutions such as dark-dark, bright-dark, and higher-order solitons travelling on a continuos wave background.

1.2 Motivations and Purposes

In the recent years MI has been proposed as a possible mechanism for the generation of rogue waves. *"In oceanography, rogue waves are defined as waves whose height is more than twice the significant wave height, that is the average height of the highest one-third of the waves in a wave record"* [66, 23].

From an experimental point of view, researchers are interested on their reproducibility and observability in wave tank experiments. From a mathematical point of view, this is equivalent to study the linear stability of solutions which can describe the dynamics of rogue waves.

The dynamics and the physical features of rogue waves can be described by solutions of the NLS equation, such as the homoclinic orbirts [67] of an unstable Stokes wave. Calini and collaborators [69] discovered that, beside the mechanism of MI, rogue waves are created as a result of phase modulation. Using the gauge form of the Bäcklund transformation [68], they constructed the associated solution of the linearised NLS equation, i.e. a squared eigenfunction and so they explored the stability of Stokes waves. Finally, they stated the following selection criterion for rogue waves: *"among the homoclinic orbits of a Stokes wave with M unstable modes, the only 'good' candidate for rogue wave is the maximally iterated homoclinic orbit, with all its spatial modes coalesced through phase modulation"* [69].

A similar investigation was performed on the spatially periodic breathers on an unstable plane wave background, obtaining a similar conclusion [70].

If one considers two coupled NLS equations (CNLS), besides the already mentioned non-focusing instabilities between two unstable and two stable CNLS fields [71] or between a stable and an unstable CNLS field [52], baseband MI can exists. It is triggered by zero-frequency disturbances, and it is believed to be responsible for the formation of rogue waves [72, 73, 74].

Between all the possible kinds of solutions suitable to model rogue waves, we focus on rational solutions: they are solutions with a rational, or semi-rational [7], dependence on the variables x and t, in contrast with the standard solitons whose expression is given in terms of exponentials only. They are also solutions of multicomponent wave equations such as the CNLS equation and the 3WRI system [75, 76, 77]. In this thesis we take into account the system of a resonant triad, not only because it encloses this kind of solitons, but even because the nonlinearity term is the simplest that can occur between three interacting waves [78, 79], and the interaction of waves under resonance conditions is of great interest in many fields of research (see, for instance, [80, 81] and the literature therein). We investigate the linear stability of the 3WRI model by considering solutions on finite background.

[7] Here, semi-rational solutions are meant to have an expression that is both rational and exponential in the variables x and t.

Due to the technical mathematical issues already stated in the previous section, the linear stability of this system and the mechanism leading to its linear instability are less studied than those of other systems, such as the CNLS equations. However, further outcomes can be obtained thanks to the approach developed in [64], and we have applies such an approach to the plane wave solutions of the 3WRI system in order to investigate their linear stability and to confirm if linear instability can be considered a necessary condition to explain the formation of rogue waves mathematically represented by rational solutions. In order to do that, we take advantage of the integrability of this system [82, 83]. This fact is not obvious at all, since the stability of a solution is a local phenomenon, while the integrability is a global characteristic of the equation. As it has already been mentioned (see [62, 63]), solutions of a linearised equation can be written by squared eigenfunctions, and, in turn, by means of the associated Lax pair. If an equation is Lax-integrable [84], the stability of its solutions can be analysed (see, for instance, [71] and [52]). Once the squared eigenfunctions are obtained, we look at their temporal behaviour: if they have an exponential growth in time (i.e. the gain function is different from zero), then the provided solution of the nonlinear equation is (neutrally) linearly unstable. We underline that this approach allows us to generalise the formalism to $N \times N$ matrices. As a consequence, the solutions of the Lax pair equations are written in matrix form and the squared eigenfunctions are more general than those ones used so far.

In addition, we use the spectral method developed in [64] for a technical reason: IST is algebrically cumbersome and it becomes more and more complicated to apply if one wants to find solutions which are rational, semi-rational or, more generally, with a finite background. Indeed, it is necessary to solve the inverse problem to see if localised structures exist asymptotically (after the interaction). For the 3WRI system, the linear stability analysis which can lead to the formation of solitons on vanishing background has leaded to the conclusion that the envelope with intermediate velocity can decay surrounding all its N solitons and, after the interaction, the fast and the slow envelopes own additional N solitons each one. However, it has been impossible to find the final N soliton solutions which, instead, were written only in implicit form and the findings were supported by numerical analysis [58]. Instead, this alternative approach [64] allows us to use Darboux Dressing Transformation (DDT) [85, 86] for envelopes whose background are plane waves interacting resonantly, and in this respect, it turns out that DDT is potentially more useful and algebrically simpler

for finding rational solutions [76]. Another reason for choosing this method is that this approach does not depend on the functional class of the potential, contrary to the IST, which requires the imposition of boundary conditions. Therefore, a wider class of solutions can be taken into account, such as rational or semi-rational solitons, whose dependence on space x and time t usually is asymptotically polynomial, but also other solutions such as breathers. We have numerically observed the generation of potential rogue waves and breathers generated via the linear instability of such a system. This remarkable observation would not have been possibile without the application of the approach [64], which is tailor-made for multi-component systems with solutions on finite background.

In this thesis, first, we carry out a comprehensive topological classification of the stability spectra of the 3WRI system in the parameters space, where the parameters in question are combinations of the physical parameters involved in the plane waves and in the system. This classification is topological and we associate a gain function to any topology. We observe that the stability spectra of the CNLS system are included in this classification and, indeed, the gain function shows the presence of MI-baseband-like and MI-passband-like for such spectra. However, the stability analysis for the 3WRI system is richer, because it presents additional topological features. Indeed, we observe a new gain function associated to such topological features which can be considered neither a MI-passband type nor a MI-baseband type, and are, instead, associated to a stronger linear instability around the zero wave number. In particular, we have observed, via numerical simulations, that this kind of topology and its gain is associated to explosive instability, i.e. the three interacting waves blow up in a finite time [60, 61].

We show that the plane wave solutions of the 3WRI system are linearly unstable in time for any choice of the physical parameters, including those ones associated to the solutions that are explosive. The linear instability of the plane wave correspond to the observation of a positive gain-function.

Although the onset of the linear instability of the 3WRI system has not been clarified, this thesis is meant to be a prelude for its understanding. Indeed, we aim to investigate the mechanism leading to this phenomenon in future research works. It is worth highlighting that, in the research work [87], the authors have analysed the stability of two coupled ordinary differential equations (instead of three PDEs) whose forcing term is the interaction with a third wave, with large amplitude, which does not obey the same dynamical equa-

tions of the other two interacting waves with finite amplitudes [88]. They speculate that the third wave is a cosine as a function of the time.The authors claimed that a sufficient and necessary condition for the onset of instability is that the two interacting waves have modes of opposite sign.

In this thesis, we perform the linear stability analysis on three coupled PDEs, and after linearising every equation, the wave solution interacts with the perturbations of the other two waves. Moreover, every solution propagates with different velocity and we cannot find a reference frame in which they have the same velocity. Instead, we can obtain a system of three ordinary differential equations only in the particular case in which the three waves propagate at the same velocity [57]. For the 3WRI system with wave solutions propagating at the same velocity, the Hasselmann's criterion [89, 90] states that instability occurs if the two sidebands modes sum together with the same signs, and in the case they interact resonantly with the same signs, there is neutral stability.

Hence, we underline the relation between the presence of baseband MI type and the possible existence of rational solitons which can model rogue waves, and in this regard, we provide a necessary condition for the existence of rational solutions on a finite background constructed by means of the DDT method. For sake of simplicity, we will refer sometimes to these rational and semi-rational solutions as rational solutions of Darboux type or DT-FB rational solutions, FB standing for "finite background". We do that by the stability analysis of the plane waves which are solutions of the 3WRI system. These plane waves are meant as the possible background for solitons, namely as the seed solutions for the algebraic construction of rational solutions of Darboux type. When needed, we will specify if we deal with semi-rational solutions, instead of purely rational solutions.

The motivation to conduct this research is because, so far, the mechanism which causes rogue waves formation is unknown, although several hypothesis have been formulated and MI (like passband and baseband) is one of them [91], we assume that their onset can be due to the more general phenomenon of the linear instability, that is a phenomenon that can occur in the 3WRI system. Moreover, rogue waves are ubiquitous in nature and are observed in several physical settings, such as in water tank [92], in fibre optics [24] and in plasma [93]. They are also predicted in the atmosphere [94], in superfluids [95], in Bose-Einstein condensates [96] and in capillary waves [97].

1.3 Overview of the thesis

In Chapter 2, we describe the spectral method developed in [64] and we use the NLS equation as a case study.

In Chapter 3, we give the 'set up' of the formalism for the 3WRI system: Lax pair and Lax operators, construction of the squared eigenfunctions, characteristic polynomials and useful rescalings of the physical parameters of the problem.

In Chapter 4, we conduct the stability linear analysis through the topological classification of the stability-spectra in the parameters space and the associated gain functions. Thus, we state a necessary criterium for the existence of rational and semi-rational solitons on a finite background of Darboux type. However, the computations of the expressions of these solutions is not the aim of this thesis.

In Chapter 5, we show some numerical observations of breathers and potential rogue waves.

Chapter 2

Linear Stability of Plane Waves of the NLS and CNLS Systems

In this chapter we present the formalism developed in [64] by providing the NLS equation as an example. Because NLS is a scalar equation, the space stability spectrum coincides with the spectrum of the spatial part of the Lax pair [64]. This coincidence is not met in the general case of the multi-component systems. Thus, in order to understand where the spatial stability spectrum comes from, we provide the CNLS system as a further example [64]. In this way we are able to write the general definition of stability spectra for multi-component systems.

2.1 Universal Nature of the Nonlinear Schrödinger Equation and Modulational Instability

The origin of the Nonlinear Schrödinger equation is rooted in the theory of self-focusing waves in electrical fields. In 1964, R. Y. Chiao et al. wrote a NLS-type equation [98]. They considered the wave equation for an electric field plus a nonlinear term and concluded that an optical beam of a single frequency, whose dynamics is described by such equation, cannot spread in a nonlinear media, namely the beam is self-focused. Since then, more investigations were carried out on the self-focusing phenomenon (see, for instance, [99, 100])

and, in this context, the NLS equation was derived in [99] as we know it today,

$$u_t - iu_{xx} + 2is|u|^2u = 0, \qquad s^2 = 1\,, \tag{2.1}$$

where the subscripts denote the derivatives with respect to the space x and the time t, $|\cdot|$ is the module of the classical field $u(x,t)$, and s is a sign.

The NLS equation with the sign $s = -1$ is known as focusing NLS equation and was written for the first time in the research paper on the self-focusing optical beams in dispersive and nonlinear media [99]. Using the IST method, Zakharov and Shabat derived its solutions classified as bright solitons which decay at zero at the spatial infinity, and as breathers which decay at a constant background at the spatial infinity [29].

For $s = 1$, the equation is named defocusing NLS. Its solutions are known as dark solitons due to their feature to have a nontrivial background intensity and a spatial local dip. They were obtained by IST in [101].

The universal nature of the NLS equation lies in the fact that it describes the dynamics of many systems in nature whose behaviour is that one of an envelope of a monochromatic wave packet in a dispersive and nonlinear media when the dissipation can be neglected [19]. Zakharov was the first to derive the NLS equation in the context of water waves [103]. Nevertheless, it can be derived in the limit of weak nonlinearity from several equations via the multiple scale method, for instance, by the Sine-Gordon equation [15]. The defocusing NLS equation can also be derived from the KdV equation and the focusing NLS equation from the modified-KdV (see for example [102]).

After Stokes wrote the approximate solutions of the Laplace problem [22], i.e. the Stokes waves, Benjamin and Feir discovered that nonlinear Stokes waves are modulationally unstable [13]. It is well known the pivotal role of the NLS equation in the study of MI and the NLS equation is one of the most used equation for modelling modulation of waves. In this regard, we refer the reader to the book [15] for the linear stability analysis of plane waves, solutions of the NLS equation.

Because the NLS equation had a key role in the understanding of the MI and because it is a scalar equation, in the next section, we shall describe the spectral method developed in [64], by using the NLS equation as a case study.

2.2 Matrix Form of the Nonlinear Schrödinger Equation

Before we proceed with the stability analysis, we make a 'set up' for a new formalism in which the NLS is meant as a matrix equation, where the matrices involved are 2×2. In order to do that, we take advantage of mathematical techniques provided by the integrability. Indeed, since the NLS equation is integrable [29], it admits a representation via two differential equations, which are called Lax equations,

$$\psi_x = X\psi, \qquad \psi_t = T\psi, \tag{2.2}$$

where the subscripts are the derivatives with respect to the spatial variable x and the time variable t, X and T are 2×2 matrices named Lax operators, being $\psi = \psi(x,t,\kappa)$ a common solution of the two linear differential matrix equations (2.2), while $X = X(x,t,\kappa)$ and $T = T(x,t,\kappa)$ depend on the variables x, t and on a complex quantity κ called spectral parameter, according to the definitions

$$X = i\kappa\sigma_3 + Q, \tag{2.3a}$$

$$T = 2i\kappa^2\sigma_3 + 2\kappa Q + i\sigma_3(Q^2 - Q_x), \tag{2.3b}$$

where

$$\sigma_3 = \begin{pmatrix} 1 & 0 \\ 0 & -1 \end{pmatrix}, \tag{2.4}$$

is a Pauli matrix. The matrix $Q = Q(x,t)$ depends on the variables x and t, contains the complex dynamical variable $u = u(x,t)$ and introduces the sign $s^2 = 1$

$$Q = \begin{pmatrix} 0 & su^* \\ u & 0 \end{pmatrix}, \tag{2.5}$$

where u^* is the complex conjugate of the dynamical variable u. We are interested in non-trivial common solutions ψ of the Lax equations (2.2), which are given by the compatibility condition

$$\psi_{xt} = \psi_{tx}. \tag{2.6}$$

The NLS equation can be obtained by (2.6), because it is integrable. By using both (2.2) and (2.6), we get an equation for the Lax operators X and T

$$X_t - T_x + [X, T] = 0, \tag{2.7}$$

where $[X, T] = XT - TX$ is the commutator of the two matrices X and T [1]. Finally, by the definitions of the Lax operators (2.3) and using the fact that

$$Q^2 = s||Q||^2\mathbf{I}_{2\times 2}, \tag{2.9}$$

where $\mathbf{I}_{2\times 2}$ is the 2×2 identity matrix and $||\cdot||$ denotes [2] the spectral norm of Q, we obtain the scalar NLS equation in matrix form

$$Q_t + i\sigma_3 Q_{xx} - 2is\sigma_3||Q||^2 Q = 0. \tag{2.10}$$

In computing the equation (2.10), we have used the property of the Pauli matrix σ_3 to be involutory, that is $\sigma_3^2 = \mathbf{I}_{2\times 2}$. Moreover, the anti-commutators $\{\sigma_3, Q\} = 0$ and $\{\sigma_3, Q_x\} = 0$. The anti-commutator between two matrices A and B is defined as $\{A, B\} = AB + BA$. One can check that (2.10) includes the NLS equation in scalar form. By writing (2.10) as follows

$$\begin{pmatrix} 0 & s(u_t^* + iu_{xx}^* - 2isuu^{*2}) \\ u_t - iu_{xx} + 2isu^*u^2 & 0 \end{pmatrix} = 0_{2\times 2}, \tag{2.11}$$

where $0_{2\times 2}$ denotes the null matrix 2×2, hence,

$$u_t^* + iu_{xx}^* - 2isuu^{*2} = 0, \tag{2.12a}$$

[1] By (2.2), the left-hand side and the right-hand side of the condition (2.6) are rewritten in the following way

$$\psi_{xt} = (X\psi)_t = X_t\psi + X\psi_t = X_t\psi + XT\psi, \tag{2.8a}$$

and

$$\psi_{tx} = (T\psi)_x = T_x\psi + T\psi_x = T_x\psi + TX\psi. \tag{2.8b}$$

[2] The spectral norm of Q is defined as

$$||Q|| = \sqrt{\tau_{\max}}, \quad Q\dagger = \begin{pmatrix} 0 & u^* \\ su & 0 \end{pmatrix},$$

where $\tau_{\max}$ is the biggest eigenvalue of the matrix $QQ^\dagger$, where $Q^\dagger$ is the conjugate transpose of the matrix Q.

$$u_t - iu_{xx} + 2isu^*u^2 = 0, \tag{2.12b}$$

where the equation (2.12a) is the complex conjugate of the equation (2.12b). In particular, (2.12b) is the NLS equation for u and (2.12a) is the NLS equation for u^*.

2.3 Integrability and Linear Stability

In addition to the matrix NLS equation, we need to introduce Lax operators which are independent of the spatial variable x and of the time variable t. In this way, the resulting Lax equations are integrable by the separation of variables method and the obtained solution is mapped into the solution of the original Lax problem [31].

2.3.1 Lax Problem Revisited

Let us consider the simplest solution of the NLS equation (2.12b), namely the plane wave

$$u_0(x,t) = ae^{i(qx-\eta t)}, \tag{2.13}$$

depending on x and t, where a is the amplitude, q is the wave number and η is the frequency of the wave solution. Let $a \in \mathbb{R}$ be independent of the variables x and t. The frequency depends on a and q by the relation

$$\eta = q^2 + 2sa^2, \tag{2.14}$$

that is obtained by substituting (2.13) in the NLS equation (2.12b).
In order to simplify the calculations, we introduce the transformation on the matrix solution $Q_0 = Q_0(x,t)$,

$$Q_0 = \begin{pmatrix} 0 & su_0^* \\ u_0 & 0 \end{pmatrix} = G \begin{pmatrix} 0 & sa \\ a & 0 \end{pmatrix} G^{-1}, \tag{2.15}$$

where $u_0 = u_0(x,t)$ is the plane wave given in (2.13), u_0^* is its complex conjugate, $G = G(x,t)$ is a diagonal matrix which contains all the dependence on the variables x and t,

and $G^{-1} = G^{-1}(x,t)$ is its inverse. More in detail, the matrix G can be written as follows (see Appendix A):

$$G = e^{-\frac{i}{2}[qx-(q^2+2sa^2)t]\sigma_3}. \tag{2.16}$$

The transformation (2.15) induces also a transformation on the solution ψ of the Lax pair (2.2),

$$\psi = G\phi, \tag{2.17}$$

such that it introduces the function $\phi = \phi(x,t)$.
By putting the transformation (2.17) into the the Lax pair (2.2), we obtain the PDEs (see Appendix B):

$$\phi_x = iW\phi, \qquad \phi_t = -iZ\phi, \tag{2.18}$$

where the operators $W = W(\kappa)$ and $Z = Z(\kappa)$ are defined as follows

$$iW = G^{-1}XG - G^{-1}G_x, \tag{2.19a}$$

$$-iZ = G^{-1}TG - G^{-1}G_t. \tag{2.19b}$$

The operators W and Z in (2.19) are 2×2 matrices independent of x and t and depending only on the spectral parameter κ, whose expressions, in terms of their entries, are [3]

$$W = \begin{pmatrix} \kappa + \frac{q}{2} & -isa \\ -ia & -\kappa - \frac{q}{2} \end{pmatrix}, \qquad Z = \begin{pmatrix} -2\kappa^2 + \frac{q^2}{2} & isa(2\kappa - q) \\ ia(2\kappa - q) & 2\kappa^2 - \frac{q^2}{2} \end{pmatrix}, \tag{2.20}$$

and, in addition, they are related with one another is

$$Z = -2\left(\kappa - \frac{q}{2}\right)W. \tag{2.21}$$

[3] We have used the formulas

$$G^{-1}G_x = -\frac{i}{2}q\sigma_3, \quad G^{-1}G_t = \frac{i}{2}(q^2 + 2sa^2)\sigma_3,$$

and the anti-commutators

$$\{\sigma_3, Q\} = 0.$$

The advantage of the revisited Lax Pair (2.18) is that we can integrate it by separation of variables and a solution is

$$\phi = e^{i(Wx-Zt)}, \tag{2.22}$$

where we have used the fact that $[W, Z] = 0$. In turn, by using the transformation (2.17), the solution of the Lax Pair (2.2) is

$$\psi = e^{-\frac{i}{2}[qx-(q^2+2sa^2)t]\sigma_3} e^{i(Wx-Zt)}. \tag{2.23}$$

2.4 Investigating Stability via Lax Pair

The perturbations of the NLS equation can be written as combinations of the SEs which are solutions of the linearised equation [44]. Since the SEs are written starting form the Lax operators, it turns out that one can characterise the solutions of the linearised equation by using such operators.

2.4.1 Squared Eigenfunctions

The starting point of our investigation is the Lax problem (2.2) for the NLS equation. Using the solutions ψ and ψ^{-1} of the Lax problem (2.2), we define the SE $\Psi = \Psi(x, t)$

$$\Psi = \psi M \psi^{-1}, \tag{2.24}$$

where $M = M(\kappa)$ is a 2×2 matrix dependent only on the spectral parameter κ. By (2.2), Ψ satisfies the PDEs [64]

$$\Psi_x = [X, \Psi], \qquad \Psi_t = [T, \Psi], \tag{2.25}$$

which are compatible with one another because of (2.7).
The transformation (2.17) induces the similarity transformation

$$\Psi = G\Phi G^{-1}, \tag{2.26}$$

where the matrix G is given in (2.16), and $\Phi = \Phi(x,t)$, defined as

$$\Phi := \phi M \phi^{-1}, \tag{2.27}$$

satisfies the PDEs (Appendix C)

$$\Phi_x = i[W, \Phi], \quad \Phi_t = -i[Z, \Phi], \tag{2.28}$$

whose solution is [4]

$$\Phi = e^{i(Wx - Zt)} \Phi(0,0) e^{-i(Wx - Zt)}. \tag{2.29}$$

where $\Phi(0,0)$ is the initial condition at $x = 0$ and $t = 0$. Because of (2.27) and (2.22), $\Phi(0,0) \equiv M(\kappa)$. Finally, because of the transformations (2.26) and (2.17), the SE, solution of the PDEs (2.25), reads

$$\Psi = G\,\phi\,\Phi(0,0)\,\phi^{-1}\,G^{-1} = \psi\,\Phi(0,0)\,\psi^{-1}, \tag{2.30}$$

where ψ is provided by (2.23).

2.4.2 Solution of the Linearised Equation and its Connection with Integrability

In this section we introduce the linearised equation (LE) obtained perturbing a generic solution of the NLS.

[4] Let us suppose $\Phi(x,t) = \alpha(x)\beta(t)$, by integrating in x the first of the equations (2.28)

$$\alpha(x) = \alpha(0) + i \int_0^x [W, \alpha(x_1)] \mathrm{dx}_1,$$

and, via iteration,

$$\alpha(x) = \alpha(0) + i \int_0^x [W, \alpha(0)] \mathrm{dx}_1 - \int_0^x \left[W, \int_0^{x_1} [W, \alpha(x_2)]\, \mathrm{dx}_2 \right] \mathrm{dx}_1 = \alpha(0) + i[W, \alpha(0)]x - \int_0^x \left[W, \int_0^{x_1} [W, \alpha(x_2)]\, \mathrm{dx}_2 \right] \mathrm{dx}_1.$$

Similarly, by integrating in t the second of the equations (2.25), one gets

$$\beta(t) = \beta(0) - i[Z, \beta(0)]t - \int_0^t \left[Z, \int_0^{t_1} [Z, \alpha(t_2)]\, \mathrm{dt}_2 \right] \mathrm{dt}_1,$$

thus,

$$\Phi(x,t) = \alpha(x)\beta(t) = \alpha(0)\beta(0) + i[W, \alpha(0)\beta(0)]x - i[Z, \alpha(0)\beta(0)]t + \ldots.,$$

and, by setting $\alpha(0)\beta(0) = \Phi(0,0)$, the solution is (2.29).

Let us suppose to have a solution of a nonlinear equation and to add to it a small perturbation, so that the perturbed solution is $u + \delta u$. As a consequence, the matrix solution is perturbed

$$Q \to Q + \delta Q, \tag{2.31}$$

and the perturbed Lax operators are

$$X \to X + \delta X, \qquad T \to T + \delta T. \tag{2.32}$$

By substituting (2.32) in the equations (2.7), at the first order in the perturbation, we get the LE

$$(\delta X)_t - (\delta T)_x + [\delta X, T] + [X, \delta T] = 0, \tag{2.33}$$

which is an evolution equation for the perturbation δQ. Moreover, we stress that the expression of the linearised equation, as it is written in (2.33), is independent of the model until one chooses the Lax pair, namely the matrix Q and, for this reason, the LE (2.33) is written more generally as follows

$$A_t - B_x + [A, T] + [X, B] = 0. \tag{2.34}$$

We are interested in searching for solutions $A = A(x, t, \kappa)$ and $B = B(x, t, \kappa)$ related to the fundamental matrix solution ψ of the Lax pair. In this respect, we provide the following propositions, which are also stated in [64].

Proposition 2.4.1. *If the pair A, B solves the linearised equation (2.34), then also the pair $F = F(x, t)$, $H = H(x, t)$ defined as*

$$F = [A, \Psi], \qquad H = [B, \Psi], \tag{2.35}$$

satisfies the linearised equation (2.34), namely

$$F_t - H_x + [F, T] + [X, H] = 0. \tag{2.36}$$

This is a consequence of the Jacobi identity and of the fact that Ψ is a solution of (2.25) [64].

Proposition 2.4.2. *The following expressions*

$$F = \left[\frac{\partial X}{\partial \kappa}, \Psi\right], \qquad H = \left[\frac{\partial T}{\partial \kappa}, \Psi\right], \tag{2.37}$$

are solutions of the linearised equation (2.36).

The validity of this statement follows from the fact that the matrices

$$A = \frac{\partial X}{\partial \kappa}, \qquad B = \frac{\partial T}{\partial \kappa}, \tag{2.38}$$

are solutions of the equation (2.34) and from the Proposition 2.4.1 [64].
A consequence of the Proposition 2.4.2 is that any sum or integral of F over the spectral variable κ is a solution δQ of the LE (2.33). As in the paper [64], we assume that the perturbation δQ has the integral representation

$$\delta Q = \int \mathrm{d}\kappa \, F(x,t,\kappa), \tag{2.39}$$

which provides a solution δQ bounded and localised in x at any fixed time t. We require that the perturbation is localised, so that the absolute value of the perturbed solution goes to a constant as $|x| \to \infty$.
The matrix $F(x,t,\kappa)$ and the perturbation δQ satisfy the same linearised equation (2.33) provided that only local terms are involved in their expressions [64]. The solution F plays the same role as the exponential solution of any linearised equation with constant coefficients, namely, by varying κ over the spectrum, it provides the set of "Fourier-like" modes of the linear PDE (2.33) and it takes the general expression [64]

$$F(x,t,\kappa) = G(x,t) \sum_{j,m=1}^{N} \mu_{jm}(\kappa) e^{i[(x(w_j - w_m) - t(z_j - z_m)]} F^{(jm)}(\kappa) G^{-1}(x,t)\,, \tag{2.40}$$

where w_j and z_j are the eigenvalues of the matrices W and Z, respectively and N is the dimension of the matrices W and Z. The coefficients $\mu_{jk}(\kappa)$ are arbitrary functions of the spectral parameter κ, whereas $F^{(jm)}(\kappa)$ constitute a basis (we will obtain explicitly the formula (2.77) in the section 2.5).
If we want δQ to be bounded, then the solution F must be bounded in x for any fixed t and κ, and the subset of the complex κ-plane, over which the integral (2.39) runs, constitutes the so-called stability x-spectrum of the solution Q, denoted by $\mathbf{S}_x$ [64]. The spacial spectrum $\mathbf{S}_x$ can be geometrically defined as follows:

Definition 2.4.3. *The x-spectrum $\mathbf{S}_x$, namely the spectral curve on the complex κ-plane, is the set of values of the spectral variable κ such that at least one of these complex numbers $k_j = w_{j+1} - w_{j+2}$, $j = 1, 2, ..., N \pmod N$ is real.*

Similarly, one can define the stability t-spectrum, denoted by S_t, for which the perturbation δQ and the solution F is bounded and localised in time for any fixed x and κ. Here, we are interested in finding the values of the spectral parameter κ for which the perturbation δQ is bounded in space but it can grow up in time, such that the solution Q can even be linearly unstable in time [64]. In the case of the NLS equation, we will do that by finding both the $\mathbf{S}_x$ and $\mathbf{S}_t$ spectrum. The values of κ belonging to the $\mathbf{S}_x$ spectrum, but not to the $\mathbf{S}_t$ spectrum are those ones for which linear instability occurs. We highlight that, for the scalar NLS equation, the spectrum of the operator $\frac{d}{dx} - X$ and the spectrum of the operator $\frac{d}{dt} - T$ coincide with the stability spectrum $\mathbf{S}_x$ and with the stability spectrum $\mathbf{S}_t$, respectively (see [64] for more details about this point).

In the following, we find the general expression of F for the NLS equation. Although H is also a solution of the LE, we choose to work with F only for the sake of simplicity. Because we are in the case of 2×2 matrices, we use the algebraic basis generated by the Pauli matrices.

From (2.37), the solution F can be written as

$$F = 2i\sigma_3\Psi^{(o)}, \tag{2.41}$$

where we have used the commutation rules between the Pauli matrices. Therefore, we are interested only on the computation of the off-diagonal part of the SE Ψ; in particular, because G is a diagonal matrix [5], we consider only the following SE:

$$\Psi^{(o)} = G\Phi^{(o)}G^{-1}, \tag{2.42}$$

where $\Phi^{(o)} = e^{i(W_0x - Z_0t)}\Phi^{(o)}(0,0)e^{-i(W_0x - Z_0t)}$ (see [64] for more details about the procedure for obtaining this solution after the diagonalisation of the matrices W and Z), where W_0 and Z_0 are the diagonalised matrices of W and Z, and the latter are simultaneously

[5] By the definition of Ψ (2.26), we have

$$\Psi = G\Phi G^{-1} = G(\Phi^{(o)} + \Phi^{(d)})G^{-1} = G\Phi^{(o)}G^{-1} + \Phi^{(d)},$$

where $\Phi^{(o)}$ and $\Phi^{(d)}$ are the off-diagonal part and the diagonal part of the matrix Φ, respectively.

diagonalised because they commute with one another. We cannot have the term proportional to $\Phi^{(d)}(0,0)$, because, when $x=0$ and $t=0$, the solution must be still off-diagonal. Thus, we impose $\Phi^{(o)}(0,0) \equiv \Phi(0,0)$ and $\Phi^{(d)}(0,0) \equiv 0$. Moreover, if the matrices W and Z were not diagonalised, then $\Phi(x,t)$ would have also had entries on its diagonal part, but we want to take only its off-diagonal entries. Indeed, once put $\Phi^{(o)}(0,0) \equiv \Phi(0,0)$, one can check this by assuming that the exponential $e^{i((W^{(d)}+W^{(o)})x-(Z^{(d)}+Z^{(o)})t)}$ can be approximated by the Taylor series $\mathbf{I}_{2\times 2} + i((W^{(d)}+W^{(o)})x-(Z^{(d)}+Z^{(o)})t) + ...$ and, then, by substituting it into the expression of $\Phi(x,t)$.

Let us suppose that the expression of the initial condition is

$$\Phi^{(o)}(0,0) = \alpha\sigma_1 + \beta\sigma_2, \tag{2.43}$$

where α and β are arbitrary constants, and σ_1 and σ_2 are the Pauli matrices

$$\sigma_1 = \begin{pmatrix} 0 & 1 \\ 1 & 0 \end{pmatrix}, \quad \sigma_2 = \begin{pmatrix} 0 & -i \\ i & 0 \end{pmatrix}.$$

Let W_0 and Z_0 be proportional to σ_3. Indeed, because of the property of the trace to be invariant under cyclic permutations, it turns out that the trace of the similarity transformations for diagonalising the matrices W and Z in (2.19) is zero as well as W_0 and Z_0 are 2×2 traceless matrices.

Since the off-diagonal Pauli matrices, σ_1 and σ_2, anti-commute with the diagonal Pauli matrix σ_3, we get

$$\Psi^{(o)} = \alpha\sigma_1 e^{-2i(W_0x-Z_0t)}e^{i(qx-(q^2+2a^2)t)\sigma_3}, \quad \text{if} \quad \text{s=+1}, \tag{2.44}$$

$$\Psi^{(o)} = \beta\sigma_2 e^{-2i(W_0x-Z_0t)}e^{i(qx-(q^2-2a^2)t)\sigma_3}, \quad \text{if} \quad \text{s=-1}. \tag{2.45}$$

We have supposed $\beta = 0$ for the defocusing case $s=+1$ in (2.44), and $\alpha = 0$ for the focusing case $s=-1$ in (2.45). This is because Q is an off-diagonal matrix equals to $Q = a\sigma_1 e^{i(qx-(q^2+2a^2)t)\sigma_3}$ if s=+1, and equals to $Q = -ia\sigma_2 e^{i(qx-(q^2-2a^2)t)\sigma_3}$ if $s=-1$, and we choose to perturb with a matrix δQ with amplitude proportional to σ_1 if $s=+1$ or proportional to σ_2 if $s=-1$. Moreover, since F satisfies the same evolution equation of δQ and they are related with one another in (2.39), then the perturbation δQ and F must be proportional to the same Pauli matrix. In turn, F is given in (2.41), so that the squared

eigenfunctions must be those in (2.44) and (2.45). Finally, using the commutation and anti-commutation rules of the Pauli matrices applied to the expression (2.41), the solution of the LE is

$$F = -2\alpha\sigma_2 e^{-2i(W_0 x - Z_0 t)} e^{i(qx-(q^2+2a^2)t)\sigma_3}, \quad \text{if} \quad s = +1, \tag{2.46}$$

$$F = 2\beta\sigma_1 e^{-2i(W_0 x - Z_0 t)} e^{i(qx-(q^2-2a^2))t\sigma_3}, \quad \text{if} \quad s = -1. \tag{2.47}$$

We observe that, in the case of the NLS equation written via 2×2 matrices, the differences of the egeinvalues w_j and z_j are $w_j - w_{j+1} = 2w_j$ and $z_j - z_{j+1} = 2z_j$ for $j = 1, 2 \bmod(2)$, because of the commutation rules of the Pauli matrices. This does not hold for matrices W and Z whose dimension is $N > 2$.

2.4.3 Spectral Stability Analysis

The matrices W and Z are simultaneously diagonalised and are related one with the other by means of formula (2.21) and thus their eigenvalues are related as well [6],

$$w = \pm\sqrt{\kappa^2 - sa^2}, \qquad z = -2\kappa w, \tag{2.48}$$

where we are considering the plane wave with $q = 0$.
In both the focusing and defocusing ($s = -1$ and $s = +1$) cases, the eigenvalues w and z are reals if and only if $\kappa \in \mathbf{S}_x$ and $\mathbf{S}_t$, respectively. In the defocusing case $s = +1$ the solution $u = ae^{-2ia^2 t}$ is linearly stable because the x-spectrum

$$\mathbf{S}_x = \{-\infty < \kappa \leq -a\} \oplus \{a \leq \kappa < +\infty\}, \tag{2.49}$$

is included in the spectrum of the operator T

$$\mathbf{S}_t = \mathbf{S}_x \oplus \{\kappa = i\gamma : -\infty < \gamma < +\infty\}. \tag{2.50}$$

Both the spectra are shown in the figure 2.1.

In the focusing case $s = -1$, the solution $u = ae^{2ia^2 t}$ is linearly unstable. Indeed, the

[6] In order to obtain the eigenvalues w and z, we have solved the equations

$$\mathrm{Det}(W - w\,\mathbf{I}_{2\times 2}) = 0, \quad \mathrm{Det}(Z - z\,\mathbf{I}_{2\times 2}) = 0,$$

with unknowns w and z, and $\mathrm{Det}(\cdot)$ is the determinant.

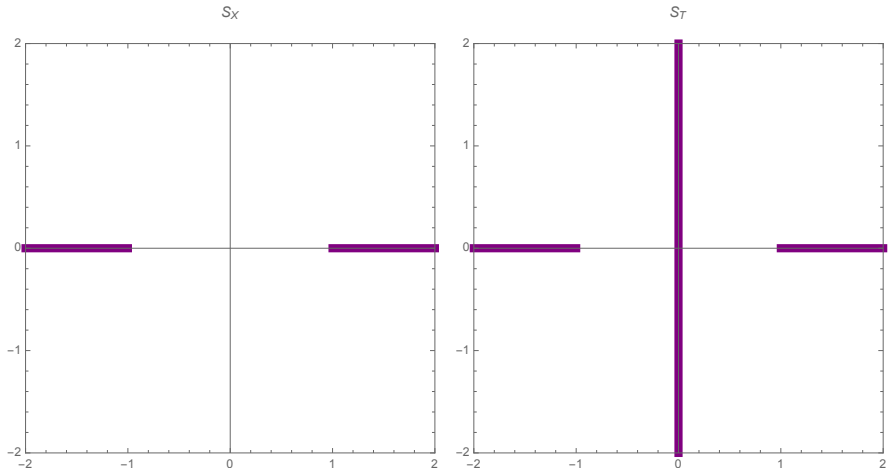

Figure 2.1: Defocusing case, a=1.

x-spectrum is

$$\mathbf{S}_x = \{-\infty < \kappa < +\infty\} \oplus \{\kappa = -i\gamma : -a \leq \gamma \leq +a\}, \tag{2.51}$$

while t-spectrum is

$$\mathbf{S}_t = \{-\infty < \kappa < +\infty\} \oplus \{\kappa = i\gamma : \gamma < -a \quad \text{or} \quad \gamma > +a\}. \tag{2.52}$$

In this case the branch $-a < \gamma < +a$ belongs to $\mathbf{S}_x$ but not to $\mathbf{S}_t$, as shown in the figure 2.2. This is related to the MI phenomenon, indeed, in such a case, the squared

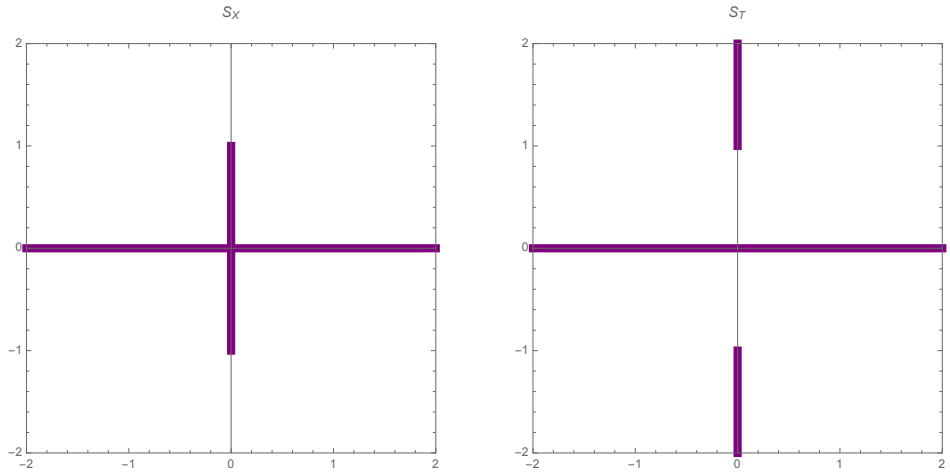

Figure 2.2: Focusing case, a=1.

eigenfunctions in (2.46) and (2.47) grow exponentially as time goes on.

2.5 Wave Coupling and Solution of the Linearised Equation for the CNLS System

In the following we give an introduction to the linear stability problem of the plane wave solutions of the CNLS system within the integrability framework to prove that the main objects to be computed are the eigenmodes' wave numbers and frequencies defined on the stability spectrum. In the presentation, we will follow [64].

For the CNLS system, we start by choosing the Lax operators $X(x,t,\kappa)$ and $T(x,t,\kappa)$ to be

$$X(\kappa) = i\kappa\Sigma + Q\,, \quad T(\kappa) = 2i\kappa^2\Sigma + 2\kappa Q + i\Sigma(Q^2 - Q_x)\,, \tag{2.53}$$

where Σ, Q are matrix-valued functions of x and t, and κ is the spectral parameter, and

$$\Sigma = \begin{pmatrix} 1 & 0 & 0 \\ 0 & -1 & 0 \\ 0 & 0 & -1 \end{pmatrix}, \tag{2.54a}$$

$$Q = \begin{pmatrix} 0 & v_1^* & v_2^* \\ u_1 & 0 & 0 \\ u_2 & 0 & 0 \end{pmatrix}. \tag{2.54b}$$

Here and below the asterisk denotes complex conjugation and the four field variables u_1, u_2, v_1, v_2 are considered as independent functions of x and t, and are conveniently arranged as two two-dimensional vectors, that is

$$\mathbf{u} = \begin{pmatrix} u_1 \\ u_2 \end{pmatrix}, \quad \mathbf{v} = \begin{pmatrix} v_1 \\ v_2 \end{pmatrix}. \tag{2.55}$$

Then the matrix PDE (2.7) becomes, in this case,

$$Q_t = -i\Sigma(Q_{xx} - 2Q^3)\,, \tag{2.56}$$

which is equivalent to the two vector PDEs

$$\begin{aligned} \mathbf{u}_t &= i[\mathbf{u}_{xx} - 2(\mathbf{v}^\dagger\mathbf{u})\mathbf{u}] \\ \mathbf{v}_t &= i[\mathbf{v}_{xx} - 2(\mathbf{u}^\dagger\mathbf{v})\mathbf{v}]\,, \end{aligned} \tag{2.57}$$

equivalent to the CNLS system upon setting

$$v_1 = s_1 u_1, \tag{2.58a}$$

$$v_2 = s_2 u_2. \tag{2.58b}$$

Here the dagger notation denotes the Hermitian conjugation (which takes column-vectors into row-vectors). In this simpler setting, if $Q(x,t)$ is a given solution of the equation (2.56), the linearised equation (2.33) for a small change $\delta Q(x,t)$ reads

$$\delta Q_t = -i\Sigma[\delta Q_{xx} - 2(\delta Q Q^2 + Q\delta Q Q + Q^2 \delta Q)]\,. \tag{2.59}$$

Moreover, the Propositions 2.4.1 and 2.4.2 are still satisfied for the CNLS system (and any multi-component system, satisfying certain hypothesis, see [64]), and the fact that the perturbation δQ and the solution F are linked by the integral (2.39) guarantees that the matrix $F(x,t,\kappa)$ satisfies this same linear PDE, namely

$$F_t = -i\Sigma[F_{xx} - 2(FQ^2 + QFQ + Q^2 F)]\ , \tag{2.60}$$

and, for $\kappa \in \mathbf{S}_x$, these solutions should be considered as eigenmodes of the linearised equation.

The spectral analysis is based on the following

Proposition 2.5.1. *The matrix*

$$F = i[\Sigma\,,\,\Psi]\,, \tag{2.61}$$

defined in the Proposition 2.4.2, along with (2.53), in the case of the CNLS system, satisfies the same linear equation satisfied by δQ.

The Proposition 2.5.1 has been specialised to the case of the CNLS equation, but it is stated in a general form in [64] (see Proposition 4 of the paper), in which it is formulated for any multi-component system provided that each term in the expression of the Lax operators has a local character.

We can compute analytically the matrix F if the fundamental matrix solution $\psi(x,t,\kappa)$ of

the Lax pair corresponding to the solution $Q(x,t)$ is explicitly known. Here we devote our attention to the stability of the plane wave solution of (2.56), or of the equivalent vector system (2.57),

$$\mathbf{u}(x,t) = e^{i(qx\sigma_3 - \nu t)}\mathbf{a}\,, \quad \mathbf{v}(x,t) = e^{i(qx\sigma_3 - \nu t)}\mathbf{b}\,, \quad \nu = q^2 + 2\mathbf{b}^\dagger\mathbf{a}\,. \tag{2.62}$$

In these expressions a and b are arbitrary, constant and, with no loss of generality, real 2-dim vectors:

$$\mathbf{a} = \begin{pmatrix} a_1 \\ a_2 \end{pmatrix}\,, \quad \mathbf{b} = \begin{pmatrix} b_1 \\ b_2 \end{pmatrix}\,. \tag{2.63}$$

The plane wave solution of the CNLS system is obtained by setting

$$b_1 = s_1 a_1, \tag{2.64a}$$

$$b_2 = s_2 a_2. \tag{2.64b}$$

The reduced version of this system is the NLS one-component version, for $u_2 = v_2 = 0, v_1 = -u_1$, that turns out to be a good model of the Benjamin-Feir (or modulational) instability which is of great physical relevance (see Chapter 2).

The main focus of this section is to understand how the spectrum $\mathbf{S}_x$ changes by varying the parameters a_1, a_2, b_1, b_2 and q. In matrix notation, see (2.54b), this plane wave solution (2.62) reads

$$Q = G\,\Xi\,G^{-1}\,, \quad \Xi = \begin{pmatrix} 0 & b_1 & b_2 \\ a_1 & 0 & 0 \\ a_2 & 0 & 0 \end{pmatrix}\,, \quad G(x,t) = e^{i(qx\sigma - q^2 t\sigma^2 + pt\Sigma)}\,, \tag{2.65}$$

where the matrix Σ has the expression (2.54a) while the matrix σ is

$$\sigma = \begin{pmatrix} 0 & 0 & 0 \\ 0 & 1 & 0 \\ 0 & 0 & -1 \end{pmatrix}, \tag{2.66}$$

and we conveniently introduce the real parameters

$$p = b_1 a_1 + b_2 a_2 \tag{2.67a}$$

$$r = b_1 a_1 - b_2 a_2 \tag{2.67b}$$

which will be handy in the following. Next we observe that a fundamental matrix solution $\psi(x,t,\kappa)$ of the Lax equations has the expression

$$\psi(x,t,\kappa) = G(x,t) e^{i(xW(\kappa) - tZ(\kappa))}\,, \tag{2.68}$$

where the x, t-independent matrices W and Z are found to be

$$W(\kappa) = \begin{pmatrix} \kappa & -ib_1 & -ib_2 \\ -ia_1 & -\kappa - q & 0 \\ -ia_2 & 0 & -\kappa + q \end{pmatrix} = \kappa\Sigma - q\sigma - i\,\Xi\,, \tag{2.69}$$

$$Z(\kappa) = \begin{pmatrix} -2\kappa^2 & i(2\kappa - q)b_1 & i(2\kappa + q)b_2 \\ i(2\kappa - q)a_1 & 2\kappa^2 - q^2 - a_2 b_2 & a_1 b_2 \\ i(2\kappa + q)a_2 & a_2 b_1 & 2\kappa^2 - q^2 - a_1 b_1 \end{pmatrix} = \kappa^2 - 2\kappa W(\kappa) - W^2(\kappa) - p\,, \tag{2.70}$$

with the property that they commute, $[W\,,\,Z] = 0$, consistently with the compatibility condition $\psi_{xt} = \psi_{tx}$. We consider here the eigenvalues $w_j(\kappa)$ and $z_j(\kappa)$, $j = 1,2,3$, of $W(\kappa)$ and, respectively, of $Z(\kappa)$ as simple, as indeed they are for generic values of κ. In this case both $W(\kappa)$ and $Z(\kappa)$ are diagonalized by the same matrix $U(\kappa)$, namely

$$\begin{aligned} &W(\kappa) = U(\kappa) W_D(\kappa) U^{-1}(\kappa)\,, \quad W_D = \mathrm{diag}\{w_1,\, w_2,\, w_3\} \\ &Z(\kappa) = U(\kappa) Z_D(\kappa) U^{-1}(\kappa)\,, \quad Z_D = \mathrm{diag}\{z_1,\, z_2,\, z_3\}\,. \end{aligned} \tag{2.71}$$

Next we construct the matrix $F(x,t,\kappa)$ via its definition, see (2.61), (2.26) and (2.27),

$$F(x,t,\kappa) = [\Sigma\,,\, \phi(x,t,\kappa) M(\kappa) \phi^{-1}(x,t,\kappa)]\,, \tag{2.72}$$

which, because of the explicit expression (2.68), reads

$$F(x,t,\kappa) = G(x,t) \left[\Sigma\,,\, e^{i(xW(\kappa) - tZ(\kappa))} M(\kappa) e^{-i(xW(\kappa) - tZ(\kappa))}\right] G^{-1}(x,t)\,. \tag{2.73}$$

As for the matrix $M(\kappa)$, it lies in a nine-dimensional linear space whose standard basis is given by the matrices $B^{(jm)}$, whose entries are

$$B^{(jm)}_{kn} = \delta_{jk}\delta_{mn}\,, \tag{2.74}$$

where δ_{jk} is the Kronecker symbol ($\delta_{jk} = 1$ if $j = k$ and $\delta_{jk} = 0$ otherwise). However the alternative basis $V^{(jm)}$, which is obtained via the similarity transformation

$$V^{(jm)}(\kappa) = U(\kappa)B^{(jm)}U^{-1}(\kappa)\,, \tag{2.75}$$

where $U(\kappa)$ diagonalizes W and Z (see (2.71)), is more convenient to our purpose. Indeed, expanding the generic matrix $M(\kappa)$ in this basis as

$$M(\kappa) = \sum_{j,m=1}^{3} \mu_{jm}(\kappa)V^{(jm)}(\kappa)\,, \tag{2.76}$$

the scalar functions μ_{jm} being its components, and inserting this decomposition into the expression (2.73), leads to the following representation of F

$$F(x,t,\kappa) = G(x,t)\sum_{j,m=1}^{3} \mu_{jm}(\kappa)e^{i[(x(w_j-w_m)-t(z_j-z_m)]}F^{(jm)}(\kappa)G^{-1}(x,t)\,, \tag{2.77}$$

where we have introduced the x, t-independent matrices

$$F^{(jm)}(\kappa) = \left[\Sigma\,,\, V^{(jm)}(\kappa)\right]\,. \tag{2.78}$$

The advantage of expression (2.77) is to explicitly show the dependence of the matrix F on the six exponentials $e^{i[(x(w_j-w_m)-t(z_j-z_m)]}$.

The elements $\mu_{jk}(\kappa)$ are arbitrary because they are the coefficients on the basis $V^{jk}(\kappa)$ used to write the matrix $M(\kappa)$ in (2.76), that is, in turn, arbitrary.

2.6 Eigenmodes' Wave Numbers and Frequencies for Multi-Components Systems

The Proposition 2.5.1 stated in the previous section guarantees that, for any choice κ of the functions $\mu_{jm}(\kappa)$, the expression (2.77) be a solution of the linearized equation (2.59), see (2.60). The requirement to have δQ bounded is equivalent to require F bounded. Looking at the formula (2.77), since μ_{jk} are arbitrary, it is sufficient to impose that only one difference, say $k_1 - k_2$, is real and the corresponding $\mu_{12} \neq 0$, and to impose that the other coefficients are $\mu_{23} = \mu_{31} = 0$.' The further condition that the solution $\delta Q(x,t)$ be bounded in x at any fixed time t results in integrating expression (2.77) with respect to the

variable κ over the spectral curve $\mathbf{S}_x$ of the complex κ-plane:

$$\delta Q(x,t) = \int_{\mathbf{S}_x} \mathrm{d}\kappa\, F(x,t,\kappa)\,. \tag{2.79}$$

The spacial spectrum $\mathbf{S}_x$ can be geometrically defined as follows:

Definition 2.6.1. *The x-spectrum $\mathbf{S}_x$, namely the spectral curve on the complex κ-plane, is the set of values of the spectral variable κ such that at least one of the three complex numbers $k_j = w_{j+1} - w_{j+2}$, $j = 1,2,3\,(\mathrm{mod}\,3)$, or explicitly*

$$k_1(\kappa) = w_2(\kappa) - w_3(\kappa)\,, \quad k_2(\kappa) = w_3(\kappa) - w_1(\kappa)\,, \quad k_3(\kappa) = w_1(\kappa) - w_2(\kappa)\,, \tag{2.80}$$

is real.

Observe that the k_j's play the role of eigenmode wave-numbers (see (2.77)).
The requirement to have δQ bounded is equivalent to require F bounded. Looking at the formula (2.77), since μ_{jk} are arbitrary, it is sufficient to impose that only one difference, say $k_1 - k_2$, to be real and the corresponding $\mu_{12} \neq 0$ and to impose that the other coefficients are $\mu_{23} = \mu_{31} = 0$.

To the purpose of establishing the stability properties of the continuous wave solution (2.62) we do not need to compute the integral representation (2.79) of the solution δQ of (2.59). Indeed, it is sufficient to compute the eigenfrequencies

$$\omega_1(\kappa) = z_2(\kappa) - z_3(\kappa)\,, \quad \omega_2(\kappa) = z_3(\kappa) - z_1(\kappa)\,, \quad \omega_3(\kappa) = z_1(\kappa) - z_2(\kappa)\,, \tag{2.81}$$

as suggested by the exponentials which appear in (2.77). Their expression follows from the matrix relation (2.70)

$$z_j = \kappa^2 - 2\kappa w_j - w_j^2 - p\,, \tag{2.82}$$

and read

$$\omega_j = -k_j(2\kappa + w_{j+1} + w_{j+2})\,, \quad j = 1,2,3\ (\mathrm{mod}\,3)\,. \tag{2.83}$$

This expression looks even simpler by using the relation $w_1 + w_2 + w_3 = -\kappa$ implied by the trace of the matrix $W(\kappa)$ (see (2.69)) and finally reads

$$\omega_j = k_j(w_j - \kappa)\ , \ \ j = 1,\, 2,\, 3\ . \tag{2.84}$$

The consequence of this expression (2.84), which is relevant to our stability analysis, is given by the following

Proposition 2.6.2. *The continuous wave solution (2.62) is* stable *against perturbations* δQ *whose representation (2.39) is given by an integral which runs* only *over those values of* $\kappa \in \mathbf{S}_x$ *which are strictly* real.

The proof of this Proposition is provided in [64].

Chapter 3

The 3-Wave Resonant Interaction Model

In this Chapter we introduce the 3WRI system and we reformulate it in order to include all the possible velocity orderings and all the possible choices of signs in just one Lax pair. This reformulation simplifies the computations in view of a complete classification of the spatial stability spectra in the parameters space (see Chapter 4). Then, we apply the formalism developed in [64] as introduced in the Chapter 2. Finally, we write the differences of the eigenvalues of the matrices W in terms of the differences of the eigenvalues of the matrices Z.

3.1 Linear Stability Analysis of the 3WRI Equations: Historical Overview and State of the Research

The 3-wave resonant interaction (3WRI) model describes the dynamics of three waves interacting by a quadratic nonlinearity and without dispersion and dissipation. The nonlinearity term can be considered like a perturbation at the first order of the linear dynamics [55, 78]. The weak, quadratic nonlinearity and the neglected dispersion make the system the simplest model to be analysed in case of resonant interaction. The interaction is called 'resonant' because it takes place only when the frequencies η_j and the wave numbers ν_j of each wave

with $j = 1, 2, 3$ satisfy particular relations, named *resonant conditions*:

$$\eta_1 + \eta_2 + \eta_3 = 0, \quad \nu_1 + \nu_2 + \nu_3 = 0. \tag{3.1}$$

Moreover, the dispertionless dynamics entails that for time going to $\pm\infty$ the solutions are well separated and do not decay, and the model is integrable [58]. The dynamics with dispersion can be also described by adding a dispersive term that, in general, makes the model non-integrable, unless it is a second order correction to the linear dynamics that acts in a timescale longer than the nonlinearity. However, this correction affects substantially the stability of the system. For instance, in the research work [56], a triplet of dark solitons with locked velocity has been found to be always unstable. Nevertheless, a quasi-negligible second order dispersion balances the nonlinearity effect so that a stable triplet of dark solitons can propagate.

In this thesis we are interested in the linear stability analysis of the simplest solutions of the 3WRI system, i.e. the plane waves. The stability of a resonant triad was studied first in 1967 by Hasselmann for spatially uniform plane waves and he formulated a stability criterion (named *Hasselmann's criterion*)[89]:

"the nonlinear coupling between two infinitesimal components 1 *and* 2 *and a finite component* 3 *whose wave-numbers and frequencies satisfy the resonant-interaction conditions*

$$\eta_1 \pm \eta_2 = \eta_3, \qquad \nu_1 \pm \nu_2 = \nu_3,$$

is unstable for the sum interaction and neutrally stable for the difference interaction."

In other words, the criterion above states that the wave with highest frequency exhibits instability [44, 90]. The dynamics of a conservative system of coupled plane waves with amplitudes modulated in time is described by the ordinary differential equations

$$\begin{aligned} \frac{dA_1}{dt} &= s_1 A_2^* A_3^*, \\ \frac{dA_2}{dt} &= s_2 A_1^* A_3^*, \\ \frac{dA_3}{dt} &= s_3 A_1^* A_2^*, \end{aligned} \tag{3.2}$$

where $A_j = A_j(t)$, with $j = 1, 2, 3$, are complex slowly varying amplitudes, s_j are signs such that $s_j^2 = 1$, and the asterisk denotes the complex conjugation. Let us suppose that the wave A_3 is the 'pump', whose amplitude is initially finite and it is approximately constant in time, while the amplitudes of the other two interacting waves are infinitesimal

and dependent on time. These assumptions lead the system (3.2) to reduce to [44, 57]

$$\begin{aligned} \frac{dA_1}{dt} &= s_1 A_2^* A_3^* \,, \\ \frac{dA_2}{dt} &= s_2 A_1^* A_3^* \,, \\ \frac{dA_3}{dt} &= 0 \,. \end{aligned} \tag{3.3}$$

and because A_3 is constant in time, we obtain

$$\frac{d^2 A_j}{dt^2} \approx s_1 s_2 A_j |A_3|^2, \qquad j = 1, 2. \tag{3.4}$$

If $s_1 = s_2 = 1$ and $s_3 = -1$, then the infinitesimal amplitudes grow exponentially until the linear approximation is not longer valid, the amplitudes A_1 and A_2 become comparable to the amplitude A_3 which, in turn, depletes. However, this process is periodic, in the sense that, after an exact period $2t_0$ [1], A_1 and A_2 deplete and A_3 grows [57]. Thus, A_1 and A_2 are periodic, and A_3 is nonlinearly unstable: the linear approximation is not valid anymore when the infinitesimal amplitudes reach the value of the finite one. If $s_1 = s_2 = s_3$, all the three amplitudes grow indefinitely and the system exhibits explosive instability [57, 60, 61, 104]. Beside research works on the system of ordinary differential equations (3.2), further research has been carried out on the system (3.2) and on the stability of its solutions. In particular, if the amplitudes A_j depend on both time and space, such that the system (3.2) involves partial derivatives with respect to both time t and space x, general solutions are wave packets [105, 106]. The starting point of the investigation in this thesis is the 3WRI model, that is written in general form as an integrable system of three PDEs in $1+1$ dimensions [55]

$$\begin{cases} q_{1t} + c_1 q_{1x} = s_1 q_2^* q_3^* \,, \\ q_{2t} + c_2 q_{2x} = s_2 q_1^* q_3^* \,, \\ q_{3t} + c_3 q_{3x} = s_3 q_1^* q_2^* \,, \end{cases} \tag{3.5}$$

where $q_j = q_j(x,t)$ are complex amplitudes, c_j is the group velocity of the jth-packet, s_j such that $s_j^2 = 1$. The subscripts x and t denote the partial derivatives with respect to space x and time t, respectively, while the asterisk stands for the complex conjugation.

By assuming that the resonant conditions (3.1) are satisfied, the system (3.5) describes

[1] t_0 is the time that the infinitesimal solutions A_1 and A_2 take to become comparable to the amplitude A_3.

several processes that can be classified mainly by the signs s_j and by the ordering of the velocities c_j [57]. Indeed, the system (3.5) comes from perturbing the differential equation $u_{TT} + \Omega(-i\partial_X)^2 u = N(u)$, where $\Omega(\eta)$ is a real nonnegative polynomial, with $\Omega^2(0) > 0$, and N is twice differentiable function, with $N(0) = N'(0) = 0$, enclosing nonlinear terms [55, 78, 79]. After using the multi-scale method, one gets an equation for the lower order error term and, in order to avoid that this term grows linearly, we need to set equal to zero some terms such that, after rescaling, we obtain the system (3.5) with signs $s_j = \mathrm{sgn}(N''(0)\nu_j)$, $j = 1, 2, 3$ [55]. Therefore, the system (3.5), with the resonant conditions (3.1) and with a sign s_j different from the other two signs, is associated to decay instability. On the other hand, the system (3.5) can also be obtained, with the same procedure described above, by replacing the term $N(u)$ with the term [2] $N(u_x)$, such that the signs are defined as $s_j = -\mathrm{sgn}(\mathrm{N}''(0)\nu_\mathrm{j}\eta_\mathrm{m}\eta_\mathrm{l})$, for j, l, $m = 1, 2, 3$ and all distinct [55]. As a result, the conditions (3.1) are satisfied for $s_1 = s_2 = s_3$, provided that the ratios $\frac{\eta_j}{\nu_j}$ are all positive. This is the case known as explosive instability. Indeed, by considering wave packets as solutions, we can individuate the solutions with explosive behaviour via the analysis of the *Manley-Rowe relations* [3] [107]

$$\int_{\mathbb{R}} |q_1|^2 \,\mathrm{dx} - s_1 s_2 \int_{\mathbb{R}} |q_2|^2 \,\mathrm{dx} = I_{12}, \tag{3.6a}$$

$$\int_{\mathbb{R}} |q_2|^2 \,\mathrm{dx} - s_2 s_3 \int_{\mathbb{R}} |q_3|^2 \,\mathrm{dx} = I_{23}, \tag{3.6b}$$

$$\int_{\mathbb{R}} |q_3|^2 \,\mathrm{dx} - s_1 s_3 \int_{\mathbb{R}} |q_1|^2 \,\mathrm{dx} = I_{31}, \tag{3.6c}$$

with q_j being a smooth function satisfying the condition $|q_j|^2 \to 0$ for $|x| \to \infty$, where $|\cdot|$ is the modulus [4] and I_{12}, I_{23} and I_{13} being constants. The equations (3.6) are conservation

[2] The subscript x denotes the derivative with respect to x of the solution u.

[3] If we multiply each equation for the envelope q_j by its complex conjugate q_j^*, and if we add to this equation the equation for q_j^* multiplied by q_j, we obtain an equation for the action of every envelope [55] (that is the energy of the wave divided by η_j [57])

$$\frac{d}{dt}\int_{\mathbb{R}} |q_j|^2 \mathrm{dx} = 2 s_j \int_{\mathbb{R}} \mathrm{Re}\{q_1 q_2 q_3\} \mathrm{dx}, \qquad j = 1, 2, 3,$$

and $\mathrm{Re}\{\cdot\}$ is the real part of the product $q_1 q_2 q_3$. Finally, by summing two by two these equations and by integrating them with respect to the time, we get the Manley-Rowe relations. [55]

[4] This is a consequence of the fact that the solutions q_j are wave packets and so they are also square-integrable $\int_{\mathbb{R}} |q_j|^2 \,\mathrm{dx} < \infty$.

laws of the action exchanged between the interacting envelopes [108, 109].

By looking at the relations (3.6), we deduce that when all the signs s_j are equal one to another, the system (3.5) can exhibit solutions with spikes at a finite time because the conserved quantity I_{kj} may not bound the action $\int_{\mathbb{R}} |q_j|^2 \, \mathrm{dx}$ of any packet in the left-hand side of the equations (3.6). Indeed, the envelope can grow up indefinitely and blow up at a finite time although their mutual exchange of action allows I_{kj} to remain constant [60, 55, 110]. If instead one sign is different from the others, the system (3.5) describes two kind of interactions: decay instability or stimulated backscatter [57]. For example, let us consider $s_3 = -1$ and $s_1 = s_2 = 1$, then the *Manley-Rowe relations* become [5]

$$\int_{\mathbb{R}} |q_1|^2 \, \mathrm{dx} - \int_{\mathbb{R}} |q_2|^2 \, \mathrm{dx} = I_{12}, \tag{3.7a}$$

$$\int_{\mathbb{R}} |q_3|^2 \, \mathrm{dx} + \int_{\mathbb{R}} |q_1|^2 \, \mathrm{dx} = I_{13}, \tag{3.7b}$$

$$\int_{\mathbb{R}} |q_2|^2 \, \mathrm{dx} + \int_{\mathbb{R}} |q_3|^2 \, \mathrm{dx} = I_{23}. \tag{3.7c}$$

With this choice of signs, the constants I_{kj} are nonnegative and bound any norm of the envelopes at any time, such that the solutions do not grow up indefinitely and remain bounded (see [55] and [110] for more details). This process is interesting because, during the interaction between the envelopes, linear instability may occur. In this respect, in [111], by using the IST formalism and numerical techniques, the authors studied the stability of a finite amplitude wave interacting with two initially infinitesimal amplitude waves. In this way, the system (3.5) reduces to a system of two linear equations for the initial infinitesimal waves. Because the small amplitudes can grow up during the interaction, after a certain time, nonlinearity comes into play and the linear approximation is not valid. However, there is a connection between the linearisation of the 3WRI model and the Zakharov-Shabat problem describing its nonlinear evolution. In particluar, after some transformations, the 3WRI model describing the interaction between a 'pump' and two infinitesimal sidebands, reduces to three Zhakarov-Shabat problems [57]. This is because the system is dispersionless, the envelopes are well separated in the initial and the final states, and hence the

[5] Only two conserved quantities I_{kj} are linearly independent. Indeed, for I_{12} and I_{13} linearly independent, then $I_{23} = I_{12} - I_{13}$.

Zhakarov-Shabat scattering data contain all the information about the final state. A conclusion about the linear stability analysis of the 3WRI model is that, if the highest-frequency pump has the middle velocity and contains solitons, then linear instability occurs and in the final state the pump can show a spike at a finite time (explosive instability) or can deplete (decay instability) [57]. We highlight that this analysis was conducted by supposing that the potential of the eigenvalues problem goes to zero as $x \to \pm\infty$ (see also [58]).

Although, the *Manley-Rowe relations* are useful to predict if square-integrable solutions blow up at a finite time, we can not use them when plane waves solutions are considered. For this reason, even if we do not exclude the possibility of the existence of solutions with explosive instability, in our analysis, we need to consider any choice of signs, also that one in general associated to explosive instability, i.e. $s_1 = s_2 = s_3$.

Moreover, most of the research works lead so far dealt with wave packets, not with plane waves as, instead, we shall do. In addition, the linear stability analysis was carried out by considering the two side-bands and the pump as solutions of the three 3WRI system. The framework of our research is more general, in the sense that we deal with a system of three plane waves, we perturb every solution and then every solution interacts with the perturbations of the other two interacting waves. In other words, we are considering a system of three pumps interacting in resonance one with each other and every pump interacts with two side-bands.

In the literature, the system (3.5) has been written in different forms, obtained by redefining the variables q_j and the velocities c_j. This is because, from the computational point of view and depending on the applications, a form may be more convenient than others. For instance, let us consider the case in which one sign is different from the others. If one puts $q_1 = \bar{q}_1$, $q_2 = \bar{q}_2^*$ and $q_3 = \bar{q}_3$ and $s_1 = -p_1$, $s_2 = p_2$ and $s_3 = -p_3$, the system (3.5) can be written in a more general form by introducing a complex coupling constant K [112][56]

$$\begin{cases} \bar{q}_{1t} + c_1\bar{q}_{1x} = -p_1K^*\bar{q}_2\bar{q}_3^*\,, \\ \bar{q}_{2t} + c_2\bar{q}_{2x} = p_2K\bar{q}_1\bar{q}_3\,, \\ \bar{q}_{3t} + c_3\bar{q}_{3x} = -p_3K^*\bar{q}_1^*\bar{q}_2. \end{cases} \tag{3.8}$$

Although the equations (3.8) describe the interactions between three waves in a homogeneous medium [58, 111], they can be mapped into a system with a phase factor describing the interactions in a medium with weak inhomogeneity and an IST problem is formulated in order to understand the effect of inhomogeneities on the three waves interaction [112].

In this thesis we apply the spectral analysis method developed in [64] to plane waves only. On the other hand, several other researches were carried out on more complicated solutions of the 3WRI system. In fact, it is well known that the 3WRI model has solutions that are triplets of solitons travelling together with a common velocity, the so called *simultons*. Interesting research works were conducted on simultons in the last years [82, 113, 114, 115, 116]. Indeed, the system (3.12) has also been used in a covariant form [56] obtained transforming the fields $\bar{q}_j$ as $u_1(z,y) = K\sqrt{\frac{c_2}{c_1-c_2}}\,\bar{q}_1(x,t)$, $u_2(z,y) = K\sqrt{\frac{c_1}{c_2-c_1}}\,\bar{q}_2(x,t)$, $u_3(z,y) = K\sqrt{c_1c_2}\,\bar{q}_3(x,t)$ and with 'velocities' of the solitons $V_1 = \frac{1}{c_1-c_3}$, $V_2 = \frac{1}{c_2-c_3}$ satisfying the condition $0 < V_1 < V_2$. After that transformations, z and y are the temporal and the spatial variable, respectively. The equations so obtained have a simulton solution constituted by three dark solitons which are always unstable unless the 3WRI system is perturbed via a weak dispersion. It was observed that this weak dispersion reduces the MI [56]. Even if the perturbed system should not have solitons, the dispersion parameters are chosen such that only the shape of the soliton are slightly modified and at the same time the instability is reduced [56]. In the same work, the analysis and the classification of the stabilities according to the signs is carried out. The stability of a simulton composed by two bright and a dark solitons (BBD) was studied in the paper [114]. Let c_1, c_2 and c_3 be the velocities of the triad solutions of the 3WRI system and c be the velocity of the simulton. It was found that when c is brought below a critical value, that is

$$c_{uns} = \frac{2c_1c_2}{c_1 + c_2 - Q(c_1 - c_2)}\,, \tag{3.9}$$

the simulton becomes unstable. Q depends on the parameters involved on the expression of the simulton, and when $-1 < Q < 1$, we have $c_1 < c_{uns} < c_2$. Furthermore, an unstable simulton decays in a stable one emitting a pulse when c is brought above the value c_{uns} and the simulton becomes a 'boomeron' in the sense that its final velocity is different from the initial one. The stability was also analysed under collision between two stable simultons, and it was found they can pass through each other maintaining their shape if their velocities are different, and repulse or attract each other if their velocities are the same. A similar analysis was carried out on the interaction between a stable or an unstable simulton with a linear wave [115]. Bearing in mind the outcomes described above, an interesting future direction of research is the stability analysis of rational triads, whose analytical expressions were found by Darboux Dressing Transformation in [72, 83].

3.2 Lax Pair

As explained in Chapter 1, the main aim of this thesis is to individuate values of the physical parameters for which linear instability occurs. In general, we observe that a change of the ordering of the velocities is reflected into a change of the Lax pair associated to the system. This would be quite impractital in view of a complete classification of the instabilities (and of the stability spectra that we will introduce later in this work) with respect to the parameters. For this reason, in the following discussion, first we observe some symmetries in the 3WRI system, and then we use such symmetries to write a general expression for the Lax operators including all possible orderings of the velocities. This general expression allows us to compute all the necessary analytic tools and, only in the end, deduce what happens if we change the velocities ordering without further complicated computations.

3.2.1 Symmetries

The Lax operators associated with the system (3.5) [53, 58] make our computations hard to carry out because of the square roots in their expressions. In order to write the Lax operators in the easy form, one can rescale the fields q_j as follows [55]

$$q_j = \sqrt{\frac{\Delta_1\Delta_2\Delta_3}{\Delta_j}}\, s_j u_j, \quad j = 1, 2, 3, \tag{3.10}$$

where $s_j^2 = 1$ and

$$\Delta_1 = c_2 - c_3, \quad \Delta_2 = c_1 - c_3, \quad \Delta_3 = c_1 - c_2, \tag{3.11}$$

and the system (3.5) becomes

$$\begin{cases} u_{1t} + c_1 u_{1x} = s_2 s_3 |\Delta_1| u_2^* u_3^*\,, \\ u_{2t} + c_2 u_{2x} = s_1 s_3 |\Delta_2| u_1^* u_3^*\,, \\ u_{3t} + c_3 u_{3x} = s_1 s_2 |\Delta_3| u_1^* u_2^*\,. \end{cases} \tag{3.12}$$

The symbol $|\cdot|$ denotes the absolute value of the differences of the velocities which is defined as

$$|c_i - c_j| = \begin{cases} c_i - c_j & \text{if} \quad c_i > c_j\,, \\ c_j - c_i & \text{if} \quad c_j > c_i\,, \end{cases} \qquad i,\, j = 1, 2, 3. \tag{3.13}$$

Thus, once fixed, say, the velocity c_3, the system (3.12) takes two different expressions corresponding to the orderings $c_1 > c_2$ and $c_2 > c_1$. The same argument holds when c_1, or c_2, is fixed. Therefore, the system (3.12) encloses six systems associated to every velocities ordering [6] and they correspond to six Lax Pairs. We can not write all the six Lax pairs in one, because the differences of the velocities appear only after computing the compatibility condition for the Lax operators. Every Lax operator contains terms proportional to the single velocities c_j, but not terms proportional to their differences, that, instead, appear after the computation of the commutator between the two operators. Precisely, the six 3WRI systems are:

$C_1)$ $c_1 > c_2 > c_3$

$$\begin{cases} u_{1t} + c_1 u_{1x} = s_2 s_3 (c_2 - c_3) u_2^* u_3^* \,, \\ u_{2t} + c_2 u_{2x} = s_1 s_3 (c_1 - c_3) u_1^* u_3^* \,, \\ u_{3t} + c_3 u_{3x} = s_1 s_2 (c_1 - c_2) u_1^* u_2^* \,, \end{cases} \tag{3.14}$$

$C_2)$ $c_1 > c_3 > c_2$

$$\begin{cases} u_{1t} + c_1 u_{1x} = -s_2 s_3 (c_2 - c_3) u_2^* u_3^* \,, \\ u_{2t} + c_2 u_{2x} = s_1 s_3 (c_1 - c_3) u_1^* u_3^* \,, \\ u_{3t} + c_3 u_{3x} = s_1 s_2 (c_1 - c_2) u_1^* u_2^* \,, \end{cases} \tag{3.15}$$

$C_3)$ $c_3 > c_1 > c_2$

$$\begin{cases} u_{1t} + c_1 u_{1x} = -s_2 s_3 (c_2 - c_3) u_2^* u_3^* \,, \\ u_{2t} + c_2 u_{2x} = -s_1 s_3 (c_1 - c_3) u_1^* u_3^* \,, \\ u_{3t} + c_3 u_{3x} = s_1 s_2 (c_1 - c_2) u_1^* u_2^* \,, \end{cases} \tag{3.16}$$

$C_4)$ $c_3 > c_2 > c_1$

$$\begin{cases} u_{1t} + c_1 u_{1x} = -s_2 s_3 (c_2 - c_3) u_2^* u_3^* \,, \\ u_{2t} + c_2 u_{2x} = -s_1 s_3 (c_1 - c_3) u_1^* u_3^* \,, \\ u_{3t} + c_3 u_{3x} = -s_1 s_2 (c_1 - c_2) u_1^* u_2^* \,, \end{cases} \tag{3.17}$$

[6] In this discussion, we are not considering the choices of the signs.

$C_5)$ $c_2 > c_3 > c_1$

$$\begin{cases} u_{1t} + c_1 u_{1x} = s_2 s_3 (c_2 - c_3) u_2^* u_3^* \,, \\ u_{2t} + c_2 u_{2x} = -s_1 s_3 (c_1 - c_3) u_1^* u_3^* \,, \\ u_{3t} + c_3 u_{3x} = -s_1 s_2 (c_1 - c_2) u_1^* u_2^* \,, \end{cases} \tag{3.18}$$

$C_6)$ $c_2 > c_1 > c_3$

$$\begin{cases} u_{1t} + c_1 u_{1x} = s_2 s_3 (c_2 - c_3) u_2^* u_3^* \,, \\ u_{2t} + c_2 u_{2x} = s_1 s_3 (c_1 - c_3) u_1^* u_3^* \,, \\ u_{3t} + c_3 u_{3x} = -s_1 s_2 (c_1 - c_2) u_1^* u_2^* \,. \end{cases} \tag{3.19}$$

Since our aim is to classify the spectra of the Lax operators with regard to the parameters involved in the 3WRI model, we should examine every Lax Pair (3.14)-(3.19) to get a complete classification. Nevertheless, our analysis can be further simplified because in the system of equations (3.12) only the product of signs appear. This implies there are only four possible products of signs, each one corresponding to two different combinations of the signs [7]:

$S_1)$ for $s_1 = s_2 = -s_3$

$$\begin{cases} s_2 s_3 = -1, \\ s_1 s_3 = -1, \\ s_1 s_2 = 1, \end{cases} \tag{3.20}$$

$S_2)$ for $s_1 = s_3 = -s_2$

$$\begin{cases} s_2 s_3 = -1, \\ s_1 s_3 = 1, \\ s_1 s_2 = -1, \end{cases} \tag{3.21}$$

[7] For example, the case $s_1 = s_2 = -s_3$ encloses two combinations of signs that are $s_1 = s_2 = -1$ and $s_3 = 1$ or $s_1 = s_2 = 1$ and $s_3 = -1$.

$S_3)$ for $s_2 = s_3 = -s_1$

$$\begin{cases} s_2 s_3 = 1, \\ s_1 s_3 = -1, \\ s_1 s_2 = -1, \end{cases} \tag{3.22}$$

$S_4)$ for $s_1 = s_2 = s_3$

$$\begin{cases} s_2 s_3 = 1, \\ s_1 s_3 = 1, \\ s_1 s_2 = 1. \end{cases} \tag{3.23}$$

At this point, it is worth reminding that we are including also the "explosive case" (i.e. the case (3.23)). In fact, as already mentioned, we do not have reason to exclude this case. A priori, we cannot know if the system with the combination of signs in (3.23) is actually explosive for the plane wave solutions because we can not predict the possibility of explosive behaviour via the Manley-Rowe relations, for the plane wave solutions are not square-integrable.

By combining the systems (3.14)-(3.19) with every possible choice of signs (3.20)-(3.23), we get in total twenty-four systems of equations, everyone denoted by the letter C_j, associated to a Lax pair, and by the letter S_j, associated to the choice of signs. Therefore, for instance, the system of equations $C_1 S_1$ is the one corresponding to the Lax pair C_1 with a choice of signs S_1. However, only twelve cases are relevant because the others can be obtained by the former via symmetry, as will be shown below.

Proposition 3.2.1. *For every fixed choice of signs, if the velocities ordering is reversed, the resulting system is symmetric to the former one by relabelling of the indices, that is equivalent to exchange the bigger velocity with the smaller velocity.*

Proof. Let us consider, say, the velocities orderings C_1, (3.14), and C_4, (3.17), and let us suppose that the signs $s_1 s_2$, $s_1 s_3$ and $s_2 s_3$ are fixed and are the same for both systems. In the system (3.14) the differences of the velocities are all positive, while in the system (3.17) they are all negative. However, there is a minus in front of the negative differences in (3.17), such that the sign in front of the interaction term is the same of the system

(3.14). In particular, the systems (3.14) and (3.17) are equivalent, in the sense that one can be obtained from the other by a relabelling. Indeed, after the substitutions $1 \to 3$, $3 \to 1$ and $2 \to 2$ in the system (3.17) we get the system (3.14), and vice versa. Thus, if we consider first the system (3.17) in which the solution u_1 has the smaller velocity and u_3 has the bigger one, after relabelling, u_1 has the bigger velocity and u_3 has the smaller one. This reasoning can be extended to all orderings of velocities. □

As a consequence of the Proposition 3.2.1, we may consider only three orderings instead of six. In particular, the equivalent orderings are: C_1 with C_4, C_2 with C_5 and C_3 with C_6. We note that once the signs are fixed, for example after choosing the signs S_4, the signs of the interactions are positive in all the systems (3.14)-(3.19), and this is a consequence of the presence of the modulus $|\Delta_j|$ in the system (3.5). Since the choice $s_1 s_2 = s_1 s_3 = s_2 s_3 = -1$ is not allowed, it looks like the negative interactions are not allowed. Nevertheless, there is another symmetry in the model that makes the interaction of any sign possible.

Proposition 3.2.2. *For any choice of signs and any velocities ordering, the 3WRI system admits interaction with both positive and negative signs.*

Proof. Let us consider the system (3.14) with fixed signs. If we change every solution $u_j \to -u_j$ and then we define $-u_j = \bar{u}_j$, then we get that the solutions $\bar{u}_j$ satisfy the same system of u_j with the same interaction, namely, $\bar{u}_j$ are also solutions of the model. On the other hand, if we come back to u_j, we get a 3WRI system for u_j, but with the sign of the interaction opposite to the former, i.e. negative. □

Proposition 3.2.1 and Proposition 3.2.2 suggest that we can change the interaction sign by changing simultaneously the signs of all the amplitudes of the solutions u_j. Below, we shall show that, once the ordering of the velocities is fixed, the systems for $\bar{u}_j$ and for u_j describe the same processes.

3.2.2 A General Expression for the 3WRI System

In order to fulfil the stability analysis, we need to deal with six Lax pairs (or with three Lax pairs if we want to rediscover the other three orderings by symmetry) and, once fixed the velocities ordering, we will vary the signs to reproduce the four cases S_1, S_2, S_3 and S_4. However, our analysis can be simplified further because the cases analysed in the previous section can be rediscovered if the 3WRI model is interpreted and written in a particular fashion (as explained below).

Let us consider the 3WRI model

$$\begin{cases} u_{1t} + c_1 u_{1x} = s_1(c_2 - c_3)u_2^* u_3^*\,, \\ u_{2t} + c_2 u_{2x} = s_2(c_1 - c_3)u_1^* u_3^*\,, \\ u_{3t} + c_3 u_{3x} = s_3(c_1 - c_2)u_1^* u_2^*\,, \end{cases} \tag{3.24}$$

where s_j are signs such that $s_j^2 = 1$, $j = 1, 2, 3$, and the velocities and their orderings can be whatever [8]. Indeed, in some of the systems (3.14)-(3.19), the differences $c_j - c_{j+1}$ appear with a minus in front of them. In the system (3.24), the sign minus is included in the definition of s_j and, for this reason, there are eight possible choices of signs:

$\mathcal{S}_1^+)$ $s_1 = s_2 = 1$, $s_3 = -1$;

$\mathcal{S}_1^-)$ $s_1 = s_2 = -1$, $s_3 = 1$;

$\mathcal{S}_2^+)$ $s_1 = s_3 = 1$, $s_2 = -1$;

$\mathcal{S}_2^-)$ $s_1 = s_3 = -1$, $s_2 = 1$;

$\mathcal{S}_3^+)$ $s_2 = s_3 = 1$, $s_1 = -1$;

$\mathcal{S}_3^-)$ $s_2 = s_3 = -1$, $s_1 = 1$;

$\mathcal{S}_4^+)$ $s_1 = s_2 = s_3 = -1$;

$\mathcal{S}_4^-)$ $s_1 = s_2 = s_3 = 1$.

[8] We are taking into account also the combinations of signs not included in the classification of the choices S_j.

The combination $\mathcal{S}_1^+$ is obtained from the combination $\mathcal{S}_1^-$ by a symmetry. To prove that, let us consider the 3WRI system for the solution $u = u(x,t)$

$$\begin{cases} u_{1t} + c_1 u_{1x} = s_1(c_2 - c_3)u_2^* u_3^*, \\ u_{2t} + c_2 u_{2x} = s_2(c_1 - c_3)u_1^* u_3^*, \\ u_{3t} + c_3 u_{3x} = s_3(c_1 - c_2)u_1^* u_2^*. \end{cases} \tag{3.25}$$

Proposition 3.2.3. *In the system (3.25), the interaction term is left invariant by changing all the signs s_j, (see also [57]).*

Proof. The system (3.25) admits solutions like $\bar{u}_j = e^{i\theta_j} u_j$, where θ_j are arbitrary phases. We also write $\bar{s}_j = |\bar{s}_j| e^{i \arg(\bar{s}_j)}$, with $|\bar{s}_j| = 1$ and

$$\arg(\bar{s}_j) = \begin{cases} 0 & \text{if} \quad \bar{s}_j = 1, \\ \pi & \text{if} \quad \bar{s}_j = -1, \end{cases} \qquad j = 1,2,3, \tag{3.26}$$

the signs $\bar{s}_j$ are mapped into the signs s_j via the following transformation

$$\bar{s}_j = e^{i(\arg(s_j) + \phi_j)}, \quad j = 1,2,3 \tag{3.27}$$

and when we come back to the system for u_j, we have

$$\begin{cases} u_{1t} + c_1 u_{1x} = (c_2 - c_3)u_2^* u_3^* e^{-i(\theta_1+\theta_2+\theta_3 - \arg(s_1) - \phi_1)} \\ u_{2t} + c_2 u_{2x} = (c_1 - c_3)u_1^* u_3^* e^{-i(\theta_1+\theta_2+\theta_3 - \arg(s_2) - \phi_2)} \\ u_{3t} + c_3 u_{3x} = (c_1 - c_2)u_1^* u_2^* e^{-i(\theta_1+\theta_2+\theta_3 - \arg(s_3) - \phi_3)}. \end{cases} \tag{3.28}$$

The system (3.28) is equivalent to the system

$$\begin{cases} \bar{u}_{1t} + c_1 \bar{u}_{1x} = (c_2 - c_3)\bar{u}_2^* \bar{u}_3^* e^{i \arg(\bar{s}_1)} \\ \bar{u}_{2t} + c_2 \bar{u}_{2x} = (c_1 - c_3)\bar{u}_1^* \bar{u}_3^* e^{i \arg(\bar{s}_2)} \\ \bar{u}_{3t} + c_3 \bar{u}_{3x} = (c_1 - c_2)\bar{u}_1^* \bar{u}_2^* e^{i \arg(\bar{s}_3)}, \end{cases} \tag{3.29}$$

only if $\phi_1 = \phi_2 = \phi_3 \equiv \phi$ and $\phi = \theta_1 + \theta_2 + \theta_3$. Because s_j and $\bar{s}_j$ are just signs, ϕ has value π or 0. Moreover, looking at the system for the solution $\bar{u}_j$, one has also $e^{-i(\theta_1+\theta_2+\theta_3 - \arg(\bar{s}_j))} = e^{-i(\theta_1+\theta_2+\theta_3 - \arg(s_j) - \phi)}$, with $j = 1,2,3$, and so $e^{i(\arg(\bar{s}_j))} = e^{i(\arg(s_j)+\phi)}$, such that $\arg(\bar{s}_j) = \arg(s_j) + \phi$. Let us suppose $\bar{s}_1 = 1$, $\bar{s}_2 = -1$ and $\bar{s}_3 = -1$, there are two possibilities: $\phi = 0$, and $\arg(s_1) = 0$, $\arg(s_2) = \arg(s_3) = \pi$, or $\phi = \pi$, and

	Velocities ordering					
signs s_j	C_1	C_2	C_3	C_4	C_5	C_6
$\mathcal{S}_1^+$	$-S_1C_1$	S_2C_2	$-S_4C_3$	S_1C_4	$-S_2C_5$	S_4C_6
$\mathcal{S}_1^-$	S_1C_1	$-S_2C_2$	S_4C_3	$-S_1C_4$	S_2C_5	$-S_4C_6$
$\mathcal{S}_2^+$	$-S_2C_1$	S_1C_2	$-S_3C_3$	S_2C_4	$-S_1C_5$	S_3C_6
$\mathcal{S}_2^-$	S_2C_1	$-S_1C_2$	S_3C_3	$-S_2C_4$	S_1C_5	$-S_3C_6$
$\mathcal{S}_3^+$	$-S_3C_1$	S_4C_2	$-S_2C_3$	S_3C_4	$-S_4C_5$	S_2C_6
$\mathcal{S}_3^-$	S_3C_1	$-S_4C_2$	S_2C_3	$-S_3C_4$	S_4C_5	$-S_2C_6$
$\mathcal{S}_4^+$	$-S_4C_1$	S_3C_2	$-S_1C_3$	S_4C_4	$-S_3C_5$	S_1C_6
$\mathcal{S}_4^-$	S_4C_1	$-S_3C_2$	S_1C_3	$-S_4C_4$	S_3C_5	$-S_1C_6$

Table 3.1: 3WRI cases.

$\arg(s_1) = \pi$, $\arg(s_2) = \arg(s_3) = 0$.

This means that if we want to leave unchanged the interaction, we need to change both the signs s_j and the signs of all the amplitudes, i.e. $\bar{u}_j = -u_j$. In other words, changing all the signs s_j is equivalent to changing all the signs in front of the amplitudes of the solutions u_j. □

As a consequence of the Proposition 3.2.3, we take into account only four possible choices of signs (instead of eight) that, combined with the six possible velocities orderings, give twenty-four systems in total, although we expect twelve relevant cases only. This means there is another symmetry, in fact the Proposition 3.2.1 holds for the system (3.24) as well. We can associate every case of the 3WRI model (3.12) to every case of the model described by the system (3.24), as shown in the Table 3.1. Let us focus on the choices $\mathcal{S}_1^+$ and $\mathcal{S}_1^-$. Once the signs $\mathcal{S}_1^+$ are fixed, the system 3WRI (3.24) gives us the right cases S_2C_2, S_1C_4 and S_4C_6 for the solution u_j, while the other remaining cases are reversed, $-S_1C_1$, $-S_4C_3$, $-S_2C_5$ and the sign minus denotes this reversion. Nevertheless, these cases are the right ones for $\bar{u}_j = -u_j$, and can be also obtained with the right signs by changing the signs $s_j \to -s_j$. Moreover, by the Proposition 3.2.1, the case S_1C_1 is equivalent to the case S_1C_4. The same argument holds for the other orderings.

Finally, we observe that with the model (3.12) one would have to deal with three Lax pairs and then, to obtain the other orderings, we have to swap the bigger velocity with the smaller

one. As we show in the following, with (3.24) we deal with only one Lax pair and, if we wish, we can cover all cases by a change of sign or by changing the values of the velocities without changing Lax pair.

3.3 Plane Wave Solutions

The system (3.24) admits as solutions the plane waves

$$u_1 = a_1 e^{i(\eta_1 t - \nu_1 x)}, \qquad u_2 = a_2 e^{i(\eta_2 t - \nu_2 x)}, \qquad u_3 = a_3 e^{i(\eta_3 t - \nu_3 x)}, \tag{3.30}$$

where a_j are the amplitudes, η_j are the frequencies and ν_j are the wave numbers.
By choosing the reference frame moving with the wave u_3, such that the velocity $c_3 = 0$ and by substituting the solution u_3 in the last equation of the system (3.24), we get the *resonant conditions*

$$\eta_1 + \eta_2 + \eta_3 = 0, \qquad \nu_1 + \nu_2 + \nu_3 = 0. \tag{3.31}$$

The amplitude a_3 takes the expression

$$a_3 = i s_3 a_1 a_2 \frac{c_1 - c_2}{\eta_1 + \eta_2}, \qquad a_1, a_2 \in \mathbb{R}, \tag{3.32}$$

thus, the solution u_3 is

$$u_3 = i s_3 a_1 a_2 \frac{c_1 - c_2}{\eta_1 + \eta_2} e^{-i((\eta_1+\eta_2)t - (\nu_1+\nu_2)x)}. \tag{3.33}$$

Moreover, by setting the expression (3.33) and the other two plane waves u_1 and u_2 in (3.30) into the first two equations of the system (3.24), the nonlinear *dispersion relations* are obtained

$$\begin{aligned} \nu_1 &= \frac{\eta_1}{c_1} + s_1 s_3 a_2^2 \frac{c_2(c_1 - c_2)}{c_1(\eta_1 + \eta_2)}, \\ \nu_2 &= \frac{\eta_2}{c_2} + s_2 s_3 a_1^2 \frac{c_1(c_1 - c_2)}{c_2(\eta_1 + \eta_2)}. \end{aligned} \tag{3.34}$$

3.3.1 Galilean Invariance

The system (3.24) is invariant under the substitutions

$$u_j(x,t) = \bar{u}_j(\bar{x}, \bar{t}), \tag{3.35}$$

where space x and time t transform as the Galilei transformations

$$\begin{cases} x = \bar{x} + v\bar{t}\,, \\ t = \bar{t}\,, \end{cases} \tag{3.36}$$

and the characteristic, linear velocities are

$$c_j = \bar{c}_j + v, \quad j = 1, 2, 3. \tag{3.37}$$

Furthermore, by replacing the plane wave solutions in (3.35), we get [9]

$$\eta_j = \bar{\eta}_j + v\bar{\nu}_j, \qquad \bar{\nu_j} = \nu_j, \qquad \bar{a}_j = a_j, \qquad \forall j = 1, 2, 3. \tag{3.38}$$

By the Galilean transformations for the frequencies and for the wave numbers (3.38), without loss of generality, we choose, for example, $\eta_1 = q$ and $\eta_2 = \pm q$. However, due to the resonant conditions (3.31), we can put $\eta_1 = \eta_2 = q$ only, otherwise three wave resonance does not occur.

From now on, we shall choose the reference frame in which $c_3 = 0$, and we shall fix $\eta_1 = \eta_2 = q$ and, as a consequence, $\eta_3 = -2q$. In this way, the plane waves (3.30) become

$$u_1 = a_1 e^{i(qt - \nu_1 x)}, \quad u_2 = a_2 e^{i(qt - \nu_2 x)}, \quad u_3 = i s_3 a_1 a_2 \frac{c_1 - c_2}{2q} e^{-i(2qt - (\nu_1 + \nu_2)x)}, \tag{3.39}$$

where the frequencies are

$$\begin{aligned} \nu_1 &= \frac{q}{c_1} + s_1 s_3 a_2^2 \frac{c_2(c_1 - c_2)}{2qc_1}, \\ \nu_2 &= \frac{q}{c_2} + s_2 s_3 a_1^2 \frac{c_1(c_1 - c_2)}{2qc_2}. \end{aligned} \tag{3.40}$$

[9] Indeed,

$$u_j(x,t) = \bar{u}_j(\bar{x}, \bar{t}),$$

entails

$$a_j e^{i(\eta_j t - \nu_j x)} = \bar{a}_j e^{i(\bar{\eta}_j \bar{t} - \bar{\nu}_j \bar{x})},$$

and, by substituting (3.36),

$$a_j e^{i(\eta_j t - \nu_j x)} = a_j e^{i((\eta_j - v\nu_j)\bar{t} - \nu_j \bar{x})},$$

from which the formulas (3.38).

3.4 Lax Pair Formulation

The phenomenon of the linear stability, is analysed using the feature of the 3WRI model to be Lax-integrable. Indeed, a squared combination of fundamental solutions of the Lax pair is presented like a combination of the 'eigenmode-solutions' of the linearised equation [64]. In this respect, the differences of the eigenvalues of the Lax operators are necessary to write a solution of the linearised equation. In this section we give the explicit expressions of the Lax operators involved in the Lax formulation of the problem. We show how a similarity transformation allows us to break free the Lax operators from the dependence of space and time variables, such that the Lax equation is reduced to the Liouville equations, whose integration is trivial. A further gauge transformation simplifies our computations and makes our formula easier to handle. Finally, we find out that every Lax operator, obtained after such transformations, is written as a polynomial expression in the other Lax operator. Therefore, we obtain the relation between the differences of the eigenvalues of the Lax operators, and the solution of the linearised equation is provided in detail.
In the following, we apply the theory for multi-component systems provided in Chapter 2.

3.4.1 Linearised Equation

In this section we present the Lax pair and the linearised equation, following the research work [64].
Since the 3WRI is Lax-integrable, we associate to the system (3.24) the Lax operators $\tilde{X} \equiv \tilde{X}(x,t,\kappa)$ and $\tilde{T} \equiv \tilde{T}(x,t,\kappa)$

$$\tilde{X} = -i\kappa\tilde{C} + U, \qquad \tilde{T} = i\kappa\tilde{D} + V, \tag{3.41}$$

where x and t are the space and time variables, respectively, κ is the spectral parameter, and $\tilde{C}$ and $\tilde{D}$ are 3×3 matrices depending only on the linear velocities c_j

$$\tilde{C} = \begin{pmatrix} -\frac{1}{3}(c_1+c_2) & 0 & 0 \\ 0 & \frac{1}{3}(2c_2-c_1) & 0 \\ 0 & 0 & \frac{1}{3}(2c_1-c_2) \end{pmatrix}, \tag{3.42}$$

$$\tilde{D} = \frac{c_1 c_2}{3} \begin{pmatrix} -2 & 0 & 0 \\ 0 & 1 & 0 \\ 0 & 0 & 1 \end{pmatrix}. \tag{3.43}$$

The matrices $U = U(x,t)$ and $V = V(x,t)$ involve the solutions [10] u_j of the system (3.24), the signs s_j and the velocities c_j, and they are defined as follows

$$U = \begin{pmatrix} 0 & s_1 u_1 & -s_1 s_2 s_3 u_2^* \\ s_1 s_2 s_3 u_1^* & 0 & s_3 u_3 \\ s_2 u_2 & s_1 s_2 s_3 u_3^* & 0 \end{pmatrix}, \tag{3.44}$$

$$V = \begin{pmatrix} 0 & -s_1 c_1 u_1 & s_1 s_2 s_3 c_2 u_2^* \\ -s_1 s_2 s_3 c_1 u_1^* & 0 & 0 \\ -s_2 c_2 u_2 & 0 & 0 \end{pmatrix}. \tag{3.45}$$

Let us introduce the Lax pair

$$\tilde{\psi}_x = \tilde{X}\tilde{\psi}, \quad \tilde{\psi}_t = \tilde{T}\tilde{\psi}, \tag{3.46}$$

whose solution $\tilde{\psi} = \tilde{\psi}(x,t,\kappa)$ is a 3×3 matrix which satisfies the compatibility condition

$$\tilde{\psi}_{xt} = \tilde{\psi}_{tx}, \tag{3.47}$$

that is equivalent to the equation for the Lax operators

$$\tilde{X}_t - \tilde{T}_x + [\tilde{X}, \tilde{T}] = 0, \quad \forall \tilde{\psi}, \tag{3.48}$$

or, equivalently,

$$U_t - V_x + [U, V] = 0, \quad \forall \tilde{\psi}. \tag{3.49}$$

Here and thereafter the brackets $[\cdot,\cdot]$ denote the commutator between the operators.

Proposition 3.4.1. *The following two operators*

$$X = -i\kappa C + U, \qquad T = i\kappa D + V, \tag{3.50}$$

where

$$C = \tilde{C} + \frac{1}{3}(c_1 + c_2)\mathbf{I}, \quad D = \tilde{D} + \frac{2}{3}c_1 c_2 \mathbf{I}, \tag{3.51}$$

[10] We remind the reader that the asterisk stands for complex conjugation.

and $\mathbf{I}$ *is the identity matrix* 3×3*, constitute a Lax pair*

$$\psi_x = X\psi, \quad \psi_t = T\psi, \tag{3.52}$$

whose solution transforms as

$$\psi = \tilde{\psi} e^{i\frac{2}{3}\kappa c_1 c_2 t - i\frac{\kappa}{3}(c_1+c_2)x}. \tag{3.53}$$

Proof. Indeed the matrices $\tilde{C}$ and $\tilde{D}$, involved in (3.41), are

$$\tilde{C} = -\frac{1}{3}(c_1 + c_2)\mathbf{I} + (c_1 + c_2)(\Sigma_+ + \Sigma_-), \tag{3.54}$$

$$\tilde{D} = -\frac{2}{3}c_1 c_2 \mathbf{I} + c_1 c_2(\Sigma_+ + \Sigma_-), \tag{3.55}$$

where

$$\Sigma_+ = \begin{pmatrix} 0 & 0 & 0 \\ 0 & 1 & 0 \\ 0 & 0 & 0 \end{pmatrix}, \quad \Sigma_- = \begin{pmatrix} 0 & 0 & 0 \\ 0 & 0 & 0 \\ 0 & 0 & 1 \end{pmatrix}. \tag{3.56}$$

This means that the Lax operators X and T have a diagonal part proportional to Σ_+ and Σ_-, and with entries X_{11} and T_{11} which are null elements. Looking at the compatibility conditions (3.48) and (3.49), we see that the terms $-i\frac{2}{3}\kappa c_1 c_2 \mathbf{I}$ and $-\frac{i}{3}\kappa(c_1 + c_2)\mathbf{I}$ do not affect the computation of the 3WRI equations and then the stability analysis. Moreover, by substituting $\tilde{X} = X + i\frac{\kappa}{3}(c_1 + c_2)$ and $\tilde{T} = T - i\frac{2}{3}\kappa c_1 c_2$ in the Lax pair (3.41), we have the equations

$$\tilde{\psi}_x - i\frac{\kappa}{3}(c_1 + c_2)\tilde{\psi} = X\tilde{\psi}, \tag{3.57a}$$

$$\tilde{\psi}_t + i\frac{2}{3}\kappa c_1 c_2 \tilde{\psi} = T\tilde{\psi}, \tag{3.57b}$$

and, by defining $\psi = \tilde{\psi} e^{i\frac{2}{3}\kappa c_1 c_2 t - i\frac{\kappa}{3}(c_1+c_2)x}$, the equations (3.57) become the Lax pair (3.52). □

If we perturb the solutions $u_j \to u_j + \delta u_j$, we have, as a consequence, that also the Lax operators become perturbed $X \to X + \delta X$, $T \to T + \delta T$. If we set these perturbed

operators in the compatibility condition (3.48), at the first order in the perturbation, we get the equation for the perturbations δX and δT [64]

$$\delta X_t - \delta T_x + [\delta X, T] + [X, \delta T] = 0, \tag{3.58}$$

named *linearised equation*. In order to find a solution of the linearised equation related to the solution of the Lax pair (3.46), we define the squared eigenfunction $\Psi = \Psi(x, t, \kappa)$ by the following similarity transformation

$$\Psi = \psi M \psi^{-1}, \tag{3.59}$$

where $M = M(\kappa)$, is a constant matrix, independent on x and t and ψ^{-1} is the inverse of the matrix $\psi = \psi(x, t, \kappa)$. After that, two propositions, stated in the paper [64], are given below.

Proposition 3.4.2. *If the pair E, J solve the linearised equation (3.58), then also the pair*

$$F = [E, \Psi], \quad H = [J, \Psi], \tag{3.60}$$

is a solution of the linearised equation (3.58), namely

$$F_t - H_x + [F, T] + [X, H] = 0. \tag{3.61}$$

Proposition 3.4.3. *The following expressions,*

$$F = \left[\frac{\partial X}{\partial \kappa}, \Psi\right], \quad H = \left[\frac{\partial T}{\partial \kappa}, \Psi\right], \tag{3.62}$$

provide solutions of the linearised equation (3.58).

One notes that, to obtain the solution F, one needs to know the explicit expression of the squared eigenfunction (3.59) related to the solution of the Lax pair. This will be the aim of the next section.

3.4.2 Similarity Transformation of the Lax Pair

Once the Lax operators are provided, we see that only the matrices U and V enclose the solutions u_j and, so, the dependence on the variables x and t. Below, we introduce a

similarity transformation by which the Lax pair becomes a pair of Liouville equations simple to integrate. In this way, one can obtained the squared eigenfunctions.
Let $G = G(x,t,\kappa)$ be a matrix such that

$$U = GU_0G^{-1}, \qquad V = GV_0G^{-1}, \tag{3.63}$$

with G^{-1} the inverse of $G = G(x,t,\kappa)$ and

$$U_0 = \begin{pmatrix} 0 & s_1a_1 & -s_1s_2s_3a_2 \\ s_1s_2s_3a_1 & 0 & s_3a_3 \\ s_2a_2 & s_1s_2s_3a_3^* & 0 \end{pmatrix}, \quad V_0 = \begin{pmatrix} 0 & -s_1c_1a_1 & s_1s_2s_3c_2a_2 \\ -s_1s_2s_3c_1a_1 & 0 & 0 \\ -s_2c_2a_2 & 0 & 0 \end{pmatrix}, \tag{3.64}$$

so that the Lax operators are independent of x and t.
More in details, the explicit expression of the matrix G is (Appendix D)

$$G = e^{-\frac{i}{2}(\nu_1-\nu_2)x\mathbf{I}}e^{-i(qt-\nu_1x)\Sigma_+}e^{i(qt-\nu_2x)\Sigma_-}, \tag{3.65}$$

and $[\Sigma_+,\Sigma_-] = 0$. In addition, this transformation induces the similarity transformation $\psi = G\phi$ on the solution of the Lax problem [11], and, so, on its squared eigenfunctions (see definition in [64])

$$\Psi = G\Phi G^{-1}, \tag{3.66}$$

[11] The operator X is

$$X = G(-i\kappa C + U_0)G^{-1};$$

this, substituted in $\psi_x = X\psi$, gives

$$\psi_x = G(-i\kappa C + U_0)G^{-1}\psi,$$

and, by multiplying to the left by G^{-1},

$$G^{-1}\psi_x = (-i\kappa C + U_0)G^{-1}\psi.$$

Since $G^{-1}\psi_x = (G^{-1}\psi)_x - (G^{-1})_x\psi$ and $(G^{-1}G)_x = (G^{-1})_xG + G^{-1}G_x = 0$, we obtain

$$(G^{-1}\psi)_x = (-i\kappa C + U_0 - G^{-1}G_x)(G^{-1}\psi);$$

this, after defining $\phi = G^{-1}\psi$ and $iW_0 = i\kappa C + U_0 - G^{-1}G_x$, becomes

$$\phi_x = iW_0\phi.$$

and on the Lax operators (appendix E)

$$iW_0 = G^{-1}XG - G^{-1}G_x, \qquad -iZ_0 = G^{-1}TG - G^{-1}G_t. \tag{3.67}$$

Therefore, the Lax pair becomes

$$\Phi_x = i[W_0, \Phi], \qquad \Phi_t = -i[Z_0, \Phi], \tag{3.68}$$

whose solution is

$$\Phi = e^{i(W_0 x - Z_0 t)}\Phi(0,0)e^{-i(W_0 x - Z_0 t)}, \tag{3.69}$$

with $\Phi(0,0)$ initial condition. Explicitly, we have

$$W_0 = \begin{pmatrix} \frac{\nu_1-\nu_2}{2} & -is_1a_1 & is_1s_2s_3a_2 \\ -is_1s_2s_3a_1 & -\kappa c_2 - \frac{\nu_1+\nu_2}{2} & -is_3a_3 \\ -is_2a_2 & -is_1s_2s_3a_3^* & -\kappa c_1 + \frac{\nu_1+\nu_2}{2} \end{pmatrix}, \tag{3.70a}$$

$$Z_0 = \begin{pmatrix} 0 & -is_1c_1a_1 & is_1s_2s_3c_2a_2 \\ -is_1s_2s_3c_1a_1 & -\kappa c_1c_2 - q & 0 \\ -is_2c_2a_2 & 0 & -\kappa c_1c_2 + q \end{pmatrix}, \tag{3.70b}$$

with wave-numbers ν_1 and ν_2 given by (3.40) and $[W_0, Z_0] = 0$.

3.4.3 Gauge Transformation

In order to carry out our stability analysis, we need to know the eigenvalues of the matrices W_0 and Z_0, and so it is necessary to compute the characteristic polynomials of such matrices. However, the expressions (3.70a) and (3.70b) make the computation of their characteristic polynomials difficult. For this reason, we introduce a gauge transformation simplifyng the form of the polynomials that we will introduce in the next sections.
The matrices G, W_0 and Z_0 in (3.63) and (3.70) can be generalised as follows (see formulas (D.7) in the Appendix D),

$$G = \begin{pmatrix} e^{i(mqt - l\nu_1 x - n\nu_2 x)} & 0 & 0 \\ 0 & e^{i((m-1)qt - (l-1)\nu_1 x - n\nu_2 x)} & 0 \\ 0 & 0 & e^{i((m+1)qt - l\nu_1 x - (n+1)\nu_2 x)} \end{pmatrix}, \tag{3.71}$$

or,

$$G = e^{i(mqt-(l\nu_1+n\nu_2)x)\mathbf{I}} e^{-i(qt-\nu_1 x)\Sigma_+} e^{i(qt-\nu_2 x)\Sigma_-}, \tag{3.72}$$

$$W_0(\kappa; l, n) = \begin{pmatrix} \nu_1 l + \nu_2 n & -is_1 a_1 & is_1 s_2 s_3 a_2 \\ -is_1 s_2 s_3 a_1 & -\kappa c_2 + \nu_1(l-1) + \nu_2 n & -is_3 a_3 \\ -is_2 a_2 & -is_1 s_2 s_3 a_3^* & -\kappa c_1 + \nu_1 l + \nu_2(n+1) \end{pmatrix}, \tag{3.73}$$

$$Z_0(\kappa; m) = \begin{pmatrix} mq & -is_1 c_1 a_1 & is_1 s_2 s_3 c_2 a_2 \\ -is_1 s_2 s_3 c_1 a_1 & -\kappa c_1 c_2 + q(m-1) & 0 \\ -is_2 c_2 a_2 & 0 & -\kappa c_1 c_2 + q(m+1) \end{pmatrix}, \tag{3.74}$$

where l, m and n are rational numbers.

They reduce to (3.65), (3.70a) and (3.70b) by setting $m = 0$, $l = \frac{1}{2}$ and $n = -\frac{1}{2}$.

Let us define the gauge transformation

$$\bar{G} = Ge^{-i(mqt-(l\nu_1+n\nu_2)x)\mathbf{I}}, \tag{3.75}$$

such that,

$$\bar{\psi} = \bar{G}\bar{\phi} = G\phi = \psi, \tag{3.76}$$

with $\bar{\phi} = e^{i(mqt-(l\nu_1+n\nu_2)x)\mathbf{I}}\phi$. The Lax pair becomes [12]

$$\begin{cases} \bar{\psi}_x = \bar{X}\bar{\psi}\,, \\ \bar{\psi}_t = \bar{T}\bar{\psi}\,. \end{cases} \tag{3.77}$$

By combining the Lax pair (3.77) with (3.76), we get

$$\begin{cases} \bar{\phi}_x = i\bar{W}\bar{\phi}\,, \\ \bar{\phi}_t = -i\bar{Z}\bar{\phi}\,. \end{cases} \tag{3.78}$$

On the other hand (Appendix G)

$$\begin{cases} \phi_x = iW_0\phi\,, \\ \phi_t = -iZ_0\phi\,, \end{cases} \tag{3.79}$$

[12] In this case, $\bar{X} \equiv X$ and $\bar{T} \equiv T$.

and therefore,

$$\bar{W} = W_0 - (l\nu_1 + n\nu_2)\mathbf{I}, \qquad \bar{Z} = Z_0 - mq\mathbf{I}, \tag{3.80}$$

with l, n and m which are, in general, rational numbers.

By using the gauge transformations (3.75) and (3.80), by setting $m = 0$, $l = \frac{1}{2}$, $n = -\frac{1}{2}$ and multiplying W by $2c_1c_2q$, we shall work with the matrices

$$W = 2c_1c_2q \begin{pmatrix} 0 & -is_1a_1 & is_1s_2s_3a_2 \\ -is_1s_2s_3a_1 & -\kappa c_2 - \nu_1 & -is_3a_3 \\ -is_2a_2 & -is_1s_2s_3a_3^* & -\kappa c_1 + \nu_2 \end{pmatrix}, \tag{3.81}$$

and

$$Z = \begin{pmatrix} 0 & -is_1c_1a_1 & is_1s_2s_3c_2a_2 \\ -is_1s_2s_3c_1a_1 & -\kappa c_1c_2 - q & 0 \\ -is_2c_2a_2 & 0 & -\kappa c_1c_2 + q \end{pmatrix}. \tag{3.82}$$

This choice will prove convenient in the light of the treatment illustrated in the next chapter.

3.4.4 Relations between the Transformed Lax Operators and the Differences of their Eigenvalues

The matrix W is expressible as a polynomial of the matrix Z (Appendix H) as follows

$$W = (c_1 - c_2)Z^2 - c_1(-q - c_1c_2\kappa)Z + c_2(q - c_1c_2\kappa)Z - (c_1 - c_2)(a_2^2c_2^2s_1s_3 - a_1^2c_1^2s_2s_3)\mathbf{I}, \tag{3.83}$$

and vice versa, the matrix Z as function of the matrix W (Appendix H) is

$$\begin{aligned} Z\left[\frac{a_2^2s_1s_3(c_1 - c_2)}{2c_1q} - \frac{a_1^2s_2s_3(c_1 - c_2)}{2c_2q} - \frac{(c_2 + c_1)q}{c_1c_2(c_1 - c_2)} + \kappa\right] &= \frac{W^2}{4c_1^2c_2^2q^2} - \\ - \frac{W}{2c_1c_2q}\left[\frac{a_1^2s_2s_3c_1(c_1 - c_2)}{2c_2q} - \frac{a_2^2s_1s_3c_2(c_1 - c_2)}{2c_1q} + \frac{q(c_1 - c_2)}{c_1c_2} - (c_1 + c_2)\kappa + \frac{2q}{c_1 - c_2}\right] - \\ - (a_2^2s_1s_3 - a_1^2s_2s_3)\mathbf{I}. \end{aligned} \tag{3.84}$$

In addition, if w_j and z_j, $j = 1, 2, 3$ are the eigenvalues of W and Z, respectively, then

$$w_j = (c_1 - c_2)z_j^2 - c_1(-q - c_1c_2\kappa)z_j + c_2(q - c_1c_2\kappa)z_j - (c_1 - c_2)(a_2^2c_2^2s_1s_3 - a_1^2c_1^2s_2s_3), \quad j = 1, 2, 3,$$

(3.85)

and

$$z_j\left[\frac{a_2^2 s_1 s_3(c_1-c_2)}{2c_1 q}-\frac{a_1^2 s_2 s_3(c_1-c_2)}{2c_2 q}-\frac{(c_2+c_1)q}{c_1c_2(c_1-c_2)}+\kappa\right]=\frac{w_j^2}{4c_1^2c_2^2q^2}-$$
$$-\frac{w_j}{2c_1c_2q}\left[\frac{a_1^2s_2s_3c_1(c_1-c_2)}{2c_2q}-\frac{a_2^2s_1s_3c_2(c_1-c_2)}{2c_1q}+\frac{q(c_1-c_2)}{c_1c_2}-(c_1+c_2)\kappa+\frac{2q}{c_1-c_2}\right]-$$
$$-(a_2^2s_1s_3-a_1^2s_2s_3),\quad j=1,2,3, \tag{3.86}$$

hence, the differences of the eigenvalues of W are (Appendix I)

$$w_j-w_{j+1}=(z_j-z_{j+1})(c_1-c_2)\left(-z_{j+2}-c_1c_2\kappa+q\frac{c_1+c_2}{c_1-c_2}\right),\quad j=1,2,3,\quad \mathrm{mod}(3). \tag{3.87}$$

and the differences between the eigenvalues of Z are (Appendix I)

$$(z_j-z_{j+1})\left(2a_2^2s_1s_3c_2(c_1-c_2)-2a_1^2s_2s_3c_1(c_1-c_2)-2q^2\frac{(c_2+c_1)}{(c_1-c_2)}+2c_1c_2q\kappa\right)=$$
$$=-(w_j-w_{j+1})\left(\frac{w_{j+2}}{2c_1c_2q}+\frac{2q}{c_1-c_2}\right). \tag{3.88}$$

3.4.5 Characteristic Polynomials and Rescaled Differences of the Eigenvalues

Although in the previous sections we use some transformations to greatly simplify the Lax operators and the Lax pair, the characteristic polynomials are still hard to handle. However, we can do some further substitutions to obtain a more elegant expression of the characteristic polynomials.

First of all, we can rescale some parameters by q. Once the characteristic polynomials of W and Z are denoted with $\tilde{P}_W(\tilde{w};\kappa)$ and $\tilde{P}_Z(\tilde{z};\kappa)$, respectively, then the amplitudes, the unknowns $\tilde{w}$ and $\tilde{z}$, and the spectral parameter can be rescaled as follows:

$$a_1=q\alpha_1,\quad a_2=q\alpha_2\,, \tag{3.89a}$$

$$\tilde{w}=q^2w,\quad \tilde{z}=qz, \tag{3.89b}$$

$$\kappa = \frac{q\lambda}{c_1 c_2}. \tag{3.89c}$$

At this point, we rename the characteristic polynomials

$$P_W(w;\lambda) = -\frac{\tilde{P}(w;\kappa)}{q^6}, \quad P_Z(z;\lambda) = -\frac{\tilde{P}(z;\kappa)}{q^3}. \tag{3.90}$$

The coefficients of these characteristic polynomials are expressions of the rescaled amplitudes to the second and to the fourth and we benefit from further substitutions,

$$p_1 = \frac{c_1^2 s_1 \alpha_1^2 + c_2^2 s_2 \alpha_2^2}{s_1 s_2 s_3}, \quad p_2 = \frac{c_1^2 s_1 \alpha_1^2 - c_2^2 s_2 \alpha_2^2}{s_1 s_2 s_3}, \tag{3.91}$$

and combinations of the velocities

$$\frac{c_1 - c_2}{c_1 + c_2} = p_3, \qquad c_1 + c_2 = p_4, \quad p_4 \neq 0. \tag{3.92}$$

We highlight that later in our analysis we will consider also the limiting case $p_3 \to \infty$ (that is $p_4 \to 0$).

The computations of the characteristic polynomials after the substitutions above show that, after multiplying the variable w by a factor p_4, we can rescale once more the polynomial $P_W(w;\lambda)$ by a factor p_4^3. Finally, the characteristic polynomials become

$$\begin{aligned} P_W(w;\lambda) &= w^3 + \left[2\lambda - p_3(2+p_2)\right] w^2 + \\ &+ \left[p_2(1+2p_3^2 - p_3\lambda) + p_1 p_3(-3+p_3\lambda) - (p_3^2-1)(\lambda^2-1)\right] w + \\ &+ \left[p_2(\lambda - p_3(-1+p_2+p_3(p_3+\lambda)))\right] - p_1^2 p_3^3 + \\ &+ p_1\left[-1 + p_3(p_3 + 2p_2 p_3 - \lambda + p_3^2\lambda)\right], \end{aligned} \tag{3.93}$$

and

$$P_Z(z;\lambda) = z^3 + 2\lambda z^2 + (\lambda^2 + p_2 - 1)z + p_2\lambda - p_1. \tag{3.94}$$

Moreover, by setting the substitutions above, we rewrite the formulas (3.83) and (3.84) respectively as follows

$$W = p_3 Z^2 + q(1+p_3\lambda)Z + p_3 p_2 q^2, \tag{3.95}$$

and

$$\begin{aligned} Z = &-\frac{p_3}{1 - p_3\left(\lambda + p_3^2(p_1-\lambda) - p_2 p_3 + p_3\right)} W^2 + \frac{\left(p_2 p_3^2 - 2\lambda p_3^2 + p_3^2 + 1\right)}{1 - p_3\left(\lambda + p_3^2(p_1-\lambda) - p_2 p_3 + p_3\right)} W + \\ &+ \frac{2p_1 p_3^2 - p_2 p_3^3 - p_2 p_3}{1 - p_3\left(\lambda + p_3^2(p_1-\lambda) - p_2 p_3 + p_3\right)}, \end{aligned}$$

(3.96)

hence, the differences between the eigenvalues become

$$w_j - w_{j+1} = (z_j - z_{j+1}) \left[(-p_3 z_{j+2} + q(1 - \lambda p_3)) \right], \tag{3.97}$$

for $j = 1, 2, 3, \mod(3)$, and

$$\begin{aligned} & z_j - z_{j+1} = \\ & - \frac{(w_1 - w_2) \left(p_3 \left(-p_3(-2\lambda + p_2 + 1) + p_4 q^2((p_2 + 2)p_3 - 2\lambda) - w_3 \right) - 1 \right)}{1 - p_3 \left(\lambda + p_3^2(p_1 - \lambda) - p_2 p_3 + p_3 \right)}, \end{aligned} \tag{3.98}$$

for $j = 1, 2, 3, \mod(3)$. Furthermore, we give some useful formulas. Because the trace is invariant under cyclic permutations, the eigenvalues w_j and z_j satisfy the following relations

$$w_1 + w_2 + w_3 = ((2 + p_2)p_3 - 2\lambda), \tag{3.99}$$

$$z_1 + z_2 + z_3 = -2\lambda, \tag{3.100}$$

with $p_4 = c_1 + c_2$, and by the computation of the determinant of the matrices W and Z, we get

$$z_1 z_2 z_3 = p_1 - \lambda p_2, \tag{3.101}$$

$$w_1 w_2 w_3 = p_1^2 p_3^3 - p_1 \left[p_3 \left(-\lambda + 2p_2 p_3 + \lambda p_3^2 + p_3 \right) - 1 \right] + p_2 \left[p_2 p_3 + \left(p_3^2 - 1 \right) (\lambda + p_3) \right]. \tag{3.102}$$

Obviously, the formulas above are satisfied for both complex and real λ.

Because a solution of the linearised equation can be expressed as combination of the exponentials $e^{i(x(w_j - w_{j+1}) - t(z_j - z_{j+1}))}$ [64], we have completed the preliminary calculations in order to prepare the work for the stability analysis.

Chapter 4

Spectra and Linear Instabilities of the 3WRI Equations

In this Chapter we will follow the theory for multi-component systems provided in Chapter 2 and we will use all the preliminary computations carried out in Chapter 3.
We provide the definition of $\mathbf{S}_x$-spectrum as composed by the values of the spectral parameter λ which are the roots of the polynomial $\mathcal{P}(\xi, \lambda)$ of the squares of the differences $\xi = (w_1 - w_2)^2$. The analysis of the nature of the λ-roots allows us to obtain a full topological classification of the stability spectra in the parameters space. Using a numerical routine implemented in MATLAB R2017a, for any generic choice of the physical parameters, we plot the stability spectrum and its associated gain function (see definition below). The fact that this function is always different from zero indicates that linear instability occurs for any generic choice of the parameters p_1, p_2 and p_3.

4.1 Spatial and Temporal Stability Spectra

Given the real parameters p_1, p_2 and p_3 (see formulas (3.91) and (3.92)), we are interested in finding the values of the complex spectral parameter λ such that the plane waves are bounded in space and see if they are linearly stable or unstable in time. In other words, let w_j be the eigenvalues of the matrix W and z_j the eigenvalues of Z; them we aim to search

those values of the spectral parameter λ corresponding to real differences $k_j = w_{j+1} - w_{j+2}$, whereas the differences $\omega_j = z_{j+1} - z_{j+2}$ can be real or complex. This latter point can be understood for the differences k_j are linked to the differences ω_j by the formula

$$k_j = \omega_j(-p_3 z_j + q(1 - \lambda p_3)), \quad j = 1, 2, 3. \tag{4.1}$$

Therefore, values of the spectral parameter λ corresponding to real k_j may correspond to complex ω_j and so linear instability may occur.

In the following, we will refer to the eigenvalues w (resp. z) of the matrix W (resp. Z) also as w-roots (resp. z-roots) of the characteristic polynomial $P_W(w;\lambda)$ (resp. $P_Z(z;\lambda)$), namely, the polynomial roots of the equation $P_W(w;\lambda) = 0$ (resp. $P_Z(z;\lambda) = 0$), solved with respect to w (resp. z). From here on, we fix $q = 1$, without loss of generality, because of the Galileian invariance (Chapter 3).

Definition 4.1.1. *The spatial stability spectrum $\mathbf{S}_x$ for the plane wave solutions of the 3WRI system (3.5), is defined as the locus of the λ-plane identified with $\mathbb{C}$ such that, for fixed values of the physical parameters p_1, p_2 and p_3, the characteristic polynomial $P_W(w;\lambda)$, admits at least two w-roots such that their difference is a real number, namely, the set of the spectral parameter λ for which there exist at least two eigenvalues w_ℓ and w_m for the matrix W, for some ℓ and m, for which $(w_\ell - w_m) \in \mathbb{R}$.*

Definition 4.1.2. *The temporal stability spectrum $\mathbf{S}_t$ for the plane wave solutions of the 3WRI system (3.5), is defined as the locus of the λ-plane identified with $\mathbb{C}$ such that, for fixed values of the physical parameters p_1, p_2 and p_3, the characteristic polynomial $P_Z(z;\lambda)$ admits at least two z-roots such that their difference is a real number, namely, the set of values of the spectral parameter λ such that there exist at least two eigenvalues z_ℓ and z_m for the matrix Z, for some ℓ and m, for which $(z_\ell - z_m) \in \mathbb{R}$.*

In the following, we give the definition of the components of the stability spectrum $\mathbf{S}_x$.

Definition 4.1.3. *Real values of the spectral parameter λ, not belonging to $\mathbf{S}_x$ constitute a* gap *(G). A gap, including a single isolated real point within its real endpoints, will be renamed as* split gap *(SG).*

Complex values of the spectral parameter λ, belonging to $\mathbf{S}_x$ correspond to branches *(B) and* loops *(L), which are open and closed curves, respectively. Figure of eight loops, self-intersecting on the real axis, will be referred to as* twisted loops *(TL).*

Once the parameter p_3 is fixed, the topological classification of the spacial stability spectra $\mathbf{S}_x$ in the (p_1, p_2) parameters space, can be obtained by means of the algebraic-geometric procedure described in the next sections [1].

4.1.1 Polynomials of the Squares of the Differences

Let us write the characteristic polynomials (3.93) and (3.94) in a general form

$$P_W(w;\lambda) \equiv P_W(w;\lambda;p_1,p_2,p_3) = \sum_{j=0}^{3} a_j^{(W)} w^j = \prod_{j=1}^{3}(w-w_j), \quad a_3^{(W)} = 1, \tag{4.2a}$$

$$P_Z(z;\lambda) \equiv P_Z(z;\lambda;p_1,p_2,p_3) = \sum_{j=0}^{3} a_j^{(Z)} z^j = \prod_{j=1}^{3}(z-z_j), \quad a_3^{(Z)} = 1. \tag{4.2b}$$

By combinations of the coefficients $\{a_j^{(W)}\}_{j=0}^{3}$, we construct the coefficients of the polynomial $\mathcal{P}_W(\xi;\lambda) \equiv \mathcal{P}_W(\xi;\lambda;p_1,p_2,p_3)$ of degree 3 in the variable ξ, whose ξ-roots are the squares of all the possible differences of the roots of the polynomial $P_W(w;\lambda)$ (Appendix J),

$$\mathcal{P}_W(\xi;\lambda) \equiv \mathcal{P}_W(\xi;\lambda;p_1,p_2,p_3) = \prod_{\substack{j,h=1 \\ j<h}}^{3} \left[\xi - (w_j - w_h)^2\right] , \tag{4.3}$$

that is a 2-variate polynomial in ξ and λ. For the sake of simplicity, we will refer to $\mathcal{P}_W(\xi;\lambda)$ as the *polynomial of the squares of the differences*. A ξ-root (resp. λ-root) of $\mathcal{P}_W(\xi;\lambda)$ is a polynomial root of the equation $\mathcal{P}_W(\xi;\lambda) = 0$, solved with respect to ξ (resp. λ).
For any fixed p_1, p_2 and p_3 parameters, the spectrum $\mathbf{S}_x$ is the locus of the λ-roots of $\mathcal{P}_W(\xi;\lambda)$ for all $\xi \in \mathbb{R}$, $\xi \geq 0$. In other words, the spatial spectrum $\mathbf{S}_x$ can be seen as a one-parameter algebraic variety over the complex numbers, and it is defined as

$$\mathbf{S}_x = \{\lambda \in \mathbb{C} \,|\, \mathcal{P}_W(\xi;\lambda) = 0,\, \xi \in \mathbb{R},\, \xi \geq 0\} \ . \tag{4.4}$$

Similarly, by combinations of the coefficients $\{a_j^{(Z)}\}_{j=0}^{3}$, we can construct the coefficients of the polynomial $\mathcal{P}_Z(\eta;\lambda) = \mathcal{P}(\eta;\lambda;p_1,p_2,p_3)$, that is a polynomial of degree 3 in the

[1] An analogous procedure can be implemented for deriving the temporal stability spectra $\mathbf{S}_t$, starting from Z instead of W.

variable η and whose η-roots are the squares of the differences of the roots of the polynomial $P_Z(z;\lambda)$ (Appendix J),

$$\mathcal{P}_Z(\eta;\lambda) \equiv \mathcal{P}_Z(\eta;\lambda;p_1,p_2,p_3) = \prod_{\substack{j,h=1 \\ j\neq h}}^{3} \left[\eta - (z_j - z_h)^2\right] , \tag{4.5}$$

that is a 2-variate polynomial in η and λ. A η-root (resp. λ-root) of $\mathcal{P}_Z(\eta;\lambda)$ is a polynomial root of the equation $\mathcal{P}_Z(\eta;\lambda) = 0$, solved with respect to η (resp. λ).
For any fixed p_1, p_2 and p_3 parameters, the temporal spectrum $\mathbf{S}_t$ is the locus of the λ-roots of $\mathcal{P}_Z(\eta;\lambda)$ for all $\eta \in \mathbb{R}$, $\eta \geq 0$. In other words, the spectrum $\mathbf{S}_t$ can be seen as the one-parameter algebraic variety over the complex numbers, and it is defined as

$$\mathbf{S}_t = \{\lambda \in \mathbb{C} \,|\, \mathcal{P}_Z(\eta;\lambda) = 0,\, \eta \in \mathbb{R},\, \eta \geq 0\} \ . \tag{4.6}$$

4.2 Real Spectrum

In this section we take into account only real λ-roots. By bearing in mind this assumption, and because $P(w;\lambda)$ is a cubic polynomial, the existence of a real w-root implies that the other two w-roots are real too, otherwise there are two complex conjugate w-roots and a w-real root. Therefore, in the first case the differences k_j are all real and the corresponding λ values belong to the spectrum $\mathbf{S}_x$. In the second case, they are all complex and λ values belong to a *gap*.
By denoting by $\Delta_y(\mathcal{P}(y))$ the discriminant with respect to y of the polynomial $P(y)$, we observe that the polynomial of the squares of the differences $\mathcal{P}_W(0;\lambda)$ (resp. $\mathcal{P}_Z(0;\lambda)$) is equal to the discriminant with respect to w (resp. z) of the characteristic polynomial $P_W(w;\lambda)$ (resp. $P_Z(z;\lambda)$) with the opposite sign,

$$\mathcal{P}_W(0;\lambda) = -\Delta_w(P_W(w;\lambda)), \quad \mathcal{P}_Z(0;\lambda) = -\Delta_z(P_Z(z;\lambda)), \tag{4.7}$$

and they are related as follows

$$\mathcal{P}_W(0;\lambda) = \mathcal{P}_Z(0;\lambda)\mathcal{R}^2(\lambda), \tag{4.8}$$

where

$$-\mathcal{P}_Z(0;\lambda) = 4\lambda^4 - 27p_1^2 - 4\lambda^3 p_1 + 18\lambda p_1(p_2+2) + \lambda^2((p_2-20)p_2-8) - 4(p_2-1)^3, \tag{4.9}$$

and

$$\mathcal{R}(\lambda) = \left(p_3\left(\lambda + p_3^2(p_1 - \lambda) - p_2 p_3 + p_3\right) - 1\right). \tag{4.10}$$

Since we impose k_j to be real, we consider only $\mathcal{P}_W(0;\lambda) \leq 0$.

Indeed, by assuming $\mathcal{R}(\lambda) \neq 0$, $\mathcal{P}_Z(0;\lambda) \leq 0$ if and only if $\mathcal{P}_W(0;\lambda) \leq 0$, that is, by (4.8), if $\mathcal{P}_Z(0;\lambda)$ is negative or zero, then $\mathcal{P}_W(0;\lambda)$ is like that, and vice versa.

There is also the limiting case $\mathcal{R}(\lambda) = 0$, satisfied for

$$\lambda = \frac{p_3^2(p_1 p_3 - p_2 + 1) - 1}{p_3\left(p_3^2 - 1\right)}, \tag{4.11}$$

for which $\mathcal{P}_W(0;\lambda) = 0$, but $\mathcal{P}_Z(0;\lambda)$ can be zero, positive or negative. In the following proposition we prove that only the real part of $\mathbf{S}_x$ contributes to the stability, namely that, if $\mathbf{S}_x$ has an off-real component, then the solution is expected to be unstable.

Proposition 4.2.1. *For a generic choice of the physical parameters, the plane wave solution of the 3WRI system is stable against perturbations δQ integrated only over values of λ in $\mathbf{S}_x$ strictly real, with the exception of the point separating a split gap.*

Proof. Let us suppose $\lambda \in \mathbb{R}$, so that w_j and z_j are roots of third degree polynomials with real coefficients. As a consequence, the characteristic polynomials can have: three real and distinct w-roots; or a real triple w-root; or a w-real double root and a real simple w-root or two complex conjugate w-roots and a real w-root. We impose that $w_j - w_{j+1}$ be real [2], thus we exclude the case in which the characteristic polynomial $P(w;\lambda)$ has two complex conjugate w-roots and a real w-root.

Let us assume $\mathcal{R}(\lambda) \neq 0$ and let w_j be real and all distinct, i.e. $\mathcal{P}_W(0;\lambda) < 0$. Thus, since $p_4 \in \mathbb{R}$, all the differences $w_j - w_{j+1}$ are also real and all distinct

$$w_j - w_{j+1} = (z_j - z_{j+1})(-z_{j+2}p_3 - \lambda p_3 + 1), \quad j = 1,2,3, \quad \mathrm{mod}(3), \tag{4.12}$$

and then the product $(z_j - z_{j+1})(-z_{j+2}p_3 - \lambda p_3 + 1)$ is real too. For $\lambda \in \mathbb{R}$, we cannot have $(z_j - z_{j+1}) \in \mathbb{C}$ and $(-z_{j+2}p_3 - \lambda p_3 + 1) \in \mathbb{C}$ so that $(z_j - z_{j+1})(-z_{j+2}p_3 - \lambda p_3 + 1) \in \mathbb{R}$ because, by the relation (4.8), we would have $\mathcal{P}_Z(0;\lambda) > 0$, and so $\mathcal{P}_W(0;\lambda) > 0$, in contradiction with the hypothesis. Instead, we can have $(z_j - z_{j+1}) \in \mathbb{R}$ and $(-z_{j+2}p_3 - \lambda p_3 + 1) \in$

[2] Since w_j are roots of a third degree polynomial with real coefficients, then the requerement to have at least a real difference implies that all the differences $w_j - w_{j+1}$ are real too.

$\mathbb{R}$, so that their product is real, and then $w_j - w_{j+1} \in \mathbb{R}$, $\forall j = 1, 2, 3$.
Moreover, we remind that if also only two roots coincide, then $\mathcal{P}_Z(0;\lambda) = 0$, and this condition pushes $\mathcal{P}_W(0;\lambda) = 0$ to vanish, but we are imposing $\mathcal{P}_W(0;\lambda)$ to be strictly positive.
Therefore we conclude that if $\lambda \in \mathbb{R}$ and $\mathcal{R}(\lambda) \neq 0$, then $\mathcal{P}_W(0;\lambda) < 0$ if and only if $\mathcal{P}_Z(0;\lambda) < 0$.

Let us suppose $\mathcal{P}_W(0;\lambda) = 0$ and $P(w;\lambda)$ has a double real root and a simple real root. For the sake of simplicity, we impose $w_1 = w_2$, while w_3 is different from the other two. From the formula (4.12) and by considering $p_3 \neq 0$, we distinguish three cases corresponding to all the possibilities for which we have $w_1 - w_2 = 0$:

1. $z_1 - z_2 = 0$ and $-z_3 p_3 - \lambda p_3 + 1 = 0$, ($\mathcal{P}_Z(0;\lambda) = 0$ and $\mathcal{R}(\lambda) = 0$);
2. $z_1 - z_2 = 0$ and $-z_3 p_3 - \lambda p_3 + 1 \neq 0$, ($\mathcal{P}_Z(0;\lambda) = 0$ and $\mathcal{R}(\lambda) \neq 0$);
3. $z_1 - z_2 \neq 0$ and $-z_3 p_3 - \lambda p_3 + 1 = 0$, ($\mathcal{P}_Z(0;\lambda) \neq 0$ and $\mathcal{R}(\lambda) = 0$).

In the following we shall discuss the reverse arguments: starting from the hypothesis 1., 2., and 3., we show that $w_1 = w_2$, and the w-roots are all real, i.e. if $\mathcal{P}_Z(0;\lambda) = 0$, then $\mathcal{P}_W(0;\lambda) = 0$.

1. If $z_1 = z_2$, then z_1 and z_2 are real, then z_3 is necessarily real, and for this particular case we get

$$z_3 = \frac{1}{p_3} - \lambda, \tag{4.13}$$

and by (3.100)

$$z_1 = z_2 = -\frac{1}{2}\left(\frac{1}{p_3} + \lambda\right). \tag{4.14}$$

Moreover,

$$z_2 - z_3 = -\frac{1}{2}\left(\frac{3}{p_3} - \lambda\right), \quad z_3 - z_1 = \frac{1}{2}\left(\frac{3}{p_3} - \lambda\right), \tag{4.15}$$

so that

$$z_1 - z_2 = 0, \quad (z_2 - z_3) = -(z_3 - z_1). \tag{4.16}$$

By keeping in mind formulas (4.13) and (4.12), we compute the differences $w_j - w_{j+1}$ and get

$$w_1 - w_2 = 0, \quad w_2 - w_3 = -(w_3 - w_1) = -\frac{p_4}{2}\left(\frac{3}{p_3} - \lambda\right)(-z_1 p_3 - \lambda p_3 + 1), \tag{4.17}$$

all real, because all the parameters involved and all the three z_j are real.

Thus, we conclude that $\mathcal{P}_Z(0;\lambda) = 0$ implies $\mathcal{P}_W(0;\lambda) = 0$.

Furthermore, the characteristic polynomial $P(z_3;\lambda)$ becomes proportional to $\mathcal{R}(\lambda)$,

$$P(z_3;\lambda) = \frac{1 - p_3\left(\lambda + p_3^2(p_1 - \lambda) - p_2 p_3 + p_3\right)}{p_3^3} = -\frac{1}{p_3^3}\mathcal{R}(\lambda). \tag{4.18}$$

This implies that, if $z_3 = \frac{1}{p_3} - \lambda$ is a zero of the characteristic polynomial $P(z;\lambda)$, then $\mathcal{R}(\lambda) = 0$ and λ has the expression (4.11). The reverse argument is also true: if $\mathcal{R}(\lambda) = 0$, then $z_3 = \frac{1}{p_3} - \lambda$ is a zero of the characteristic polynomial $P(z;\lambda)$.

2. We assume $z_1 = z_2$ and z_1 and z_2 are both real. As a consequence z_3 is real, but we impose that z_3 does not satisfy the formula (4.13) any more. Nevertheless, by the formulas (3.100) and (3.101), we have that

$$2z_j^3 + 2\lambda z_j^2 + (1 - \lambda)p_2 = 0, \quad z_j = z_1 = z_2, \tag{4.19}$$

and once z_j is obtained [3] , we can use (3.100) to get $z_3 = -2(z_j + \lambda)$. Therefore, the relations (4.17) and (4.16) are still satisfied, indeed

$$z_1 = z_2, \quad z_3 - z_1 = -(z_2 - z_3) = -(3z_j + 2\lambda), \quad z_j = z_1 = z_2, \tag{4.20}$$

and then,

$$w_1 = w_2, \quad w_2 - w_3 = -(w_3 - w_1) = (3z_j + 2\lambda)(-p_3 z_j - p_3\lambda + 1), \quad z_j = z_1 = z_2, \tag{4.21}$$

and all the three differences $(w_j - w_{j+1})$ are real. Even for this case $\mathcal{P}_Z(0;\lambda) = 0$ implies $\mathcal{P}_W(0;\lambda) = 0$. In this case $\mathcal{R}(\lambda)$ is different from zero.

3. Let us consider the most general case in which all the three z_j are different from one another. $\mathcal{P}_W(0;\lambda) = 0$ when $\mathcal{R}(\lambda) = 0$. We identify two sub-cases:

[3] It is not the aim of our analysis to find the explicit expression of the solutions $z_j = z_1 = z_2$.

3a) $\mathcal{P}_Z(0;\lambda) < 0$, and the characteristic polynomial $P(z;\lambda)$ has three real z-roots all distinct;

3b) $\mathcal{P}_Z(0;\lambda) > 0$, and the characteristic polynomial $P(z;\lambda)$ has two complex conjugate z-roots and a real z-root.

Furthermore, since $\mathcal{R}(\lambda) = 0$, then $\mathcal{P}_W(0;\lambda) = 0$, and $P(w;\lambda)$ has a) a real double w-root and a simple w-root or b) a triple real w-root.

3a) Let us suppose z_j are all different, but $z_3 = \frac{1}{p_3} - \lambda$. By substituting $\lambda = \frac{1}{p_3} - z_3$, into the other two differences $w_2 - w_3$ and $w_3 - w_1$, we get

$$w_2 - w_3 = -p_3(z_2 - z_3)(z_1 - z_3), \quad w_3 - w_1 = p_3(z_2 - z_3)(z_1 - z_3), \tag{4.22}$$

that is

$$w_2 - w_3 = -(w_3 - w_1), \tag{4.23}$$

and in addition

$$w_1 - w_2 = 0. \tag{4.24}$$

However, this case is impossible. Indeed, by using the formula (4.22) and matching the two formulas

$$w_2 - w_3 = (z_2 - z_3)(-p_3 z_1 - p_3\lambda + 1), \tag{4.25}$$

$$w_3 - w_1 = (z_3 - z_1)(-p_3 z_2 - p_3\lambda + 1), \tag{4.26}$$

via (4.23), we get the equation

$$(z_2 - z_3)(-p_3 z_1 - p_3\lambda + 1) = (z_1 - z_3)(-p_3 z_2 - p_3\lambda + 1), \tag{4.27}$$

that is satisfied for $z_1 = z_2$. However, this is a contradiction to the hypothesis $\mathcal{P}_Z(0;\lambda) < 0$. Thus, we can not have $\mathcal{P}_Z(0;\lambda) < 0$, and instead we have $\mathcal{P}_Z(0;\lambda) = 0$. Note that because of the formula (4.8), we have $\mathcal{R}(\lambda) = 0$.

The case b) is impossible. Indeed, because $w_1 = w_2 = w_3$ has to be verified, we need to impose $z_1 = z_2 = z_3 = \frac{1}{p_3} - \lambda$, that is a contradiction to the hypothesis $\mathcal{P}_Z(0;\lambda) < 0$.

3b) If $\mathcal{P}_Z(0;\lambda) > 0$, the characteristic polynomial $P(z;\lambda)$ has two complex conjugate roots, say, z_1 and z_2, and a real root z_3. In order the case a) to be verified, the relation $z_3 = \frac{1}{p_3} - \lambda$ has to be satisfied. We can not have $(-z_j p_3 - \lambda p_3 + 1) = 0$, for $j = 1, 2$, because this equation would be satisfied only for z-roots all real, but we are in the hypothesis $\mathcal{P}_Z(0;\lambda) > 0$. We note that, since $\mathrm{Re}(z_1) = \mathrm{Re}(z_2)$ and $\mathrm{Im}(z_1) = -\mathrm{Im}(z_2)$, then $z_2 - z_3$ and $z_3 - z_1$ are complex with the same imaginary part and $z_1 - z_2 = 2i\mathrm{Im}(z_1)$. Moreover, because $w_2 - w_3 = -(w_3 - w_1) = -p_3(z_1 - z_3)(z_2 - z_3)$, the differences $w_2 - w_3$ and $w_3 - w_1$ are real, in particular

$$w_2 - w_3 = -(w_3 - w_1) = -p_3\left((\mathrm{Re}(z_j) - z_3)^2 + (\mathrm{Im}(z_j))^2\right), \quad z_j = z_1 = z_2, \tag{4.28}$$

and we have that if $p_3 p_4 > 0$, then $w_2 - w_3 < 0 < w_3 - w_1$, and if $p_3 p_4 < 0$, then $w_3 - w_1 < 0 < w_2 - w_3$.
Moreover, z_3 coincides with the solution of $\mathcal{R}(\lambda)$ and the formula (4.18) is still satisfied.
The case b) is impossible because, since we require a priori that all the roots z_j must be different from each other, we have to impose $(-z_j p_3 - \lambda p_3 + 1) = 0$, $\forall j = 1, 2, 3$ in order to have all the three w_j coinciding and real, which gives us all z_j coinciding and real, but this is a contradiction to the hypothesis $\mathcal{P}_Z(0;\lambda) > 0$.

Let us suppose $P(w;\lambda)$ has a triple real root, that is $\mathcal{P}_W(0;\lambda) = 0$. We distinguish two cases:

1. $z_1 = z_2 = z_3$, but $-p_3 z_j - p_3\lambda + 1 \neq 0$, $\quad (\mathcal{P}_Z(0;\lambda) = 0$ and $\mathcal{R}(\lambda) \neq 0)$;
2. $z_1 = z_2 = z_3$, and $-p_3 z_j - p_3\lambda + 1 = 0$, $\quad (\mathcal{P}_Z(0;\lambda) = 0$ and $\mathcal{R}(\lambda) = 0)$.

All the cases above are trivial to show, but in the case 2., we have that, by making the sum of all the three z_j solutions of the equation $-p_3 z_j - p_3\lambda + 1 = 0$, $\forall j = 1, 2, 3$, we get $z_1 + z_2 + z_3 = 3\left(\frac{1}{p_3} - \lambda\right)$ with $p_3 \neq 0$, in contrast with the trace (3.100), unless $\lambda = \frac{3}{p_3}$.
Finally, we conclude that if $\mathcal{R}(\lambda) = 0$ and $\mathcal{P}_Z(0;\lambda) > 0$, then $\mathcal{P}_W(0;\lambda) = 0$ and $P(w;\lambda)$

has a double real root and a simple real root.

If $\mathcal{P}_Z(0;\lambda) > 0$, we have that all the three real differences $w_j - w_{j+1}$ correspond to the three differences $z_j - z_{j+1}$, all complex.

On the other hand, let us assume now that λ is complex, $\lambda = \mu + i\rho$, with nonvanishing imaginary part, $\rho \neq 0$. Let $w_j = \alpha_j + i\beta_j$ be the (generically complex) roots of $P_W(w;\lambda)$. With this notation, we have that one of the wave numbers, say $k_3 = w_1 - w_2$, will be real only if $\beta_1 = \beta_2 = \beta$. Then, from (3.98) , we have that $\omega_3 = z_1 - z_2$ will also be real only if the following equation is satisfied:

$$-\beta_3\left(-1 + p_3(p_3 - p_2p_3 + p_3^2(p_1 - \mu) + \mu])\right) + \left(-1 + p_3^2\right)\left(-1 + p_3^2 - p_3\alpha_3\right)\rho. \quad (4.29)$$

Writing the polynomial $P_W(w;\lambda)$ as $P_W(w;\lambda) = \prod_{j=1}^{3}(w - \alpha_j - i\,\beta_j)$, and comparing the real and imaginary parts of the coefficients of same powers of w from this expression with those obtained from (3.93), we get, in addition to equation (4.29), six further polynomial equations, constituting overall a system of seven polynomial equations for the seven unknowns α_1, α_2, α_3, β, β_3, μ, ρ, each equation being of degree 1, 2 or 3 in the unknowns:

$$\begin{aligned} &p_2^2p_3 + p_1^2p_3^3 - \alpha_1\alpha_2\alpha_3 + \alpha_3\beta^2 + \alpha_1\beta\beta_3 + \alpha_2\beta\beta_3 + p_2(-1 + p_3^2)(p_3 + \mu) - \\ &- p_1(-1 + p_3(p_3 + 2p_2p_3 - \mu + p_3^2\mu)), \end{aligned} \quad (4.30a)$$

$$-(\alpha_1 + \alpha_2)\alpha_3\beta + (-\alpha_1\alpha_2 + \beta^2)\beta_3 + (p_2 - p_1p_3)(-1 + p_3^2)\rho, \quad (4.30b)$$

$$\begin{aligned} &1 + \alpha_1\alpha_2 + (\alpha_1 + \alpha_2)\alpha_3 - \beta(\beta + 2\beta_3) - \mu]^2 + p_1p_3(3 - p_3\mu) + \\ &p_2(-1 + p_3(-2p_3 + \mu])) + \rho]^2 + p_3^2(-1 + \mu^2 - \rho^2), \end{aligned} \quad (4.30c)$$

$$(\alpha_1 + \alpha_2 + 2\alpha_3)\beta + (\alpha_1 + \alpha_2)\beta_3 + (-2\mu + p_3(p_2 - p_1p_3 + 2p_3\mu))\rho, \quad (4.30d)$$

$$(2 + p_2)p_3 - \alpha_1 - \alpha_2 - \alpha_3 - 2\mu, \quad (4.30e)$$

$$-2\beta - \beta_3 - 2\rho. \quad (4.30f)$$

Using an algebraic manipulation software (like Mathematica or Maple), after a long and tedious work (we apply the method developed in [65]), one shows that, for a *generic* choice of the parameters p_1, p_2 and p_3, system (4.30) either does not have real solutions or features at most 72 complex solutions. This excludes, for a generic choice of the parameters p_1, p_2 and p_3, that there exist sets of non-vanishing measure off the real axis on the λ-plane for which z_1 and z_2 generate a real difference when w_1 and w_2 generate a real difference, namely for which either side of (3.98) is real. As the set of exceptional complex values of λ for which either side of (3.98) is real has generically at most vanishing measure, it does not contribute to the integral in (2.79); therefore, for a generic choice of the parameters p_1, p_2, and p_3, the plane wave solution is stable against the perturbation δQ integrated only over values of λ in $\mathbf{S}_x$ strictly real, with the exception of the isolated points in the split gaps. The discussion of the non-generic choices of the parameters p_1, p_2 and p_3, possibly allowing a set of non-vanishing measure off the real axis on the λ-plane providing a stable contribution to the integral of the perturbation, is left to future investigation. □

We stress that for both the cases 1. and 2., if $P(z;\lambda)$ has a double real root and a simple real root, then it is the same also for $P(w;\lambda)$.
Whatever the labelling is, we have always three real differences $w_j - w_{j+1}$. Moreover, the relations $z_j - z_{j+1} = 0$ and $z_{j+1} - z_{j+2} = -(z_{j+3} - z_j)$ imply $w_j - w_{j+1} = 0$ and $w_{j+1} - w_{j+2} = -(w_{j+3} - w_j)$ for $j = 1, 2, 3, \mathrm{mod}(3)$. In particular, one can prove that, for real λ, there is an *order relation* for the differences $z_j - z_{j+1}$ and $w_j - w_{j+1}$, and there exist a bijective relation between the two orderings of the differences, but this argument will not be discussed in this thesis.

4.2.1 Gaps and Branches

In this section we give a topological description of the components of the spectrum $\mathbf{S}_x$ which are referred to as gaps and branches. We impose that the eigenvalues of W are non-simple and we take into account the polynomial $\mathcal{P}_W(0;\lambda)$ and its relation with the polynomial $\mathcal{P}_Z(0;\lambda)$ given by (4.8). In fact, as discussed in the previous section, by (4.8), the eigenvalues w_j are non-simple if and only if the eigenvalues z_j are non-simple, with the

exception of a point on the real axis of the $\mathbf{S}_x$ spectrum [4]. Thus, one can study first the discriminant with respect to λ of $\mathcal{P}_Z(0;\lambda)$ to get the main structure of the $\mathbf{S}_x$ spectrum [5], but then one needs to introduce a resultant, which will be defined later, to know for which values of the physical parameters a split-gap occurs. Therefore, it is useful to introduce the discriminant $\Delta_\lambda \mathcal{P}_Z(0;\lambda)$ which can be factorised as

$$\Delta_\lambda \mathcal{P}_Z(0;\lambda) = \prod_j D_j(p_1,p_2)^{d_j}, \quad \forall p_3 \in \mathbb{R}, \tag{4.31}$$

and the resultant $\mathrm{Res}_\lambda(\mathcal{P}_Z(0;\lambda),\mathcal{R}(\lambda))$ which can be factorised as

$$\mathrm{Res}_\lambda(\mathcal{P}_Z(0;\lambda),\mathcal{R}(\lambda)) = \prod_j R_j(p_1,p_2,p_3)^{r_j}. \tag{4.32}$$

Let $\mathcal{D}_j$ be the real-analytic variety in the parameter space (p_1,p_2), implicitly defined as

$$\mathcal{D}_j = \{p_1,p_2,p_3 \in \mathbb{R} : D_j(p_1,p_2)=0,\ R_j(p_1,p_2,p_3)=0\}. \tag{4.33}$$

Once the value of the parameter p_3 is fixed, a first topological classification of the possible curves in the λ-plane in terms of the choices of the parameters (p_1,p_2) can be made by observing the nature of the λ-roots for which the matrix Z (resp. W) has non-simple eigenvalues. This corresponds to analysing the sign of (4.31). By imposing (4.31) to be negative, we obtain a set of regions in the (p_1,p_2)-plane in which Z (resp. W) is not diagonalisable for two real values of λ and for a pair of complex conjugate values of λ. This values of λ identify the end-points of a gap and of a branch, respectively. On the contrary, if (4.31) is positive, we obtain regions in the (p_1,p_2)-plane in which Z (resp. W) is not diagonalisable either for four real values of λ corresponding to the end-points of two gaps, or for two pairs of complex conjugate values of λ corresponding to the end-points of two branches. In addition, besides the λ-roots of the polynomial $\mathcal{P}_Z(0;\lambda)$, the polynomial $\mathcal{P}_W(0;\lambda)$ has also one real double λ-root, that is the λ-root of the polynomial $\mathcal{R}(\lambda)$. The value of this λ-root depends on the parameters p_1, p_2 and p_3, and so it varies as p_j vary, and it varies in the (p_1,p_2)-plane once the value of p_3 is fixed. Interestingly, we have found that also the sign of the resultant (4.32) is relevant for the classification of gaps and it is a determining factor for defining the so called *split-gap*. In particular, a split-gap exists in

[4] We can have at most one split-gap. This is a consequence of the formula (4.8), in which $\mathcal{R}(\lambda)$ is a first degree polynomial in λ, and the only root gives the point between the two endpoints of a gap.

[5] One observes that the discriminant with respect to λ of $\mathcal{P}_W(0;\lambda)$ is always zero because the polynomial $\mathcal{P}_W(0;\lambda)$ has a double real λ-root for any choice of the parameters p_j.

the regions of the (p_1, p_2)-plane for which the resultant is negative (see below).
Finally, the curves defined by (4.33) are the boundaries of the regions in the (p_1, p_2)-plane associated to different topologies of the spectra $\mathbf{S}_x$.

In order to define the number of gaps and branches, we compute the discriminant $\Delta_z(P(z;\lambda)) = -\mathcal{P}_Z(0;\lambda)$, that is a polynomial in λ, with parameters p_1, p_2, and p_3. The polynomial $\mathcal{P}_Z(0;\lambda)$ is negative whenever the three roots z_j are real, and it is positive if only one root z_j is real. As a consequence, for fixed values of p_1, p_2, and p_3, the polynomial $\mathcal{P}_Z(0;\lambda)$ is positive (resp. negative) for those values of λ inside (resp. outside) the gap, and they become zero at the end-points of gaps. Gaps and branches appear or disappear at the multiple-zeros of the polynomial $\mathcal{P}_Z(0;\lambda)$ (as discussed more in details later), thus at the zeros of the discriminant [6] $\Delta_\lambda \mathcal{P}_Z(0;\lambda)$, namely when

$$\Delta_\lambda \mathcal{P}_Z(0;\lambda) = -256(p_1 - p_2)(p_1 + p_2)\left(27p_1^2 - (p_2 - 1)(p_2 + 8)^2\right)^3 = 0. \tag{4.34}$$

The three polynomial factors appearing in (4.34) bound the regions in the (p_1, p_2)-plane characterised by different numbers of gaps and branches. We denote such curves as follows

$$\mathcal{D}_1 = \{(p_1, p_2) \in \mathbb{R}^2 : p_1 - p_2 = 0\}, \tag{4.35}$$

$$\mathcal{D}_2 = \{(p_1, p_2) \in \mathbb{R}^2 : p_1 + p_2 = 0\}, \tag{4.36}$$

$$\mathcal{D}_3 = \{(p_1, p_2) \in \mathbb{R}^2 : \left(27p_1^2 - (p_2 - 1)(p_2 + 8)^2\right)^3 = 0\}. \tag{4.37}$$

On the curves (4.35)-(4.37), two real values of λ-roots collide by closing a gap, or they separate by opening a gap. Whenever two real λ-roots collide to close a gap, they become two complex conjugate roots, and so they identify the end-points of a gap. Vice versa, if two complex conjugate λ-roots become two real λ-roots, we expect that a gap appears. As a result, the (p_1, p_2)-plane is divided in domains identified by different number of gaps and branches.

Proposition 4.2.2. *The $\mathbf{S}_x$-spectrum has the gaps and branches structure described in*

Table 4.1: Gaps and branches structure.

Regions in the (p_1, p_2)-plane	$\#G$	$\#B$	λ-roots of $\mathcal{P}_z(0;\lambda)$
$0 < p_2 < \gamma \cap -p_2 < p_1 < p_2$	$2G$	$0B$	4 distinct and real
$\gamma < p_2 < p_1 \cap \gamma < p_1$	$2G$	$0B$	4 distinct and real
$\gamma < p_2 < -p_1 \cap \gamma < -p_1$	$2G$	$0B$	4 distinct and real
$p_2 > \gamma \cap -p_2 < p_1 < p_2$	$1G$	$1B$	2 distinct and real, 2 complex conjugate
$p_1 < p_2 < -p_1 \cap p_1 < 0$	$1G$	$1B$	2 distinct and real, 2 complex conjugate
$-p_1 < p_2 < p_1 \cap p_1 > 0$	$1G$	$1B$	2 distinct and real, 2 complex conjugate
$p_2 < 0 \cap p_2 < p_1 < -p_2$	$0G$	$2B$	2 pairs of complex conjugate roots

table 4.1. where the polynomial γ is defined as

$$\gamma = 27p_1^2 - (p_2 - 1)(p_2 + 8)^2, \tag{4.38}$$

and the intervals in the parameter space are written in implicit form.

The classification of gaps and branches in the (p_1, p_2)-plane has been obtained by studying simultaneously the sign of the discriminant $\Delta_\lambda(\mathcal{P}_Z(0;\lambda))$ and the signs of the following polynomials [117]

$$\Delta_{01} = 8a_2a_4 - 3a_3^2, \tag{4.39a}$$

$$\Delta_{02} = 64a_0a_4^3 - 16a_1a_3a_4^2 - 16a_2^2a_4^2 + 16a_2a_3^2a_4 - 3a_3^4, \tag{4.39b}$$

$$\Delta_{03} = 8a_1a_4^2 - 4a_2a_3a_4 + a_3^3, \tag{4.39c}$$

$$\Delta_{04} = 12a_0a_4 - 3a_1a_3 + a_2^2, \tag{4.39d}$$

[6] Note that the discriminant w.r.t. λ of both the discriminant $\Delta_z(P(z;\lambda))$ and of the polynomial $\mathcal{P}_Z(0;\lambda)$ is actually the same, although $\Delta_z(P(z;\lambda))$ and $\mathcal{P}_Z(0;\lambda)$ have opposite signs.

where a_j are the coefficients of [7]

$$\mathcal{P}_Z(0;\lambda) = a_4\lambda^4 + a_3\lambda^3 + a_2\lambda^2 + a_1\lambda + a_0. \tag{4.40}$$

Let us identify, case by case, the conditions on the polynomials (4.39a)-(4.39d) and on the discriminant $\Delta_\lambda(\mathcal{P}_Z(0;\lambda))$ within the regions in the (p_1, p_2)-plane [117].

- By imposing $\Delta_\lambda\mathcal{P}_Z(0;\lambda) > 0$, $\Delta_{01} < 0$ and $\Delta_{02} < 0$, we have 4 distinct real λ-roots which identify the four end-points of 2 gaps and 0 branches.
- When $\Delta_\lambda\mathcal{P}_Z(0;\lambda) < 0$, we have 2 distinct real λ-roots and 2 complex conjugate λ-roots. In this case we have 1 gap and 1 branch.
- The conditions to obtain the regions in the (p_1, p_2)-plane corresponding two pairs of complex conjugate roots, are

  1. $\Delta_\lambda\mathcal{P}_Z(0;\lambda) > 0$, $\Delta_{01} > 0$ and $\Delta_{02} > 0$;
  2. $\Delta_\lambda\mathcal{P}_Z(0;\lambda) > 0$, $\Delta_{01} < 0$ and $\Delta_{02} > \frac{\Delta_{01}^2}{4}$;
  3. $\Delta_\lambda\mathcal{P}_Z(0;\lambda) > 0$, $\Delta_{01} > 0$ and $\Delta_{02} < 0$.

  Thus, we have 0 gaps and 2 branches.
- The condition to have 4 real roots all coincident, that is $\Delta_\lambda\mathcal{P}_Z(0;\lambda) = 0$, $\Delta_{04} = 0$ and $\Delta_{02} = 0$, is never satisfied.
- There are some extreme points of gaps domains. Indeed, the condition $\Delta_\lambda\mathcal{P}_Z(0;\lambda) = 0$ and $\Delta_{04} = 0$ is verified at the points $(4, 4)$ and $(-4, 4)$ for which we have a triple real root and a simple real root, thus we have 1 gap. The condition $\Delta_\lambda\Delta_z\mathcal{P}(z) = 0$, $\Delta_{02} = 0$ and $\Delta_{01} < 0$ is verified only at the point $(0, 0)$ for which we have two double real roots and 1 gap.
- Furthermore, there are some exceptional points for which, although they are corresponding to 0 gaps, the nature of the roots is different from that in their neighbourhood. In more detail, we have two pairs of complex conjugate λ-roots at the point

[7] Strictly speaking, we should have written

$$-\mathcal{P}_Z(0;\lambda) = a_4\lambda^4 + a_3\lambda^3 + a_2\lambda^2 + a_1\lambda + a_0,$$

but the sign on front of the polynomial $\mathcal{P}_Z(0;\lambda)$ is completely irrelevant after the computation of the discriminant w.r.t. λ.

$(0,-8)$, that is when $\Delta_\lambda \mathcal{P}_Z(0;\lambda)=0$ and $\Delta_{02}>0$, or a real double root and two complex conjugate roots for 1) $\Delta_\lambda \mathcal{P}_Z(0;\lambda)=0$ and $\Delta_{02}>0$, or 2) $\Delta_\lambda \mathcal{P}_Z(0;\lambda)=0$, $\Delta_{01}>0$ and $\Delta_{03}\neq 0$, and the corresponding domains belonging to the curves D_1 and D_2, and they are:

$$-8+4\sqrt{3}<p_2<0, \quad \{p_1=p_2 \cup p_1=-p_2\}, \tag{4.41a}$$

$$p_2<-8-4\sqrt{3}, \quad \{p_1=p_2 \cup p_1=-p_2\}, \tag{4.41b}$$

or,

$$-4<p_2<-20+8\sqrt{6}, \quad \{p_1=p_2 \cup p_1=-p_2\}, \tag{4.42a}$$

$$-20-8\sqrt{6}<p_2<-4, \quad \{p_1=p_2 \cup p_1=-p_2\}. \tag{4.42b}$$

We have also 4 real distinct λ-roots for $\Delta_\lambda \mathcal{P}_Z(0;\lambda)>0$, $\Delta_{01}<0$ and $0<\Delta_{02}<\frac{\Delta_{01}^2}{4}$

Other limiting cases can be discussed, but this is not the aim of our research work because we are interested in generic cases only.

The same classification for branches and gaps was obtained in [64] for the CNLS equation.

Split Gaps

Looking at the expressions (4.35), (4.36) and (4.37), we deduce that the gaps structure described so far can change by varying p_1 and p_2 only. Nevertheless, since $\mathcal{P}_W(0;\lambda)=\mathcal{P}_Z(0;\lambda)\mathcal{R}^2(\lambda)$, $\mathcal{P}_W(0;\lambda)$ can be zero when $\mathcal{R}(\lambda)=0$ also if $\mathcal{P}_Z(0;\lambda)$ is negative or positive. Since $\mathcal{R}(\lambda)$ is a first degree polynomial and it has real coefficients, the equality $\mathcal{R}(\lambda)=0$ may be verified just at one point of the real $\mathbf{S}_x$-spectrum [8]. Moreover, because of the expression of $\mathcal{R}(\lambda)$, for values of p_1 and p_2 varying in an interval so that we have a fixed number of gaps, this point can move inside or can coincide with an endpoint of gap. Since $\mathcal{R}(\lambda)$ depends on p_3 as well, we expect that the regions in the (p_1,p_2)-plane

[8] This point is also a real double-zero of the polynomial $\mathcal{R}^2(\lambda)$.

in which the zero of $\mathcal{R}(\lambda)$ is inside a gap move by varying p_3. Moreover, when $\mathcal{R}(\lambda) = 0$ then $\mathcal{P}_W(0;\lambda) = 0$ too, and for this reason we have only two possible scenarios:

1. $\mathcal{P}_Z(0;\lambda) > 0$ and the double-zero is within a gap, i.e. a split-gap;
2. $\mathcal{P}_Z(0;\lambda) = 0$ and the double-zero is a triple-zero of the polynomial $\mathcal{P}_W(0;\lambda)$, and it coincides with the end-point of a gap.

We underline that the situation in which $\mathcal{P}_Z(0;\lambda) < 0$ and $\mathcal{P}_W(0;\lambda) = 0$ never occurs because of the Proposition 4.2.1.
We define a transition in the evolution of gaps structure, also in the case in which, a split-gap appears because a point falls within an existent gap (or, vice versa, a split-gap becomes an effective gap because a point shifts from the inside of a gap to the end-point of the gap). To see for which values of the parameters p_j such a transition occurs, we have to understand for which values of the parameters p_1, p_2 and p_3 the zero of $\mathcal{R}(\lambda)$ collides with a zero of $\mathcal{P}_Z(0;\lambda)$, or, in other words, when $\mathcal{P}_Z(0;\lambda)$ has a common root with the polynomial $\mathcal{R}(\lambda)$. This analysis is conducted by studying the resultant with respect to λ between the two polynomials $\mathcal{P}_Z(0;\lambda)$ and $\mathcal{R}(\lambda)$. The discriminant with respect to λ of the product $\mathcal{P}_Z(0;\lambda)\mathcal{R}^2(\lambda)$ does not give us further information about this kind of transition, since the quantity [9]

$$\begin{aligned}\Delta_\lambda(\mathcal{P}_Z(0;\lambda)\mathcal{R}^2(\lambda)) &= \Delta_\lambda(\mathcal{P}_Z(0;\lambda)\mathcal{R}(\lambda))(\mathrm{Res}_\lambda(\mathcal{P}_Z(0;\lambda)\mathcal{R}(\lambda),\mathcal{R}(\lambda)))^2\Delta_\lambda(\mathcal{R}(\lambda)) = \\ &= \Delta_\lambda\mathcal{P}_Z(0;\lambda)(\Delta_\lambda\mathcal{R}(\lambda))^2(\mathrm{Res}_\lambda(\mathcal{P}_Z(0;\lambda),\mathcal{R}(\lambda)))^4(\mathrm{Res}_\lambda(\mathcal{R}(\lambda),\mathcal{R}(\lambda)))^2,\end{aligned} \tag{4.43}$$

is always zero because of the resultant $\mathrm{Res}_\lambda(\mathcal{R}(\lambda),\mathcal{R}(\lambda)) = 0$. However, the other terms might or might not be zero. Therefore, the useful quantity to analyse is the resultant $\mathrm{Res}_\lambda(\mathcal{P}_Z(0;\lambda),\mathcal{R}(\lambda))$: in other words, we are interested to understand for which values of the parameters p_1, p_2 and p_3 the resultant

$$\begin{aligned}\mathrm{Res}_\lambda(\mathcal{P}_Z(0;\lambda),\mathcal{R}(\lambda)) &= \left(p_3^2\left(-2p_1p_3+(p_2-1)p_3^2+p_2+2\right)-1\right)^2 \\ &\left(p_3\left(p_3^3\left(p_1^2-4p_2+4\right)-2p_1(p_2-2)p_3^2-4p_1+(p_2(p_2+4)-8)p_3\right)+4\right),\end{aligned} \tag{4.44}$$

is zero or not. In the discussion below, we shall prove that, in (4.44), the polynomial factor that appears squared does not correspond to any transition, while the other polynomial

[9] Note that $\Delta_\lambda\mathcal{R}(\lambda) = 1$.

factor identifies a curve bounding the regions in the (p_1, p_2)-plane where there exist split gaps; we define such a curve as,

$$\mathcal{D}_4 = \{p_1,\, p_2,\, p_3 \in \mathbb{R} : R_4(p_1, p_2, p_3) = 0\}, \tag{4.45}$$

where the polynomial $R_4(p_1, p_2, p_3) = R_4$ is

$$R_4 = p_3\left(p_3^3\left(p_1^2 - 4p_2 + 4\right) - 2p_1(p_2 - 2)p_3^2 - 4p_1 + (p_2(p_2 + 4) - 8)p_3\right) + 4. \tag{4.46}$$

Proposition 4.2.3. *In the (p_1, p_2)-plane, the curve $\mathcal{D}_4$, defined in (4.45), identifies the transition curve for the existence of split gaps. In particular, once the values of p_3 is fixed, the values of the parameters p_1 and p_2 for which the polynomial R_4 is negative correspond to regions where there are split gaps.*

Proof. Let us write $\mathcal{P}_Z(0;\lambda)$ and $\mathcal{R}(\lambda)$ in a more general form

$$\mathcal{P}_Z(0;\lambda) = a_4\lambda^4 + a_3\lambda^3 + a_2\lambda^2 + a_1\lambda + a_0, \tag{4.47}$$

$$\mathcal{R}(\lambda) = b_1\lambda + b_0, \tag{4.48}$$

and let τ_j and θ_j be the roots of $\mathcal{P}_Z(0;\lambda)$ and $\mathcal{R}(\lambda)$ respectively, so that the resultant with respect to λ can be written as

$$\mathrm{Res}_\lambda(\mathcal{P}_Z(0;\lambda), \mathcal{R}(\lambda)) = a_4 b_1^4 \prod_{k=1}^{4}\prod_{j=1}^{1}(\tau_k - \theta_j). \tag{4.49}$$

Let us suppose that, say, τ_j are all real and distinct, such that we have two gaps. Let us consider the initial situation in which $\theta_1 = \tau_1 < \tau_2 < \tau_3 < \tau_4$, which corresponds to having (4.49) equal to zero and the point θ_1 coinciding with an end-point of a gap. Then, we vary the values of the parameters p_1 and p_2 so that θ_1 increases until we have $\tau_1 < \theta_1 < \tau_2 < \tau_3 < \tau_4$, and we have that (4.49) is negative [10] and θ_1 is inside the gap. In particular, we have the so called split-gap [11]. Thus, the resultant (4.49), and so (4.44), is negative for this kind of gap structure. Finally, we conclude that the relevant part of the resultant is only

[10] $a_4 b_1^4$ is positive, because $a_4 = 4$.

[11] If, per absurdum, it was $\mathcal{R}(\lambda) = 0$ also in the case in which $\mathcal{P}_Z(0;\lambda) < 0$, then (4.49) would be positive for the ordering $\tau_1 < \tau_2 < \theta_1 < \tau_3 < \tau_4$.

the second polynomial. Indeed, by rescaling λ by $\tilde{\lambda} = a\lambda$, with $a \in \mathbb{R}$, in both $\mathcal{P}_Z(0;\lambda)$ and $\mathcal{R}(\lambda)$. In this way, we get the resultant $Res_\lambda(\mathcal{P}_Z(0;\tilde{\lambda}), \mathcal{R}(\tilde{\lambda})) = a^4 Res_\lambda(\mathcal{P}_Z(0;\lambda), \mathcal{R}(\lambda))$. Therefore, λ can be rescaled to eliminate the squared polynomial, or, in other words, such a polynomial is arbitrary.

Let us consider another situation in which we have two distinct real roots and two complex conjugate roots (1G 1B), and we focus only on the product $\prod_{k=1}^{4}\prod_{j=1}^{1}(\tau_k - \theta_j)$. One can show that the product between the terms $(\tau_k - \theta_j)$ corresponding to the two complex conjugate τ_k is always real and positive. Indeed, let $\tau_1 = c + i\,d$ and $\tau_2 = \tau_1^* = c - i\,d$ be the two complex conjugate roots. Since θ is always real, then the following product

$$(\tau_1 - \theta)(\tau_1^* - \theta) = (c + id - \theta)(c - id - \theta) = c^2 + d^2 + \theta^2 - 2\theta = d^2 + (\theta - c)^2, \quad (4.50)$$

is positive. At this point, the proof above on the case for the four distinct real roots can be repeated also here, by considering only the two factors of the resultant corresponding to the two distinct real roots τ_k.

The proof for the other cases, showed in table 4.1, is straightforward. □

By taking into account the regions associated to split gaps, a general classification of gaps structure is given below.

Proposition 4.2.4. *Besides the gaps structure described in table 4.1, the* $\mathbf{S}_x$*-spectrum may feature split gaps for the following choices of the parameters:*

1) *if* $-1 < p_3 < 1$, $\sigma_1 < p_1 < \sigma_2$ *and* $p_2 > 1 - \frac{1}{p_3^2}$ *with* $1 - \frac{1}{p_3^2} < 0$*;*

2) *if* $p_3 < -1$ *or* $p_3 > 1$, $\sigma_1 < p_1 < \sigma_2$ *and* $p_2 > 1 - \frac{1}{p_3^2}$ *with* $1 - \frac{1}{p_3^2} > 0$*;*

where

$$\sigma_1 = \frac{2}{p_3^3} + \frac{p_2 - 2}{p_3} - \frac{2|p_3^2 - 1|\sqrt{1 + (p_2 - 1)p_3^2}}{|p_3|^3}, \quad (4.51)$$

$$\sigma_2 = \frac{2}{p_3^3} + \frac{p_2 - 2}{p_3} + \frac{2|p_3^2 - 1|\sqrt{1 + (p_2 - 1)p_3^2}}{|p_3|^3}, \quad (4.52)$$

and the intervals in **1)** *and* **2)** *are written in implicit form.*

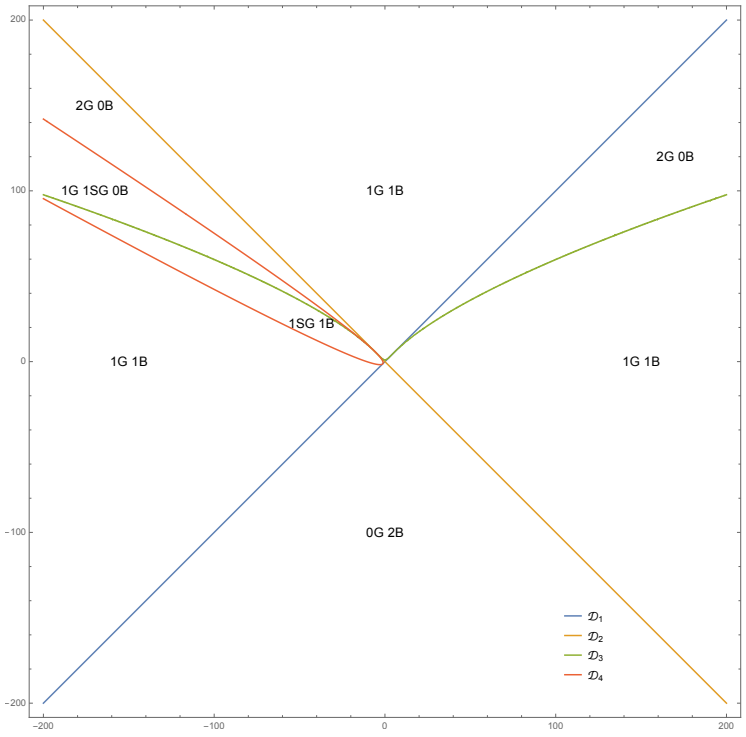

(a) (p_1, p_2)-plane, $p_3 = -0.6$.

Figure 4.1: (p_1, p_2)-plane, when $p_3 = -0.6$. Split gaps appear inside the region bounded by the curve $\mathcal{D}_4$.

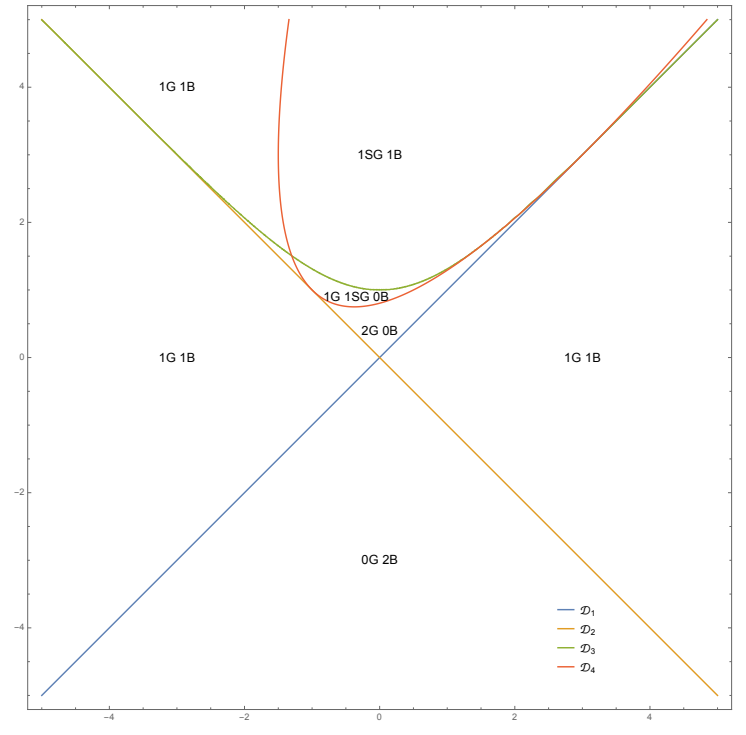

(a) (p_1, p_2)-plane, $p_3 = 2$.

Figure 4.2: (p_1, p_2)-plane, when $p_3 = 2$. Split gaps appear inside the region bounded by the curve $\mathcal{D}_4$.

The Figures 4.1(a) and 4.2(a) show where there exist split gaps. By overlaying the results of the Table 4.1 to the findings of the Proposition 4.2.4, the total number of gaps and split gaps is predicted. For example, looking at the Figure 4.1(a), we have a total of 1G and 1SG in the region between the curves $\mathcal{D}_3$ and $\mathcal{D}_4$, while we have 1G and 1SG in the region between $\mathcal{D}_4$ and $\mathcal{D}_3$. Instead, in Figure 4.2(a), the region below $\mathcal{D}_3$ has 1G and 1SG, while that one above $\mathcal{D}_3$ has 1G and 1SG.

Symmetries and Gaps

In the following discussion, we take advantage of the symmetries in the (p_1, p_2)-plane to classify gaps as p_3 changes. Indeed, since $\Delta_\lambda \mathcal{P}_Z(0;\lambda)$ is invariant under transformations $p_1 \to -p_1$ and $p_2 \to p_2$, the plot of the curves $\mathcal{D}_1$, $\mathcal{D}_2$ and $\mathcal{D}_3$ are symmetric with respect to the p_2-axis. The curve $\mathcal{D}_4$ depends also on p_3, and it has symmetries $p_1 \to -p_1$, $p_2 \to p_2$ and $p_3 \to -p_3$. Nevertheless, for finite values of p_3, such a curve is not symmetric with respect to p_2-axis and moves in the (p_1, p_2)-plane as p_3 varies. In particular, by changing p_3 to $-p_3$, the $\mathcal{D}_4$ plot is reflected with respect to p_2-axis. The curve $\mathcal{D}_4$ can be written by expressing p_2 as a function of p_1 and p_3

$$p_2(p_1, p_3) = -2 + p_3 p_1 + 2p_3^2 \pm \frac{2|p_3 - p_3^3|\sqrt{p_3 p_1 + p_3^2 - 1}}{p_3^2}, \tag{4.53}$$

and by changing $p_3 \to -p_3$, we get

$$p_2(p_1, -p_3) = -2 - p_3 p_1 + 2p_3^2 \pm \frac{2|p_3 - p_3^3|\sqrt{-p_3 p_1 + p_3^2 - 1}}{p_3^2}, \tag{4.54}$$

that is $p_2(p_1, -p_3) = p_2(-p_1, p_3)$, and one can define

$$\bar{p}_2(\bar{p}_1, p_3) = -2 + p_3 \bar{p}_1 + 2p_3^2 \pm \frac{2|p_3 - p_3^3|\sqrt{p_3 \bar{p}_1 + p_3^2 - 1}}{p_3^2}, \tag{4.55}$$

where $\bar{p}_1 = -p_1$ and the bar denotes the parameters p_1 and p_2 after the transformations. Thus, $\bar{p}_2(\bar{p}_1, p_3)$ is the curve $p_2(p_1, p_3)$, reflected with respect to the p_2-axis.
On the other hand, as p_3 approaches infinity, $\mathcal{D}_4$ becomes symmetric to the p_2-axis. In the following, we shall discuss the symmetries of $\mathcal{D}_4$ in more detail.

Proposition 4.2.5. *For $-1 < p_3 < 1$, and for $p_3 < -1$ or $p_3 > 1$, the curve $\mathcal{D}_4$ is asymmetric with respect to the p_2-axis. For $p_3 \to \pm\infty$, D_4 is symmetric with respect to p_2-axis. For $p_3 = 0$, $\mathcal{D}_4$ disappears. For $p_3 = 1$, $\mathcal{D}_4$ coincides with $\mathcal{D}_1$, while for $p_3 = -1$,*

$\mathcal{D}_4$ coincides with $\mathcal{D}_2$. For $p_3 = 0$, $p_3 = 1$ and $p_3 = -1$, there are not split gaps and the gaps structure is described only by table 4.1.

Proof. By looking at the expression of $\mathcal{D}_4$ written as a function of p_1, i.e. (4.53), we see that $p_2(p_1)$ is neither even nor odd. Nevertheless, by dividing (4.45) by the maximum power of p_3, after taking the limit $p_3 \to \pm\infty$, we obtain

$$p_2(p_1) = 1 - \frac{p_1^2}{4}, \tag{4.56}$$

which is clearly an even function, and so it is symmetric with respect to the p_2-axis.
Furthermore, the domain of the function (4.53) is

$$\left\{ \forall p_3 \in \mathbb{R}/_{\{0\}},\ (p_1 \in \mathbb{R} : p_1 \geq \left(\frac{1}{p_3} - p_3 \right) \right\}. \tag{4.57}$$

The curve $\mathcal{D}_4$ is not defined for $p_3 = 0$. In addition, once we chose $p_3 = \pm 1$, (4.53) can be considered as a function of p_1 only, whose explicit expression is

$$p_2(p_1) = \pm p_1, \tag{4.58}$$

that are $\mathcal{D}_1$ and $\mathcal{D}_2$ for $p_3 = 1$ and $p_3 = -1$, respectively [12]. In these cases the curve $\mathcal{D}_4$ becomes $(p_1 - p_2)^2$ or $(p_1 + p_2)^2$, which are positive and, as a result, there are no split gaps, and the discussion reduces to Table 4.1 only. □

Because of curve symmetries on the (p_1, p_2)-plane, here and thereafter we consider only negative values of p_3.
The Figures 4.3 and 4.4 are plots of the (p_1, p_2)-plane with the entire topological classification of gaps and branches components for $p_3 = -0.6$. We choose $p_3 = -0.6$ without loss of generality, indeed for $|p_3| > 1$ the curve $\mathcal{D}_4$ moves in the regions with 1G and 0G by creating a split-gap, and the discussion is the same.

4.3 Complex Spectrum

In the previous section we have considered the characteristic polynomial $P(w; \lambda)$ and we have analysed the situations in which two w_j-roots coincide. We can summarise the classification of λ-roots at which at least one difference $w_j - w_k$ is zero, i.e. $\xi = 0$:

[12] The domain of the function $p_2(p_1)$ becomes $\{p_1 \in \mathbb{R}\}$ for this case.

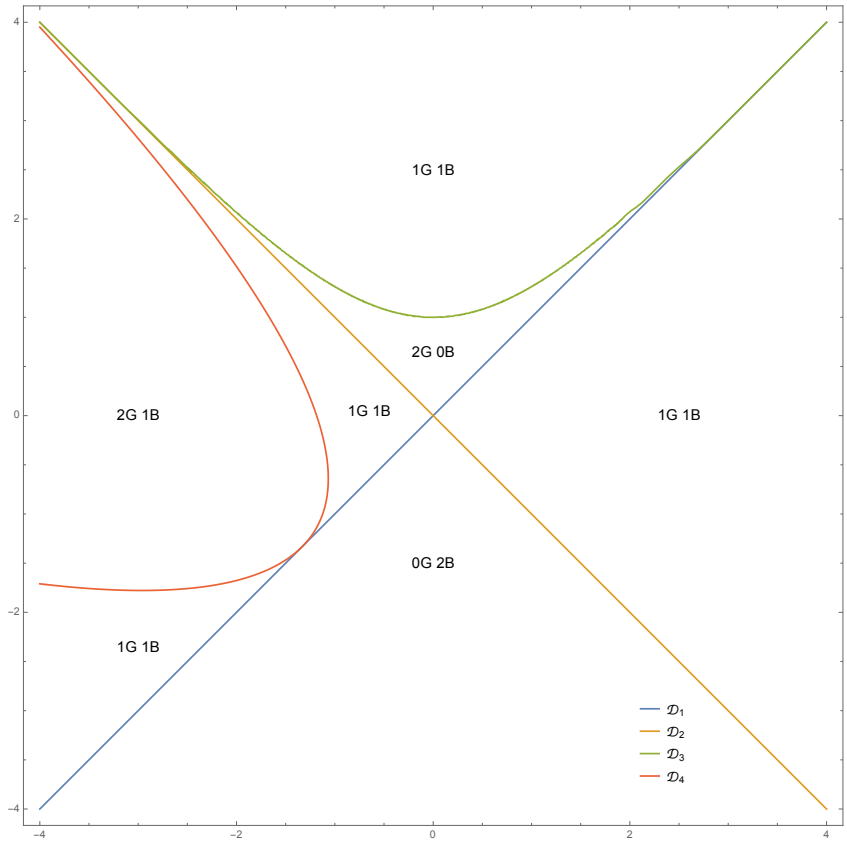

Figure 4.3: (p_1, p_2)-plane, $p_3 = -0.6$

1. 4 distinct real roots and/or 1 double real root (2G 0SG 0B or 1G 1SG 0B);

2. 2 distinct real roots, 2 complex conjugate roots and/or 1 double root (1G 0SG 1B or 0G 1SG 1B);

3. 2 pairs of complex conjugate roots (0G 0SG 2B).

Let us consider the polynomial of the squares of the differences $\mathcal{P}_W(\xi;\lambda)$, defined in (4.3), which is a sixth degree polynomial in λ and a third degree polynomial in ξ^2. We construct the polynomial $\mathcal{Q}(\xi) \equiv \mathcal{Q}(\xi; p_1, p_2, p_3)$, that is the discriminant with respect to λ of $\mathcal{P}_W(\xi;\lambda)$

$$\mathcal{Q}(\xi) \equiv \Delta_\lambda \, \mathcal{P}_W(\xi;\lambda)\,. \tag{4.59}$$

Then, we perform the polynomial factorisation of $\mathcal{Q}(\xi)$ with respect to ξ. This results in the following form

$$\mathcal{Q}(\xi) = \xi \, \mathcal{Q}_1^2(\xi) \, \mathcal{Q}_2(\xi)\,, \tag{4.60}$$

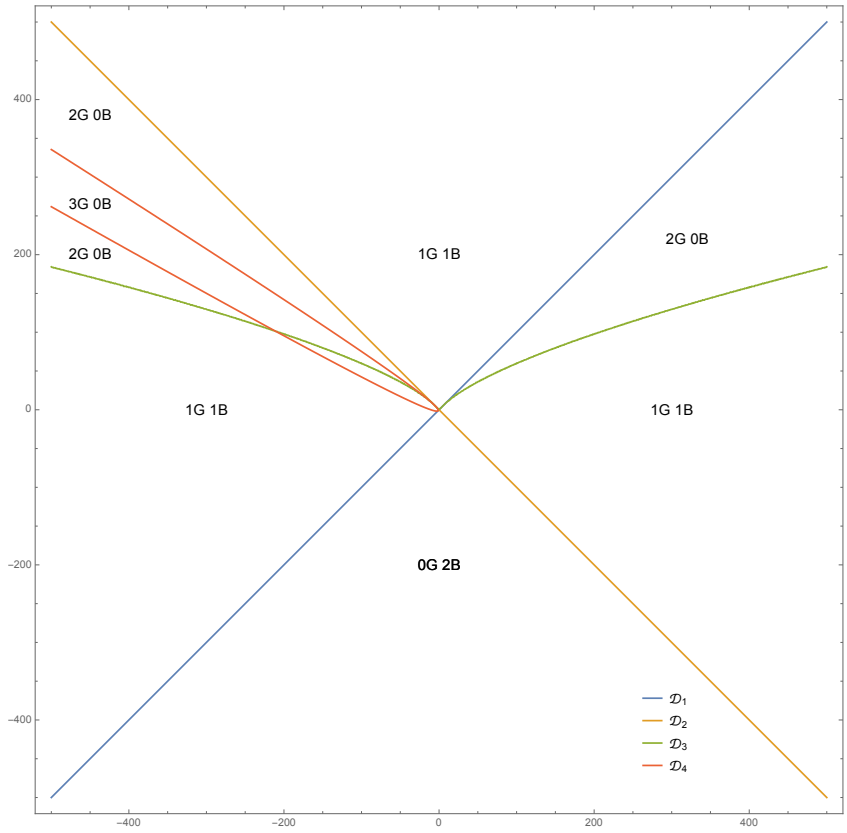

Figure 4.4: (p_1, p_2)-plane, $p_3 = 2$

where $\mathcal{Q}_1(\xi) \equiv \mathcal{Q}_1(\xi; p_1, p_2, p_3)$ and $\mathcal{Q}_2(\xi) \equiv \mathcal{Q}_2(\xi; p_1, p_2, p_3)$ are two polynomials in the variable ξ, whose degree are four and six respectively, and $\mathcal{Q}_{1,2}(0) \neq 0$. We will refer to $\mathcal{Q}_1$ and $\mathcal{Q}_2$ as the *even* and *odd* parts of $\mathcal{Q}(\xi)$, respectively.

Proposition 4.3.1. *Let $\bar{\xi}$ be the largest positive root of $\mathcal{Q}_2(\xi)$. Then, for $\xi > \bar{\xi}$, all the λ-roots of $\mathcal{P}_W(\xi; \lambda)$ are real; therefore, the stability spectra always contains part of the real axis and never features a gap containing the point at infinity.*

Proof. The polynomial of the squares of the differences is written as (Appendix J)

$$\mathcal{P}_W(\xi; \lambda) = \xi^3 - f_1 \xi^2 + \frac{f_1^2}{4}\xi - \frac{f_2}{6}, \tag{4.61}$$

where $f_1 \equiv f_1(\lambda; p_1, p_2, p_3)$ and $f_2 \equiv f_2(\lambda; p_1, p_2, p_3)$ are polynomials whose unknown is the spectral parameter λ and they are depending also by the physical parameters p_1, p_2 and p_3. In particular, for the 3WRI model, these polynomials have the general expressions

$$f_1 = \alpha_0 + \alpha_1 \lambda + \alpha_2 \lambda^2, \tag{4.62a}$$

$$f_2 = \beta_0 + \beta_1\lambda + \beta_2\lambda^2 + \beta_3\lambda^3 + \beta_4\lambda^4 + \beta_5\lambda^5 + \beta_6\lambda^6. \tag{4.62b}$$

The polynomial of the squares of the differences (4.61) vanishes for any λ-root

$$\xi^3 - f_1\xi^2 + \frac{f_1^2}{4}\xi - \frac{f_2}{6} = 0 \tag{4.63}$$

and, by diving (4.63) by ξ^3, we get the equation

$$1 - \frac{f_1}{\xi} + \frac{f_1^2}{4\,\xi^2} - \frac{f_2}{6\,\xi^3} = 0. \tag{4.64}$$

Since $\frac{1}{\xi} \to 0$ as $\xi \to +\infty$, we define $\frac{1}{\xi} \equiv \epsilon$, so that the equation (4.64) becomes

$$1 - f_1\epsilon + \frac{f_1^2}{4}\epsilon^2 - \frac{f_2}{6}\epsilon^3 = 0. \tag{4.65}$$

At this point, we note that for $\epsilon = 0$, we have the impossible equality $1 = 0$, that means all the three roots approach infinity as ϵ goes to zero. Thus, we deal with a singular perturbation problem and, in order to solve the equation (4.65), we set the rescaled variable $\lambda = \frac{y}{\delta(\epsilon)}$ into the equation (4.65) and substitute f_1 and f_2, scuh that

$$\begin{aligned} &1 + \alpha_0^2\frac{\epsilon^2}{4} - \alpha_0\epsilon - \frac{\beta_0\epsilon^3}{6} + \frac{y}{\delta}\left(\frac{\alpha_0\alpha_1}{2}\epsilon^2 - \alpha_1\epsilon - \frac{b_1}{6}\epsilon^3\right) + \frac{y^2}{2\delta^2}\alpha_0\alpha_2\epsilon^2 + \\ &+ \frac{y^2}{4\delta^2}\alpha_1^2\epsilon^2 - \frac{y^2}{\delta^2}\alpha_2\epsilon - \frac{y^2}{6\delta^2}\beta_2\epsilon^3 + \\ &+ \frac{y^3}{2\delta^3}\alpha_1\alpha_2\epsilon^2 - \frac{y^3}{6\delta^3}\beta_3\epsilon^3 + \frac{y^4}{4\delta^4}\alpha_2^2\epsilon^2 - \frac{y^4}{6\delta^4}\beta_4\epsilon^3 - \frac{y^5}{6\delta^5}\beta_5\epsilon^3 - \frac{y^6}{6\delta^6}\beta_6\epsilon^3 = 0. \end{aligned} \tag{4.66}$$

By using the principle of dominant balance, we require that at least two leading-order terms have the same order of magnitude. By imposing the condition

$$\frac{\epsilon^3}{\delta^5} = \frac{\epsilon^3}{\delta^6}, \tag{4.67}$$

we get

$$\delta = 1, \tag{4.68}$$

that gives us solutions not approaching infinity as $\epsilon \to 0$, so we have to rule out this choice. The right expression for δ is given by the condition

$$\frac{\epsilon^3}{\delta^6} = \frac{\epsilon^2}{\delta^4}, \tag{4.69}$$

hence,

$$\delta = \epsilon^{\frac{1}{2}}. \tag{4.70}$$

By substituting (4.70) in (4.66), we obtain

$$\begin{aligned} &1 + \frac{\alpha_0^2\epsilon^2}{4} - \alpha_0\epsilon - \frac{\beta_0\epsilon^3}{6} + \\ &+ y^2\left(\frac{\alpha_0\alpha_2\epsilon}{2} + \frac{\alpha_1^2\epsilon}{4} - \alpha_2 - \frac{\beta_2\epsilon^2}{6}\right) + y\left(\frac{1}{2}\alpha_0\alpha_1\epsilon^{3/2} - \alpha_1\sqrt{\epsilon} - \frac{1}{6}\beta_1\epsilon^{5/2}\right) + \\ &+ y^3\left(\frac{1}{2}\alpha_1\alpha_2\sqrt{\epsilon} - \frac{1}{6}\beta_3\epsilon^{3/2}\right) + y^4\left(\frac{\alpha_2^2}{4} - \frac{\beta_4\epsilon}{6}\right) - \frac{1}{6}\beta_5 y^5\sqrt{\epsilon} - \frac{\beta_6 y^6}{6} = 0. \end{aligned} \tag{4.71}$$

Therefore, we look for solutions of the kind[13]

$$y = y_0 + \epsilon^{\frac{1}{2}} y_1 + O(\epsilon)\,, \tag{4.72}$$

and by putting the expansion above into the equation (4.71) and collecting the terms with respect to equal powers of ϵ

$$\begin{aligned} &\sqrt{\epsilon}\left(\frac{1}{2}\alpha_1\alpha_2 y_0^3 - \alpha_1 y_0 + \alpha_2^2 y_0^3 y_1 - 2\alpha_2 y_0 y_1 - \frac{\beta_5 y_0^5}{6} - \beta_6 y_0^5 y_1\right) + \\ &+ \frac{\alpha_2^2 y_0^4}{4} - \alpha_2 y_0^2 - \frac{\beta_6 y_0^6}{6} + 1 + ... = 0, \end{aligned} \tag{4.73}$$

where we have neglected the terms $O(\epsilon)$.

By expanding and matching the coefficients of ϵ^n to zero, for $n = 0, 1$, we obtain the equations

$$1 - \alpha_2 y_0^2 + \frac{\alpha_2^2 y_0^4}{4} - \frac{\beta_6 y_0^6}{6} = 0, \tag{4.74a}$$

$$\frac{1}{2}\alpha_1\alpha_2 y_0^3 - \alpha_1 y_0 + \alpha_2^2 y_0^3 y_1 - 2\alpha_2 y_0 y_1 - \frac{\beta_5 y_0^5}{6} - \beta_6 y_0^5 y_1 = 0, \tag{4.74b}$$

whose solutions [14] are y_{0j} with $j = 1, ..., 6$. To find the order of the correction, we have to substitute the solution y_{0j} into the second equations and get y_{1j}. Thus the solutions are of the kind $y_j = y_{0j} + O(\epsilon^{\frac{1}{2}})$, $j = 1, ..., 6$. Moreover, y_{0j}^2 are all reals, in fact, if one

[13] Because of (4.70), the corrections to the roots must be a regular perturbation expansion in powers of $\epsilon^{\frac{1}{2}}$, otherwise we can not match powers of an expansion having only integral powers of ϵ.

[14] For the aim of this discussion the explicit expressions of y_{0j} are not necessary.

considers the polynomial (4.74a) as a third degree polynomial whose unknown is y_0^2, the discriminant is

$$\Delta_{y_0} = \frac{2}{27}\beta_6^3 \left(\alpha_2^3 - 9\beta_6\right)^2, \tag{4.75}$$

i.e.

$$\Delta_{y_0} = 6144 p_3^6 \left(p_3^2 - 1\right)^6 \left(1295 p_3^6 + 1298 p_3^4 + 431 p_3^2 + 48\right)^2, \tag{4.76}$$

and the condition [15] $\Delta_{y_0} \geq 0$ is satisfied $\forall p_3 \in \mathbb{R}$. In addition, by the Descartes' rule of signs, it results that y_{0j}^2 are all positive, hence y_{0j} are reals.
However, we are interested in finding λ, i.e.

$$\lambda_j = y_{0j}\epsilon^{-\frac{1}{2}} + O(1), \qquad j = 1, ..., 6, \tag{4.77}$$

and, coming back to the old variables, it turns out that

$$\lambda_j = y_{0j}\sqrt{\xi_j} + O(1), \qquad j = 1, ..., 6. \tag{4.78}$$

Finally, keeping in mind the assumption $\xi_j \in \mathbb{R}^+$, the roots λ_j are all reals. Furthermore, since y_{0j} are solutions of the polynomial (4.74a) and since $\alpha_2 = 2\left(3p_3^2 + 1\right) > 0$ and $\beta_6 = (4p_3^6 - 8p_3^4 + 4p_3^2) > 0$, $\forall p_3 \in \mathbb{R}$, by using the Descarte's rule for such a polynomial, we see there are exactly 3 positive and 3 negative roots. □

Let us impose a difference $w_j - w_k$ to be real and strictly positive, i.e. $\xi > 0$. By the formula (4.59), the values of ξ for which two λ-roots collide are those ones for which $\mathcal{Q}_2(\xi)$ vanishes. After that, $\mathcal{Q}_2(\xi)$ may change sign, that is, after a collision, two λ-roots may change their nature. In more detail, two real λ-roots may become complex and vice versa. Indeed, if the polynomial of the squares of the differences is regarded as a polynomial in λ, for any fixed ξ, we expect one of these scenarios:

a) 6 distinct real λ-roots;

b) 4 distinct real λ-roots and 2 complex conjugate λ-roots;

c) 2 distinct real λ-roots and 2 pairs of complex conjugate λ-roots;

[15] That is the condition for which y_{0j}^2 are three distinct real roots or multiple real roots.

d) 3 pairs of complex conjugate λ-roots.

As ξ varies, two or more of the above scenarios can coexist. However, the case d) never occurs. There is no interval of ξ in which all the roots are complex. In other words, $\forall \xi > 0$, there are at least two real roots. This is a consequence of the fact that the polynomial of the squares of the differences $\mathcal{P}_W(\xi;\lambda)$ is equal to the square of the polynomial of the differences $w_\ell - w_m$ (Appendix J). Since the polynomial of the differences has only real coefficients, it can have a pair of complex conjugated λ-roots at most. As a result, we expect two pairs of complex conjugate λ-roots at most for the polynomial of the squares of the differences.

In this section we focus on the complex subset of the $\mathbf{S}_x$-spectrum which may lead to instability in time (besides the point separating a split-gap). This part of the spectrum consists of open and closed continuous curves named branches and loops respectively. To understand how these curves appear, we have to imagine an initial situation in which the values of the spectral parameters λ are roots of the polynomial $\mathcal{P}_W(0;\lambda)$. Then, we impose the condition $\xi > 0$, so that the values of the spectral parameters λ are roots of the polynomial $\mathcal{P}_W(\xi;\lambda)$ $\forall \xi \in \mathbb{R}$. After that, one or more of the scenarios $a)$, $b)$ or $c)$ occur as ξ varies. For example, at $\xi = 0$, let us consider the initial condition for which we have 2 distinct real λ-roots and 2 complex conjugate λ-roots. Let us suppose that the polynomial $\mathcal{P}_W(\xi;\lambda)$ has 2 distinct real λ-roots and 2 complex conjugate λ-roots for some $\xi \in \mathbb{R}$. This means that all the real roots remain on the real axis and the 2 complex conjugate roots collide at some point on the real axis and then go to infinity necessarily on the real axis (see Proposition 4.3.1). In this case, the spectrum would be composed by 1G and 1B and 0L. However, several other situations can occur as ξ varies. For instance, let $b)$ be the next situation. We have that 2 real λ-roots become a pair of complex conjugate λ-roots. Since $\forall \xi > 0$ these couple of complex roots must remain conjugate (they are the roots of a polynomial with real coefficients) and, in addition, all the roots must be real as $\xi \to \infty$, instead of having a branch we have a loop. In this case, the spectrum would be composed by 1G 1B 1L.

A loop can be regarded as a branch closed on the real axis. Sometimes, the difference with a branch is that it is created by λ-roots not corresponding to $\xi = 0$. In any case, a loop comes from two initial real λ-roots, instead of two complex conjugate λ-roots, unlike a

branch. Nevertheless, there are some situations in which a loop is created by starting from real λ-roots associated to $\xi = 0$. As ξ varies, two real λ-roots cannot travel in a branch because, if that happens, they are forced to travel it again in order to come back on the real axis when $\xi \to \infty$ (see Proposition 4.3.1). For the same reason, two initial complex conjugate roots, starting form the ends of a branch, travel such a branch but never come back on it. Therefore, they collide on the real axis and, after that, approach infinity.

Proposition 4.3.2. *The λ-roots cannot be periodic functions of ξ.*

Proof. Since λ-roots are solutions of a polynomial, they can not be periodic. In particular, once the other parameters are fixed, let us suppose, that the λ-roots are periodic functions of ξ. Then the limit of $\lambda(\xi)$ as $\xi \to \infty$ is not convergent, because they are oscillating. Thus, the $\lambda(\xi)$ must be monotonic function of ξ. □

4.3.1 Loops Classification

In this subsection we give the loops classification and so the complete spectra classification. The (p_1, p_2)-plane is divided in regions in which the spectra have the same topology and the number of gaps and the number of branches are known in every region. After choosing the values of the parameters p_1, p_2 and p_3 in any of such regions, we use MATLAB codes in order to find the ξ-roots of the polynomial $\mathcal{Q}_2(\xi)$. Between these roots we select only the real and positive ξ-roots. If we find $\bar{\xi}_1$,...,$\bar{\xi}_N$ real and positive roots, we have to consider $N + 1$ intervals: from 0 to $\bar{\xi}_1$, from $\bar{\xi}_1$ to $\bar{\xi}_2$, etc... , until the last interval from $\bar{\xi}_N$ to $+\infty$. In this way, if the polynomial of the squares of the differences $\mathcal{P}_W(\xi;\lambda)$ is meant like a polynomial in the λ variable, every coefficient of such a polynomial is a function of the ξ variable. Then, we require every coefficient to be positive within every interval $\{\bar{\xi}_j, \bar{\xi}_{j+1}\}$, with $j = 1, ..., N-1$. After that, we see that the coefficients can change their sign inside intervals whose endpoints do not coincide with the ξ-roots of $\mathcal{Q}_2(\xi)$, we denote them as $\xi_1, ..., \xi_M$, and so further intervals appear in the ξ domain. We apply the Descartes rule of signs in all the intervals $\{\xi_j, \xi_{j+1}\}$, with $j = 1, ..., M-1$, and we see how many real positive, real negative and complex conjugate roots there are. Nevertheless, different cases may be present. For example, if we have three sign changes for the polynomial in λ and for the polynomial in $-\lambda$, then we may have 3 positive roots, 3 negative roots, or

3 positive roots, 1 negative root and 2 complex conjugate roots, or 3 positive roots, 1 negative root and 2 complex conjugate roots, or 1 positive root, 1 negative root and 2 pairs of complex conjugate roots. However, only one of these options is the real one. Therefore, we choose a generic point in every interval $\{\xi_j, \xi_{j+1}\}$, $j = 1, .., M-1$, and compute again the coefficients of the polynomial of the squares of the differences. We count the number of sign changes in every interval. Thus, we exclude all the options not corresponding to the real one. By this method, as ξ varies, we can imagine the dynamic of the λ-roots on the $\mathbf{S}_x$ spectrum, and so suppose the creation of a new spectrum component, or when two λ-roots collide to return to the real axis.

Moreover, we write down a formula linking the number of branches, loops and twisted loops:

$$\#TL + 2\#L + \#B = \#\xi^+, \tag{4.79}$$

where ξ^+ stands for the positive roots of $\mathcal{Q}_2(\xi)$.

4.3.2 Spectra Classification: Descartes Rule of Signs and Sturm Chains

Here we give a detailed, but general, description of the procedure used to obtain the topological classification of the spectra in the (p_1, p_2)-plane. Then, we will apply this procedure to any region in the parameter space with a particular number of gaps and branches.

Let $P(x)$ be a polynomial in x with real coefficients, and let $\deg(P)$ be its degree. Let us suppose $P(x)$ is ordered by descending variable exponent, then the number of positive roots of the polynomial is equal to the number of sign differences between consecutive nonzero coefficients, or is less than it by en even number. Multiple roots are counted separately. In order to obtain the number of negative roots, we substitute $-x$ into the polynomial $P(x)$ to get $Q(x) \equiv P(-x)$, and we apply the Descartes rule of sign to $Q(x)$. If, for instance, $P(x)$ is a third degree polynomial, and the sequence of successive signs for $P(x)$ is $\{+ + - -\}$, we expect 1 positive root. On the other hand, let us suppose $Q(x)$ has the sequence of successive signs $\{- + + -\}$. Then, the polynomial $Q(x)$ has 2 positive roots and the polynomial $P(x)$ has 2 negative roots. Since the number of complex roots must be equal to $\deg(P)$, the minimum number of strictly complex roots is $\deg(P) - (p + n)$,

where p denotes the number of positive roots, and n denotes the number of negative roots. Thus, if we apply the Descartes rule of signs to both $P(x)$ and $Q(x)$, and the sum of the number of their positive roots does not match $\deg(P)$, we expect the polynomial $P(x)$ to have complex roots.

We apply the Descartes rule of signs to the polynomial of the squares of the differences $\mathcal{P}_W(\xi;\lambda)$, regarded as polynomial in λ, for any choice of the parameters p_1, p_2 and p_3. The polynomial $\mathcal{P}_W(\xi;\lambda)$ is a sixth degree polynomial and the coefficients of λ^6 and of λ^5 are constants and so independent on ξ. In other words, their signs are the same as ξ varies. However, the other coefficients are depending on ξ, and so their sign can change as ξ varies. Thus, after choosing the values of p_1, p_2 and p_3, we get

$$\mathcal{P}_W(\xi;\lambda) = g_6\lambda^6 + g_5\lambda^5 + g_4(\xi)\lambda^4 + g_3(\xi)\lambda^3 + g_2(\xi)\lambda^2 + g_1(\xi)\lambda + g_0(\xi), \qquad (4.80)$$

where g_6 and g_5 are numbers, while $g_j(\xi)$,with $j = 0, 1, 2, 3, 4$, are polynomials in ξ.

The trick is to require some coefficients to be positive and see for which value of ξ this condition is satisfied. For instance, let $\bar{\xi}_1$ and $\bar{\xi}_2$ be the two values of ξ at which $\mathcal{Q}(\xi)$, i.e. $\mathcal{Q}_2(\xi)$, changes sign. We impose the conditions $g_j(\xi) > 0$, $\forall j = 1, 2, 3, 4$, in every interval $0 < \xi < \bar{\xi}_1$, $\bar{\xi}_1 < \xi < \bar{\xi}_2$ and $\bar{\xi}_2 < \xi < +\infty$. Sometimes, it will happen that some polynomial coefficient is negative, for example, for $0 < \xi < \xi_1 < \bar{\xi}_1$ and instead positive for $\xi_1 < \xi < \bar{\xi}_1$. In such case, we will split the ξ-domain in intervals as $[0, \xi_1]$, $[\xi_1, \xi_2]$, $[\xi_2, \xi_3]$, $[\xi_3, +\infty)$, where we have redefined $\bar{\xi}_1 = \xi_2$ and $\bar{\xi}_2 = \xi_3$. Then, in every of this interval we apply the Descartes rule of sign. We choose a particular value of ξ, say, into the interval $\{0, \xi_1\}$, substitute it in the polynomial $\mathcal{P}_W(\xi;\lambda)$ and count the sign changes. For example, we could have the sequence of signs $\{+ + - - - + -\}$, that is associated to the possibilities: 3 positive and 1 complex conjugate λ-roots, or 1 positive and 2 complex conjugate λ-roots. Whereas, for the polynomial $\mathcal{P}_W(\xi;\lambda)$ after substituting $\lambda \to -\lambda$, we have the sequence of signs $\{+ + - + - - -\}$ associated to the possibilities: 3 negative and 0 complex conjugate λ-roots, or 1 negative and 2 complex conjugate λ-root. By combining altogether the sequences of signs we obtain the possibilities: 3 positive and 3 negatives λ-roots, 3 positive (resp. 3 negative), 1 negative (resp. 1 positive) and 2 complex conjugate λ-roots. After that, we will repeat the same procedure by choosing a particular value of ξ into the other intervals.

Once we have the intervals in which the structure of the algebraic curves in the λ-plane may change, we will apply the Sturm chains method to the polynomial $\mathcal{P}_W(\xi;\lambda)$. First

of all, we choose a value of ξ in every interval $[0,\xi_1]$,$[\xi_1,\xi_2]$, $[\xi_2,\xi_3]$ and $[\xi_3,+\infty)$, and substitute this value of ξ in the polynomial of the squares of the differences which becomes dependent only on λ, i.e. $\mathcal{P}_W(\lambda)$. From here, we construct the Sturm chain $\{\mathcal{P}_W^{(j)}\}_{j=0}^{6} = \{\mathcal{P}_W^{(0)},\mathcal{P}_W^{(1)},\mathcal{P}_W^{(2)},\mathcal{P}_W^{(3)},\mathcal{P}_W^{(4)},\mathcal{P}_W^{(5)},\mathcal{P}_W^{(6)}\}$ for every fixed ξ in any interval $[0,\xi_1]$, $[\xi_1,\xi_2]$, $[\xi_2,\xi_3]$ and $[\xi_3,+\infty)$:

$$
\begin{aligned}
\mathcal{P}_W^{(0)}(\lambda) &= \mathcal{P}_W(\lambda),\\
\mathcal{P}_W^{(1)}(\lambda) &= \frac{d}{d\lambda}\mathcal{P}_W^{(0)}(\lambda),\\
\mathcal{P}_W^{(2)}(\lambda) &= -\mathrm{Remainder}\left(\mathcal{P}_W^{(0)}(\lambda),\mathcal{P}_W^{(1)}(\lambda)\right),\\
\mathcal{P}_W^{(3)}(\lambda) &= -\mathrm{Remainder}\left(\mathcal{P}_W^{(1)}(\lambda),\mathcal{P}_W^{(2)}(\lambda)\right),\\
\mathcal{P}_W^{(4)}(\lambda) &= -\mathrm{Remainder}\left(\mathcal{P}_W^{(2)}(\lambda),\mathcal{P}_W^{(3)}(\lambda)\right),\\
\mathcal{P}_W^{(5)}(\lambda) &= -\mathrm{Remainder}\left(\mathcal{P}_W^{(3)}(\lambda),\mathcal{P}_W^{(4)}(\lambda)\right),\\
\mathcal{P}_W^{(6)}(\lambda) &= -\mathrm{Remainder}\left(\mathcal{P}_W^{(4)}(\lambda),\mathcal{P}_W^{(5)}(\lambda)\right).
\end{aligned}
$$

The result of this computation is a sequence of numbers changing as ξ changes, and we write down only the sign of every number in the sequence and, from such a sequence, we extract the sequence of the corresponding signs. This sequence of signs changes only if we choose values of ξ from intervals different from to each other.

4.4 Gain Function

In this section, we present the function $\mathcal{H}(\omega,k)$ as an implicit function of the eigenwavenumber $k = w_i - w_j$ and of the eigenfrequency $\omega = z_i - z_j$. The vanishing of the this polynomial, i.e. $\mathcal{H}(\omega,k)=0$, for fixed k, provides ω as a function of $\mathcal{H}$ and of the other parameters of the system p_1, p_2 and p_3, whose imaginary part is the gain function. However, we do not solve this polynomial because it is sixth degree polynomial in ω, instead, we will compute numerically (via a MATLAB 2018a routine) and we will display an example of the gain function for any spectrum in the classification in the next section.

In the following, we show how the function $\mathcal{H}(\omega,k)$ is obtained.

Let us consider the two characteristic polynomials $P_Z(z;\lambda)$ and $P_W(w;\lambda)$. Because the

two associate matrices commute, i.e. $[Z, W] = 0$, they have roots in common, such that their resultant must be zero for values of the parameters involved in their expressions. The resultants with respect to p_1 and p_2 read, respectively,

$$\begin{aligned}\mathrm{Res}_{p_1}(P_Z(z;\lambda);P_W(w;\lambda)) = (-p_3(p_2+z(\lambda+z))+w-z)\left(\lambda^2+p_2(p_3(\lambda+z)-1)^2+\right.\\ +p_3^2(\lambda+z-1)(\lambda+z+1)(z(\lambda+z)-1)+p_3\left(w(z(\lambda+z)-2)-z(\lambda+z)^2+z\right)+w^2+\\ \left.+2\lambda(w+z)+wz+z^2-1\right),\end{aligned} \tag{4.82}$$

$$\begin{aligned}\mathrm{Res}_{p_2}(P_Z(z;\lambda);P_W(w;\lambda)) = (-p_1p_3-p_3z+(w-z)(\lambda+z))\left(-\lambda+p_1(p_3(\lambda+z)-1)^2+\right.\\ +(\lambda+z)(p_3^2(-(\lambda+z-1))(\lambda+z+1)+p_3(w(z(\lambda+z)-2)+z(\lambda+z-1)(\lambda+z+1))+\\ \left.+(\lambda+w)(\lambda+w+z))\right).\end{aligned} \tag{4.83}$$

Because the resultants (4.82) and (4.83) are the product of two polynomials, for each one of them, we equal to zero the polynomial with the simplest expression, in this way we obtain two maps between the eigenvalue w and z,

$$w \to \frac{p_3(p_1+z)}{\lambda+z}+z, \tag{4.84}$$

and

$$w \to p_3(p_2+z(\lambda+z))+z. \tag{4.85}$$

Using the two maps (4.84) and (4.85), we define the two polynomials by taking the numerators of the following expressions

$$J_1(z_1,z_2;\lambda) = \left(4\left((\lambda+z_1)(\lambda+z_2)(k-z_1-z_2)-p_3(p_1+z_1)(\lambda+z_2)-p_3(p_1+z_2)(\lambda+z_1)\right)\right), \tag{4.86}$$

and

$$J_2(z_1,z_2;\lambda) = 4\left(k-(p_3(p_2+z_1(\lambda+z_1))+z_1-p_3(p_2+z_2(\lambda+z_2))+z_2)\right), \tag{4.87}$$

and, after the substitutions $\omega = z_1 - z_2$ and $\theta = z_1 + z_2$, they become

$$J_1(\theta;\lambda) = k\left((\theta+2\lambda)^2-\omega^2\right)+\omega\left(-\theta^2+4p_1p_3-4\lambda(\theta+\lambda+p_3)+\omega^2\right), \tag{4.88}$$

$$J_2(\theta;\lambda) = k - \omega(p_3(\theta+\lambda)+1). \tag{4.89}$$

Moreover, we introduce another polynomial, that is the polynomial of the sums of the eigenvalues z_j (Appendix K)

$$\mathcal{S}_Z(\theta,\lambda) = \theta^3 + 4\lambda\theta^2 + (5\lambda^2 + p_2 - 1)\theta + p_1 + \lambda(-2 + p_2 + 2\lambda^2). \tag{4.90}$$

Then, the Groebner basis of the three polynomial $J_1(\theta;\lambda)$, $J_2(\theta;\lambda)$ and $\mathcal{S}_Z(\theta,\lambda)$ yields a list of polynomials of which only the first is independent on λ and θ and provides the gain function

$$\begin{aligned}
&\mathcal{H}(\omega,k) = k^4\left(\omega^2-4\right) - 4k^3\omega\left(p_1p_3+\omega^2-4\right) - \\
&- k^2\omega^2\left(-12p_1p_3 + p_3^2\left(p_2^2+4p_2+2\omega^2-8\right) - 6\left(\omega^2-4\right)\right) + \\
&+ 2k\omega^3\left(p_1p_3\left(-(p_2-2)p_3^2-6\right) + p_3^2\left(p_2^2+4p_2+2\omega^2-8\right) - 2\omega^2+8\right) + \\
&+ \omega^4\left(p_3^4\left(-\left(p_1^2-4p_2+4\right)\right) + 2p_1(p_2-2)p_3^3 + 4p_1p_3 - (p_2(p_2+4)-8)p_3^2 - 4\right) + \\
&\left(p_3^2-1\right)^2\omega^6.
\end{aligned} \tag{4.91}$$

4.5 Description of the x-Stability Spectra

In this section we provide an analytical description of the spatial stability spectra obtained for any generic choice of the parameters in the (p_1,p_2)-plane and we display both the S_x-spectrum and its associated gain function $\omega_3 = \Gamma(k_3)$ in any region of the (p_1,p_2)-plane (see Appendices M and L).

Regions with 1 Gap and 1 Branch

In the regions with 1 gap and 1 branch, we note the following correspondence between the number of loops and the number of positive ξ-roots:

- 2L: 5 positive ξ-roots;

- 1L: 3 positive ξ-roots;
- 0L: 1 positive ξ-roots.

If we choose $p_1 = -0.8$, $p_2 = 0.4$ and $p_3 = -0.6$, we have that $\mathcal{Q}_2(\xi)$ changes sign 5 times at any of the following values of ξ: $\bar{\xi}_1 = 0.028$, $\bar{\xi}_2 = 1.887$, $\bar{\xi}_3 = 2.115$, $\bar{\xi}_4 = 3.146$ and $\bar{\xi}_5 = 33.419$. After applying the Descartes rule of signs to the polynomial of the squares of the differences multiplied by minus, further intervals must be considered whose end-points are: $\xi_1 = 0.028$, $\xi_2 = 0.152$, $\xi_3 = 1.887$, $\xi_4 = 2.115$, $\xi_5 = 3.146$, $\xi_6 = 6.517$, $\xi_7 = 15.021$ and $\xi_8 = 33.419$. Then, we apply the Sturm chains technique by substituting a generic ξ value on every interval $[\xi_j, \xi_{j+1}]$ into the expression of the coefficients and we count the sign changes. Finally, we can classify the nature of the λ-roots and so we can describe the whole spectrum. In particular:

- $0 < \xi < \xi_1$: 4 λ-roots on the real axis and 2 λ-roots are travelling along the branch;
- $\xi_1 < \xi < \xi_2$: 2 λ-roots on the real axis, 2 λ-roots on the branch and 2 λ-roots on a loop;
- $\xi_2 < \xi < \xi_3$: 4 λ-roots on the real axis, and 2 λ-roots on a loop or on the branch;
- $\xi_3 < \xi < \xi_4$: 6 λ-roots on the real axis;
- $\xi_4 < \xi < \xi_5$: 6 λ-roots on the real axis;
- $\xi_5 < \xi < \xi_6$: 4 λ-roots on the real axis, 2 λ-roots on the second loop;
- $\xi_6 < \xi < \xi_7$: 4 λ-roots on the real axis, 2 λ-roots on the second loop;
- $\xi_7 < \xi < \xi_8$: 4 λ-roots on the real axis, 2 λ-roots on the second loop.
- $\xi > \xi_8$: 6 λ-roots on the real axis.

We conclude that 2 loops exist for these choices of the physical parameters.

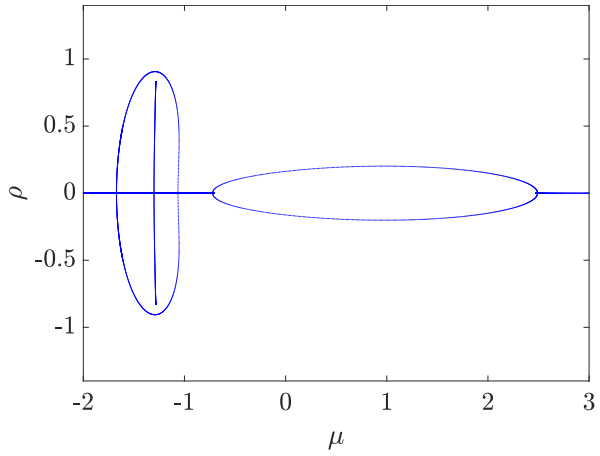

Figure 4.5: Stability spectrum for $p_1 = -0.8$, $p_2 = 0.4$, $p_3 = -0.6$. $\rho = \mathrm{Re}(\lambda)$ and $\mu = \mathrm{Im}(\lambda)$.

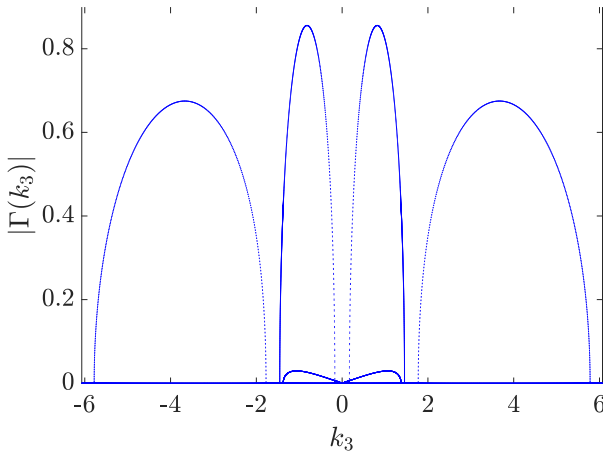

Figure 4.6: Gain function $\Gamma(k_3)$ where $k_3 = w_1 - w_2$ associated to the stability spectrum obtained at $p_1 = -0.8$, $p_2 = 0.4$, $p_3 = -0.6$.

By setting $p_1 = -4.0$, $p_2 = -3.0$ and $p_3 = -0.6$, we have that $\mathcal{Q}_2(\xi)$ changes sign 3 times at any of the following values of ξ: $\bar{\xi}_1 = 0.030$, $\bar{\xi}_2 = 31.959$ and $\bar{\xi}_3 = 49.660$. By applying the Descartes rule of signs, further intervals must be considered whose end-points are: $\xi_1 = 0.026$, $\xi_2 = 0.030$, $\xi_3 = 0.525$, $\xi_4 = 31.959$, $\xi_5 = 38.834$, $\xi_6 = 49.660$ and $\xi_7 = 52.214$. Then, we apply the Sturm chains technique and we obtain the classification of the nature of the λ-roots:

- $0 < \xi < \xi_1$: 4 λ-roots on the real axis and 2 λ-roots on the branch;

- $\xi_1 < \xi < \xi_2$: 4 λ-roots on the real axis and 2 λ-roots on the branch;
- $\xi_2 < \xi < \xi_3$: 2 λ-roots on the real axis, and 2 λ-roots on the loop and 2 λ-roots on the branch;
- $\xi_3 < \xi < \xi_4$: 2 λ-roots on the real axis and 2 λ-roots on the branch and 2 λ-roots on the loop;
- $\xi_4 < \xi < \xi_5$: 2 λ-roots on the real axis and 2 λ-roots on the branch and 2 λ-roots on the loop;
- $\xi_5 < \xi < \xi_6$: 6 λ-roots on the real axis;
- $\xi > \xi_7$: 6 λ-roots on the real axis.

Therefore, 1 loop is present in this spectrum.

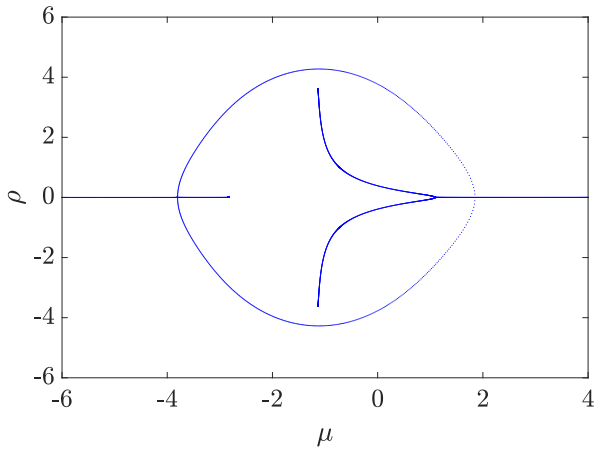

Figure 4.7: Stability spectrum at $p_1 = -4.0$, $p_2 = -3.0$, $p_3 = -0.6$. $\rho = \mathrm{Re}(\lambda)$ and $\mu = \mathrm{Im}(\lambda)$.

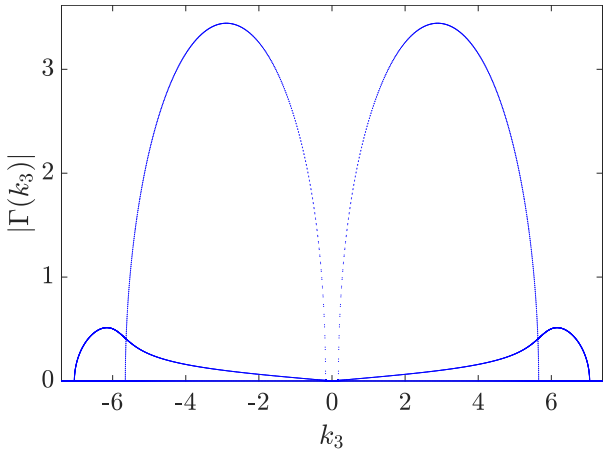

Figure 4.8: Gain function $\Gamma(k_3)$ with $k_3 = w_1 - w_2$ associated to the spectrum obtained at $p_1 = -4.0$, $p_2 = -3.0$, $p_3 = -0.6$.

By setting $p_1 = 1.0$, $p_2 = 3.0$ and $p_3 = -0.6$, we have that $\mathcal{Q}_2(\xi)$ changes sign 1 time in the point $\bar{\xi}_1 = 36.911$. After applying the Descartes rule of signs, further intervals must be considered whose end-points are: $\xi_1 = 0.079$, $\xi_2 = 3.664$, $\xi_3 = 36.911$. Then, we apply the Sturm chains technique and we get the following classification:

- $0 < \xi < \xi_1$: 4 real λ-roots and 2 λ-roots on the branch;
- $\xi_1 < \xi < \xi_2$: 4 real λ-roots and 2 λ-roots on the branch;
- $\xi_2 < \xi < \xi_3$: 4 real λ-roots and 2 λ-roots on the branch;
- $\xi > \xi_3$: 6 λ-roots on the real axis.

No loops exist into the spectrum for these choices of the physical parameters.

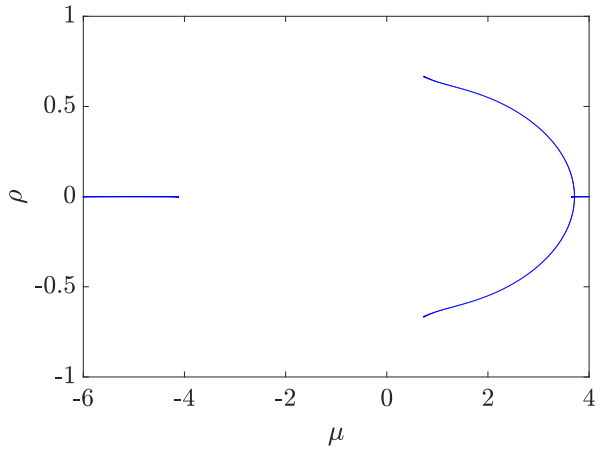

Figure 4.9: Stability spectrum at $p_1 = 1.0$, $p_2 = 3.0$, $p_3 = -0.6$. $\rho = \mathrm{Re}(\lambda)$ and $\mu = \mathrm{Im}(\lambda)$.

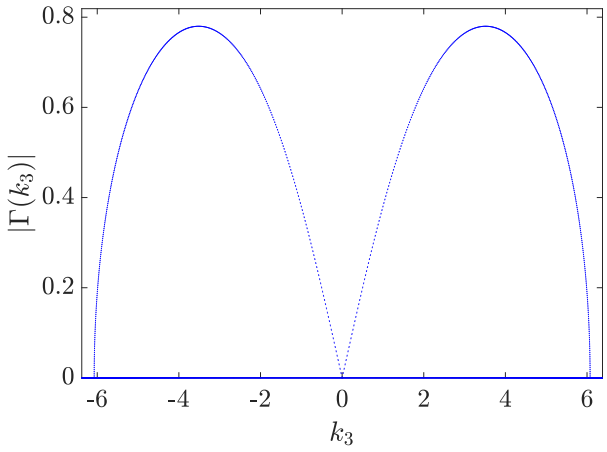

Figure 4.10: Gain function $\Gamma(k_3)$ where$k_3 = w_1 - w_2$ associated to the spectrum obtained at $p_1 = 1.0$, $p_2 = 3.0$, $p_3 = -0.6$.

4.5.1 Regions with 0 Gap and 2 Branches

In the regions with 0 gap and 2 branches, there is the following correspondence between the number of loops and the number of positive ξ-roots:

- 2L: 6 positive ξ-roots;
- 1L: 4 positive ξ-roots;

- 0L: 2 positive ξ-roots.

Let us set $p_1 = -6.2$, $p_2 = -6.3$ and $p_3 = -0.6$. For these values of the parameters the polynomial $\mathcal{Q}_2(\xi)$ change sign 6 times at the values of ξ: $\bar{\xi}_1 = 0.168$, $\bar{\xi}_2 = 1.219$, $\underline{a}r\xi_3 = 63.296$, $\bar{\xi}_4 = 63.549$, $\bar{\xi}_5 = 64.132$, $\bar{\xi}_6 = 70.732$. Then, we apply the Descartes rule of signs and we find further intervals whose end-points are: $\xi_1 = 0.168$, $\xi_2 = 0.451$, $\xi_3 = 0.839$, $\xi_4 = 1.015$, $\xi_5 = 1.219$, $\xi_6 = 2.746$, $\xi_7 = 63.296$, $\xi_8 = 64.132$, $\xi_9 = 66.267$, $\xi_{10} = 70.732$, $\xi_{11} = 71.817$, $\xi_{12} = 82.022$, $\xi_{13} = 87.860$. In this way, by the Sturm chains method, we have the classification of the λ-roots:

- $0 < \xi < \xi_1$: 2 λ-roots on the real axis, 2 λ-roots on a branch and 2 λ-roots on the other branch;
- $\xi_1 < \xi < \xi_2$: 4 λ-roots on the real axis and 2 λ-roots on a branch;
- $\xi_2 < \xi < \xi_3$: 4 λ-roots on the real axis and 2 λ-roots on a branch;
- $\xi_3 < \xi < \xi_4$: 4 λ-roots on the real axis and 2 λ-roots on a branch;
- $\xi_4 < \xi < \xi_5$: 4 λ-roots on the real axis and 2 λ-roots on a branch;
- $\xi_5 < \xi < \xi_6$: 2 λ-roots on the real axis, 2 λ-roots on a branch and 2 λ-roots on a loop;
- $\xi_6 < \xi < \xi_7$: 2 λ-roots on the real axis, 2 λ-roots on a branch and 2 λ-roots on a loop;
- $\xi_7 < \xi < \xi_8$: 6 λ-roots on the real axis;
- $\xi_8 < \xi < \xi_9$: 4 λ-roots on the real axis and 2 λ-roots on a loop;
- $\xi_9 < \xi < \xi_{10}$: 4 λ-roots on the real axis and 2 λ-roots on a loop;
- $\xi_{10} < \xi < \xi_{11}$: 6 λ-roots on the real axis;
- $\xi_{11} < \xi < \xi_{12}$: 6 λ-roots on the real axis;
- $\xi_{12} < \xi < \xi_{13}$: 6 λ-roots on the real axis;
- $\xi > \xi_{13}$: 6 λ-roots on the real axis.

Thus, we see 2 loops in this spectrum.

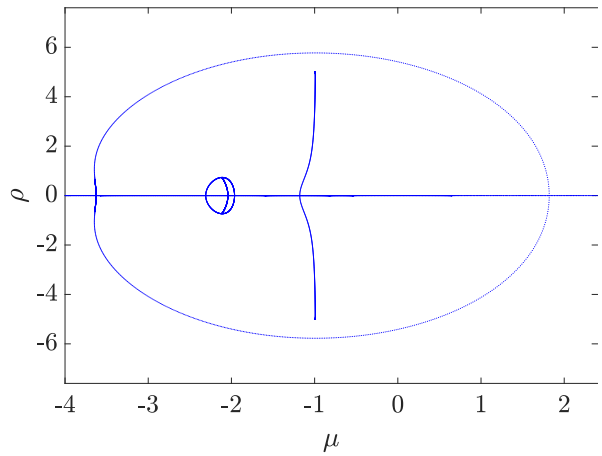

Figure 4.11: Stability spectrum with $p_1 = -6.2$, $p_2 = -6.3$, $p_3 = -0.6$. $\rho = \mathrm{Re}(\lambda)$ and $\mu = \mathrm{Im}(\lambda)$.

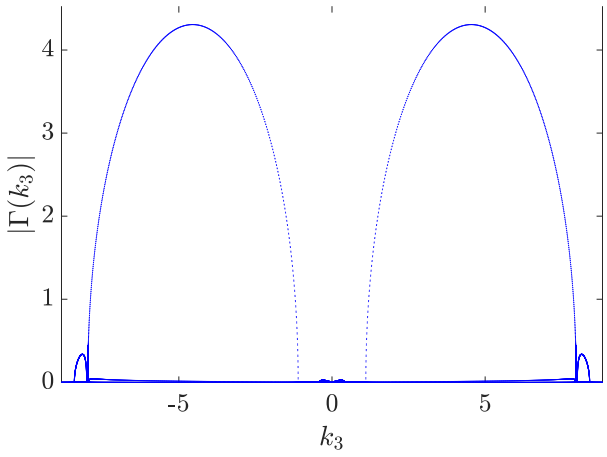

Figure 4.12: Gain function $\Gamma(k_3)$ where $k_3 = w_1 - w_2$ associated to the spectrum obtained at $p_1 = -6.2$, $p_2 = -6.3$, $p_3 = -0.6$.

If we choose $p_1 = -4.0$, $p_2 = -4.2$ and $p_3 = -0.6$, the polynomial $\mathcal{Q}_2(\xi)$ vanishes 4 times in these points: $\bar{\xi}_1 = 0.129$, $\bar{\xi}_2 = 0.240$, $\bar{\xi}_3 = 36.370$ and $\bar{\xi}_4 = 44.444$. By using the Descartes rule of signs we have: $\xi_1 = 0.129$, $\xi_2 = 0.179$, $\xi_3 = 0.240$, $\xi_4 = 0.380$, $\xi_5 = 0.495$, $\xi_6 = 1.047$, $\xi_7 = 36.370$, $\xi_8 = 43.943$, $\xi_9 = 44.444$, $\xi_{10} = 46.439$, $\xi_{11} = 49.745$, $\xi_{12} = 57.025$. By constructing the Sturm chains method, we obtain the following λ-roots classification:

- $0 < \xi < \xi_1$: 2 λ-roots on the real axis, 2 λ-roots on a branch and 2 λ-roots on the other branch;
- $\xi_1 < \xi < \xi_2$: 4 λ-roots on the real axis and 2 λ-roots on a branch;
- $\xi_2 < \xi < \xi_3$: 4 λ-roots on the real axis and 2 λ-roots on a branch;
- $\xi_3 < \xi < \xi_4$: 2 λ-roots on the real axis, 2 λ-roots on a branch and 2 λ-roots on a loop;
- $\xi_4 < \xi < \xi_5$: 2 λ-roots on the real axis, 2 λ-roots on a branch and 2 λ-roots on a loop;
- $\xi_5 < \xi < \xi_6$: 2 λ-roots on the real axis, 2 λ-roots on a branch and 2 λ-roots on a loop;
- $\xi_6 < \xi < \xi_7$: 2 λ-roots on the real axis, 2 λ-roots on a branch and 2 λ-roots on a loop;
- $\xi_7 < \xi < \xi_8$: 4 λ-roots on the real axis and 2 λ-roots on a branch or on a loop;
- $\xi_8 < \xi < \xi_9$: 4 λ-roots on the real axis and 2 λ-roots on a branch or on a loop;
- $\xi_9 < \xi < \xi_{10}$: 6 λ-roots on the real axis;
- $\xi_{10} < \xi < \xi_{11}$: 6 λ-roots on the real axis;
- $\xi_{11} < \xi < \xi_{12}$: 6 λ-roots on the real axis;
- $\xi > \xi_{12}$: 6 λ-roots on the real axis.

Only one loop is present in the spectrum.

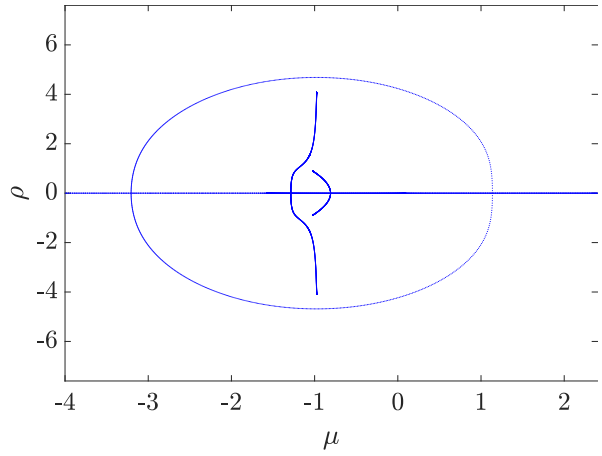

Figure 4.13: Stability spectrum with $p_1 = -4.0$, $p_2 = -4.2$, $p_3 = -0.6$. $\rho = \mathrm{Re}(\lambda)$ and $\mu = \mathrm{Im}(\lambda)$.

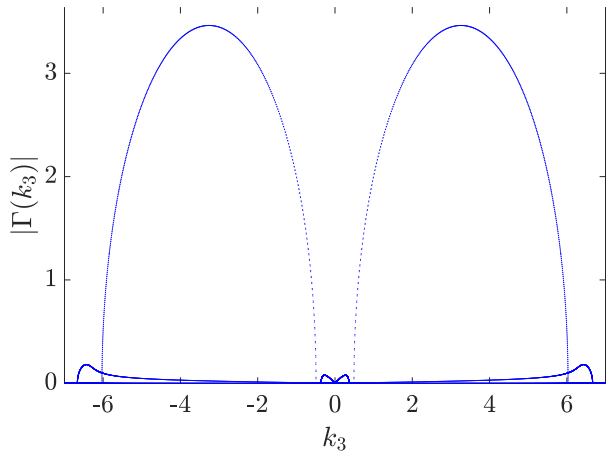

Figure 4.14: Gain function $\Gamma(k_3)$ where $k_3 = w_1 - w_2$ associated to the spectrum obtained at $p_1 = -4.0$, $p_2 = -4.2$, $p_3 = -0.6$.

If we choose $p_1 = 1.0$, $p_2 = -3.0$ and $p_3 = -0.6$, the polynomial $\mathcal{Q}_2(\xi)$ vanishes 2 times in these two points: $\bar{\xi}_1 = 8.421$ and $\bar{\xi}_2 = 13.280$. By using the Descartes rule of signs we have: $\xi_1 = 0.076$, $\xi_2 = 0.769$, $\xi_3 = 2.284$, $\xi_4 = 8.421$, $\xi_5 = 11.354$, $\xi_6 = 12.477$, $\xi_7 = 13.157$, $\xi_8 = 13.280$, $\xi_9 = 13.289$. By using Sturm chains we get the following λ-roots classification:

- $0 < \xi < \xi_1$: 2 λ-roots on the real axis, 2 λ-roots on a branch and 2 λ-roots on the other branch;

- $\xi_1 < \xi < \xi_2$: 2 λ-roots on the real axis, 2 λ-roots on a branch and 2 λ-roots on the other branch;
- $\xi_2 < \xi < \xi_3$: 4 λ-roots on the real axis, 2 λ-roots on a branch and 2 λ-roots on the other branch;
- $\xi_3 < \xi < \xi_4$: 2 λ-roots on the real axis, 2 λ-roots on a branch and 2 λ-roots on the other branch;
- $\xi_4 < \xi < \xi_5$: 4 λ-roots on the real axis, 2 λ-roots on a branch;
- $\xi_5 < \xi < \xi_6$: 4 λ-roots on the real axis, 2 λ-roots on a branch;
- $\xi_6 < \xi < \xi_7$: 4 λ-roots on the real axis, 2 λ-roots on a branch;
- $\xi_7 < \xi < \xi_8$: 4 λ-roots on the real axis, 2 λ-roots on a branch;
- $\xi_8 < \xi < \xi_9$: 6 λ-roots on the real axis;
- $\xi > \xi_9$: 6 λ-roots on the real axis.

No loop is present in the spectrum.

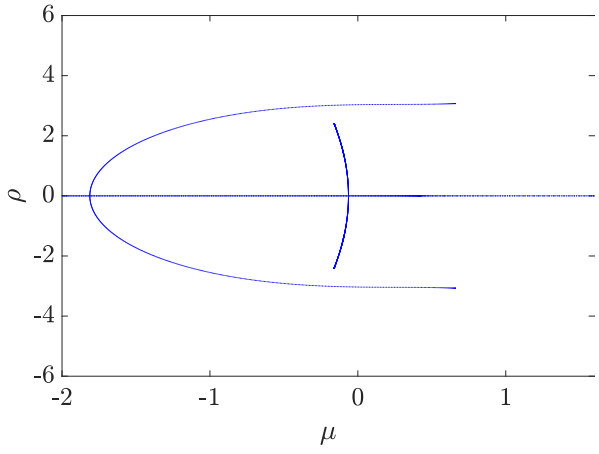

Figure 4.15: Stability spectrum with $p_1 = 1.0$, $p_2 = -3.0$, $p_3 = -0.6$. $\rho = \mathrm{Re}(\lambda)$ and $\mu = \mathrm{Im}(\lambda)$.

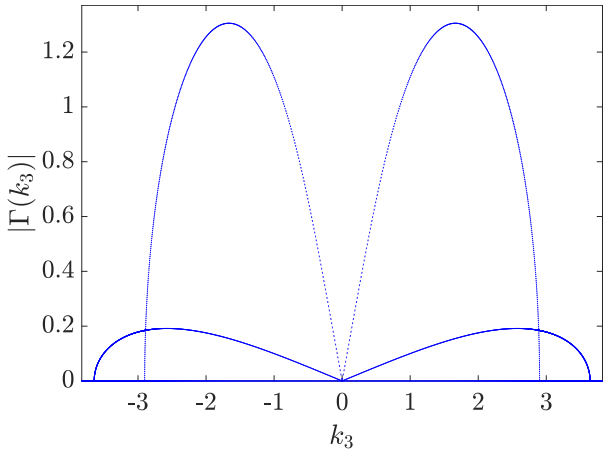

Figure 4.16: Gain function $\Gamma(k_3)$ where $k_3 = w_1 - w_2$ associated to the spectrum obtained at $p_1 = 1.0$, $p_2 = -3.0$, $p_3 = -0.6$.

4.5.2 Regions with 2 Gaps and 0 Branch

In the regions with 2 gaps and 0 branch, there is the following correspondence between the number of loops and the number of positive ξ-roots:

- 2L: 4 positive ξ-roots;
- 1L: 2 positive ξ-roots.

The region with 2 gaps, 0 branch and 0 loop does not exist. This is because the λ-roots which start to move in the interval between the 2 gaps would be trapped inside such interval and never would go to infinity: this is in contradiction of the Proposition 4.3.1.

Let us set $p_1 = -70.0$, $p_2 = 60.0$ and $p_3 = -0.6$. The polynomial $\mathcal{Q}_2(\xi)$ changes sign 4 times in the points $\bar{\xi}_1 = 1.596$, $\bar{\xi}_2 = 218.582$, $\bar{\xi}_3 = 968.174$, $\bar{\xi}_4 = 3944.396$. After applying the Descartes rule of signs, the end-point of the intervals become: $\xi_1 = 1.596$, $\xi_2 = 32.536$, $\xi_3 = 218.582$, $\xi_4 = 482.289$, $\xi_5 = 968.174$, $\xi_6 = 1480.780$, $\xi_7 = 3944.396$, $\xi_8 = 4733.800$. By using Sturm chains method, we get the following λ-roots classification:

- $0 < \xi < \xi_1$: 6 λ-roots on the real axis;

- $\xi_1 < \xi < \xi_2$: 4 λ-roots on the real axis, 2 λ-roots on a loop;
- $\xi_2 < \xi < \xi_3$: 4 λ-roots on the real axis, 2 λ-roots on a loop;
- $\xi_3 < \xi < \xi_4$: 2 λ-roots on the real axis, 2 λ-roots on a loop and 2 λ-roots on another loop;
- $\xi_4 < \xi < \xi_5$: 2 λ-roots on the real axis, 2 λ-roots on a loop and 2 λ-roots on another loop;
- $\xi_5 < \xi < \xi_6$: 4 λ-roots on the real axis, 2 λ-roots on a loop;
- $\xi_6 < \xi < \xi_7$: 4 λ-roots on the real axis, 2 λ-roots on a loop;
- $\xi_7 < \xi < \xi_8$: 6 λ-roots on the real axis;
- $\xi > \xi_8$: 6 λ-roots on the real axis.

Therefore, we see 2 loops in this spectrum.

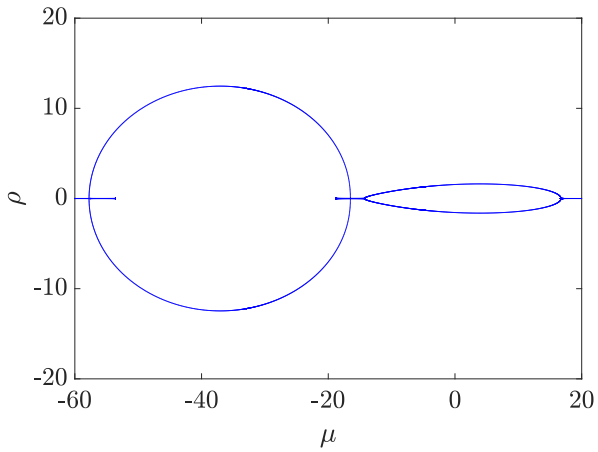

Figure 4.17: Stability spectrum with $p_1 = -70.0$, $p_2 = 60.0$, $p_3 = -0.6$. $\rho = \mathrm{Re}(\lambda)$ and $\mu = \mathrm{Im}(\lambda)$.

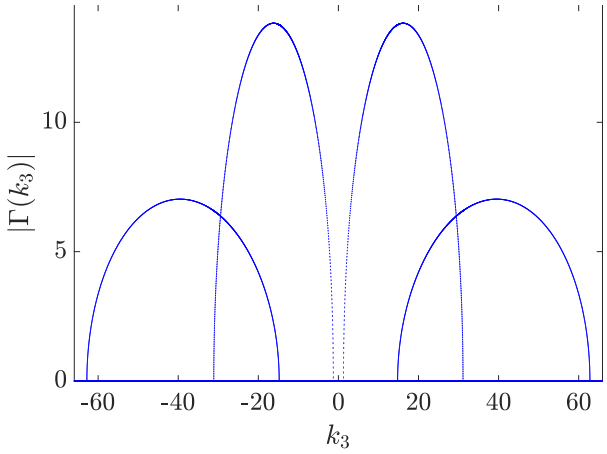

Figure 4.18: Gain function $\Gamma(k_3)$ where $k_3 = w_1 - w_2$ associated to the spectrum obtained at $p_1 = -70.0$, $p_2 = 60.0$, $p_3 = -0.6$.

Let us set $p_1 = 0.2$, $p_2 = 0.6$ and $p_3 = -0.6$. The polynomial $\mathcal{Q}_2(\xi)$ changes sign 2 times in the points $\bar{\xi}_1 = 2.348$ and $\bar{\xi}_2 = 18.989$. After applying the Descartes rule of signs ,the end-point of the intervals become: $\xi_1 = 2.348$, $\xi_2 = 6.410$ and $\xi_3 = 18.989$. After constructing the Sturm chains, the λ-roots classification is:

- $0 < \xi < \xi_1$: 6 λ-roots on the real axis;
- $\xi_1 < \xi < \xi_2$: 4 λ-roots on the real axis, 2 λ-roots on a loop;
- $\xi_2 < \xi < \xi_3$: 4 λ-roots on the real axis, 2 λ-roots on a loop;
- $\xi > \xi_3$: 6 λ-roots on the real axis.

Therefore, there is only 1 loop in this spectrum.

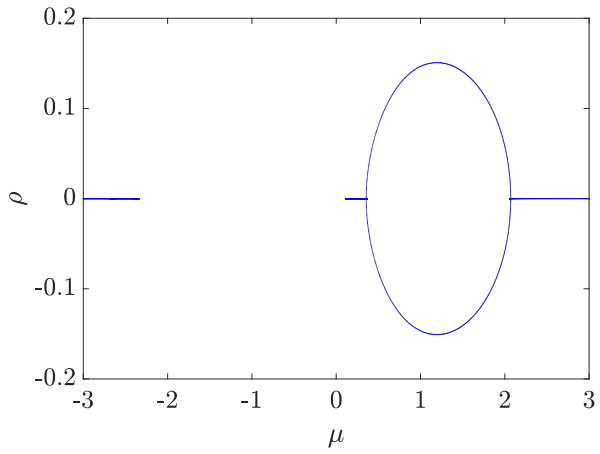

Figure 4.19: Stability spectrum with $p_1 = 0.2$, $p_2 = 0.6$, $p_3 = -0.6$. $\rho = \mathrm{Re}(\lambda)$ and $\mu = \mathrm{Im}(\lambda)$.

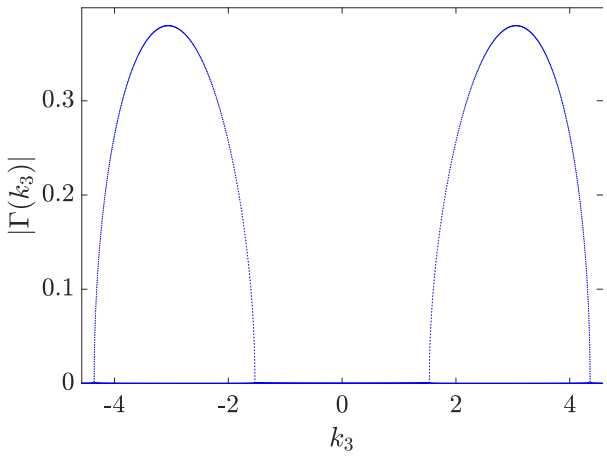

Figure 4.20: Gain function $\Gamma(k_3)$ where $k_3 = w_1 - w_2$ associated to the spectrum obtained at $p_1 = 0.2$, $p_2 = 0.6$, $p_3 = -0.6$.

4.5.3 Region with 1 Gap, 1 Split Gap and 0 Branches

There is only one possibility:

- 1L 1TL: 3 positive ξ-roots.

By choosing $p_1 = -90.0$, $p_2 = 60.0$ and $p_3 = -0.6$, the polynomial $\mathcal{Q}_2(\xi)$ vanishes in the points $\bar{\xi}_1 = 63.032$, $\bar{\xi}_2 = 2891.269$ and $\xi_3 = 4474.552$. By the Descartes rule, the ξ-

domain is split by these points: $\xi_1 = 63.032$, $\xi_2 = 267.710$, $\xi_3 = 1569.140$, $\xi_4 = 2891.269$, $\xi_5 = 4474.552$, $\xi_6 = 6153.740$. The λ-roots classification is obtained by the Sturm chains construction:

- $0 < \xi < \xi_1$: 4 λ-roots on the real axis and 2 λ-roots on a loop;
- $\xi_1 < \xi < \xi_2$: 2 λ-roots on the real axis, 2 λ-roots on a loop and 2 λ-roots on another loop;
- $\xi_2 < \xi < \xi_3$: 2 λ-roots on the real axis, 2 λ-roots on a loop and 2 λ-roots on another loop;
- $\xi_3 < \xi < \xi_4$: 2 λ-roots on the real axis, 2 λ-roots on a loop and 2 λ-roots on another loop;
- $\xi_4 < \xi < \xi_5$: 4 λ-roots on the real axis and 2 λ-roots on a loop;
- $\xi_5 < \xi < \xi_6$: 6 λ-roots on the real axis;
- $\xi > \xi_6$: 6 λ-roots on the real axis.

In this spectrum it looks like there are only two loops, but actually there are 1 loop and 1 twisted loop. Therefore, the second loop that we have found has to be counted twice. Indeed, we cannot individuate the exact value of ξ in which the two λ-roots collide on the real axis to become again two complex conjugate roots travelling the second part of the twisted loop.

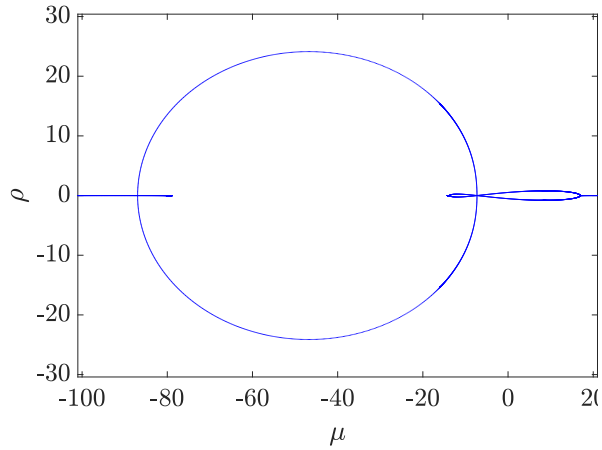

Figure 4.21: Stability spectrum with $p_1 = -90.0$, $p_2 = 60.0$, $p_3 = -0.6$. $\rho = \mathrm{Re}(\lambda)$ and $\mu = \mathrm{Im}(\lambda)$.

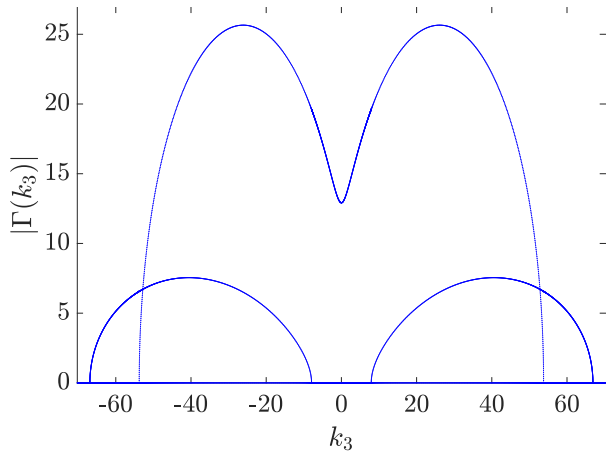

Figure 4.22: Gain function $\Gamma(k_3)$ where $k_3 = w_1 - w_2$ associated to the spectrum obtained at $p_1 = -90.0$, $p_2 = 60.0$, $p_3 = -0.6$.

4.5.4 Region with 1 Split Gap and 1 Branch

In this region we have:

- 1L 1TL: 4 positive ξ-roots;
- 1TL: 2 positive ξ-roots.

Let us fix $p_1 = -1.4$, $p_2 = -1.0$ and $p_3 = -0.6$. The polynomial $\mathcal{Q}_2(\xi)$ changes sign 4 times in the points $\bar{\xi}_1 = 9.216$, $\bar{\xi}_2 = 11.823$, $\bar{\xi}_3 = 12.195$ and $\bar{\xi}_4 = 27.053$. By the Descartes rule of signs, we get: $\xi_1 = 0.002$, $\xi_2 = 0.421$, $\xi_3 = 9.216$, $\xi_4 = 11.823$, $\xi_5 = 12.195$, $\xi_6 = 27.053$, so that, by using the Sturm chains technique, the λ-roots are classified as follows:

- $0 < \xi < \xi_1$: 2 λ-roots on the real axis, 2 λ-roots on a branch and 2 λ-roots on a loop;
- $\xi_1 < \xi < \xi_2$: 2 λ-roots on the real axis, 2 λ-roots on a branch and 2 λ-roots on a loop
- $\xi_2 < \xi < \xi_3$: 2 λ-roots on the real axis, 2 λ-roots on a branch and 2 λ-roots on a loop
- $\xi_3 < \xi < \xi_4$: 4 λ-roots on the real axis, 2 λ-roots on a branch or on a loop;
- $\xi_4 < \xi < \xi_5$: 6 λ-roots on the real axis;
- $\xi_5 < \xi < \xi_6$: 4 λ-roots on the real axis, 2 λ-roots on a loop;
- $\xi > \xi_6$: 6 λ-roots on the real axis.

In this spectrum there is 1 loop and 1 twisted loop. Also in this case it is not possible distinguish the exact value of ξ in which two λ-roots collide in the point separating a split gap and then they become again two complex conjugate roots.

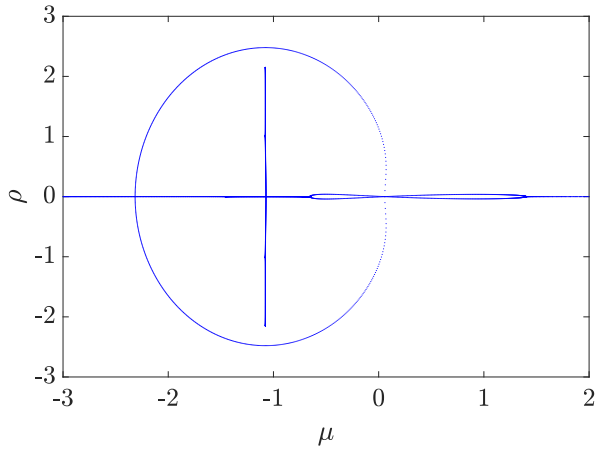

Figure 4.23: Stability spectrum with $p_1 = -1.4$, $p_2 = -1.0$, $p_3 = -0.6$. $\rho = \mathrm{Re}(\lambda)$ and $\mu = \mathrm{Im}(\lambda)$.

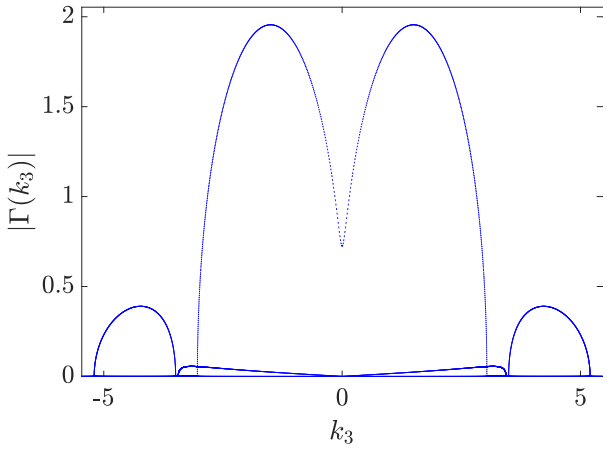

Figure 4.24: Gain function $\Gamma(k_3)$ where $k_3 = w_1 - w_2$ associated to the spectrum at $p_1 = -1.4$, $p_2 = -1.0$, $p_3 = -0.6$.

If we choose $p_1 = -4$, $p_2 = 2$ and $p_3 = -0.6$, the polynomial $\mathcal{Q}_2(\xi)$ vanishes 2 times in $\bar{\xi}_1 = 9.591$ and $\bar{\xi}_2 = 98.262$. By the Descartes rule of signs, we get the points $\xi_1 = 0.136$, $\xi_2 = 9.591$, $\xi_3 = 19.547$, $\xi_4 = 45.537$, $\xi_5 = 98.262$. The classification of the λ-roots is:

- $0 < \xi < \xi_1$: 2 λ-roots on the real axis, 2 λ-roots on a branch and 2 λ-roots on a loop;
- $\xi_1 < \xi < \xi_2$: 2 λ-roots on the real axis, 2 λ-roots on a branch and 2 λ-roots on a loop;

- $\xi_2 < \xi < \xi_3$: 4 λ-roots on the real axis, 2 λ-roots on a loop;
- $\xi_3 < \xi < \xi_4$: 4 λ-roots on the real axis, 2 λ-roots on a loop;
- $\xi_4 < \xi < \xi_5$: 4 λ-roots on the real axis, 2 λ-roots on a loop;
- $\xi > \xi_5$: 6 λ-roots on the real axis.

It looks like we have only one loop, but actually this is a twisted loop.

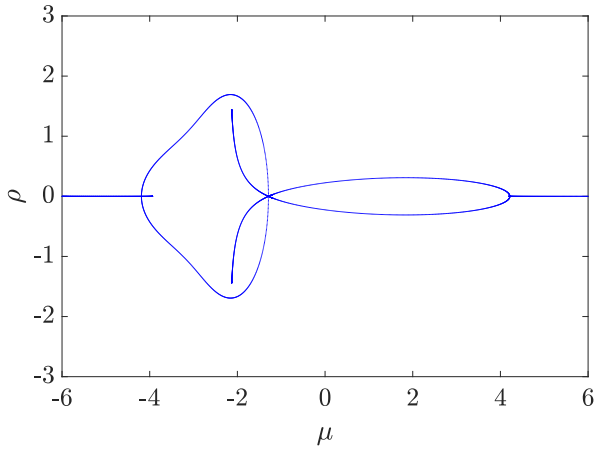

Figure 4.25: Stability spectrum with $p_1 = -4.0$, $p_2 = 2.0$, $p_3 = -0.6$. $\rho = \mathrm{Re}(\lambda)$ and $\mu = \mathrm{Im}(\lambda)$.

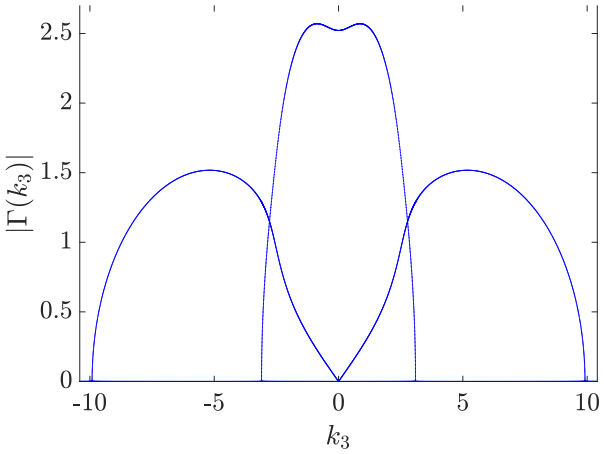

Figure 4.26: Gain function $\Gamma(k_3)$ where $k_3 = w_1 - w_2$ associated to the spectrum obtained at $p_1 = -4.0$, $p_2 = 2.0$, $p_3 = -0.6$.

Summarising, all the possibile topologies in the (p_1, p_2)-plane are:

- 1G 0SG 1B 2L 0TL;
- 1G 0SG 1B 1L 0TL;
- 1G 0SG 1B 0L 0TL;
- 0G 0SG 2B 2L 0TL;
- 0G 0SG 2B 1L 0TL;
- 0G 0SG 2B 0L 0TL;
- 2G 0SG 0B 2L 0TL;
- 2G 0SG 0B 1L 0TL;
- 1G 1SG 0B 1L 1TL;
- 0G 1SG 1B 1L 1TL;
- 0G 1SG 1B 0L 1TL.

4.6 Topological Classification of the Spectra in the Parameter Space

At this point, we can obtain the entire topological classification of the spectra in the parameter space. In order to do that, we need to describe the curves in the (p_1, p_2)-plane separating the regions with different number of gaps, branches and loops. First of all, we compute and factorise the polynomial $\mathcal{Q}_2(\xi)$ at $\xi = 0$,

$$\mathcal{Q}_2(0) = \prod_{j=1}^{4} D_j(p_1, p_2, p_3)^{d_j} , \tag{4.92a}$$

whose corresponding curves are given by (4.33), as well as the discriminant of $\mathcal{Q}_2(\xi)$ with respect to ξ,

$$\Delta_\xi \mathcal{Q}_2(\xi) = \prod_{j=0}^{4} E_j(p_1, p_2, p_3)^{e_j} , \tag{4.92b}$$

where the functions E_j depend on the parameters p_1, p_2 and p_3.
Similarly to the definition (4.33), let $\mathcal{E}_j$ be the real-analytic variety in the parameter space, implicitly defined as

$$\mathcal{E}_j = \left\{ p_1, p_2, p_3 \in \mathbb{R} \; \exists \, (p_1, p_2) \in \mathbb{R}^{1\times 1} \,|\, E_j(p_1, p_2, p_3) = 0 \right\}. \tag{4.93a}$$

The curves (4.93a) define transition regions with different topological structures. In particular, we find again the curves (4.93a), which are $\mathcal{D}_1$, $\mathcal{D}_2$, $\mathcal{D}_3$ and $\mathcal{D}_4$ coinciding with $\mathcal{E}_1$, $\mathcal{E}_2$, $\mathcal{E}_3$ and $\mathcal{E}_4$, respectively, plus another curve that we denote as $\mathcal{E}_0$.
If the matrix W features the parameters p_1, p_2 and p_3 only in polynomial form, then $\mathcal{D}_j$, with $j = 1, 2, 3, 4$, and $\mathcal{E}_0$ are algebraic varieties over the reals.

Definition 4.6.1. *Let*

$$\mathcal{C} = \left(\bigcup_{j=1,2,3,4} \mathcal{D}_j \right) \bigcup \mathcal{E}_0, \tag{4.94}$$

be the set of all the varieties $\mathcal{D}_j$ joined with $\mathcal{E}_0$. The set $\mathcal{C}$ defines the boundaries of the regions in the (p_1, p_2)-parameters space associated to different topologies of the spectra $\mathbf{S}_x$.

For instance, if the (effective[16]) parameter space is 2-dimensional, then $\mathcal{C}$ is a set of curves on the real plane.

Finally, in the figures 4.27 and 4.28, we show the curves $\mathcal{C}$ in the parameters space and the entire topological classification of the spectra in this space.

[16] The parameters p_1 and p_2 may appear in the definition of the varieties $\mathcal{D}_j$ and $\mathcal{E}$ combined in a certain number of functions, whose total number can be less than the original number of parameters; then, these functions of the parameters, on which the varieties depend, play the role of "effective" parameters.

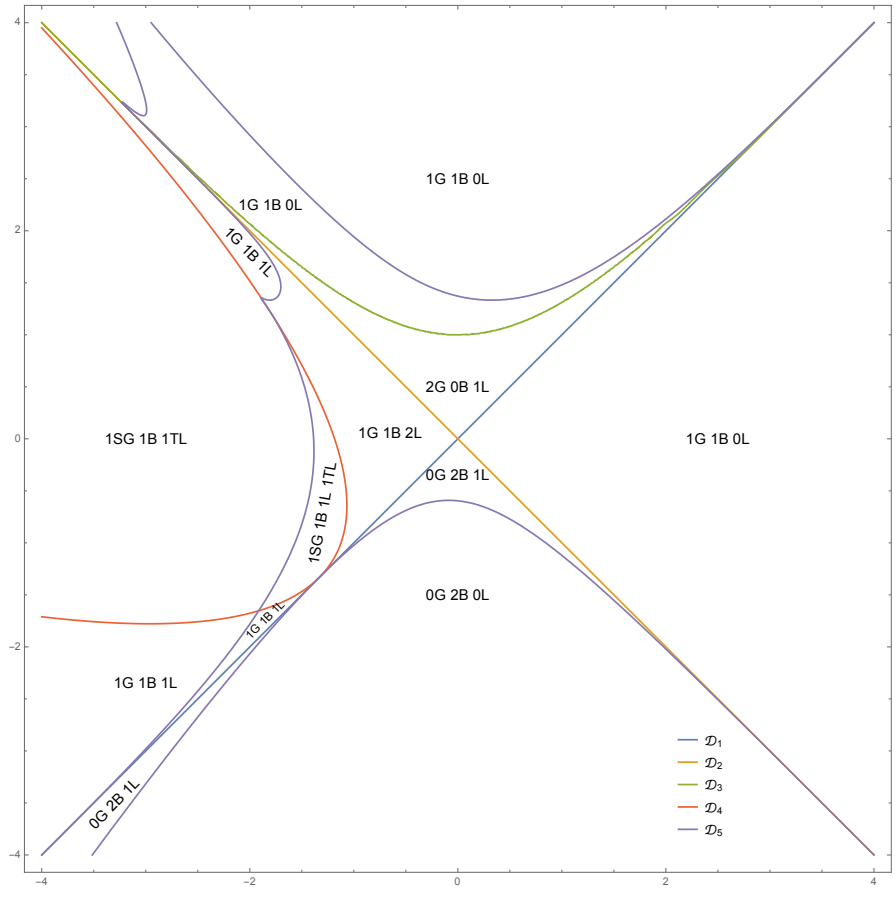

Figure 4.27: (p_1, p_2)-plane, $p_3 = -0.6$.

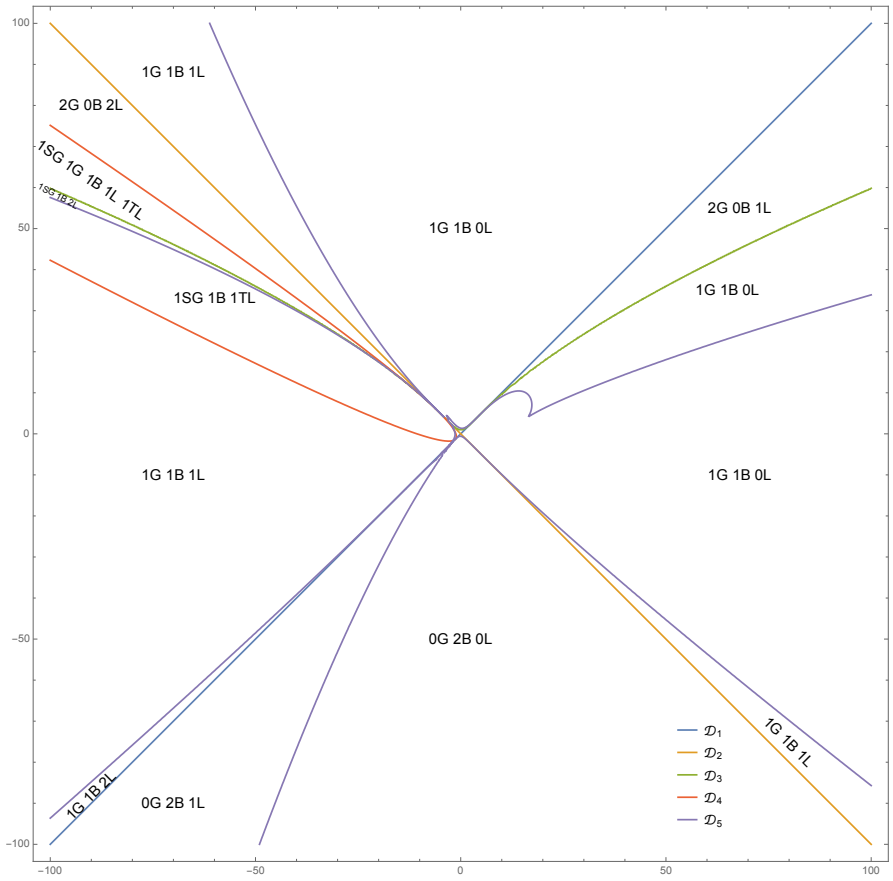

Figure 4.28: (p_1, p_2)-plane, $p_3 = -0.6$.

Chapter 5

Classification of the Stability Spectra on the Physical Parameters Space and Numerical Simulations

Based on the results obtained in the previous chapter, in the following we discuss the classification of the stability spectra in terms of the physical parameters space. We divide the parameters space in octants and in every octant we provide the values of the physical parameters. Then, we provide some examples of numerical solutions of the original 3WRI system to show that the plane wave solution is everywhere linearly unstable and that the presence of a branch into the stability spectrum can be associated, depending on the class of the perturbation, to the onset of localised structures such as breather-like solutions and potential rogue waves.

These numerical simulations have been included manly for the sake of complementing the analytical results: although the theory presented herein cannot quantitatively explain these numerical experiments, it is interesting to observe that perturbing plane waves associated to different spectra and integrating numerically (over a short time) the 3WRI system using the different perturbing waves yields different time evolutions and behaviours, hence suggesting a potential link, in the spirit of what has been done for the NLS system in [72]. This link may be the subject of future investigation.

5.1 Classification of the Stability Spectra on the Physical Parameters Space

The formulas (3.91) can be written as follows

$$s_1 s_2 s_3 p_1 = c_1^2 s_1 a_1^2 + c_2^2 s_2 a_2^2, \tag{5.1a}$$

$$s_1 s_2 s_3 p_2 = c_1^2 s_1 a_1^2 - c_2^2 s_2 a_2^2, \tag{5.1b}$$

by summing and subtracting (5.1) and (5.1b) we get, respectively,

$$c_1^2 = \frac{s_2 s_3}{2a_1^2}(p_1 + p_2), \tag{5.2a}$$

$$c_2^2 = \frac{s_1 s_3}{2a_2^2}(p_1 - p_2). \tag{5.2b}$$

Moreover, we know that

$$p_3 = \frac{c_1 - c_2}{c_1 + c_2}. \tag{5.3}$$

Let us separate the parameters space (p_1, p_2) in quadrants and let us enumerate clockwise the quadrants with the roman numbers I, II, III, IV. Then, let us separate further every quadrant in two parts or octants according to the following scheme:

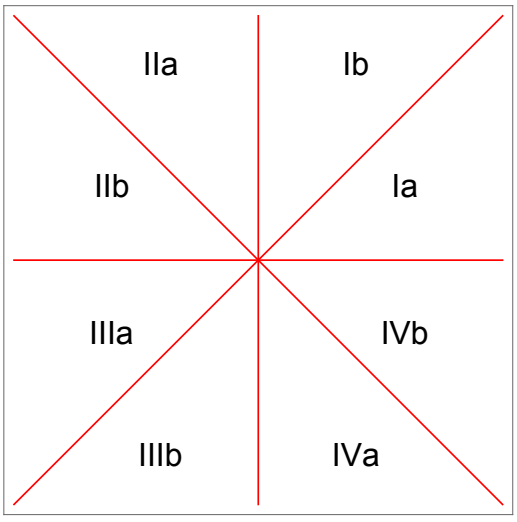

In every octant, we have the following relation between the parameters p_1 and p_2:

- Octant Ia: $|p_1| > |p_2|$, $p_1 > 0$ and $p_2 > 0$;
- Octant Ib: $|p_1| < |p_2|$, $p_1 > 0$ and $p_2 > 0$;
- Octant IIa: $|p_1| < |p_2|$, $p_1 < 0$ and $p_2 > 0$;
- Octant IIb: $|p_1| > |p_2|$, $p_1 < 0$ and $p_2 > 0$;
- Octant IIIa: $|p_1| > |p_2|$, $p_1 < 0$ and $p_2 < 0$;
- Octant IIIb: $|p_1| < |p_2|$, $p_1 < 0$ and $p_2 < 0$;
- Octant IVa: $|p_1| < |p_2|$, $p_1 > 0$ and $p_2 < 0$;
- Octant IVb: $|p_1| > |p_2|$, $p_1 > 0$ and $p_2 < 0$.

In order to see which choice of signs exists in any octant, let us take into account the formulas (5.2a) and (5.2b).

In the quadrant I, we have $p_1 > 0$ and $p_2 > 0$, then, by the formula (5.2a), it results in $s_2 s_3 = 1$, and so $s_2 = s_3 = \pm 1$. In the octant Ia, we have $p_1 > p_2$, then, by the formula (5.2b), $s_1 s_3 = 1$. This yields that the choice of signs is $\mathcal{S}_4^+$ or $\mathcal{S}_4^-$, that is $s_1 = s_2 = s_3 = \pm 1$. In the octant Ib, we have $p_1 < p_2$, thus, by the relation (5.2b), the choice of signs is $\mathcal{S}_3^+$ or $\mathcal{S}_3^-$, that is $s_1 = -1$ and $s_2 = s_3 = 1$ or $s_1 = 1$ and $s_2 = s_3 = -1$, respectively.

In the quadrant II, we have $p_1 < 0$ and $p_2 > 0$, and by the formula (5.2b), it results $s_1 s_3 = -1$, and so $s_1 = -s_3$. In the octant IIa, $p_1 > -p_2$, as a consequence of the relation (5.2a), we have $s_2 s_3 = 1$. Therefore, the choice of signs is $\mathcal{S}_3^+$ or $\mathcal{S}_3^-$, corresponding to $s_1 = -1$ and $s_2 = s_3 = 1$ or $s_1 = -$ and $s_2 = s_3 = -1$, respectively. On the other hand in the octant IIb, we have $p_1 < -p_2$. By the formula (5.2a), we obtain $s_2 s_3 = -1$. Thus we have the choices of signs $s_1 = s_2 = 1$ and $s_3 = -1$ or $s_1 = s_2 = -1$ and $s_3 = 1$ which are denoted as $\mathcal{S}_1^+$ and $\mathcal{S}_1^-$, respectively.

In the quadrant III, we have $p_1 < 0$ and $p_2 < 0$. By the relation (5.2a), we obtain $s_2 s_3 = -1$, that is $s_2 = -1$ and $s_3 = 1$ or $s_2 = 1$ and $s_3 = -1$. In the octant IIIa, $p_1 < p_2$, and as consequence of the formula (5.2b) we get $s_1 s_3 = -1$. Therefore, the combinations of signs are $s_1 = s_2 = 1$ and $s_3 = -1$ or $s_1 = s_2 = -1$ and $s_3 = 1$ corresponding to the choices $\mathcal{S}_1^+$ and $\mathcal{S}_1^-$, respectively. In the octant IIIb, we have $p_1 > p_2$, then $s_1 s_3 = 1$, that

is $s_1 = s_3 = 1$ and $s_3 = -1$ or $s_1 = s_3 = -1$ and $s_3 = 1$. They correspond to the choices $\mathcal{S}_2^+$ and $\mathcal{S}_2^-$, respectively.

In the quadrant IV, we have the relations $p_1 > 0$ and $p_2 < 0$. By the relation (5.2b), it results in $s_1 s_3 = 1$, and so $s_1 = s_3 = 1$ or $s_1 = s_3 = -1$. Moreover, in the octant IVa, $p_1 < -p_2$, then, by (5.2a) $s_2 s_3 = -1$, we obtain $s_1 = s_3 = 1$ and $s_2 = -1$ or $s_1 = s_3 = -1$ and $s_2 = 1$. These combinations of signs are denoted as $\mathcal{S}_2^+$ and $\mathcal{S}_2^-$, respectively. In the octant IVb, $p_1 > -p_2$ and, by the formula (5.2a), this yields $s_2 s_3 = 1$. Thus, we have $s_1 = s_2 = s_3 = 1$ or $s_2 = s_2 = s_3 = -1$, corresponding to te choices $\mathcal{S}_4^+$ or $\mathcal{S}_4^-$, respectively.

In the following subsection we will provide the mapping from the parameters p_1, p_2, p_3 into the parameters c_1, c_2, a_1 and a_2.

5.1.1 Octant Ia

By looking at the formulas (5.2), if $p_1 > p_2 > 0$, then $p_1 + p_2 > 0$ and $p_1 - p_2 > 0$. As a consequence, $s_1 s_3 = 1$ and $s_2 s_3 = 1$ and, so, $s_1 = s_2 = s_3$.

By subctracting (5.2a) from (5.2b)

$$c_1^2 - c_2^2 = \frac{1}{2a_1^2}(p_1 + p_2) - \frac{1}{2a_2^2}(p_1 - p_2) = \frac{1}{2a_1^2 a_2^2}[p_1(a_2^2 - a_1^2) + p_2(a_1^2 + a_2^2)]. \quad (5.4)$$

For $p_3 < 0$, we have $|c_2| > |c_1|$, so $c_1^2 - c_2^2 < 0$, and

$$0 < \frac{p_1}{p_2} < \frac{a_2^2 + a_1^2}{a_1^2 - a_2^2} \quad \text{then} \quad |a_1| > |a_2|. \quad (5.5)$$

Similarly, for $p_3 > 0$, we have $|c_2| < |c_1|$, the equation $c_1^2 - c_2^2 > 0$ gives us the condition $|a_1| > |a_2|$. We have $|a_1| \neq |a_2|$, otherwise $p_2 < 0$.

In conclusion, for both the cases $|c_2| > |c_1|$ ($p_3 < 0$) and $|c_2| < |c_1|$ ($p_3 > 0$) the amplitudes satisfy the relation $|a_1| > |a_2|$.

5.1.2 Octant Ib

By (5.2), if $p_2 > p_1 > 0$, then $p_1 + p_2 > 0$ and $p_1 - p_2 < 0$ and also we have $s_2 s_3 = 1$ and $s_1 s_3 = -1$. Thus, it results in $s_2 = s_3 = -s_1$.

By subtracting (5.2a) from (5.2b)

$$c_1^2 - c_2^2 = \frac{1}{2a_1^2}(p_1+p_2) + \frac{1}{2a_2^2}(p_1-p_2) = \frac{1}{2a_1^2a_2^2}[p_1(a_1^2+a_2^2) + p_2(a_2^2-a_1^2]) < 0. \quad (5.6)$$

For $p_3 < 0$, we have $|c_2| > |c_1|$. Thus,

$$0 < \frac{p_1}{p_2} < \frac{a_1^2 - a_2^2}{a_2^2 + a_1^2} \quad \text{then} \quad |a_1| > |a_2|. \quad (5.7)$$

It must be $|a_1| \neq |a_2|$, although we have the contradiction $p_1 < 0$.

One can show that for both $|c_2| > |c_1|$ ($p_3 < 0$) and $|c_2| < |c_1|$ ($p_3 > 0$) the amplitudes satisfy the relation $|a_1| > |a_2|$.

5.1.3 Octant IIa

By (5.2), if $p_2 > 0$ and $p_1 < 0$ and $|p_2| > |p_1|$, then $p_1 + p_2 > 0$ and $p_1 - p_2 < 0$ and $s_2 s_3 = 1$ and $s_1 s_3 = -1$. This entails $s_2 = s_3 = -s_1$.

By summing (5.2a) and (5.2b)

$$c_1^2 + c_2^2 = \frac{1}{2a_1^2}(p_1+p_2) - \frac{1}{2a_2^2}(p_1-p_2) = \frac{1}{2a_1^2a_2^2}[p_1(a_2^2-a_1^2) + p_2(a_2^2+a_1^2)] > 0. \quad (5.8)$$

Thus,

$$0 > \frac{p_1}{p_2} > \frac{a_1^2 + a_2^2}{a_1^2 - a_2^2}, \quad \text{then}, \quad |a_1| < |a_2|. \quad (5.9)$$

In this case, if $|a_1| \neq |a_2|$, otherwise $p_1 > 0$.

For both $|c_2| > |c_1|$ ($p_3 < 0$) and $|c_2| < |c_1|$ ($p_3 > 0$) the amplitudes satisfy the relation $|a_1| < |a_2|$.

5.1.4 Octant IIb

By (5.2), if $p_2 > 0$ and $p_1 < 0$ and $|p_1| > |p_2|$, then we obtain $p_1 + p_2 > 0$ and $p_1 - p_2 < 0$ and $s_2 s_3 = 1$ and $s_1 s_3 = -1$. As a result, we get $s_2 = s_3 = -s_1$. By summing (5.2a) and (5.2b)

$$c_1^2 + c_2^2 = \frac{1}{2a_1^2}(p_1+p_2) - \frac{1}{2a_2^2}(p_1-p_2) = \frac{1}{2a_1^2a_2^2}[p_1(a_2^2-a_1^2) + p_2(a_2^2+a_1^2)] > 0. \quad (5.10)$$

Therefore,

$$0 > \frac{p_2}{p_1} > \frac{a_1^2 - a_2^2}{a_2^2 + a_1^2} \quad \text{then} \quad |a_1| < |a_2|. \tag{5.11}$$

Also in this case $|a_1| \neq |a_2|$, otherwise we have a contradiction. Finally, for both $|c_2| > |c_1|$ ($p_3 < 0$) and $|c_2| < |c_1|$ ($p_3 > 0$) the amplitudes satisfy the relation $|a_1| < |a_2|$.

5.1.5 Octant IIIa

By (5.2), if $p_1 < p_2 < 0$, then $p_1 + p_2 < 0$ and $p_1 - p_2 < 0$ and $s_2 s_3 = -1$ and $s_1 s_3 - 1$. This entails $s_1 = s_2 = -s_3$.

By subtracting (5.2a) from (5.2b)

$$c_1^2 - c_2^2 = -\frac{1}{2a_1^2}(p_1 + p_2) + \frac{1}{2a_2^2}(p_1 - p_2) = \frac{1}{2a_1^2 a_2^2}[p_1(a_1^2 - a_2^2) - p_2(a_2^2 + a_1^2)] < 0. \tag{5.12}$$

Therefore,

$$0 < \frac{p_1}{p_2} < \frac{a_1^2 + a_2^2}{a_1^2 - a_2^2} \quad \text{then} \quad |a_1| > |a_2|. \tag{5.13}$$

If $|a_1| = |a_2|$, we have the contradiction $p_2 > 0$.

For both $|c_2| > |c_1|$ ($p_3 < 0$) and $|c_2| < |c_1|$ ($p_3 > 0$) the amplitudes satisfy the relation $|a_1| > |a_2|$.

5.1.6 Octant IIIb

By (5.2), if $p_2 < p_1 < 0$, then $p_1 + p_2 < 0$ and $p_1 - p_2 > 0$ and $s_2 s_3 - 1$ and $s_1 s_3 = 1$. Therefore, it turns out $s_1 = s_3 = -s_2$.

By subctring (5.2a) from (5.2b)

$$c_1^2 - c_2^2 = -\frac{1}{2a_1^2}(p_1 + p_2) - \frac{1}{2a_2^2}(p_1 - p_2) = \frac{1}{2a_1^2 a_2^2}[-p_1(a_2^2 + a_1^2) + p_2(a_1^2 - a_2^2)] < 0. \tag{5.14}$$

Thus,

$$0 < \frac{p_2}{p_1} < \frac{a_1^2 + a_2^2}{a_1^2 - a_2^2} \quad \Longrightarrow \quad |a_1| > |a_2|. \tag{5.15}$$

If $|a_1| = |a_2|$, we have the contradiction $p_1 > 0$. For both $|c_2| > |c_1|$ ($p_3 < 0$) and $|c_2| < |c_1|$ ($p_3 > 0$) the amplitudes satisfy the relation $|a_1| > |a_2|$.

5.1.7 Octant IVa

By (5.2), if $p_2 < 0$ and $p_1 > 0$ and $|p_2| > |p_1| \implies p_1 + p_2 < 0$ and $p_1 - p_2 > 0$. $s_2 s_3 = -1$ and $s_1 s_3 = 1$ entails $s_1 = s_3 = -s_2$.
By summing (5.2a) and (5.2b)

$$c_1^2 + c_2^2 = -\frac{1}{2a_1^2}(p_1 + p_2) + \frac{1}{2a_2^2}(p_1 - p_2) = \frac{1}{2a_1^2 a_2^2}[p_1(a_1^2 - a_2^2) - p_2(a_2^2 + a_1^2)] > 0. \quad (5.16)$$

Thus,

$$0 > \frac{p_1}{p_2} > \frac{a_1^2 + a_2^2}{a_1^2 - a_2^2} \quad \implies \quad |a_1| < |a_2|. \quad (5.17)$$

If $|a_1| = |a_2|$, then $p_2 < 0 \ \forall a_1, a_2$. For both $|c_2| > |c_1|$ ($p_3 < 0$) and $|c_2| < |c_1|$ ($p_3 > 0$) the amplitudes satisfy the relation $|a_1| \leq |a_2|$.

5.1.8 Octant IVb

By (5.2), if $p_2 < 0$ and $p_1 > 0$ and $|p_1| > |p_2|$ yields $p_1 + p_2 > 0$ and $p_1 - p_2 > 0$. If $s_2 s_3 = 1$ and $s_1 s_3 = 1$, then $s_1 = s_3 = s_2$. By summing (5.2a) and (5.2b)

$$c_1^2 + c_2^2 = \frac{1}{2a_1^2}(p_1 + p_2) + \frac{1}{2a_2^2}(p_1 - p_2) = \frac{1}{2a_1^2 a_2^2}[p_1(a_1^2 + a_2^2) + p_2(a_2^2 - a_1^2)] > 0. \quad (5.18)$$

Thus,

$$0 > \frac{p_1}{p_2} > \frac{a_1^2 - a_2^2}{a_1^2 + a_2^2} \quad \implies \quad |a_1| < |a_2|. \quad (5.19)$$

If $|a_1| = |a_2|$, then $p_1 > 0 \ \forall a_1, a_2$. Finally, for both $|c_2| > |c_1|$ ($p_3 < 0$) and $|c_2| < |c_1|$ ($p_3 > 0$) the amplitudes satisfy the relation $|a_1| \leq |a_2|$.

5.1.9 Transformations of the Physical Parameters

In the following we provide the transformations form the parameters p_1, p_2, p_3 and p_4 to the velocities c_1, c_2, to the amplitudes a_1, a_2 and to the signs s_1, s_2 and s_3.
The velocities c_1 and c_2 can be also written as

$$c_1 = \frac{(1 + p_3)p_4}{2}, \quad (5.20a)$$

$$c_2 = \frac{(1-p_3)p_4}{2}. \tag{5.20b}$$

In the following we provide the values of the signs s_j, $j = 1, 2, 3$, for different range of the parameters p_1 and p_2.

- if $p_2 < 0$ and $p_1 \leq p_2$: $s_1 = -1$, $s_2 = -1$, $s_3 = 1$;
- if $p_2 < 0$ and $-p_2 < p_1 < p_2$: $s_1 = -1$, $s_2 = 1$, $s_3 = -1$;
- if $p_2 < 0$ and $p_1 \geq -p_2$: $s_1 = -1$, $s_2 = -1$, $s_3 = -1$;
- if $p_2 > 0$ and $p_1 \leq -p_2$: $s_1 = -1$, $s_2 = -1$, $s_3 = 1$;
- if $p_2 > 0$ and $-p_2 < p_1 < p_2$: $s_1 = -1$, $s_2 = 1$, $s_3 = 1$;
- if $p_2 > 0$ and $p_1 \geq p_2$: $s_1 = -1$, $s_2 = -1$, $s_3 = -1$;
- if $p_2 = 0$ and $p_1 < 0$: $s_1 = -1$, $s_2 = -1$, $s_3 = 1$;
- if $p_2 = 0$ and $p_1 > 0$: $s_1 = -1$, $s_2 = -1$, $s_3 = -1$.

If $p_1 = p_2 = 0$, then $a_1 = a_2 = 0$ and is not considered.

The amplitudes transform as follows

$$a_1 = \frac{\sqrt{2s_2s_3(p_1+p_2)}}{|1+p_3||p_4|}, \tag{5.21a}$$

$$a_2 = \frac{\sqrt{2s_2s_3(p_1-p_2)}}{|1-p_3||p_4|}. \tag{5.21b}$$

5.2 Numerical Simulations

In this section we show some numerical observations of different evolution obtained by integrating numerically the 3WRI system from a perturbed plane wave solution.

We use two kinds of perturbations: a localised perturbation and a random perturbation[1].

[1] In this respect, it is right to highlight that the linear stability analysis of plane wave solutions of the scalar NLS equation when these plane waves are perturbed via periodic perturbations was carried out in [38, 39, 40, 41, 42, 43]

We fix p_1, p_2 and p_3 and we reconstruct all the physical parameters, a_1, a_2, c_1, c_2, s_1, s_2, s_3, based on the formulae in Section 5.1.9. Using these parameters, we construct the corresponding plane wave solution. We compute this plane wave solution at $t = 0$, we perturb it spatially and we use it as the initial condition for our numerical simulation. Each initial condition is perturbed alternatively in two different ways:

- through a localised perturbation, added to the initial data (individually to each $u_j's$), having the form:

$$\epsilon \cos\left(\frac{\pi x}{2L}\right) e^{-\alpha x^2}, \tag{5.22}$$

  where L is the semi-length of the numerical integration interval, ϵ is the amplitude of the perturbation (in the following $\epsilon = 10^{-3}$, unless specified differently), and α is a chosen parameter, typically set to 2 (in the following $\alpha = 2$, unless specified differently);

- through a random perturbation, added as a noise to the initial data (individually to each $u_j's$), having the form:

$$\epsilon\psi(x) \quad \text{with} \quad \psi(-L) = \psi(L) = 0, \tag{5.23}$$

  where $\psi(x)$ for $x \in (-L, L)$ is a uniform distribution in the interval $[0, 1]$, L is again the semi-length of the integration interval and ϵ is the amplitude of the perturbation; in the implementation, the random perturbation is smoothened by computing ψ on a subset of the spatial nodes and then by using a Whittaker-Shannon interpolation formula [119] over the remaining nodes (see Appendix N).

As for the numerical scheme applied, we use the method of lines with a pseudospectral, Fourier discretisation in space and an adaptive Runge-Kutta scheme in time implemented in MATLAB R2017a (see Appendix O and Appendix P). In order to apply the pseudospectral method, it is very convenient to have initial conditions independent of the space variable. Let us provide the following transformation:

$$\begin{cases} \tilde{u}_1 = e^{i\nu_1(x-c_1t)}u_1, \\ \tilde{u}_2 = e^{i\nu_2(x-c_2t)}u_2, \\ \tilde{u}_3 = e^{i(\nu_3 x+\omega t)}u_3, \end{cases} \tag{5.24}$$

where

$$\nu_1 = \frac{\eta_1}{c_1} + s_1 s_3 a_2^2 \frac{c_2}{c_1} \frac{(c_1 - c_2)}{\eta_1 + \eta_2}, \tag{5.25a}$$

$$\nu_2 = \frac{\eta_2}{c_2} + s_2 s_3 a_1^2 \frac{c_1}{c_2} \frac{(c_1 - c_2)}{\eta_1 + \eta_2}, \tag{5.25b}$$

$$\nu_3 = -(\nu_1 + \nu_2), \tag{5.25c}$$

$$\omega = c_1 \nu_1 + c_2 \nu_2 \tag{5.25d}$$

then, it is straightforward to verify that $\tilde{u}_1$, $\tilde{u}_2$, $\tilde{u}_3$ satisfy the following system of PDEs [2]

$$\begin{cases} \tilde{u}_{1t} = -c_1 \tilde{u}_{1x} + s_1 c_2 \tilde{u}_2^* \tilde{u}_3^*, \\ \tilde{u}_{2t} = -c_2 \tilde{u}_{2x} + s_2 c_1 \tilde{u}_1^* \tilde{u}_3^*, \\ \tilde{u}_{3t} = i\omega \tilde{u}_3 + s_3 (c_1 - c_2) \tilde{u}_1^* \tilde{u}_2^*, \end{cases} \tag{5.26}$$

with the following initial conditions

$$\begin{cases} \tilde{u_1}(x,0) = e^{i\nu_1 x} u_1(x,0), \\ \tilde{u_2}(x,0) = e^{i\nu_2 x} u_2(x,0), \\ \tilde{u_3}(x,0) = e^{i\nu_3 x} u_3(x,0). \end{cases} \tag{5.27}$$

We integrate system (5.26) with initial condtions (5.27) and the we invert (5.24) to obtain the solutions in terms of the $u_j' s$ starting from the solutions in terms of the $\tilde{u}_j' s$.
Observe that, if $u_j(x,t)$ is the plane wave solution (3.30), then $\tilde{u}_j(x,t)$ does not depend explicitly on the space variable x, indeed we have

$$\begin{cases} \tilde{u}_1 = a_1 e^{i(\eta_1 - \nu_1 c_1)t}, \\ \tilde{u}_2 = a_2 e^{i(\eta_2 - \nu_2 c_2)t}, \\ \tilde{u}_3 = a_3 e^{i(\eta_3 + \omega)t}, \end{cases} \tag{5.28}$$

[2] Although the solutions $\tilde{u}_j$, for $j = 1, 2, 3$ may appear simpler than those ones used in the theoretical part of the Thesis, they satisfy a system (see formula (5.26)) more complicated than that one used for the analytical computations and dealing with it would result an useless effort. On the other hand, the system (5.26) has been found useful for the numerics in this Chapter.

with a_3 as in (3.32), and $\eta_3 = -(\eta_1 + \eta_2)$.

In particular, from (5.28), we see that $\tilde{u}_j(x,0)$ does not depend on the spatial variable x, and hence the integration interval [3] $[-L, L]$ can be taken arbitrary for system (5.26) using (5.28) at $t = 0$ as initial conditions.

In the following we denote with

$$\rho_j^{(0)} = \max_{x\in[-L,L]} \frac{|u_j(x,0)|}{a_j}\,, \tag{5.29a}$$

the ratio between the initial maximum of the absolute value of the perturbed solution and a_j (that is the amplitude of the unperturbed wave); we also introduce

$$\bar{\rho}_j = \max_{x\in[-L,L],t\in[0,T]} \frac{|u_j(x,t)|}{a_j}\,, \tag{5.29b}$$

namely, the ratio between the maximum of the absolute value of the perturbed solution on the whole integration domain $[-L, L] \times [0, T]$ and a_j.

Before we show some numeric simulations, it is right to provide the following definition of rogue wave:

"*In the real ocean, rogue waves are waves that are very steep and much higher than the surrounding waves in a wave record, which is usually of 20-minute length;...There is currently no consensus on one unique definition of a rogue wave, but a common and simple approach is to define a rogue wave as a wave whose wave height or crest height exceeds some thresholds related to the significant wave height. A common definition is to apply the criteria (Haver, 2000)*:

$$\frac{H_{max}}{H_s} > 2, \quad \text{and/or} \quad \frac{C_{max}}{H_s} > 1.25,$$

where H_{max} denotes the zero-crossing wave height, C_{max} is the crest height, and H_s is the significant wave height, defined as four times the standard deviation of the surface, typically calculated from a 20-minute measurement of the surface elevation." [120].

Because of this definition, we report the value $\bar{\rho}_{max}$ for each numerical solution and this value will give us in percentage the ratio between the maximum value obtained by the numerical simulations and the background. We will state that we have a potential rogue wave any time the maximum value of the solution exceeds at least of three times the value of

[3] The range of values of L is taken as larger as possible to make sure that all the modes with higher velocities are included as well.

the background. We will state that we have a potential rogue wave any time the maximum value of the solution exceeds at least three times the value of the background.

5.2.1 2**G** 0**SG** 0**B** 1**L** 0**TL**

We investigate the region 2G 0B 1L that is located near the origin in the parameter space (see Figure 4.27).
We choose the parameters $p_1 = 0.2$, $p_2 = 0.3$, $p_3 = -0.6$ and $p_4 = 1$ corresponding to the velocities $c_1 = 0.2$, $c_2 = 0.8$, to the amplitudes $a_1 = 2.5$, $a_2 = 0.27951$ and to the choice of signs $s_1 = 1$, $s_2 = 1$, $s_3 = 1$. In particular with the localised perturbation, we observe:

- $\rho_1^{(0)} = 0.04\%$ and $\bar{\rho}_1 = 0.052206\%$;
- $\rho_2^{(0)} = 0.35777\%$ and $\bar{\rho}_2 = 0.35777\%$;
- $\rho_3^{(0)} = 0.47703\%$ and $\bar{\rho}_3 = 0.82379\%$.

By perturbing with random perturbation, we observe:

- $\rho_1^{(0)} = 0.058176\%$ and $\bar{\rho}_1 = 0.17725\%$;
- $\rho_1^{(0)} = 0.48424\%$ and $\bar{\rho}_2 = 0.61943\%$;
- $\rho_1^{(0)} = 0.57518\%$ and $\bar{\rho}_3 = 1.6717\%$.

5.2.2 0**G** 0**SG** 2**B** 1**L** 0**TL**

We investigate the region 0G 2B 1L that is located near the origin on the parameter space (see Figure 4.27).
We choose the parameters $p_1 = 0.2$, $p_2 = -0.4$, $p_3 = -0.6$ and $p_4 = 1$ corresponding to the velocities $c_1 = 0.2$, $c_2 = 0.8$, to the amplitudes $a_1 = 1.5811,$, $a_2 = 0.68465$ and to the choice of signs $s_1 = -1$, $s_2 = 1$, $s_3 = -1$. In particular with the localised perturbation (5.22), we observe:

- $\rho_1^{(0)} = 0.063246\%$ and $\bar{\rho}_1 = 333.6069\%$;
- $\rho_2^{(0)} = 0.14606\%$ and $\bar{\rho}_2 = 598.6718\%$;
- $\rho_3^{(0)} = 0.30792\%$ and $\bar{\rho}_3 = 1014.7219\%$.

By perturbing with random perturbation, we observe:

- $\rho_1^{(0)} = 0.082294\%$ and $\bar{\rho}_1 = 239.9949\%$;
- $\rho_2^{(0)} = 0.18711\%$ and $\bar{\rho}_2 = 407.9717\%$;
- $\rho_3^{(0)} = 0.52058\%$ and $\bar{\rho}_3 = 607.7822\%$.

5.2.3 1G 1SG 0B 1L 1TL

We choose the parameters $p_1 = -90.0$, $p_2 = 60.0$, $p_3 = -0.6$ and $p_4 = 1$ corresponding to the velocities $c_1 = 0.2$, $c_2 = 0.8$, to the amplitudes $a_1 = 19.3649$, $a_2 = 10.8253$ and to the choice of signs $s_1 = 1$, $s_2 = 1$, $s_3 = -1$. In this case we have explosive behaviour and, in particular, with the localised perturbation (5.22), we observe explosion at $t = 0.75$ seconds:

- $\rho_1^{(0)} = 0.005164\%$ and $\bar{\rho}_1 = 502961.1987\%$;
- $\rho_2^{(0)} = 0.0092376\%$ and $\bar{\rho}_2 = 449856.3477\%$;
- $\rho_3^{(0)} = 0.0015901\%$ and $\bar{\rho}_3 = 134122.7821\%$.

We do not report the plots fro these simulations because they are all blu coloured. We run the simulations for the solutions $|u_1|$, $|u_2|$ and $|u_3|$ in the region 1G 1SG 0B 1L 1TL after localised perturbation and the simulations run over a time $0 \leq t \leq 0.7$ and a space $-30 \leq x \leq 30$. We observe the maximum for $|u_1|$ is 97416.7 on the background with intensity 18.6, the solution $|u_2|$ reaches its maximum of intensity at 48707.7 on the background with intensity 9.2 and the solution $|u_3|$ has its maximum of intensity at 84365.7 on the background of intensity 62.8.

With the random perturbation (5.23), we observe explosion at $t = 0.71375$ seconds:

- $\rho_1^{(0)} = 0.0072695\%$ and $\bar{\rho}_1 = 502961.1987\%$;
- $\rho_2^{(0)} = 0.011944\%$ and $\bar{\rho}_2 = 478.2925\%$;
- $\rho_3^{(0)} = 0.0022268\%$ and $\bar{\rho}_3 = 140.8017\%$.

We do not report the plots fro these simulations because they are all blu coloured. We have observed the evolutions of the solutions $|u_1|$, $|u_2|$ and $|u_3|$ in the region 1G 1SG 0B 1L 1TL after random perturbation and the simulations run over a time $0 \leq t \leq 0.7$ and a space $-30 \leq x \leq 30$. The maximum reached by $|u_1|$ is 122.8 on the background with intensity 0.5, the solution $|u_2|$ reaches its maximum of intensity at 61.3 on the background with intensity 1.9 and the solution $|u_3|$ has its maximum of intensity at 122.3 on the background of intensity 60.7

Conjecture 5.2.1. *The presence of a twisted loop (or a split-gap) in a stability spectrum corresponds to a solution that is explosive in time.*

Conjecture 5.2.2. *The existence of branches in a stability spectrum is a necessary condition for the onset of rogue waves ascribable to rational or semi-rational solutions and which can be obtained by DDT.*

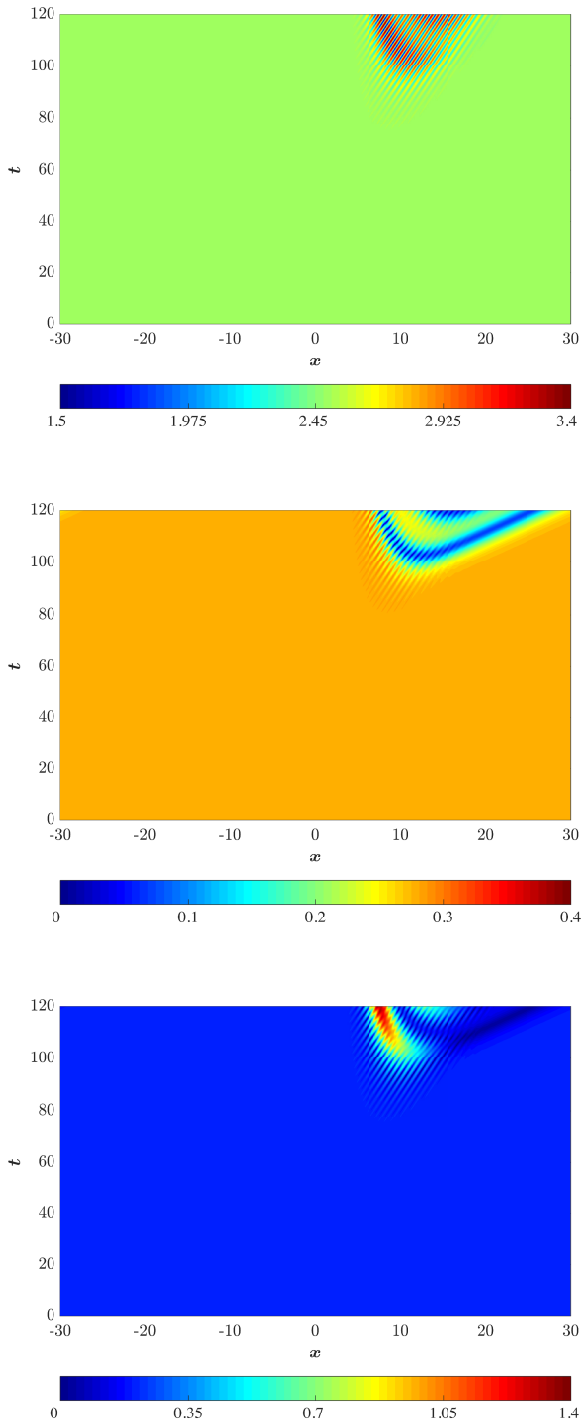

Figure 5.1: Solutions $|u_1|$, $|u_2|$ and $|u_3|$ in the region 2G 0SG 0B 1L 0TL after localised perturbation. The simulations run over a time $0 \leq t \leq 120$ and a space $-20 \leq x \leq 20$.

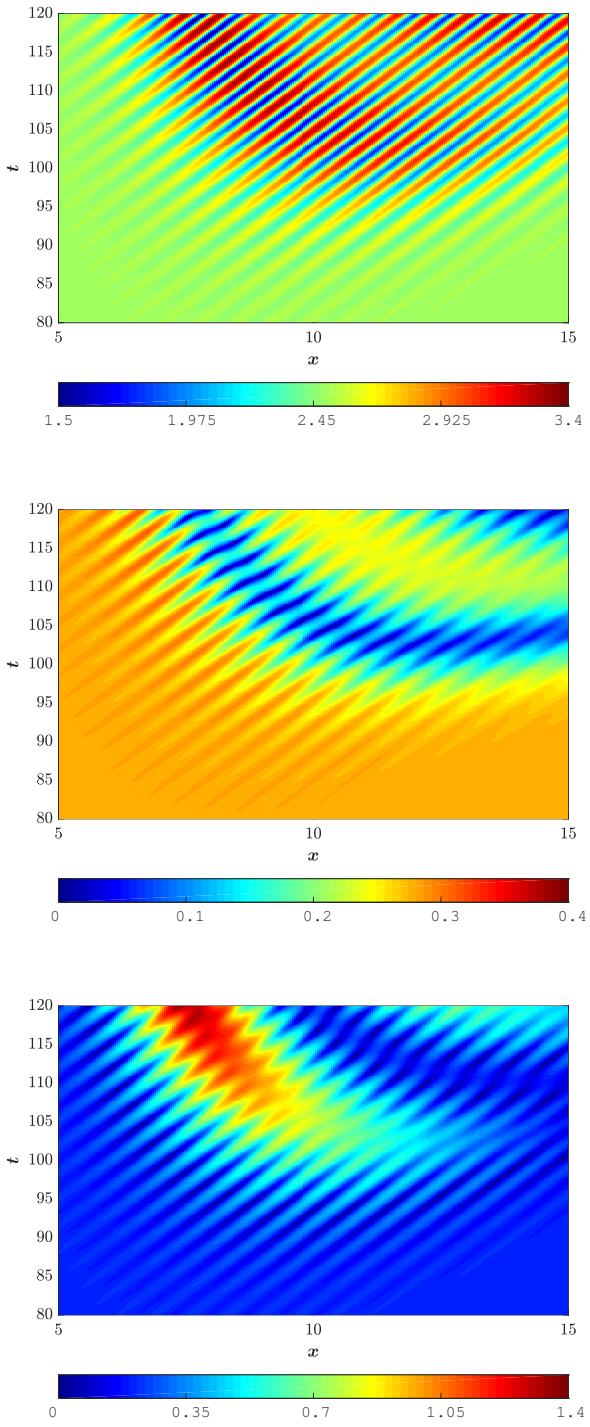

Figure 5.2: Zoom of the solutions $|u_1|$, $|u_2|$ and $|u_3|$ in the region 2G 0SG 2B 1L 0TL after localised perturbation. The simulations run over a time $80 \leq t \leq 120$ and a space $5 \leq x \leq 15$.

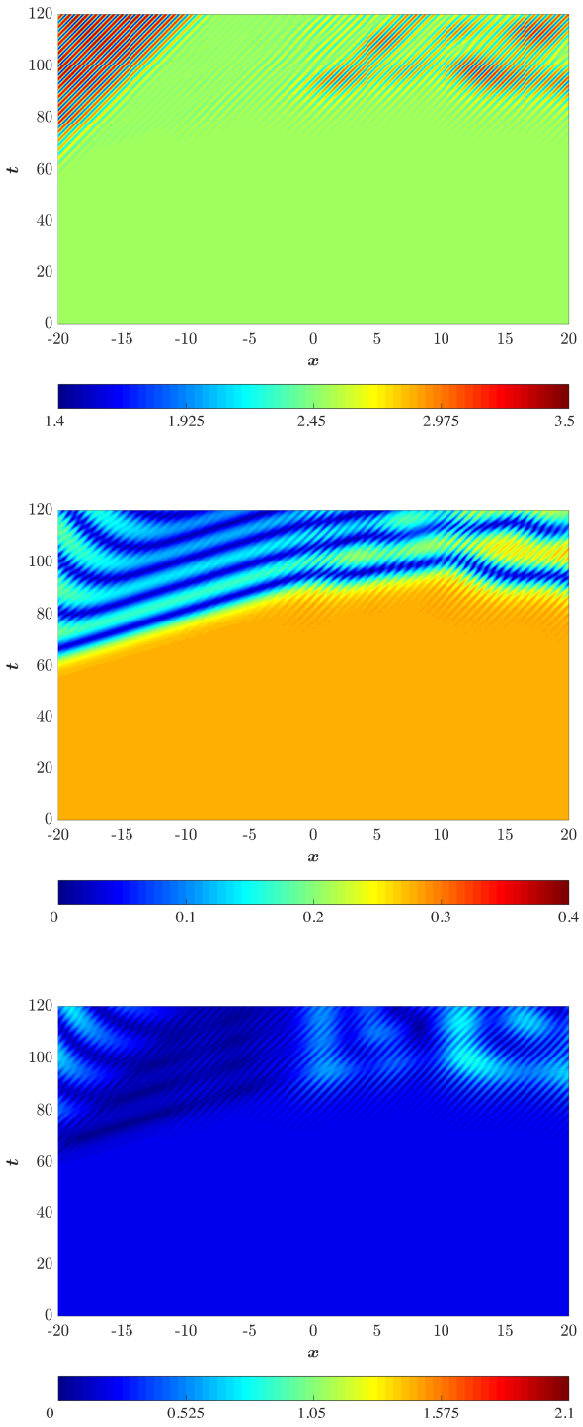

Figure 5.3: Solutions $|u_1|$, $|u_2|$ and $|u_3|$ in the region 2G 0SG 0B 1L 0TL after random perturbation. The simulations run over a time $0 \leq t \leq 120$ and a space $-20 \leq x \leq 20$.

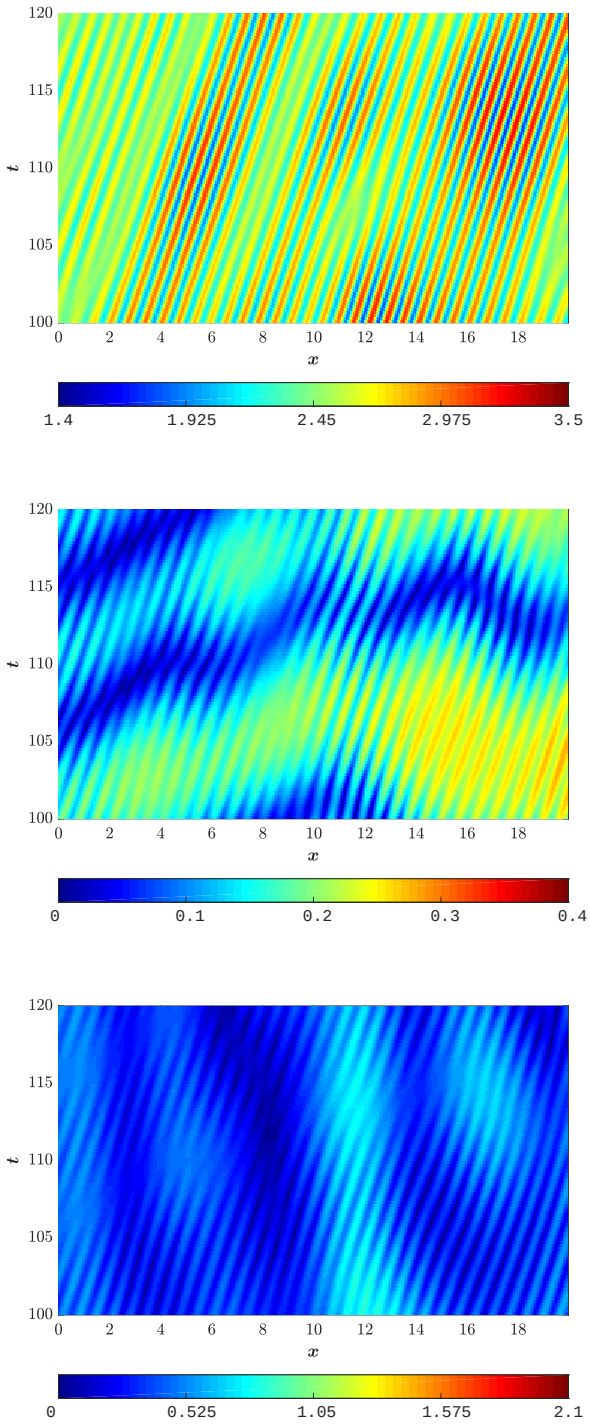

Figure 5.4: Zoom of the solutions $|u_1|$, $|u_2|$ and $|u_3|$ in the region 2G 0SG 2B 1L 0TL after random perturbation. The simulations run over a time $100 \leq t \leq 120$ and a space $0 \leq x \leq 20$.

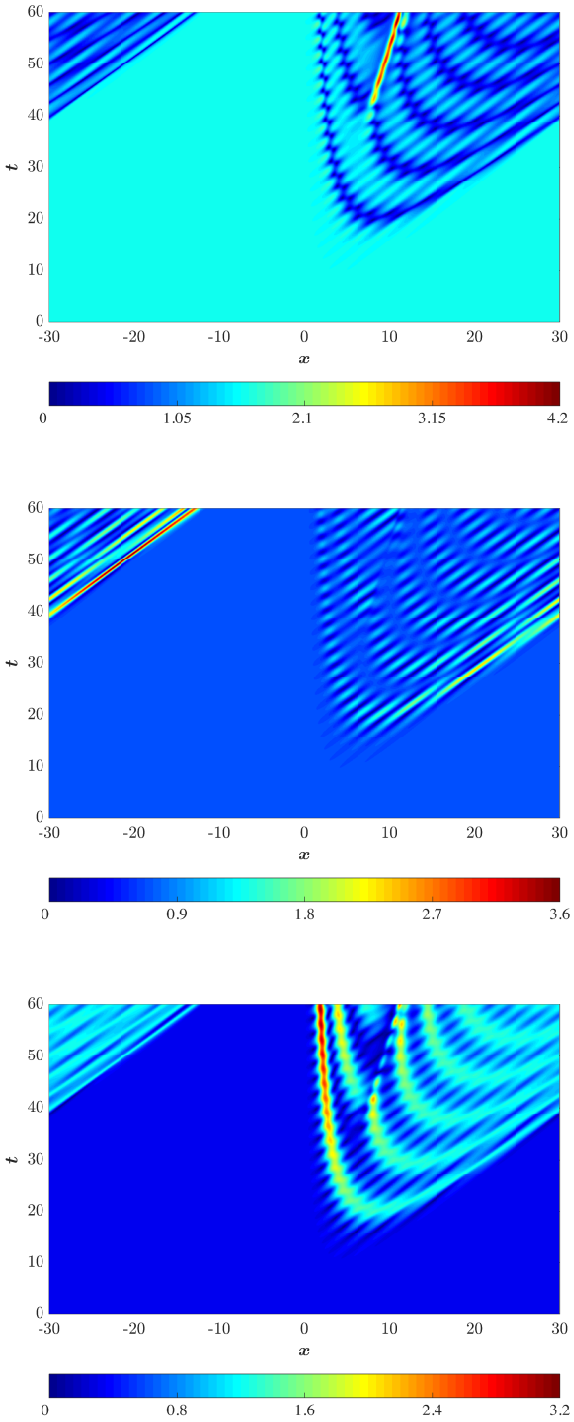

Figure 5.5: Solutions $|u_1|$, $|u_2|$ and $|u_3|$ in the region 0G 0SG 2B 1L 0TL after localised perturbation. The simulations run over a time $0 \leq t \leq 60$ and a space $-30 \leq x \leq 30$. These localised structures resemble the breather solutions of the NLS equation [121]. We observe a complementarity in the pattern and in the colours between the three solutions displayed, this suggests a well defined exchange of energy between the three solutions that is interesting to be studied deeper in future works.

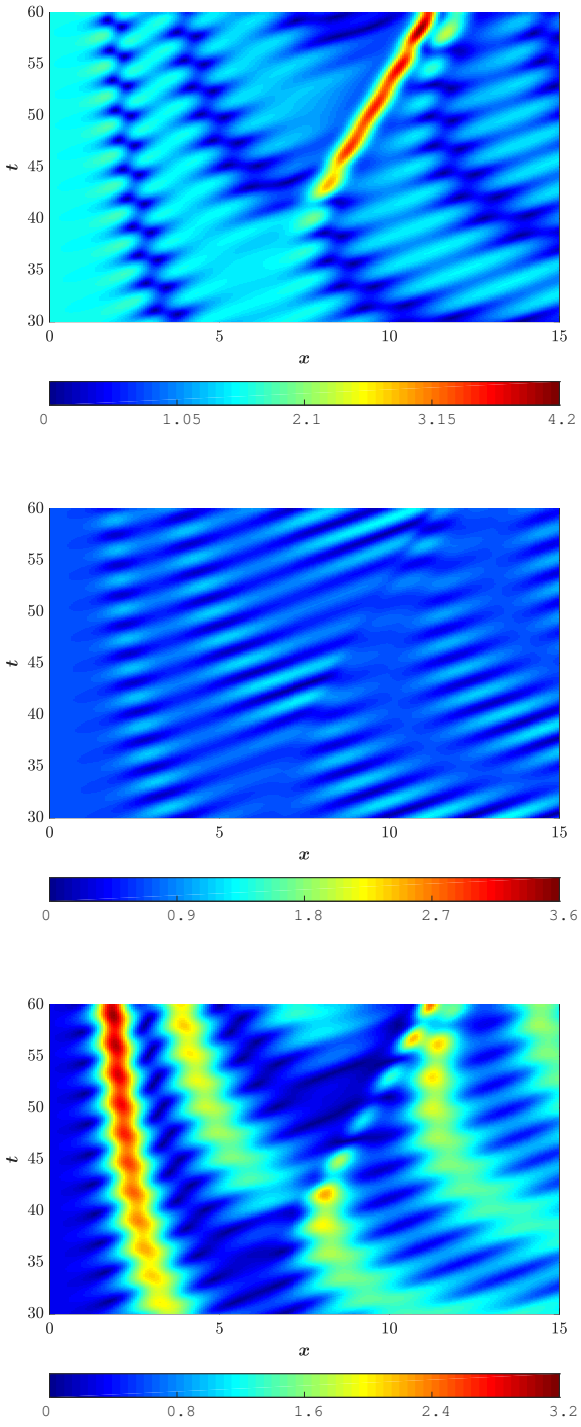

Figure 5.6: Zoom of the solutions $|u_1|$, $|u_2|$ and $|u_3|$ in the region 0G 0SG 2B 1L 0TL after localised perturbation. The simulations run over a time $0 \leq t \leq 30$ and a space $0 \leq x \leq 15$. In the plots for $|u_1|$ and $|u_3|$ we have localised structures which are breathe-like solutions with a maximum of intensity of 4.2 and 3.2 (red colour) on a background with intensity 0 (blu colour).

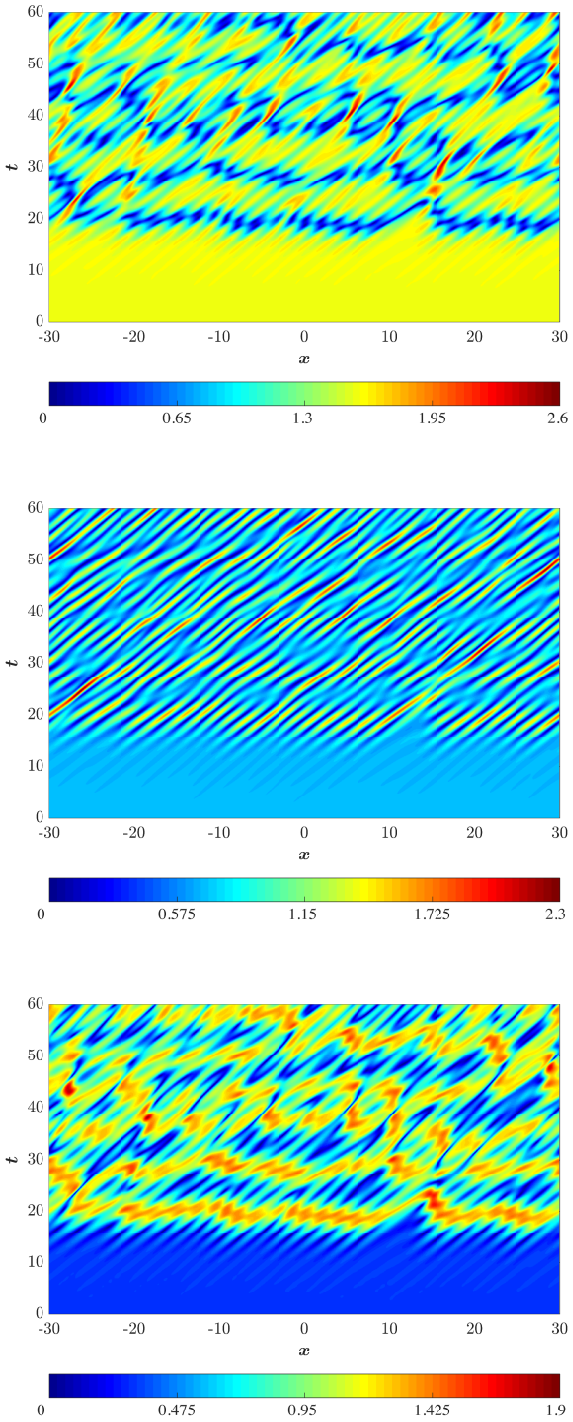

Figure 5.7: Solutions $|u_1|$, $|u_2|$ and $|u_3|$ in the region 0G 0SG 2B 1L 0TL after random perturbation. The simulations run over a time $0 \leq t \leq 60$ and a space $-30 \leq x \leq 30$. We observe a complementarity in the pattern and in the colours between the the three solutions displayed, this suggests a well defined exchange of energy between the three solutions that is interesting to be studied deeper in future works.

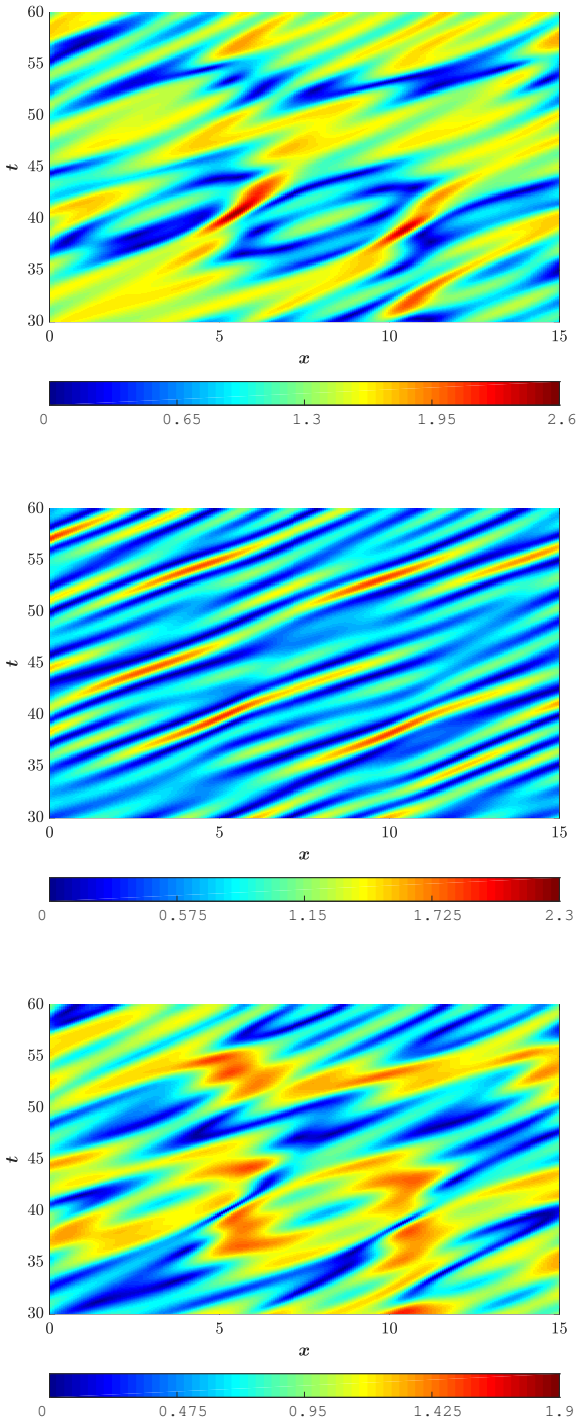

Figure 5.8: Zoom of the solutions $|u_1|$, $|u_2|$ and $|u_3|$ in the region 0G 0SG 2B 1L 0TL after random perturbation. The simulations run over a time $0 \leq t \leq 30$ and a space $0 \leq x \leq 15$. In the plots of $|u_1|$ and $|u_2|$ we have potential rogue waves with a maximum of intensity of 2.6 and 2.3 (red colour) on a background with 0 intensity (blu colour). These localised structures resemble the development of "integrable turbulence" studied for the focusing NLS equation in [39].

Chapter 6

Conclusions

6.1 Summary of the Results

The aim of this thesis has been the analysis of the spectral stability of plane wave solutions of the 3WRI model, when such solutions undergo localised perturbations. The approach is based on a spectral method recently developed in [64] to carry out the stability analysis of a nonlinear multi-component system, when the solutions have a non-vanishing background. The problem of assessing the stability of solutions of the 3WRI system had been already investigated in the literature. For instance, Kaup's research works [57, 63, 58] had focussed on the stability analysis of the 3WRI model with soliton solutions on vanishing background, which can be obtained, in principle, by the IST method [31, 30, 29, 53]. It is well known that the IST machinery, in addition to being technically cumbersome to apply to multi-component systems, depends on the boundary conditions (*e.g.* by requiring the solution and its first derivative to be in the class of potentials vanishing sufficiently fast to infinity). On the contrary, the method in [64] is independent of the class of the potentials and tailor-made for the application to multi-component systems. We have obtained several results:

- By applying the method in [64] to the 3WRI model, we have provided for the first time, a comprehensive topological classification of the spatial stability spectra (as curves on the complex plane) with respect to the parameters space and the gain functions associated to any stability spectrum.

- Interestingly, we have found that all the stability spectra of the CNLS system are also enclosed in those of the 3WRI system. Indeed, the same method has already been successfully applied to the CNLS system [64]. The topological features of the CNLS stability spectra are gaps on the real axis, and branches and loops off the real axis: the gaps correspond to the solutions which are not bounded in space, whereas the branches and loops correspond to the solutions which are instead bounded in space, but which can be linearly unstable in time.

- Compared to the CNLS system, new topological features exist in the stability sfpectra of the 3WRI model, for instance, figure-of-eight loops that we have named twisted loops. Remarkably, the gain function associated to the twisted loops is non-zero in a whole neighbourhood of the origin (origin enclosed). This fact has been conjecturally associated to explosive instability: the solutions blow up in a finite time.

- We have observed that the gain function associated to the branches is non-zero at low wave numbers, symmetrically located with respect to the zero-value of the wave number, but it is anyway zero at the origin of the plot (linear instability of baseband-type). The gain function associated to the loops is non-zero only away from the origin (linear instability of passband-type).

- We have observed linear instability in time of plane waves for any choice of the physical parameters, except for those ones associated to the solutions that are explosive and we observe the subsequent generation of coherent localised structures, such as breather-like solutions and potential rogue waves. Some of these solutions have been observed numerically and, to the best of our knowledge, they have never been observed before in the context of the linear instability of the 3WRI system. Nevertheless, the 3WRI system is a dispersionless system with only coupling terms between the different wave components [58]. Thus, the observation of localised structures is remarkable, if one considers that MI has been observed in the context of nonlinear dispersive systems, where nonlinearity and dispersion can balance each other (see, for example, [37, 45, 71, 52, 17, 49, 50, 51, 9]).

  A conclusion is that the mechanism for the onset of localised structures (e.g. potential rogue waves) in the 3WRI system, as a result of localised perturbations of plane waves, must be different. For this reason, in the context of the 3WRI system, we

have prefered to refer to this physical phenomenon as *"linear instability"* rather than as linear stage of MI.

6.2 Open Problems and Future Directions

There are several open problems related to the subject of this Thesis and to the results obtained so far. In the following, we provide some possible future directions for the research.

6.2.1 The Onset of Rogue Waves in the 3-Wave Resonant Interaction Model

We have conjectured that the existence of branches in the stability spectra is a necessary condition for the onset of rogue waves ascribable to rational or semi-rational solutions [75, 76, 77] and which can be obtained by DDT [85]. Indeed, the ends of a branch correspond to the vanishing of at least a difference between the eigenvalues of the spatial Lax operator after gauge transformation. Following [75], we see that if two eigenvalues are equal with one another, we have a necessary condition for the existence of semi-rational solitons whereas, if all the three eigenvalues are equal with one another, we have the necessary condition for the existence of rational solutions. Moreover, in the paper [72], it has been found that, for rational solutions in defocusing regime of the CNLS, potential rogue waves exist if and only if base-band MI exists. We refer to *potential* rogue waves as the rogue waves which can be modelled by rational and semi-rational solitons obtainable by DDT method.

In a future research work, we aim to write a necessary (and, possibly, also a sufficient) condition for the existence of potential rogue waves in terms of the parameters used to classify the topologies of the stability spectra, namely, we aim to understand for which values of the parameters the necessary condition is also sufficient.

6.2.2 Spectra of the Lax Operators and Stability Spectra

Following the paper [64], we have assumed that the perturbation δQ has the integral representation

$$\delta Q = \int \mathrm{d}\kappa \, F(x,t,\kappa), \tag{6.1}$$

which provides a solution δQ bounded and localised in x at any fixed time t. The boundedness condition of $F(x,t,\kappa)$ defines the spatial stability spectrum $\mathbf{S}_x$ of the solution $Q(x,t)$. As mentioned in [64], this spectrum depends on the behaviour of the matrix $Q(x)$ for large $|x|$. Indeed, if $Q(x)$ vanishes sufficiently fast as $|x| \to \infty$, then $\mathbf{S}_x$ coincides with the spectrum of the operator $\mathrm{d}/\mathrm{dx} - i\lambda\Sigma - Q(x)$, that is defined by the spatial Lax equation. Instead, if $Q(x)$ is non-vanishsing as $|x| \to \infty$, as for the case of plane waves, the spectrum $\mathbf{S}_x$ of the solution $Q(x)$ in general may not coincide with the spectrum of the differential operator $\mathrm{d}/\mathrm{dx} - i\lambda\Sigma - Q(x)$, when $Q(x)$ is $N \times N$ with $N > 2$.
In [52, 71], it has been provided a spectral criterion for the occurrence of MI in the CNLS system. The authors establish a link between the eigenmode of the linearised problem with the eigenfunctions of the Lax problem which, in turn, can be used to construct the nonlocal dynamics of the system via Bäcklund transformations [122]. Nevertheless, they impose that the solutions satisfy boundary periodic conditions and the criterium for the existence of MI refers to the Floquet spectrum of the Lax operators. In the approach developed in [64] is independent of the boundary conditions for the solutions, so that, in the context of this new spectral method, one can establish a more general correspondence between the spectra of the Lax operators and the stability spectra.

6.2.3 Exchange of Energy in the Linear Instability of the 3-Wave Resonant Interaction Model

In the simulations of all the three solutions of the 3WRI system, we have always observed the presence of colours and pattern complementarity. We conjecture that this complementarity is due to the exchange of energy between the waves during their interaction such that, when one has the maximum values of the intensity, explained as the absorption of energy, the density of another wave is at its minimum, so the latter has given away its energy.

Similar investigation on nonlinear dispersive multicomponent systems has been conducted in [49, 50, 51], both via numerical simulations and perturbative methods.

Appendix A

Transformation Matrix $G(x,t)$ for the matrix NLS Equation

Let $G = G(x,t)$ be the matrix such that the transformation (2.15) is verified. Let us suppose that its expression is

$$G = \begin{pmatrix} g_1 & 0 \\ 0 & g_2 \end{pmatrix}, \tag{A.1}$$

whose entries are $g_1 = g_1(x,t)$, $g_2 = g_2(x,t)$, and its inverse matrix is

$$G^{-1} = \begin{pmatrix} g_1^{-1} & 0 \\ 0 & g_2^{-1} \end{pmatrix}, \tag{A.2}$$

such that,

$$G \begin{pmatrix} 0 & sa \\ a & 0 \end{pmatrix} G^{-1} = \begin{pmatrix} 0 & sag_1g_2^{-1} \\ ag_1^{-1}g_2 & 0 \end{pmatrix}. \tag{A.3}$$

Since (A.3) must be equal to Q_0 provided in (2.15), after the substitution of the relation dispersion (2.14) in the plane wave (2.13), we obtain

$$g_1g_2^{-1} = e^{-i(qx-(q^2+2sa^2)t)}, \qquad g_1^{-1}g_2 = e^{i(qx-(q^2+2sa^2)t)}. \tag{A.4}$$

By (A.4) we find a relation between the entries g_1 and g_2

$$g_1 = g_2e^{-i(qx-(q^2+2sa^2)t)}. \tag{A.5}$$

With the following ansatz on the expressions of such entries

$$g_1 = e^{im(qx-(q^2+2sa^2)t)}, \qquad g_2 = e^{in(qx-(q^2+2sa^2)t)}, \tag{A.6}$$

the equation (A.5) reads

$$e^{im(qx-(q^2+2sa^2)t)} = e^{i(n-1)(qx-(q^2+2sa^2)t)}, \tag{A.7}$$

which gives us the condition

$$m = n - 1, \tag{A.8}$$

with m and n arbitrary rational numbers.

For the sake of simplicity, we choose $n = \frac{1}{2}$ and, finally, we get

$$G = e^{-\frac{i}{2}(qx-(q^2+2sa^2)t)\sigma_3}, \tag{A.9}$$

where σ_3 is the Pauli matrix (2.4).

Appendix B

Lax Equations of the NLS Equation

By the transformation (2.17) the right-hand sides of the Lax equations (3.41) become

$$X\psi = XG\phi, \quad T\psi = TG\phi, \tag{B.1}$$

and, on the other hand, the left-hand sides read

$$\psi_x = G_x\phi + G\phi_x, \quad \psi_t = G_t\phi + G\phi_t, \tag{B.2}$$

finally, matching (B.1) and (B.2)

$$G_x\phi + G\phi_x = XG\phi, \tag{B.3a}$$

$$G_t\phi + G\phi_t = TG\phi. \tag{B.3b}$$

Multiplying by G^{-1} from the left the equations (B.3), the PDEs for the solution ϕ are

$$\phi_x = iW\phi, \tag{B.4a}$$

$$\phi_t = -iZ\phi. \tag{B.4b}$$

where we have defined the operators as follows

$$iW = G^{-1}XG - G^{-1}G_x, \tag{B.5a}$$

$$-iZ = G^{-1}TG - G^{-1}G_t. \tag{B.5b}$$

Appendix C

PDEs for the SE $\Phi(x,t)$ of the NLS Equation

Since ψ is a solution of the Lax pair (2.2), the squared eigenfunction (SE) Ψ defined in (2.24) satisfies the PDEs (2.25) The transformation (2.17) induces the similarity transformation which introduces another SE Φ, solution of other PDEs that we shall find in the following discussion.

By looking at the expression of G in (2.16), one can check that the left-hand sides of the PDEs (2.25) are

$$\Psi_x = G_x\Phi G^{-1} + G\Phi_x G^{-1} + G\Phi G_x^{-1}, \tag{C.1a}$$

$$\Psi_t = G_t\Phi G^{-1} + G\Phi_t G^{-1} + G\Phi G_t^{-1}; \tag{C.1b}$$

by matching the right-hand side and the left-hand side of the PDEs (2.25), it results

$$XG\Phi G^{-1} - G\Phi G^{-1}X = G_x\Phi G^{-1} + G\Phi_x G^{-1} + G\Phi G_x^{-1}, \tag{C.2a}$$

$$TG\Phi G^{-1} - G\Phi G^{-1}T = G_t\Phi G^{-1} + G\Phi_t G^{-1} + G\Phi G_t^{-1}. \tag{C.2b}$$

Finally, by multiplying by G^{-1} from the left and by G from the right, and considering that $G_x^{-1}G = -G^{-1}G_x$, the equations (C.2) become the PDEs satisfied by Φ

$$\Phi_x = i[W,\Phi], \qquad \Phi_t = -i[Z,\Phi]. \tag{C.3}$$

Appendix D

Similarity Transformation for the 3WRI System

The transformation

$$U = GU_0G^{-1}, \tag{D.1}$$

in matrix form reads

$$\begin{pmatrix} 0 & s_1a_1e^{i(qt-\nu_1x)} & -s_1s_2s_3a_2e^{-i(qt-\nu_2x)} \\ s_1s_2s_3a_1e^{-i(qt-\nu_1x)} & 0 & s_3a_3e^{-i(2qt-(\nu_1+\nu_2))x} \\ s_2a_2e^{i(qt-\nu_2x)} & s_1s_2s_3a_3^*e^{i(2qt-(\nu_1+\nu_2))x} & \end{pmatrix} = \begin{pmatrix} 0 & s_1a_1g_1g_2^{-1} & -s_1s_2s_3a_2g_1g_3^{-1} \\ s_1s_2s_3a_1g_2g_1^{-1} & 0 & s_3a_3g_2g_3^{-1} \\ s_2a_2g_3g_1^{-1} & s_1s_2s_3a_3^*g_3g_2^{-1} & 0 \end{pmatrix}, \tag{D.2}$$

where G is

$$G = \begin{pmatrix} g_1 & 0 & 0 \\ 0 & g_2 & 0 \\ 0 & 0 & g_3 \end{pmatrix}, \tag{D.3}$$

and the entries g_1, g_2 and g_3 are unknown.

The matrix equation (D.2) gives us a system of three equations

$$\begin{cases} g_1 = g_2 e^{i(qt-\nu_1 x)}\,, \\ g_2 = g_3 e^{-i(2qt-(\nu_1+\nu_2))x}\,, \\ g_3 = g_1 e^{i(qt-\nu_2 x)}\,. \end{cases} \tag{D.4}$$

Looking at (D.4), one assumes the general expression of the unknowns g_j

$$g_1 = e^{i(m_1 qt-(l_1\nu_1+n_1\nu_2)x)}, \quad g_2 = e^{i(m_2 qt-(l_2\nu_1+n_2\nu_2)x)}, \quad g_3 = e^{i(m_3 qt-(l_3\nu_1+n_3\nu_2)x)}, \tag{D.5}$$

with m_j, n_j and l_j, $j = 1, 2, 3$, are positive or negative integers or can be zero. The expressions (D.5), substituted in the system (D.4), gives

$$\begin{cases} m_1 = m\,, \\ m_2 = m-1\,, \\ m_3 = m+1\,, \end{cases} \qquad \begin{cases} l_1 = l\,, \\ l_2 = l-1\,, \\ l_3 = l\,, \end{cases} \qquad \begin{cases} n_1 = n\,, \\ n_2 = n\,, \\ n_3 = n+1\,, \end{cases} \tag{D.6}$$

so that

$$g_1 = e^{i(mqt-(l\nu_1+n\nu_2)x)}, \quad g_2 = e^{i((m-1)qt-((l-1)\nu_1+n\nu_2)x)}, \quad g_3 = e^{i((m+1)qt-(l\nu_1+(n+1)\nu_2)x)}, \tag{D.7}$$

and for $m = 0$, $l = \frac{1}{2}$ and $n = -\frac{1}{2}$, we get

$$g_1 = e^{-\frac{i}{2}(\nu_1-\nu_2)x}, \quad g_2 = e^{-i(qt-\frac{1}{2}(\nu_1+\nu_2)x)}, \quad g_3 = e^{i(qt-\frac{1}{2}(\nu_1+\nu_2)x)}. \tag{D.8}$$

By substituting the expressions (D.8) in (D.3), the matrix G (D.3) can rewritten as in formula (3.65).

Appendix E

Liouville Equations

Let

$$\Psi = G\Phi G^{-1} \tag{E.1}$$

be a SE defined via the solution ψ of the Lax Pair (3.41) and satisfying the differential equations

$$\Psi_x = [X, \Psi], \quad \Psi_t = [T, \Psi]. \tag{E.2}$$

By differentiating (E.1) with respect to x and t, we obtain, respectively, [1]

$$\Psi_x = G_x\Phi G^{-1} + G\Phi_x G^{-1} + G\Phi(G^{-1})_x, \tag{E.3a}$$

$$\Psi_t = G_t\Phi G^{-1} + G\Phi_t G^{-1} + G\Phi(G^{-1})_t, \tag{E.3b}$$

and, on the other hand, by substituting (E.1) in the equations (E.2)

$$[X, \Psi] = XG\Phi G^{-1} - G\Phi G^{-1}X, \tag{E.4a}$$

$$[T, \Psi] = TG\Phi G^{-1} - G\Phi G^{-1}T. \tag{E.4b}$$

[1] We use the fact that $G^{-1}G = \mathbf{I}$ and $(G^{-1}G)_x = \mathbf{0}$ from which

$$(G^{-1})_x G = -G^{-1}G_x.$$

The same argument holds for the differentiation w.r.t. t.

By matching (E.3) with (E.4) and multiplying from the left by G^{-1} and from the right by G, we obtain the Liouville equations

$$\Phi_x = i[W_0, \Phi], \quad \Phi_t = -i[Z_0, \Phi], \tag{E.5}$$

where the operators

$$iW_0 = G^{-1}XG - G^{-1}G_x, \quad -iZ_0 = G^{-1}TG - G^{-1}G_t, \tag{E.6}$$

are now independent of x and t. The equations (E.2) are not simply integrable because of the dependence on x and t of the matrices X and T. However, after the similarity transformation via the matrix G, the equations (E.6) are now simply integrable and the expression of their solution is well known and it is given in (3.69).

Appendix F

Differential equations for ϕ

Let ψ be the solution of the Lax Pair

$$\psi_x = X\psi, \quad \psi_t = T\psi. \tag{F.1}$$

If we make the transformation

$$\psi = G\phi, \tag{F.2}$$

by the differential equations (F.1), we obtain the identities

$$G_x\phi + G\phi_x = XG\phi, \tag{F.3a}$$

$$G_t\phi + G\phi_t = TG\phi, \tag{F.3b}$$

and multiplied to right by G^{-1}, give us the differential equations for ϕ

$$\phi_x = (G^{-1}XG - G^{-1}G_x)\phi, \tag{F.4a}$$

$$\phi_t = (G^{-1}TG - G^{-1}G_t)\phi. \tag{F.4b}$$

If we define

$$iW_0 = G^{-1}XG - G^{-1}G_x, \quad -iZ_0 = G^{-1}TG - G^{-1}G_t \tag{F.5}$$

we have

$$\phi_x = iW_0\phi, \tag{F.6a}$$

$$\phi_t = -iZ_0\phi. \tag{F.6b}$$

Appendix G

Gauges for W and Z

We can check the expressions (3.75), by looking at the transformation

$$\bar{\phi} = e^{i(mqt-(l\nu_1+n\nu_2)x)\mathbf{I}}\phi, \tag{G.1}$$

that, differentiated, say, w.r.t. x gives

$$\bar{\phi}_x = (e^{i(mqt-(l\nu_1+n\nu_2)x)\mathbf{I}}\phi)_x = (-i(l\nu_1+n\nu_2)\phi - \phi_x)e^{i(mqt-(l\nu_1+n\nu_2)x)\mathbf{I}}, \tag{G.2}$$

on the other hand, because $\bar{\phi}_x = i\bar{W}\bar{\phi}$,

$$\begin{aligned} i\bar{W}\bar{\phi} &= (\bar{G}^{-1}\bar{X}\bar{G} - \bar{G}^{-1}\bar{G}_x)\bar{\phi} = \\ &= (G^{-1}XG - G^{-1}G_x - i(l\nu_1+n\nu_2))\bar{\phi} = \\ &= i(W_0 - (l\nu_1+n\nu_2))\bar{\phi} = \\ &= i(W_0 - (l\nu_1+n\nu_2))e^{i(mqt-(l\nu_1+n\nu_2)x)\mathbf{I}}\phi\,. \end{aligned} \tag{G.3}$$

By matching (G.2) with (G.3), we obtain the equation

$$\phi_x = iW_0\phi, \tag{G.4}$$

with

$$\bar{W} = W_0 - (l\nu_1+n\nu_2). \tag{G.5}$$

The same argument holds for the operators $\bar{Z}$ and Z_0.

Appendix H

Relation between the Lax Operators W and Z

Let us consider the matrix

$$\zeta = \left(\frac{c_1 - c_2}{2qc_1c_2}\right)\left(Z^2 - (a_2^2c_2^2s_1s_3 - a_1^2c_1^2s_2s_3)\mathbf{I}\right) =$$

$$= \begin{pmatrix} 0 & -\frac{ia_1s_1c_1(c_1-c_2)(-q-c_1c_2\kappa)}{2qc_1c_2} & \frac{ia_2s_1s_2s_3c_2(c_1-c_2)(q-c_1c_2\kappa)}{2qc_1c_2} \\ -\frac{ia_1s_1s_2s_3c_1(c_1-c_2)(-q-c_1c_2\kappa)}{2qc_1c_2} & -\frac{a_2^2s_1s_3c_2(c_1-c_2)}{2qc_1} + \frac{(c_1-c_2)(-q-c_1c_2\kappa)^2}{2qc_1c_2} & \frac{a_1a_2(c_1-c_2)}{2q} \\ -\frac{ia_2s_2c_2(c_1-c_2)(q-c_1c_2\kappa)}{2qc_1c_2} & -\frac{a_1a_2s_1s_2(c_1-c_2)}{2q} & \frac{a_1^2s_2s_3c_1(c_1-c_2)}{2qc_2} + \frac{(c_1-c_2)(q-c_1c_2\kappa)^2}{2qc_1c_2} \end{pmatrix}. \tag{H.1}$$

Let us focus on the off-diagonal-part of the matrix above. The off-block diagonal terms ζ_{ij}, which are proportional to the terms ζ_{ji}, can be handled as follows. For example, the numerator of the entry ζ_{12} is

$$-ia_1c_1s_1(c_1 - c_2)(-q - c_1c_2\kappa) = -ia_1c_1^2s_1(-q - c_1c_2\kappa) + ia_1c_1c_2s_1(-q - c_1c_2\kappa) \tag{H.2}$$

whose last term is, by adding and subtracting q into the brackets,

$$ia_1c_1c_2s_1(-q - c_1c_2\kappa) = -2iqa_1c_1c_2s_1 + ia_1c_1c_2s_1(q - c_1c_2\kappa), \tag{H.3}$$

by substituting (H.3) in (H.2), one gets

$$\begin{aligned} &- ia_1s_1c_1^2(-q - c_1c_2\kappa) - 2ia_1s_1c_1c_2q + ia_1s_1c_1c_2(q - c_1c_2\kappa) = \\ &= W_{12} + Z_{12}c_1(-q - c_1c_2\kappa) - Z_{12}c_2(q - c_1c_2\kappa), \end{aligned} \tag{H.4}$$

that is

$$\zeta_{12} = \frac{W_{12}}{2qc_1c_2} + Z_{12}\frac{c_1(-q - c_1c_2\kappa)}{2qc_1c_2} - Z_{12}\frac{c_2(q - c_1c_2\kappa)}{2qc_1c_2}. \tag{H.5}$$

Similarly, let us consider the term ζ_{22}. The first term in the sum is already in W_{22}, while the numerator of the second term can be handled as follows

$$\begin{aligned}
&(c_1 - c_2)(-q - c_1c_2\kappa)^2 = c_1(-q - c_1c_2\kappa)^2 - c_2(-q - c_1c_2\kappa)^2 = \\
&= c_1(-q - c_1c_2\kappa)^2 - c_2(-q - c_1c_2\kappa)(-q - c_1c_2\kappa) = \\
&= c_1(-q - c_1c_2\kappa)^2 - c_2(-q - c_1c_2\kappa)(-q - q + q - c_1c_2\kappa) = \\
&= c_1(-q - c_1c_2\kappa)^2 + 2qc_2(-q - c_1c_2\kappa) - c_2(-q - c_1c_2\kappa)(q - c_1c_2\kappa) = \\
&= W_{22} + Z_{22}c_1(-q - c_1c_2\kappa) - Z_{22}c_2(q - c_1c_2\kappa),
\end{aligned} \tag{H.6}$$

hence,

$$\zeta_{22} = \frac{W_{22}}{2qc_1c_2} + Z_{22}\frac{c_1(-q - c_1c_2\kappa)}{2qc_1c_2} - Z_{22}\frac{c_2(q - c_1c_2\kappa)}{2qc_1c_2}. \tag{H.7}$$

By repeating the same calculations for the other terms of the matrix (H.1), we get the matrix polynomial

$$W = Z^2(c_1 - c_2) - Zc_1(-q - c_1c_2\kappa) + Zc_2(q - c_1c_2\kappa) - (c_1 - c_2)(a_2^2c_2^2s_1s_3 - a_1^2c_1^2s_2s_3)\mathbf{I}, \tag{H.8}$$

i.e. the polynomial (3.83).

Let us consider the matrix

$$\xi = W^2 - (a_2^2s_1s_3 + a_1^2s_2s_3)\mathbf{I}, \tag{H.9}$$

whose entries are

$$\xi_{11} = 0, \tag{H.10}$$

$$\xi_{22} = 4q^2c_1^2c_2^2\left(-a_2^2s_1s_3 - a_1^2a_2^2s_1s_2\left(\frac{c_1 - c_2}{2q}\right)^2 + \left(-\frac{a_2^2s_1s_3c_2(c_1 - c_2)}{2qc_1} - \frac{q}{c_1} - c_2\kappa\right)^2\right), \tag{H.11}$$

$$\xi_{33} = 4q^2c_1^2c_2^2\left(a_1^2s_2s_3 - a_1^2a_2^2s_1s_2\left(\frac{c_1 - c_2}{2q}\right)^2 + \left(\frac{a_1^2s_2s_3c_1(c_1 - c_2)}{2qc_2} + \frac{q}{c_2} - c_1\kappa\right)^2\right),$$

(H.12)

$$\xi_{21} = s_2 s_3 \xi_{12} = 4q^2 c_1^2 c_2^2 \left(-i a_1 s_1 \left(\frac{a_2^2 s_1 s_3 (c_1 - c_2)^2}{2qc_1} - \frac{q}{c_1} - c_2 \kappa \right) \right), \tag{H.13}$$

$$\xi_{31} = -s_1 s_3 \xi_{13} = 4q^2 c_1^2 c_2^2 \left(-i a_2 s_2 \left(\frac{a_1^2 s_2 s_3 (c_1 - c_2)^2}{2qc_2} + \frac{q}{c_2} - c_1 \kappa \right) \right), \tag{H.14}$$

$$\begin{aligned} &\xi_{23} = -s_1 s_2 \xi_{32} = \\ &= 4q^2 c_1^2 c_2^2 \left(a_1 a_2 + a_1 a_2 \left(\frac{c_1 - c_2}{2q} \right) \Big(- \frac{a_2^2 s_1 s_3 c_2 (c_1 - c_2)}{2qc_1} + \right. \\ &\left. + \frac{a_1^2 s_2 s_3 c_1 (c_1 - c_2)}{2qc_2} - \frac{q}{c_1} - c_2 \kappa + \frac{q}{c_2} - c_1 \kappa \Big) \right). \end{aligned} \tag{H.15}$$

Let us handle the entry ξ_{12}, proportional to the entry ξ_{21}. The part inside the brackets becomes

$$\begin{aligned} &\frac{a_2^2 s_1 s_3 (c_1 - c_2)^2}{2qc_1} - \frac{a_1^2 s_2 s_3 (c_1 - c_2)^2}{2qc_2} + \frac{a_1^2 s_2 s_3 (c_1 - c_2)^2}{2qc_2} = \\ &= \frac{a_2^2 s_1 s_3 (c_1 - c_2)^2}{2qc_1} + \frac{a_1^2 s_2 s_3 (c_1 - c_2)^2}{2qc_2} - \frac{a_1^2 s_2 s_3 c_1 (c_1 - c_2)}{2qc_2} + \frac{a_1^2 s_2 s_3 c_2 (c_1 - c_2)}{2qc_2} = \\ &= \frac{a_2^2 s_1 s_3 (c_1 - c_2)^2}{2qc_1} + \frac{a_1^2 s_2 s_3 (c_1 - c_2)^2}{2qc_2} - \frac{a_1^2 s_2 s_3 c_1 (c_1 - c_2)}{2qc_2} + \frac{a_1^2 s_2 s_3 c_2 (c_1 - c_2)}{2qc_2} + \\ &+ \frac{a_2^2 s_1 s_3 c_1 (c_1 - c_2)}{2qc_1} - \frac{a_2^2 s_1 s_3 c_1 (c_1 - c_2)}{2qc_1}, \end{aligned} \tag{H.16}$$

on the other hand,

$$\begin{aligned} &- \frac{q}{c_1} - c_2 \kappa = \frac{2q}{c_1 - c_2} - \frac{2q}{c_1 - c_2} - \frac{q}{c_1} - c_2 \kappa + \frac{q}{c_2} - c_1 \kappa - \frac{q}{c_2} + c_1 \kappa = \\ &= \frac{2q}{c_1 - c_2} - \frac{q}{c_1} - c_2 \kappa - c_1 \kappa - \frac{q}{c_2} - \frac{2qc_1 c_2 + qc_1 (c_1 - c_2)}{c_1 c_2 (c_1 - c_2)} + c_1 \kappa = \\ &= \frac{2q}{c_1 - c_2} - \frac{q}{c_1} - c_2 \kappa - c_1 \kappa - \frac{q}{c_2} - c_1 \left(q \frac{c_2 + c_1}{c_1 c_2 (c_1 - c_2)} - \kappa \right). \end{aligned} \tag{H.17}$$

By summing the terms (H.16) and (H.17), and by putting altogether in the expression of the entry ξ_{12}, we have

$$\begin{aligned} \xi_{12} = 2qc_1 c_2 W_{12} &\left(\frac{a_2^2 s_1 s_3 (c_1 - c_2)^2}{2qc_1} + \frac{a_1^2 s_2 s_3 (c_1 - c_2)^2}{2qc_2} - \frac{a_2^2 s_1 s_3 c_1 (c_1 - c_2)}{2qc_1} + \right. \\ &\left. + \frac{a_1^2 s_2 s_3 c_2 (c_1 - c_2)}{2qc_2} + \frac{2q}{c_1 - c_2} - \frac{q}{c_1} - c_2 \kappa + \frac{q}{c_2} - c_1 \kappa \right) + \\ &+ 4q^2 c_1^2 c_2^2 Z_{12} \left(\frac{a_2^2 s_1 s_3 (c_1 - c_2)}{2qc_1} - \frac{a_1^2 s_2 s_3 (c_1 - c_2)}{2qc_2} - q \frac{c_2 + c_1}{c_1 c_2 (c_1 - c_2)} + \kappa \right). \end{aligned} \tag{H.18}$$

By following a similar procedure, we get

$$\xi_{23} = 2qc_1c_2W_{23}. \tag{H.19}$$

In matrix form, it turns out that

$$\begin{aligned}
&W^2 - (a_2^2 s_1 s_3 + a_1^2 s_2 s_3)\mathbf{I} = \\
&= 2qc_1c_2W\left(\frac{a_2^2 s_1 s_3 (c_1-c_2)^2}{2qc_1} + \frac{a_1^2 s_2 s_3 (c_1-c_2)^2}{2qc_2} - \frac{a_2^2 s_1 s_3 c_1 (c_1-c_2)}{2qc_1} + \right. \\
&\left. + \frac{a_1^2 s_2 s_3 c_2 (c_1-c_2)}{2qc_2} + \frac{2q}{c_1-c_2} - \frac{q}{c_1} - c_2\kappa + \frac{q}{c_2} - c_1\kappa\right) + \\
&+ 4Zq^2c_1^2c_2^2\left(\frac{a_2^2 s_1 s_3 (c_1-c_2)}{2qc_1} - \frac{a_1^2 s_2 s_3 (c_1-c_2)}{2qc_2} - q\frac{c_2+c_1}{c_1c_2(c_1-c_2)} + \kappa\right),
\end{aligned} \tag{H.20}$$

and finally,

$$\begin{aligned}
&Z\left(\frac{a_2^2 s_1 s_3 (c_1-c_2)}{2qc_1} - \frac{a_1^2 s_2 s_3 (c_1-c_2)}{2qc_2} - q\frac{c_2+c_1}{c_1c_2(c_1-c_2)} + \kappa\right) = \\
&\frac{W^2}{4q^2c_1^2c_2^2} - \frac{W}{2qc_1c_2}\left(\frac{a_2^2 s_1 s_3 (c_1-c_2)^2}{2qc_1} + \frac{a_1^2 s_2 s_3 (c_1-c_2)^2}{2qc_2} - \right. \\
&- \frac{a_2^2 s_1 s_3 c_1 (c_1-c_2)}{2qc_1} + \frac{a_1^2 s_2 s_3 c_2 (c_1-c_2)}{2qc_2} + \\
&\left. + \frac{2q}{c_1-c_2} - \frac{q}{c_1} - c_2\kappa + \frac{q}{c_2} - c_1\kappa\right) - (a_2^2 s_1 s_3 + a_1^2 s_2 s_3)\mathbf{I}.
\end{aligned} \tag{H.21}$$

Appendix I

Relation between the differences of the Eigenvalues of the Lax Operators W and Z

From the polynomial (3.83) we can write

$$w_j = (c_1-c_2)z_j^2 - c_1(-q-c_1c_2\kappa)z_j + c_2(q-c_1c_2\kappa)z_j - (c_1-c_2)(a_2^2c_2^2s_1s_3 - a_1^2c_1^2s_2s_3) \quad \text{(I.1)}$$

$\forall j = 1, 2, 3$, and the difference between two eigenvalues is, for example,

$$w_1 - w_2 = (c_1 - c_2)(z_1^2 - z_2^2) - c_1(-q - c_1c_2\kappa)(z_1 - z_2) + c_2(q - c_1c_2\kappa)(z_1 - z_2). \quad \text{(I.2)}$$

Furthermore, because $\mathrm{Tr}(Z) = -2c_1c_2\kappa$ and $z_1^2 - z_2^2 = (z_1 - z_2)(z_1 + z_2)$, we substitute in the previous expression

$$z_1 + z_2 = -z_3 - 2c_1c_2\kappa, \quad \text{(I.3)}$$

and, as a consequence,

$$w_1 - w_2 = (c_1 - c_2)(z_1 - z_2)(-z_3 - 2c_1c_2\kappa) - c_1(-q - c_1c_2\kappa)(z_1 - z_2) + c_2(q - c_1c_2\kappa)(z_1 - z_2). \quad \text{(I.4)}$$

The difference of the eigenvalues (I.4) can be also written in a different fashion after adding and subtracting the terms qc_1 and qc_2. Indeed, it reads

$$w_1 - w_2 = (z_1 - z_2)(-z_3(c_1 - c_2) + q(c_1 + c_2) - c_1c_2\kappa(c_1 - c_2)). \quad \text{(I.5)}$$

To compute the differences $z_j - z_{j+1}$, we repeat all the calculations above, but we need to make the substitution $w_1 + w_2 = -w_3 - \mathrm{Tr}(W)$, where

$$\mathrm{Tr}(W) = 2qc_1c_2\left(\frac{a_1^2 s_2 s_3 c_1(c_1 - c_2)}{2qc_2} - \frac{a_2^2 s_1 s_3 c_2(c_1 - c_2)}{2qc_1} - \frac{q}{c_1} - c_2\kappa + \frac{q}{c_2} - c_1\kappa\right). \tag{I.6}$$

Appendix J

Characteristic Polynomial and the Associated Polynomial of the Squares of the Differences

Let $\tilde{W}$ be the diagonalised matrix of the matrix W. The eigenvalues w_ℓ, for $\ell = 1, 2, 3$, are the roots of the characteristic polynomial

$$P(w) = w^3 - \mathrm{Tr}(\tilde{W})w^2 + \frac{1}{2}\left(\mathrm{Tr}^2(\tilde{W}) - \mathrm{Tr}(\tilde{W}^2)\right)w - \mathrm{Det}(\tilde{W}). \tag{J.1}$$

We denote the trace and the determinant of matrix with $\mathrm{Tr}(\cdot)$ and $\mathrm{Det}(\cdot)$, respectively. In (J.1) we have replaced $\mathrm{Tr}(W)$ with $\mathrm{Tr}(\tilde{W})$ by using the property of the trace to be invariant under cyclic permutations and $\mathrm{Det}(W)$ with $\mathrm{Det}(\tilde{W})$ because of the Binet theorem in order to simplify the computations.

We take advantage from the property of trace and determinant to be invariant under similarity transformation, and also from the property of the coefficients of the polynomial (J.1) to be invariants. In this respect, let us introduce the Vandermonde matrix

$$\Upsilon = \begin{pmatrix} 1 & w_1 & w_1^2 \\ 1 & w_2 & w_2^2 \\ 1 & w_3 & w_3^2 \end{pmatrix}, \tag{J.2}$$

whose determinant is

$$\mathrm{Det}(\Upsilon) = w_1^2(w_3-w_2)+w_2^2(w_1-w_3)+w_3^2(w_2-w_1) = (w_1-w_2)(w_2-w_3)(w_3-w_1), \quad \text{(J.3)}$$

and we note that [1] $(\mathrm{Det}(\Upsilon))^2 = \Delta_W P(w)$, where $\Delta_W P(w)$ is the discriminant of the polynomial (J.1) with respect to w. In some computation, we benefit from the Cayley-Hamilton Theorem to write the determinant as

$$\mathrm{Det}(\tilde{W}) = \frac{1}{6}\left(\mathrm{Tr}^3(\tilde{W}) + 2\mathrm{Tr}(\tilde{W}^3) - 3\mathrm{Tr}(\tilde{W})\mathrm{Tr}(\tilde{W}^2)\right). \quad \text{(J.4)}$$

Below, we give some useful formulas

$$2(w_1w_2 + w_2w_3 + w_3w_1) = \mathrm{Tr}^2(\tilde{W}) - \mathrm{Tr}(\tilde{W}^2), \quad \text{(J.5)}$$

and

$$\begin{aligned}&(w_1^2w_2^2 + w_2^2w_3^2 + w_3^2w_1^2 + 2w_1^2w_2w_3 + 2w_1w_2^2w_3 + 2w_1w_2w_3^2) = \\ &= (w_1^2w_2^2 + w_2^2w_3^2 + w_3^2w_1^2 + 2w_1w_2w_3\mathrm{Tr}(\tilde{W})) = \frac{1}{4}\left(\mathrm{Tr}^2(\tilde{W}) - \mathrm{Tr}(\tilde{W}^2)\right)^2,\end{aligned} \quad \text{(J.6)}$$

or

$$\begin{aligned}&(w_1^2w_2^2 + w_2^2w_3^2 + w_3^2w_1^2) = \\ &= \frac{1}{4}\left(\mathrm{Tr}^2(\tilde{W}) - \mathrm{Tr}(\tilde{W}^2)\right)^2 - \frac{1}{3}\mathrm{Tr}(\tilde{W})\left(\mathrm{Tr}^3(\tilde{W}) + 2\mathrm{Tr}(\tilde{W}^3) - 3\mathrm{Tr}(\tilde{W})\mathrm{Tr}(\tilde{W}^2)\right),\end{aligned} \quad \text{(J.7)}$$

where in the last equality we use the formula (J.4).

In the next subsections we shall show the connection between the characteristic polynomial (J.1) and the polynomial of the differences $w_\ell - w_m$ and the polynomial of the squares of the differences, that is $(w_\ell - w_m)^2$.

J.0.4 Polynomial of the Differences

Let

$$P(k) = k^3 - \mathrm{Tr}(\tilde{W}_1)k^2 + \frac{1}{2}\left(\mathrm{Tr}^2(\tilde{W}_1) - \mathrm{Tr}(\tilde{W}_1^2)\right)k - \mathrm{Det}(\tilde{W}_1), \quad \text{(J.8)}$$

be the characteristic polynomial whose roots are the differences $w_\ell - w_m = k_{\ell m}$, with $\ell \neq m$, and $\ell, m = 1, 2, 3$, so the matrix $\tilde{W}_1$ is

$$\tilde{W}_1 = \begin{pmatrix} k_{12} & 0 & 0 \\ 0 & k_{23} & 0 \\ 0 & 0 & k_{31} \end{pmatrix}. \quad \text{(J.9)}$$

[1] When two roots coincide $\mathrm{Det}(\Upsilon) = 0$.

Proposition J.0.1. *Every coefficient of the polynomial (J.8) can be expressed by the coefficients of the polynomial (J.1) plus the determinant of the Vandermonde matrix* Υ*. In particular, the polynomial (J.8) can be written as*

$$P\tilde{W}_1 = k^3 - \frac{1}{2}\left(3\mathrm{Tr}(\tilde{W}^2) - \mathrm{Tr}^2(\tilde{W})\right)k - \mathrm{Det}(\Upsilon). \tag{J.10}$$

Proof. By looking at the matrix $\tilde{W}_1$, we have

$$\mathrm{Tr}(\tilde{W}_1) = 0, \tag{J.11}$$

and, as a consequence,

$$\mathrm{Tr}^n(\tilde{W}_1) = 0, \qquad n = 1, 2, 3.... \tag{J.12}$$

On the other hand,

$$\mathrm{Tr}(\tilde{W}_1^2) = k_{12}^2 + k_{23}^2 + k_{31}^2 = 2\mathrm{Tr}(\tilde{W}^2) - 2(w_1w_2 + w_2w_3 + w_3w_1), \tag{J.13}$$

which becomes, by the relation (J.5),

$$\mathrm{Tr}(\tilde{W}_1^2) = 3\mathrm{Tr}(\tilde{W}^2) - \mathrm{Tr}^2(\tilde{W}). \tag{J.14}$$

It is trivial to see that

$$\mathrm{Det}(\tilde{W}_1) = \mathrm{Det}(\Upsilon). \tag{J.15}$$

□

Proposition J.0.2. *The eigenvalues* w_ℓ *are the roots of the characteristic polynomial (J.1)* if and only if *the differences* $k_{\ell m}$ *are roots of the characteristic polynomial (J.10).*

Proof. First of all we prove that if w_ℓ are roots of the polynomial (J.1), then the differences $k_{\ell m}$ are roots of the polynomial (J.10).
Let us substitute $k = w_\ell - w_m$ into the polynomial (J.10), we have

$$\begin{aligned}
&(w_\ell - w_m)^3 - \frac{1}{2}\left(3\mathrm{Tr}(\tilde{W}^2) - \mathrm{Tr}^2(\tilde{W})\right)(w_\ell - w_m) - \mathrm{Det}(\Upsilon) = \\
&= w_\ell^3 - w_m^3 - 3w_\ell^2 w_m + 3w_\ell w_m^2 + \frac{1}{2}\left(\mathrm{Tr}^2(\tilde{W}) - \mathrm{Tr}(\tilde{W}^2)\right)w_\ell - \\
&- \frac{1}{2}\left(\mathrm{Tr}^2(\tilde{W}) - \mathrm{Tr}(\tilde{W}^2)\right)w_m - \mathrm{Tr}(\tilde{W}^2)w_\ell + \mathrm{Tr}(\tilde{W}^2)w_m - \mathrm{Det}(\Upsilon),
\end{aligned} \tag{J.16}$$

we can identify the first and the fifth term in the polynomial satisfied by w_ℓ, while the second and the sixth term in the polynomial satisfied by w_m. Leaving aside for a moment $\mathrm{Det}(\Upsilon)$, the remaining terms are handled to give

$$\begin{aligned} &-3w_\ell^2 w_m + 3w_\ell w_m^2 - \mathrm{Tr}(\tilde{W}^2)w_\ell + \mathrm{Tr}(\tilde{W}^2)w_m = \\ &= -w_\ell^2 \mathrm{Tr}(\tilde{W}) + w_m^2 \mathrm{Tr}(\tilde{W}) + w_\ell^2(w_k - w_m) + w_m^2(w_\ell - w_k) + w_k^2(w_m - w_\ell) = \\ &= -w_\ell^2 \mathrm{Tr}(\tilde{W}) + w_m^2 \mathrm{Tr}(\tilde{W}) + \mathrm{Det}(\Upsilon). \end{aligned} \tag{J.17}$$

The first two terms to the left-hand side of the equation above correspond to the quadratic terms of the polynomial for w_ℓ and w_m, respectively. The term $\mathrm{Det}(\Upsilon)$ cancels out once substituted into the polynomial (J.10). However, we can identify the difference of the known terms of the polynomials for w_ℓ and w_m within the trivial difference $\mathrm{Det}(\Upsilon) - \mathrm{Det}(\Upsilon)$

$$\mathrm{Det}(\Upsilon) = -\mathrm{Det}(\tilde{W}) + (w_1^2(w_3 - w_2) + w_2^2(w_1 - w_3) + w_3^2(w_2 - w_1) + w_1 w_2 w_3), \tag{J.18}$$

so $\mathrm{Det}(\Upsilon) - \mathrm{Det}(\Upsilon) = \mathrm{Det}(\tilde{W}) - \mathrm{Det}(\tilde{W})$. To show that if the difference $w_\ell - w_m$ are roots of the polynomial (J.10), then w_ℓ are roots of the polynomial (J.1), we need to subtract the polynomial calculated in w_m from the polynomial calculated in w_ℓ

$$P(w_\ell) - P(w_m) = w_\ell^3 - w_m^3 - \mathrm{Tr}(\tilde{W})w_\ell^2 + \mathrm{Tr}(\tilde{W})w_m^2 + \frac{1}{2}\left(\mathrm{Tr}^2(\tilde{W}) - \mathrm{Tr}(\tilde{W}^2)\right)(w_\ell - w_m). \tag{J.19}$$

By using the formula (J.17) we replace the terms $-\mathrm{Tr}(\tilde{W})w_\ell^2 + \mathrm{Tr}(\tilde{W})w_m^2$ and write down the polynomial (J.10). □

Note that both $w_\ell - w_m = k_{\ell m}$ and $w_\ell - w_m = k_{m\ell}$ are roots of the polynomial (J.10).

J.0.5 Polynomial of the Squares of the Differences

Let

$$P\tilde{W}_2 = \xi^3 - \mathrm{Tr}(\tilde{W}_2)\xi^2 + \frac{1}{2}\left(\mathrm{Tr}^2(\tilde{W}_2) - \mathrm{Tr}(\tilde{W}_2^2)\right)\xi - \mathrm{Det}(\tilde{W}_2). \tag{J.20}$$

be the characteristic polynomial whose roots are the differences $(w_\ell - w_m)^2 = k_{\ell m}^2 = \xi_{\ell m}$, and the matrix $\tilde{W}_2$ is

$$\tilde{W}_2 = \begin{pmatrix} \xi_{12} & 0 & 0 \\ 0 & \xi_{23} & 0 \\ 0 & 0 & \xi_{31} \end{pmatrix}. \tag{J.21}$$

Proposition J.0.3. *Every coefficient of the polynomial (J.20) can be expressed by the coefficients of the polynomial (J.1) plus the square of the determinant of the Vandermonde matrix Υ. In particular, the polynomial (J.20) can be written as*

$$P\tilde{W}_2 = \xi^3 - \left(3\mathrm{Tr}(\tilde{W}^2) - \mathrm{Tr}^2(\tilde{W})\right)\xi^2 + \frac{1}{4}\left(3\mathrm{Tr}(\tilde{W}^2) - \mathrm{Tr}^2(W)\right)^2\xi - (\mathrm{Det}(\Upsilon))^2. \quad \text{(J.22)}$$

Proof. By definition of trace and by using the formula (J.5), it results in

$$\mathrm{Tr}(\tilde{W}_2) = 3\mathrm{Tr}(\tilde{W}^2) - \mathrm{Tr}^2(\tilde{W}), \quad \text{(J.23)}$$

that is the coefficient of the second power of ξ in (J.22). In general,

$$\mathrm{Tr}^n(\tilde{W}_2) = (3\mathrm{Tr}(\tilde{W}^2) - \mathrm{Tr}^2(\tilde{W}))^n, \qquad n = 1, 2, 3.... \quad \text{(J.24)}$$

On the other hand, by using the formula (J.6), we have

$$\begin{aligned}\mathrm{Tr}(\tilde{W}_2^2) &= 6\mathrm{Tr}(\tilde{W}^4) - 4\mathrm{Tr}(\tilde{W})\mathrm{Tr}(\tilde{W}^3) + \\ &+ \frac{3}{2}\left(\mathrm{Tr}^2(\tilde{W}) - \mathrm{Tr}(\tilde{W}^2)\right)^2 - 2\mathrm{Tr}(\tilde{W})\left(\mathrm{Tr}^3(\tilde{W}) + 2\mathrm{Tr}(\tilde{W}^3) - 3\mathrm{Tr}(\tilde{W})\mathrm{Tr}(\tilde{W}^2)\right).\end{aligned} \quad \text{(J.25)}$$

and since

$$6\mathrm{Tr}(\tilde{W}^4) = -2\mathrm{Tr}^4(\tilde{W}) + 3\left(\mathrm{Tr}^2(\tilde{W}) - \mathrm{Tr}(\tilde{W}^2)\right)^2 + 8\mathrm{Tr}(\tilde{W})\mathrm{Tr}(\tilde{W}^3), \quad \text{(J.26)}$$

we have

$$\mathrm{Tr}(\tilde{W}_2^2) = \frac{1}{2}\left(3\mathrm{Tr}(\tilde{W}^2) - \mathrm{Tr}^2(\tilde{W})\right)^2, \quad \text{(J.27)}$$

so that the coefficient of the first power of ξ is

$$\frac{1}{2}\left(Tr^2(\tilde{W}_2) - Tr(\tilde{W}_2^2)\right) = \frac{1}{4}\left(3Tr(\tilde{W}^2) - Tr^2(W)\right)^2. \quad \text{(J.28)}$$

Finally, the constant term is

$$(\mathrm{Det}(\Upsilon))^2 = (w_1 - w_2)^2(w_2 - w_3)^2(w_3 - w_1)^2, \quad \text{(J.29)}$$

i.e. $\mathrm{Det}(\tilde{W}_2)$. □

Note that $(\mathrm{Det}(\Upsilon))^2 = \Delta_W P(w)$ and when two eigenvalues w_ℓ coincide this term is zero. Before we move on, we focus on the characteristic polynomial of the matrix $\tilde{W}^2 = Y$

$$Y = \begin{pmatrix} y_1 & 0 & 0 \\ 0 & y_2 & 0 \\ 0 & 0 & y_3 \end{pmatrix}, \qquad y_\ell = w_\ell^2 \quad \text{(J.30)}$$

that is

$$P(y) = y^3 - \mathrm{Tr}(Y)y^2 + \frac{1}{2}\left(\mathrm{Tr}^2(Y) - \mathrm{Tr}(Y^2)\right)y - \mathrm{Det}(Y). \tag{J.31}$$

The polynomial (J.31) can be written in terms of the eigenvalues w_ℓ as

$$P(w^2) = w^6 - \mathrm{Tr}(\tilde{W}^2)w^4 + \frac{1}{2}\left(\mathrm{Tr}^2(\tilde{W}^2) - \mathrm{Tr}(\tilde{W}^4)\right)w^2 - \mathrm{Det}(\tilde{W}^2), \tag{J.32}$$

and, from the Fundamental Theorem of Algebra, we expect six roots of the polynomial (J.32). However, the polynomial (J.31) is a third degree polynomial for the variable y, and this means that, for $\ell = 1, 2, 3$, we have three roots $w_\ell^2 = y_\ell$, but actually they are corresponding to six roots $w_\ell = \pm\sqrt{y_\ell}$ of the polynomial (J.32). As a direct result, at first sight, it looks like that between these six roots, everyone satisfying the polynomials (J.31) and (J.32), only three roots are solutions of the polynomial (J.1). In particular, we are interested only on those ones that satisfy the conditions $w_1 + w_2 + w_3 = \mathrm{Tr}(\tilde{W})$ and $w_1w_2w_3 = \mathrm{Det}(\tilde{W})$, also if all the six solutions of (J.32) satisfy the conditions $w_1^2 + w_2^2 + w_3^2 = \mathrm{Tr}(\tilde{W}^2)$ and $w_1^2w_2^2w_3^2 = \mathrm{Det}(\tilde{W}^2)$.

Thus, the roots are of the polynomial (J.22) are the six roots: $\pm(w_1 - w_2)$, $\pm(w_2 - w_3)$, $\pm(w_3 - w_1)$. One can ask: which of these differences correspond to those one for the roots of the polynomial (J.1)?

Let us consider the following diagonal matrices

$$W_1 = \begin{pmatrix} w_1 & 0 & 0 \\ 0 & w_2 & 0 \\ 0 & 0 & w_3 \end{pmatrix}, \quad W_2 = \begin{pmatrix} w_2 & 0 & 0 \\ 0 & w_1 & 0 \\ 0 & 0 & w_3 \end{pmatrix}, \tag{J.33}$$

it is simple to check that the two matrices above have the same characteristic polynomial and they are connected by a similarity transformation. Indeed, let W be the non-diagonalised matrix, we have

$$W = U_1^{-1}W_1U_1, \qquad W = U_2^{-1}W_2U_2, \tag{J.34}$$

hence

$$W_1 = U_3^{-1}W_2U_3, \tag{J.35}$$

where $U_3 = U_2 U_1^{-1}$. If the matrix of the squares of the differences associated to W_1 is

$$W_{12} = \begin{pmatrix} (w_1 - w_2)^2 & 0 & 0 \\ 0 & (w_2 - w_3)^2 & 0 \\ 0 & 0 & (w_3 - w_1)^2 \end{pmatrix}, \tag{J.36}$$

then, by following the same algorithm for the construction of the matrix above, we get the matrix associated to the matrix W_2, that is

$$W_{22} = \begin{pmatrix} (w_2 - w_1)^2 & 0 & 0 \\ 0 & (w_1 - w_3)^2 & 0 \\ 0 & 0 & (w_3 - w_2)^2 \end{pmatrix}. \tag{J.37}$$

The characteristic polynomial for the matrix W_{12} has the roots: $\pm(w_1 - w_2)$, $\pm(w_2 - w_3)$, $\pm(w_3 - w_1)$. The roots of the characteristic polynomial of the matrix W_{22} are: $\pm(w_2 - w_1)$, $\pm(w_1 - w_3)$, $\pm(w_3 - w_2)$. Let us suppose, that we are working with the matrix W_{12} and the right triplet is the differences $+(w_1 - w_2)$, $+(w_2 - w_3)$, $+(w_3 - w_1)$ that coincide with the same differences of the matrix W_{22} but with the reversed sign. This means that choosing the other combinations of signs in front of the differences corresponds to choose another eigenspace connected to the first eigenspace by a similarity transformation. This means that the polynomial (J.22) encloses all the possible differences associated to any possible eigenspace.

Proposition J.0.4. *The differences $w_\ell - w_m = k_{\ell m}$ are roots of the characteristic polynomial (J.10) if and only if $(w_\ell - w_m)^2 = \xi_{\ell m}$ are roots of the characteristic polynomial (J.22).*

Proof. Let us compute the square of the polynomial $P\tilde{W}_1$ (J.10)

$$\begin{aligned} &(P\tilde{W}_1)^2 = (k^3 - \frac{1}{2}\left(3\mathrm{Tr}(\tilde{W}^2) - \mathrm{Tr}^2(\tilde{W})\right)k - \mathrm{Det}(\Upsilon))^2 = \\ &= k^6 + \frac{1}{4}\left(3\mathrm{Tr}(\tilde{W}^2) - \mathrm{Tr}^2(\tilde{W})\right)^2 k^2 + \\ &+ (\mathrm{Det}(\Upsilon))^2 - k^4\left(3\mathrm{Tr}(\tilde{W}^2) - \mathrm{Tr}^2(\tilde{W})\right) - 2\mathrm{Det}(\Upsilon)k^3 + \mathrm{Det}(\Upsilon)\left(3\mathrm{Tr}(\tilde{W}^2) - \mathrm{Tr}^2(\tilde{W})\right)k, \end{aligned} \tag{J.38}$$

that can be also written as

$$\begin{aligned}
&(P\tilde{W}_1)^2 = \\
&= k^6 + \frac{1}{4}\left(3\mathrm{Tr}(\tilde{W}^2) - \mathrm{Tr}^2(\tilde{W})\right)^2 k^2 - \\
&- k^4\left(3\mathrm{Tr}(\tilde{W}^2) - \mathrm{Tr}^2(\tilde{W})\right) - \mathrm{Det}(\Upsilon)\left(k^3 - \frac{1}{2}\left(3\mathrm{Tr}(\tilde{W}^2) - \mathrm{Tr}^2(\tilde{W})\right)k\right) - \\
&- \mathrm{Det}(\Upsilon)\left(k^3 - \frac{1}{2}\left(3\mathrm{Tr}(\tilde{W}^2) - \mathrm{Tr}^2(\tilde{W})\right)k - \mathrm{Det}(\Upsilon)\right),
\end{aligned} \tag{J.39}$$

and we note that the term within the parenthesis multiplied by $\mathrm{Det}(\Upsilon)$ in the last line is $P\tilde{W}_1$ and it is zero when the roots are the eigenvalues $k_{\ell m} = w_\ell - w_m$, and, in the second line, the term multiplied by $\mathrm{Det}(\Upsilon)$ is still $\mathrm{Det}(\Upsilon)$ for the same roots. Moreover, if we do the substitution $k^2 = \xi$, the last equation is $P\tilde{W}_2$

$$(P\tilde{W}_1)^2 = P\tilde{W}_2 = \xi^3 - \xi^2\left(3\mathrm{Tr}(\tilde{W}^2) - \mathrm{Tr}^2(\tilde{W})\right) + \frac{1}{4}\left(3\mathrm{Tr}(\tilde{W}^2) - \mathrm{Tr}^2(\tilde{W})\right)^2 \xi - (\mathrm{Det}(\Upsilon))^2. \tag{J.40}$$

On the other hand,

$$P\tilde{W}_1 = \pm\sqrt{P\tilde{W}_2}. \tag{J.41}$$

□

Lemma J.0.5. *The roots w_ℓ are solutions of the characteristic polynomial (J.1) if and only if the roots $(w_\ell - w_m)^2 = \xi_{\ell m}$ are solutions of the polynomial (J.22).*

Lemma J.0.6. *is a consequence of the Propositions J.0.2 and J.0.4.*

Every result obtained in this appendix is general and can be applied to any matrix, and so to both the matrices W and Z.

Appendix K

Polynomial $\mathcal{S}_Z(\theta;\lambda)$ of the sums of the eigenvalues z_j

In this appendix we show the construction of the polynomial $\mathcal{S}_Z(\theta;\lambda)$ of the sums of the eigenvalues z_j.

The characteristic polynomial of the matrix Z is the polynomial whose roots are the eigenvalues z_j, with $j = 1, 2, 3$, and, so, it takes the expression

$$P_Z(z;\lambda) = (z - z_1)(z - z_2)(z - z_3). \tag{K.1}$$

On the other hand, we can construct the polynomial of the sums of the eigenvalues z_j, defined as the polynomial whose roots are $z_1 + z_2$, $z_2 + z_3$ and $z_3 + z_1$, that is

$$\mathcal{S}_Z(x;\lambda) = (x - (z_1 + z_2))(x - (z_2 + z_3))(x - (z_1 + z_3)). \tag{K.2}$$

$$\text{that} \quad \text{is}\, \mathcal{S}_Z(x;\lambda) = x^3 - 2x^2 Tr(Z) + \frac{x}{2}\left(3Tr^2(Z) - Tr(Z^2)\right) - \frac{1}{3}\left(Tr^3(Z) - Tr(Z^3)\right). \tag{K.3}$$

Hence, the coefficients of the polynomial $\mathcal{S}_Z(x;\lambda)$ in (K.3) can be written in terms of the coefficients of the polynomial $P_Z(z;\lambda)$ in (K.1), and, so, we obtain

$$\mathcal{S}_Z(\theta;\lambda) = \theta^3 + 4\lambda\theta^2 + (5\lambda^2 + p_2 - 1)\theta + p_1 + \lambda(-2 + p_2 + 2\lambda^2). \tag{K.4}$$

that is the polynomial of the sums of the eigenvalues z_j.

Appendix L

Space Stability Spectra

```
% Parameters to be assigned
%p1=-0.8; p2=0.4; p3=-0.6; %1G 1B 2L
%p1=-4.0; p2=-3.0; p3=-0.6;%1G 1B 1L
%p1=1.0; p2=3.0; p3=-0.6; %1G 1B 0L
p1=-6.2; p2=-6.3; p3=-0.6; %0G 2B 2L
%p1 = -4.0; p2 = -4.2; p3 = -0.6; %0G 2B 1L
%p1=1.0; p2=-3.0; p3=-0.6; %0G 2B 0L
%p1=-70.0; p2=60.0; p3=-0.6; %2G 0B 2L
%p1 = 0.2; p2 =0.6; p3 = -0.6;  %2G 0B 1L
%p1=-90.0; p2=60.0; p3=-0.6; %1G 1SG 0B 1L 1TL
%p1=-1.4; p2=-1.0; p3=-0.6; %0G 1SG 1B 1L 1TL
%p1=-4.0; p2=2.0; p3=-0.6;  %0G 1SG 1B 0L 1TL
%p1 = 2; p2 = -4; p3 = -0.6;
Nx = 2*1e3;

% Saveflag. If 'saveflag=0' no figure is saved. If 'saveflag
    =1', all
% figures are saved.
saveflag = 0;

```

```
% Dataflag. If 'dataflag=0' no data is generated. If 'dataflag=1', data is
% generated.
dataflag = 1;

% Computation of the curve on the lambda-plane, parametrized as a function
% of x = k3^2;
if dataflag==1
    [x,lambda] = branchsolver1(p1,p2,p3,Nx);
end

% NB: If the curves are not well centered in the lambda-plane, then the
% instruction for the array AXISLAMBDA below has to be modified.

% %%%%%%%%%%%%%%%%%%%%%%%%%%%%%%%%%%%%%%%%%%%%%%%%%%%%%%%%%%%%%%%%%%%%%%%%%%%%
% Roots of Q2(x)
% %%%%%%%%%%%%%%%%%%%%%%%%%%%%%%%%%%%%%%%%%%%%%%%%%%%%%%%%%%%%%%%%%%%%%%%%%%%%
% For a given choice of r and p, the roots of the polynomial Q2(x) are
% evaluated. Let Q(x) be the discriminant of the polynomial whose roots are
% the squares of the differences of the roots of the characteristic
% polynomial PW; then Q(x) = Q1(x)^2 * Q2(x); thus Q2(x) is the polynomial
```

```
% that describes the changes of sign of Q(x).

% Let X be the set of the real, non-negative zeros of Q2(x). X has at most
% four elements and it is shown that it has at least one element. Let Xj be
% its elements, where j spans between 1 and the total number of real
% non-negative roots of Q2(x), sorted in ascending order.
%
% This values are utilised for plotting the regions of x where Q is
% positive (green color) and where Q is negative (red color).

coeffdiscr = qcoef(p1,p2,p3);
xr = roots(coeffdiscr); % roots of Q2
xr_real = sort( real( xr( (abs(imag(xr))<1e-10) & (real(xr)>=0) ) ) );
xspan = [0 4*max(xr_real)];
disp(['*****************************************************************'])
disp(['Roots of Q2(x) for p1 = ',num2str(1),' , p2 = ',num2str(p2),' , p3 = ',num2str(p3)])
xr(:) % displays the roots of Q2
disp(['*****************************************************************'])

% %%%%%%%%%%%%%%%%%%%%%%%%%%%%%%%%%%%%%%%%%%%%%%%%%%%%%%%%%%%%%%%%%%%%%%%%%%%
```

```
% Columnization of lambda and x
% %%%%%%%%%%%%%%%%%%%%%%%%%%%%%%%%%%%%%%%%%%%%%%%%%%%%%%%%%%%%%%%%%%%%%%%%%%%%%%%%%%%%%%%%%%%%%%%%%%%%%%%%
lambdacol = lambda(:);
lambdacol2 = conj(lambdacol).*lambdacol;
xcol = [x(:); x(:); x(:); x(:); x(:); x(:)];

% %%%%%%%%%%%%%%%%%%%%%%%%%%%%%%%%%%%%%%%%%%%%%%%%%%%%%%%%%%%%%%%%%%%%%%%%%%%%%%%%%%%%%%%%%%%%%%%%%%%%%%%%
% Stereographic projection
% %%%%%%%%%%%%%%%%%%%%%%%%%%%%%%%%%%%%%%%%%%%%%%%%%%%%%%%%%%%%%%%%%%%%%%%%%%%%%%%%%%%%%%%%%%%%%%%%%%%%%%%%
Sy = 2*real(lambdacol)./(1+lambdacol2);
Sz = 2*imag(lambdacol)./(1+lambdacol2);
Sx = (1-lambdacol2)./(1+lambdacol2);

lambda2_1 = conj(lambda(:,1)).*lambda(:,1);
Sy1 = 2*real(lambda(:,1))./(1+lambda2_1);
Sz1 = 2*imag(lambda(:,1))./(1+lambda2_1);
Sx1 = (1-lambda2_1)./(1+lambda2_1);

lambda2_2 = conj(lambda(:,2)).*lambda(:,2);
Sy2 = 2*real(lambda(:,2))./(1+lambda2_2);
Sz2 = 2*imag(lambda(:,2))./(1+lambda2_2);
Sx2 = (1-lambda2_2)./(1+lambda2_2);

lambda2_3 = conj(lambda(:,3)).*lambda(:,3);
Sy3 = 2*real(lambda(:,3))./(1+lambda2_3);
Sz3 = 2*imag(lambda(:,3))./(1+lambda2_3);
```

```
Sx3 = (1-lambda2_3)./(1+lambda2_3);

lambda2_4 = conj(lambda(:,4)).*lambda(:,4);
Sy4 = 2*real(lambda(:,4))./(1+lambda2_4);
Sz4 = 2*imag(lambda(:,4))./(1+lambda2_4);
Sx4 = (1-lambda2_4)./(1+lambda2_4);

lambda2_5 = conj(lambda(:,5)).*lambda(:,5);
Sy5 = 2*real(lambda(:,5))./(1+lambda2_5);
Sz5 = 2*imag(lambda(:,5))./(1+lambda2_5);
Sx5 = (1-lambda2_5)./(1+lambda2_5);

lambda2_6 = conj(lambda(:,6)).*lambda(:,6);
Sy6 = 2*real(lambda(:,6))./(1+lambda2_6);
Sz6 = 2*imag(lambda(:,6))./(1+lambda2_6);
Sx6 = (1-lambda2_6)./(1+lambda2_6);

% %%%%%%%%%%%%%%%%%%%%%%%%%%%%%%%%%%%%%%%%%%%%%%%%%%%%%%%%%%%%%%%%%%%%%%%%%%%%
% Omega3 and Gain (gamma)
% %%%%%%%%%%%%%%%%%%%%%%%%%%%%%%%%%%%%%%%%%%%%%%%%%%%%%%%%%%%%%%%%%%%%%%%%%%%%

% Omega3, k3 and the gain are computed only for the values of lambda (and
% the corresponding values of x) for which lambda has a non-zero imaginary
% part. k3 = sqrt(x). gain = imag(omega3).

 lambdacom = lambdacol(abs(imag(lambdacol))~=0);
 xcom = xcol(abs(imag(lambdacol))~=0);
```

```
 k3 = sqrt(xcom);
 if dataflag==1
     omega3 = omegaextractor2(p1,p2,p3,k3,lambdacom);
 end
 gamma = imag(omega3);

 kk3 = sqrt(x);
 if dataflag==1
     omega3H = omegaextractorH(p1,p2,p3,kk3);
 end
 omega3Hcol = omega3H(:);
 gammaH = imag(omega3Hcol);

%%%%%%%%%%%%%%%%%%%%%%%%%%%%%%%%%%%%%%%%%%%%%%%%%%%%%%%%%%%%%%%%%%%%%%%%%%%%%%%%%%%%%
% Optimizing the axes ranges in order to centre the lambda-cruves for the
% user (AXISLAMBDA)
%%%%%%%%%%%%%%%%%%%%%%%%%%%%%%%%%%%%%%%%%%%%%%%%%%%%%%%%%%%%%%%%%%%%%%%%%%%%%%%%%%%%%

lambdacol_nonzeroimag = lambdacol((imag(lambdacol)~=0)&(abs(real(lambdacol))>1e-9));
maxlambdare = max(real(lambdacol_nonzeroimag));
minlambdare = min(real(lambdacol_nonzeroimag));
maxlambdaim = max(imag(lambdacol_nonzeroimag));
minlambdaim = min(imag(lambdacol_nonzeroimag));
maxlambdare = max([maxlambdare max(real(lambda(1,:)))]);
minlambdare = min([minlambdare min(real(lambda(1,:)))]);
if maxlambdaim==0
    maxlambdaim = 1;
```

```
end
if minlambdaim==0
    minlambdaim = -1;
end
axislambda = [minlambdare maxlambdare minlambdaim maxlambdaim]*(15/10);
axislambda = 2*[-3.0,3.0,-5.5,5.5];

% %%%%%%%%%%%%%%%%%%%%%%%%%%%%%%%%%%%%%%%%%%%%%%%%%%%%%%%%%%%%%%%%%%%%%%%%%%%%%%%%%%%%
% Computation of s1, s2 and a1, a2 corresponding to the given values of r,p
% %%%%%%%%%%%%%%%%%%%%%%%%%%%%%%%%%%%%%%%%%%%%%%%%%%%%%%%%%%%%%%%%%%%%%%%%%%%%%%%%%%%
% if (abs(p)>=abs(r))&&(r>=0)&&(p>=0)
%     s1 = 1; s2 = 1;
% elseif (abs(p)<abs(r))&&(r>=0)&&(p>=0)
%     s1 = 1; s2 = -1;
% elseif (abs(p)>=abs(r))&&(r>=0)&&(p<0)
%     s1 = -1; s2 = -1;
% elseif (abs(p)<abs(r))&&(r>=0)&&(p<0)
%     s1 = 1; s2 = -1;
% elseif (abs(p)>=abs(r))&&(r<0)&&(p>=0)
%     s1 = 1; s2 = 1;
% elseif (abs(p)<abs(r))&&(r<0)&&(p>=0)
%     s1 = -1; s2 = 1;
% elseif (abs(p)>=abs(r))&&(r<0)&&(p<0)
%     s1 = -1; s2 = -1;
% elseif (abs(p)<abs(r))&&(r<0)&&(p<0)
%     s1 = -1; s2 = 1;
```

```
% end
%
% a1 = sqrt(s1*(p+r)/2); a2 = sqrt(s2*(p-r)/2);
% disp([s1 s2; a1 a2]);

% %%%%%%%%%%%%%%%%%%%%%%%%%%%%%%%%%%%%%%%%%%%%%%%%%%%%%%%%%%%%%%%%%%%%%%%%%%%%%%%%%%%%%%%%
% Computation of the two critical curves on the (r,p)-plane
% %%%%%%%%%%%%%%%%%%%%%%%%%%%%%%%%%%%%%%%%%%%%%%%%%%%%%%%%%%%%%%%%%%%%%%%%%%%%%%%%%%%%%%%
% delta2 = 2^(2/3); delta4 = delta2^2;
% pden = @(x) (x+sqrt(4+x.^2)).^(2/3);
% pcurve1 = @(x) -5 + 3*(delta2./pden(x) + pden(x)/delta2);
% pcurve2 = @(x) -sqrt(16-12*delta2*((x.^2).^(1/3))+3*delta4
    *((x.^4).^(1/3)));
% if r<=4
%     rmin = 0;
%     rmax = 4;
% else
%     rmin = 4;
%     rmax = 2*r-8;
% end
% dr = (rmax-rmin)/1e3;
% rvec = [rmin:dr:rmax];
% pvec1 = pcurve1(rvec);
% pvec2 = pcurve2(rvec);

% %%%%%%%%%%%%%%%%%%%%%%%%%%%%%%%%%%%%%%%%%%%%%%%%%%%%%%%%%%%%%%%%%%%%%%%%%%%%%%%%%%%%%%%%
```

```
% Computation of the critical curves on the (a1,a2)-plane
% %%%%%%%%%%%%%%%%%%%%%%%%%%%%%%%%%%%%%%%%%%%%%%%%%%%%%%%%%%%%%%%%%%%%%%%%%%%%%%%%%%
% rval = linspace(-100,100,1e4);
% pval1 = pcurve1(rval);
% pval2 = pcurve2(rval);
% a1val1 = sqrt(s1*(pval1+rval)/2); a2val1 = sqrt(s2*(pval1-rval)/2);
% a1val2 = sqrt(s1*(pval2+rval)/2); a2val2 = sqrt(s2*(pval2-rval)/2);
% a1vec1 = a1val1((imag(a1val1)==0)&(imag(a2val1)==0));
% a2vec1 = a2val1((imag(a1val1)==0)&(imag(a2val1)==0));
% a1vec2 = a1val2((imag(a1val2)==0)&(imag(a2val2)==0));
% a2vec2 = a2val2((imag(a1val2)==0)&(imag(a2val2)==0));

% %%%%%%%%%%%%%%%%%%%%%%%%%%%%%%%%%%%%%%%%%%%%%%%%%%%%%%%%%%%%%%%%%%%%%%%%%%%%%%%%%%
% PLOTS
% %%%%%%%%%%%%%%%%%%%%%%%%%%%%%%%%%%%%%%%%%%%%%%%%%%%%%%%%%%%%%%%%%%%%%%%%%%%%%%%%%%
redfac = 0.85;
hf1 = figure(1);
clf
subplot(6,9,[1 2 10 11])
%       plot(rvec,pvec1,'k')
%       hold on
%      %plot(rvec,pvec2,'r')
%       plot(rvec,-pvec2,'r')
%       plot(rvec,rvec,'b')
```

```
213 %     plot(rvec,-rvec,'b')
214 %     plot(r,p,'ko','Marker','o','MarkerFaceColor','c','
    MarkerEdgeColor','k','MarkerSize',4)
215 %     hold off
216 %     axis([rmin rmax -rmax rmax])
217 %     xlabel('$r$','interpreter','latex')
218 %     ylabel('$p$','interpreter','latex')
219 %     title(['$(r,p)$-plane, $r=$',num2str(r),' $p=$',num2str(
    p)],'interpreter','latex')
220 %     tmp = get(gca,'position');
221 %     set(gca,'position',[tmp(1) tmp(2) redfac*tmp(3) redfac*
    tmp(4)]);
222 subplot(6,9,[19 20 28 29])
223 %     plot(rvec,pvec1,'k')
224 %     hold on
225 %     %plot(rvec,pvec2,'r')
226 %     plot(rvec,-pvec2,'r')
227 %     plot(rvec,rvec,'b')
228 %     plot(rvec,-rvec,'b')
229 %     plot(r,p,'ko','Marker','o','MarkerFaceColor','c','
    MarkerEdgeColor','k','MarkerSize',4)
230 %     hold off
231 %     axis([rmin 4 -4 4])
232 %     xlabel('$r$','interpreter','latex')
233 %     ylabel('$p$','interpreter','latex')
234 %     %title('$(r,p)$-plane','interpreter','latex')
235 %     tmp = get(gca,'position');
236 %     set(gca,'position',[tmp(1) tmp(2) redfac*tmp(3) redfac*
    tmp(4)]);
237 subplot(6,9,[37 38 46 47])
238 %     plot(rvec,pvec1,'k')
239 %     hold on
```

```
240 %     %plot(rvec,pvec2,'r')
241 %      plot(rvec,-pvec2,'r')
242 %      plot(rvec,rvec,'b')
243 %      plot(rvec,-rvec,'b')
244 %      plot(r,p,'ko','Marker','o','MarkerFaceColor','c','
    MarkerEdgeColor','k','MarkerSize',4)
245 %      hold off
246 %      axis([4 rmax -rmax rmax])
247 %      xlabel('$r$','interpreter','latex')
248 %      ylabel('$p$','interpreter','latex')
249 %     %title('$(r,p)$-plane','interpreter','latex')
250 %      tmp = get(gca,'position');
251 %      set(gca,'position',[tmp(1) tmp(2) redfac*tmp(3) redfac*
    tmp(4)]);
252 subplot(6,9,[3:6])
253      Nxx = 1e4; xx = linspace(x(1),x(end),Nxx);
254      imgc = zeros(2,Nxx,3);
255      for k=1:Nxx
256          if polyval(coeffdiscr,(xx(k)))>0
257              imgc(:,k,1) = 0;
258              imgc(:,k,2) = 1;
259              imgc(:,k,3) = 0;
260          else
261              imgc(:,k,1) = 1;
262              imgc(:,k,2) = 0;
263              imgc(:,k,3) = 0;
264          end
265      end
266      imagesc(xx,[-1 1],imgc)
267      hold on
268      plot(xx,zeros(size(xx)),'k','MarkerSize',3)
269      y = linspace(-1,1,10);
```

```
270     for k=1:length(xr_real)
271         plot(xr_real(k)*ones(size(y)),y,'k','MarkerSize',3)
272     end
273     %xpl = plot(x(1),0,'o','MarkerFaceColor','k','MarkerSize
            ',5);
274     hold off
275     axis([x(1) x(end) -1 1])
276     xlabel('$k_{3}^{2}$','interpreter','latex')
277     title(['Sign of $\Delta$ for squares of differences: green
            -pos, red-neg'],'interpreter','latex')
278     tmp = get(gca,'position');
279     set(gca,'position',[tmp(1) tmp(2) redfac*tmp(3) redfac*tmp
            (4)]);
280 subplot(6,9,[12:15,21:24,30:33,39:42,48:51])
281     plot(real(lambda(:,1)),imag(lambda(:,1)),'b.','MarkerSize'
            ,2)
282     hold on
283     plot(real(lambda(:,2)),imag(lambda(:,2)),'b.','MarkerSize'
            ,2)
284     plot(real(lambda(:,3)),imag(lambda(:,3)),'b.','MarkerSize'
            ,2)
285     plot(real(lambda(:,4)),imag(lambda(:,4)),'b.','MarkerSize'
            ,2)
286     plot(real(lambda(:,5)),imag(lambda(:,5)),'b.','MarkerSize'
            ,2)
287     plot(real(lambda(:,6)),imag(lambda(:,6)),'b.','MarkerSize'
            ,2)
288 %     pl1 = plot(real(lambda(1,1)),imag(lambda(1,1)),'o','
    MarkerFaceColor','red','MarkerSize',4);
289 %     pl2 = plot(real(lambda(1,2)),imag(lambda(1,2)),'o','
    MarkerFaceColor','red','MarkerSize',4);
```

```
290 %     pl3 = plot(real(lambda(1,3)),imag(lambda(1,3)),'o','
    MarkerFaceColor','red','MarkerSize',4);
291 %     pl4 = plot(real(lambda(1,4)),imag(lambda(1,4)),'o','
    MarkerFaceColor','red','MarkerSize',4);
292 %     pl5 = plot(real(lambda(1,5)),imag(lambda(1,5)),'o','
    MarkerFaceColor','red','MarkerSize',4);
293 %     pl6 = plot(real(lambda(1,6)),imag(lambda(1,6)),'o','
    MarkerFaceColor','red','MarkerSize',4);
294     hold off
295     xlabel('$\mu$','interpreter','latex')
296     ylabel('$\rho$','interpreter','latex')
297     title(['$\lambda$, $p_1=$',num2str(p1),', $p_2=$',num2str(
        p2),', $p_3=$',num2str(p3)],'interpreter','latex')
298     axis(axislambda)
299     tmp = get(gca,'position');
300     set(gca,'position',[tmp(1) tmp(2) redfac*tmp(3) redfac*tmp
        (4)]);
301 subplot(6,9,[7:9,16:18,25:27])
302     set(gcf,'color','w');
303     [sph1,sph2,sph3] = sphere(64);
304     hs = surfl(sph1,sph2,sph3);
305     set(hs,'FaceAlpha',0.6)
306     shading interp
307     colormap(bone)
308     hold on
309     plot3(Sx,Sy,Sz,'k.','MarkerSize',2,'LineWidth',2)
310     plot3(1,0,0,'r.','MarkerSize',15)
311     plot3(-1,0,0,'g.','MarkerSize',15)
312     axis equal % or square
313     box off
314     grid off
315     axis off
```

```
316      view(70,5)
317 %      spl1 = plot3(Sx1(1),Sy1(1),Sz1(1),'o','MarkerFaceColor
    ','b','MarkerSize',3);
318 %      spl2 = plot3(Sx2(1),Sy2(1),Sz2(1),'o','MarkerFaceColor
    ','b','MarkerSize',3);
319 %      spl3 = plot3(Sx3(1),Sy3(1),Sz3(1),'o','MarkerFaceColor
    ','b','MarkerSize',3);
320 %      spl4 = plot3(Sx4(1),Sy4(1),Sz4(1),'o','MarkerFaceColor
    ','b','MarkerSize',3);
321 %      spl5 = plot3(Sx5(1),Sy5(1),Sz5(1),'o','MarkerFaceColor
    ','b','MarkerSize',3);
322 %      spl6 = plot3(Sx6(1),Sy6(1),Sz6(1),'o','MarkerFaceColor
    ','b','MarkerSize',3);
323      hold off
324      title(['$\lambda$, $p_1=$',num2str(p1),', $p_2=$',num2str(
           p2),', $p_3=$',num2str(p3)],'interpreter','latex')
325 subplot(6,9,[34:36,43:45,52:54])
326       plot(k3,abs(gamma),'b.','MarkerSize',3)
327       hold on
328       plot(-k3,abs(gamma),'b.','MarkerSize',3)
329       plot(sqrt(xcol),abs(gammaH),'r.','MarkerSize',3)
330       plot(-sqrt(xcol),abs(gammaH),'r.','MarkerSize',3)
331 %      gpl1 = plot(sqrt(x(1)),abs(gamma1(1)),'o','
    MarkerFaceColor','red','MarkerSize',4);
332 %      gpl2 = plot(sqrt(x(1)),abs(gamma2(1)),'o','
    MarkerFaceColor','red','MarkerSize',4);
333 %      gpl3 = plot(sqrt(x(1)),abs(gamma3(1)),'o','
    MarkerFaceColor','red','MarkerSize',4);
334 %      gpl4 = plot(sqrt(x(1)),abs(gamma4(1)),'o','
    MarkerFaceColor','red','MarkerSize',4);
335 %      gpl5 = plot(sqrt(x(1)),abs(gamma5(1)),'o','
    MarkerFaceColor','red','MarkerSize',4);
```

```
336 %     gpl6 = plot(sqrt(x(1)),abs(gamma6(1)),'o','
    MarkerFaceColor','red','MarkerSize',4);
337 %     axis([-k3max k3max 0 gammamax]*(12/10))
338       hold off
339       xlabel('$k_{3}$','interpreter','latex')
340       ylabel('$|\Gamma(k_{3})|$','interpreter','latex')
341       title(['Modulus of Gain $p_1=$',num2str(p1),', $p_2=$',
             num2str(p2),', $p_3=$',num2str(p3)],'interpreter','
             latex')
342       tmp = get(gca,'position');
343       set(gca,'position',[tmp(1) tmp(2) redfac*tmp(3) redfac*
             tmp(4)]);
344
345 %file_name = ['GBL_r=',num2str(r),'_p=',num2str(p)];
346 %print(hf1,[pwd '/Figures/' file_name '.jpeg'],'-djpeg')
347
348 % for j=2:100:length(x)
349 %     pl1.XData = real(lambda(j,1)); pl1.YData = imag(lambda(j
    ,1));
350 %     pl2.XData = real(lambda(j,2)); pl2.YData = imag(lambda(j
    ,2));
351 %     pl3.XData = real(lambda(j,3)); pl3.YData = imag(lambda(j
    ,3));
352 %     pl4.XData = real(lambda(j,4)); pl4.YData = imag(lambda(j
    ,4));
353 %     pl5.XData = real(lambda(j,5)); pl5.YData = imag(lambda(j
    ,5));
354 %     pl6.XData = real(lambda(j,6)); pl6.YData = imag(lambda(j
    ,6));
355 %     xpl.XData = x(j);
356 %     gpl1.XData = sqrt(x(j)); gpl1.YData = abs(gamma1(j));
357 %     gpl2.XData = sqrt(x(j)); gpl2.YData = abs(gamma2(j));
```

```
358 %     gpl3.XData = sqrt(x(j)); gpl3.YData = abs(gamma3(j));
359 %     gpl4.XData = sqrt(x(j)); gpl4.YData = abs(gamma4(j));
360 %     gpl5.XData = sqrt(x(j)); gpl5.YData = abs(gamma5(j));
361 %     gpl6.XData = sqrt(x(j)); gpl6.YData = abs(gamma6(j));
362 %     spl1.XData = Sx1(j); spl1.YData = Sy1(j); spl1.ZData =
        Sz1(j);
363 %     spl2.XData = Sx2(j); spl2.YData = Sy2(j); spl2.ZData =
        Sz2(j);
364 %     spl3.XData = Sx3(j); spl3.YData = Sy3(j); spl3.ZData =
        Sz3(j);
365 %     spl4.XData = Sx4(j); spl4.YData = Sy4(j); spl4.ZData =
        Sz4(j);
366 %     spl5.XData = Sx5(j); spl5.YData = Sy5(j); spl5.ZData =
        Sz5(j);
367 %     spl6.XData = Sx6(j); spl6.YData = Sy6(j); spl6.ZData =
        Sz6(j);
368 %     drawnow
369 % end
370
371
372 figure(2)
373 subplot(1,3,1)
374       plot(k3,abs(gamma),'b.','MarkerSize',3)
375       hold on
376       plot(-k3,abs(gamma),'b.','MarkerSize',3)
377       plot(sqrt(xcol),abs(gammaH),'r.','MarkerSize',3)
378       plot(-sqrt(xcol),abs(gammaH),'r.','MarkerSize',3)
379       hold off
380       xlabel('$k_{3}$','interpreter','latex')
381       ylabel('$|\Gamma(k_{3})|$','interpreter','latex')
382       title(['Modulus of Gain, $p_1=$',num2str(p1),', $p_2=$',
            num2str(p2),', $p_3=$',num2str(p3)],'interpreter','
```

```
        latex')
383     tmp = get(gca,'position');
384     set(gca,'position',[tmp(1) tmp(2) redfac*tmp(3) redfac*
        tmp(4)]);
385 subplot(1,3,2)
386     plot(k3,abs(gamma),'b.','MarkerSize',3)
387     hold on
388     plot(-k3,abs(gamma),'b.','MarkerSize',3)
389     hold off
390     xlabel('$k_{3}$','interpreter','latex')
391     ylabel('$|\Gamma(k_{3})|$','interpreter','latex')
392     title(['Modulus of Gain from numerics, $p_1=$',num2str(p1
        ),', $p_2=$',num2str(p2),', $p_3=$',num2str(p3)],'
        interpreter','latex')
393     tmp = get(gca,'position');
394     set(gca,'position',[tmp(1) tmp(2) redfac*tmp(3) redfac*
        tmp(4)]);
395 subplot(1,3,3)
396     plot(sqrt(xcol),abs(gammaH),'r.','MarkerSize',3)
397     hold on
398     plot(-sqrt(xcol),abs(gammaH),'r.','MarkerSize',3)
399     hold off
400     xlabel('$k_{3}$','interpreter','latex')
401     ylabel('$|\Gamma(k_{3})|$','interpreter','latex')
402     title(['Modulus of Gain from $H$, $p_1=$',num2str(p1),',
        $p_2=$',num2str(p2),', $p_3=$',num2str(p3)],'
        interpreter','latex')
403     tmp = get(gca,'position');
404     set(gca,'position',[tmp(1) tmp(2) redfac*tmp(3) redfac*
        tmp(4)]);
405
```

```
% %%%%%%%%%%%%%%%%%%%%%%%%%%%%%%%%%%%%%%%%%%%%%%%%%%%%%%%%%%%%%%%%%%%%%%%%%%%%%%
%% PLOTS
% %%%%%%%%%%%%%%%%%%%%%%%%%%%%%%%%%%%%%%%%%%%%%%%%%%%%%%%%%%%%%%%%%%%%%%%%%%%%%%
fslabels = 28;
fsticks = 24;

%% hf1 = figure(1);
%% clf
%% plot(rvec,rvec,'k','LineWidth',2)
%% hold on
%% plot(rvec,-rvec,'k','LineWidth',2)
%% plot(rvec,pvec1,'r','LineWidth',2)
%% plot(rvec,pvec2,'b','LineWidth',2)
%% plot(r,p,'ko','Marker','o','MarkerFaceColor','g','MarkerEdgeColor','k','MarkerSize',9)
%% hold off
%% axis([rmin rmax -rmax rmax])
%% axis square
%% xlabel('$r$','interpreter','latex','fontsize',fslabels,'fontweight','bold')
%% ylabel('$p$','interpreter','latex','fontsize',fslabels,'fontweight','bold')
%% ax = gca; ax.FontSize = fsticks;
%%
%% hf2 = figure(2);
%% clf
%% if max(a1,a2)<3
%%     a1max = 3; a2max = a1max;
```

```
%% else
%%     a1max = 5;%1.5*max(a1,a2);
%%     a2max = a1max;
%% end
%% if s1==1&&s2==1
%%     plot(a1vec1,a2vec1,'r','LineWidth',2)
%%     hold on
%% elseif s1==-1&&s2==1
%%     plot(a1vec2,a2vec2,'b','LineWidth',2)
%%     hold on
%%     plot(a1vec1,a2vec1,'r','LineWidth',2)
%% elseif s1==-1&&s2==-1
%%     plot(a1vec2,a2vec2,'b','LineWidth',2)
%%     hold on
%% elseif s1==1&&s2==-1
%%     plot(a1vec2,a2vec2,'b','LineWidth',2)
%%     hold on
%%     plot(a1vec1,a2vec1,'r','LineWidth',2)
%% end
%% plot(a1,a2,'ko','Marker','o','MarkerFaceColor','g','
   MarkerEdgeColor','k','MarkerSize',9)
%% hold off
%% axis([0 a1max 0 a2max])
%% axis square
%% xlabel('$a_{1}$','interpreter','latex','fontsize',fslabels
   ,'fontweight','bold')
%% ylabel('$a_{2}$','interpreter','latex','fontsize',fslabels
   ,'fontweight','bold')
%% ax = gca; ax.FontSize = fsticks;
%% ax.XTick = [0:a1max]; ax.YTick = [0:a2max];
%
hf3 = figure(3);
```

```
460 clf
461 plot(real(lambda(:,1)),imag(lambda(:,1)),'b.','MarkerSize',2)
462 hold on
463 plot(real(lambda(:,2)),imag(lambda(:,2)),'b.','MarkerSize',2)
464 plot(real(lambda(:,3)),imag(lambda(:,3)),'b.','MarkerSize',2)
465 plot(real(lambda(:,4)),imag(lambda(:,4)),'b.','MarkerSize',2)
466 plot(real(lambda(:,5)),imag(lambda(:,5)),'b.','MarkerSize',2)
467 plot(real(lambda(:,6)),imag(lambda(:,6)),'b.','MarkerSize',2)
468 %plot(real(lambda(1,1)),imag(lambda(1,1)),'ko','Marker','o','
       MarkerFaceColor','r','MarkerEdgeColor','k','MarkerSize',5)
469 %plot(real(lambda(1,2)),imag(lambda(1,2)),'ko','Marker','o','
       MarkerFaceColor','r','MarkerEdgeColor','k','MarkerSize',5)
470 %plot(real(lambda(1,3)),imag(lambda(1,3)),'ko','Marker','o','
       MarkerFaceColor','r','MarkerEdgeColor','k','MarkerSize',5)
471 %plot(real(lambda(1,4)),imag(lambda(1,4)),'ko','Marker','o','
       MarkerFaceColor','r','MarkerEdgeColor','k','MarkerSize',5)
472 %plot([r/(2*p),0],'ko','Marker','o','MarkerFaceColor','b','
       MarkerEdgeColor','k','MarkerSize',5)
473 hold off
474 xlabel('$\mu$','interpreter','latex','fontsize',fslabels,'
       fontweight','bold')
475 ylabel('$\rho$','interpreter','latex','fontsize',fslabels,'
       fontweight','bold')
476 axis(axislambda)
477 ax = gca;
478 ax.FontSize = fsticks;
479 ax.FontWeight = 'normal';
480 ax.TickLabelInterpreter = 'latex';
481 outerpos = ax.OuterPosition;
482 ti = ax.TightInset;
483 left = outerpos(1) + ti(1);
484 bottom = outerpos(2) + ti(2);
```

```
485 ax_width = outerpos(3) - ti(1) - ti(3);
486 ax_height = outerpos(4) - ti(2) - ti(4);
487 ax.Position = [left bottom ax_width ax_height];
488 fig = gcf;
489 fig.PaperPositionMode = 'auto';
490 fig_pos = fig.PaperPosition;
491 fig.PaperSize = [fig_pos(3) fig_pos(4)];
492
493 %% hf4 = figure(4);
494 %% clf
495 %% plot(k3,abs(gamma),'b.','MarkerSize',4)
496 %% hold on
497 %% plot(-k3,abs(gamma),'b.','MarkerSize',4)
498 %% hold off
499 %% xlabel('$k_{3}$','interpreter','latex','fontsize',fslabels
    ,'fontweight','bold')
500 %% ylabel('$|\Gamma(k_{3})|$','interpreter','latex','fontsize
    ',fslabels,'fontweight','bold')
501 %% axis([-max(k3) max(k3) 0 max(abs(gamma))]*1.05)
502 %% axis square
503 %% ax = gca; ax.FontSize = fsticks;
504 %%
505 %% hf5 = figure(5);
506 %% clf
507 %% set(gcf,'color','w');
508 %% [sph1,sph2,sph3] = sphere(64);
509 %% hs = surfl(sph1,sph2,sph3);
510 %% set(hs,'FaceAlpha',0.6)
511 %% shading interp
512 %% colormap(bone)
513 %% hold on
514 %% plot3(Sx,Sy,Sz,'k.','MarkerSize',1,'LineWidth',1)
```

```
515 %% plot3(1,0,0,'co','Marker','o','MarkerFaceColor','c','
        MarkerEdgeColor','c','MarkerSize',5)
516 %% plot3(-1,0,0,'yo','Marker','o','MarkerFaceColor','y','
        MarkerEdgeColor','y','MarkerSize',5)
517 %% axis equal % or square
518 %% box off
519 %% grid off
520 %% axis off
521 %% view(70,5) %view(70,5)
522 %% hold off
523 %
524 ds = 5;
525 hf6 = figure(6);
526 clf
527 plot(real(lambda(1:ds:end,1)),imag(lambda(1:ds:end,1)),'b.','
        MarkerSize',2)
528 hold on
529 plot(real(lambda(1:ds:end,2)),imag(lambda(1:ds:end,2)),'b.','
        MarkerSize',2)
530 plot(real(lambda(1:ds:end,3)),imag(lambda(1:ds:end,3)),'b.','
        MarkerSize',2)
531 plot(real(lambda(1:ds:end,4)),imag(lambda(1:ds:end,4)),'b.','
        MarkerSize',2)
532 plot(real(lambda(1:ds:end,5)),imag(lambda(1:ds:end,5)),'b.','
        MarkerSize',2)
533 plot(real(lambda(1:ds:end,6)),imag(lambda(1:ds:end,6)),'b.','
        MarkerSize',2)
534 %plot(real(lambda(1,1)),imag(lambda(1,1)),'ko','Marker','o','
        MarkerFaceColor','r','MarkerEdgeColor','k','MarkerSize',5)
535 %plot(real(lambda(1,2)),imag(lambda(1,2)),'ko','Marker','o','
        MarkerFaceColor','r','MarkerEdgeColor','k','MarkerSize',5)
```

```
536 %plot(real(lambda(1,3)),imag(lambda(1,3)),'ko','Marker','o','
        MarkerFaceColor','r','MarkerEdgeColor','k','MarkerSize',5)
537 %plot(real(lambda(1,4)),imag(lambda(1,4)),'ko','Marker','o','
        MarkerFaceColor','r','MarkerEdgeColor','k','MarkerSize',5)
538 %plot([r/(2*p),0],'ko','Marker','o','MarkerFaceColor','b','
        MarkerEdgeColor','k','MarkerSize',5)
539 hold off
540 xlabel('$\mu$','interpreter','latex','fontsize',fslabels,'
        fontweight','bold')
541 ylabel('$\rho$','interpreter','latex','fontsize',fslabels,'
        fontweight','bold')
542 axis(axislambda)
543 ax = gca;
544 ax.FontSize = fsticks;
545 ax.FontWeight = 'normal';
546 ax.TickLabelInterpreter = 'latex';
547 outerpos = ax.OuterPosition;
548 ti = ax.TightInset;
549 left = outerpos(1) + ti(1);
550 bottom = outerpos(2) + ti(2);
551 ax_width = outerpos(3) - ti(1) - ti(3);
552 ax_height = outerpos(4) - ti(2) - ti(4);
553 ax.Position = [left bottom ax_width ax_height];
554 fig = gcf;
555 fig.PaperPositionMode = 'auto';
556 fig_pos = fig.PaperPosition;
557 fig.PaperSize = [fig_pos(3) fig_pos(4)];
558
559
560 %% hf7 = figure(7);
561 %% clf
```

```
%% plot(k3(1:ds:end),abs(gamma(1:ds:end)),'b.','MarkerSize',4)
%% hold on
%% plot(-k3(1:ds:end),abs(gamma(1:ds:end)),'b.','MarkerSize',4)
%% hold off
%% xlabel('$k_{3}$','interpreter','latex','fontsize',fslabels,'fontweight','bold')
%% ylabel('$|\Gamma(k_{3})|$','interpreter','latex','fontsize',fslabels,'fontweight','bold')
%% axis([-max(k3) max(k3) 0 max(abs(gamma))]*1.05)
%% axis square
%% ax = gca; ax.FontSize = fsticks;

hf7 = figure(7);
clf
plot(sqrt(xcol),abs(gammaH),'b.','MarkerSize',2)
hold on
plot(-sqrt(xcol),abs(gammaH),'b.','MarkerSize',2)
hold off
xlabel('$k_{3}$','interpreter','latex','fontsize',fslabels,'fontweight','bold')
ylabel('$|\Gamma(k_{3})|$','interpreter','latex','fontsize',fslabels,'fontweight','bold')
axis([-max(k3) max(k3) 0 max(abs(gamma))]*1.05)
ax = gca;
ax.FontSize = fsticks;
ax.FontWeight = 'normal';
ax.TickLabelInterpreter = 'latex';
outerpos = ax.OuterPosition;
ti = ax.TightInset;
left = outerpos(1) + ti(1);
```

```
588 bottom = outerpos(2) + ti(2);
589 ax_width = outerpos(3) - ti(1) - ti(3);
590 ax_height = outerpos(4) - ti(2) - ti(4);
591 ax.Position = [left bottom ax_width ax_height];
592 fig = gcf;
593 fig.PaperPositionMode = 'auto';
594 fig_pos = fig.PaperPosition;
595 fig.PaperSize = [fig_pos(3) fig_pos(4)];
596
597
598 hf8 = figure(8);
599 clf
600 plot(sqrt(xcol(1:ds:end)),abs(gammaH(1:ds:end)),'b.','
    MarkerSize',2)
601 hold on
602 plot(-sqrt(xcol(1:ds:end)),abs(gammaH(1:ds:end)),'b.','
    MarkerSize',2)
603 hold off
604 xlabel('$k_{3}$','interpreter','latex','fontsize',fslabels,'
    fontweight','bold')
605 ylabel('$|\Gamma(k_{3})|$','interpreter','latex','fontsize',
    fslabels,'fontweight','bold')
606 axis([-max(k3) max(k3) 0 max(abs(gamma))]*1.05)
607 ax = gca;
608 ax.FontSize = fsticks;
609 ax.FontWeight = 'normal';
610 ax.TickLabelInterpreter = 'latex';
611 outerpos = ax.OuterPosition;
612 ti = ax.TightInset;
613 left = outerpos(1) + ti(1);
614 bottom = outerpos(2) + ti(2);
615 ax_width = outerpos(3) - ti(1) - ti(3);
```

```
ax_height = outerpos(4) - ti(2) - ti(4);
ax.Position = [left bottom ax_width ax_height];
fig = gcf;
fig.PaperPositionMode = 'auto';
fig_pos = fig.PaperPosition;
fig.PaperSize = [fig_pos(3) fig_pos(4)];


%
    %%%%%%%%%%%%%%%%%%%%%%%%%%%%%%%%%%%%%%%%%%%%%%%%%%%%%%%%%%%%%%%%%%%%%%%%%%%%%%%%%%%%
%% Saving the figures
%
    %%%%%%%%%%%%%%%%%%%%%%%%%%%%%%%%%%%%%%%%%%%%%%%%%%%%%%%%%%%%%%%%%%%%%%%%%%%%%%%%%%%%
if saveflag==1
    file_name = ['spectrum_p1=',num2str(p1),'_p2=',num2str(p2)
        ,'_p3=',num2str(p3)];
    print(hf3,[pwd '/Figures/' file_name '_lambda.jpeg'],'-
        djpeg')
    print(hf6,[pwd '/Figures/' file_name '_lambda.eps'],'-
        depsc','-tiff')
    print(hf3,[pwd '/Figures/' file_name '_lambda.pdf'],'-dpdf
        ')
    print(hf7,[pwd '/Figures/' file_name '_gain.jpeg'],'-djpeg
        ')
    print(hf8,[pwd '/Figures/' file_name '_gain.eps'],'-depsc'
        ,'-tiff')
    print(hf7,[pwd '/Figures/' file_name '_gain.pdf'],'-dpdf')
end
```

Appendix M

Gain Function

```
function omega=omegaextractor2(p1,p2,p3,k,lambda)

omega = zeros(size(k));
jmax = length(k);

for j=1:jmax
    kk = k(j); ll = lambda(j);
    pw_coeff = fliplr([(-1).*p1.^2.*p3.^3+p1.*((-1)+p3.*(p3
        +2.*p2.*p3+(-1).*ll+p3.^2.*ll))+p2.*(ll+(-1).*p3.*((-1)
        +p2+p3.*(p3+ll))),...
                p2.*(1+2.*p3.^2+(-1).*p3.*ll)+p1.*p3.*((-3)+p3
                    .*ll)+(-1).*((-1)+p3.^2).*((-1)+ll.^2)
                    ,((-2)+(-1).*p2).*p3+2.*ll,1]);
    pz_coeff = [1,2*ll,p2-1+ll^2,p2*ll-p1];
    wroots = roots(pw_coeff);
    %zroots = roots(pz_coeff);

    wdiff = wroots-wroots([2,3,1]);
    [foo, mind] = min(abs(abs(wdiff)-kk));
    wroots0 = [wroots; wroots(1)];
    w1 = wroots0(mind); w2 = wroots0(mind+1);
```

```
18      cz1 = [p3,1+p3*ll,p2*p3-w1];
19      cz2 = [p3,1+p3*ll,p2*p3-w2];
20      z1roots = roots(cz1);
21      z1val = abs(polyval(pz_coeff,z1roots));
22      [fooz1,indz1] = min(z1val); z1 = z1roots(indz1);
23      z2roots = roots(cz2);
24      z2val = abs(polyval(pz_coeff,z2roots));
25      [fooz2,indz2] = min(z2val); z2 = z2roots(indz2);
26      theta = z1+z2;
27      omega(j) = kk/(1+p3*(theta+ll));
28      disp(['omegaextraction: p1 = ',num2str(p1),', p2 = ',
            num2str(p2),', p3 = ',num2str(p3),...
29          ' diff = ',num2str(foo),' , k3 = ',num2str(kk),...
30          ': j = ',int2str(j),', final j = ',int2str(jmax)]);
31  end
32  return
```

```
1   function omega = omegaextractorH(p1,p2,p3,k)
2
3   jmax = length(k);
4   omega = zeros(jmax,6);
5
6   for j=1:jmax
7       kk = k(j);
8       polH = fliplr([(-4).*kk.^4,(-4).*kk.^3.*((-4)+p1.*p3),kk
            .^2.*((-24)+kk.^2+12.*p1.* ...
9           p3+(-1).*((-8)+p2.*(4+p2)).*p3.^2),2.*kk.*(8+(-2).*kk
                .^2+((-8)+p2.*( ...
10          4+p2)).*p3.^2+p1.*p3.*((-6)+(-1).*((-2)+p2).*p3.^2))
                ,(-4)+4.*p1.* ...
11          p3+(-1).*((-8)+p2.*(4+p2)).*p3.^2+2.*p1.*((-2)+p2).*p3
                .^3+(-1).*( ...
```

```
12          4+p1.^2+(-4).*p2).*p3.^4+(-2).*kk.^2.*((-3)+p3.^2),4.*
                kk.*((-1)+ ...
13          p3.^2),((-1)+p3.^2).^2]);
14      omega(j,:) = roots(polH);
15      disp(['omegaextractionH: p1 = ',num2str(p1),', p2 = ',
            num2str(p2),', p3 = ',num2str(p3),...
16          ': j = ',int2str(j),', final j = ',int2str(jmax)]);
17  end
18  return
```

Appendix N

Sinc Interpolation

```
function y_new = sincinterpr(y_old,x_old,x_new)
%if nargin==3
%dx = x_old(2)-x_old(1);
%end
dxold = x_old(2)-x_old(1);
dxnew = x_new(2)-x_new(1);
size_x_old = size(x_old);
size_x_new = size(x_new);
size_y_old = size(y_old);

% rotates input arrays conveniently
if min(size_x_old)~=1||min(size_y_old)~=1||min(size_x_new)~=1
    error(['sincinterp error: input arguments of sincinterp
        mustbe vectors'])
end
if max(size_x_old)~=max(size_y_old)
    error(['sincinterp error: dimension mismatch in input
        arguments'])
end
if size_x_old(1)~=min(size_x_old)
    X_old = x_old.';
```

```
20 else
21     X_old = x_old;
22 end
23 if size_x_new(1)~=min(size_x_new)
24     X_new = x_new.';
25 else
26     X_new = x_new;
27 end
28 if size_y_old(1)~=min(size_y_old)
29     Y_old = y_old;
30     rot_flag = 0;
31 else
32     Y_old = y_old.';
33     rot_flag = 0;
34 end
35
36 %shift
37     %[Y_old(1) Y_old(end)]
38     [Y_min_ext, ind_min_ext] = min([abs(Y_old(1)) abs(Y_old(
           end))]);
39     if ind_min_ext==1
40         sig_min_ext = sign(Y_old(1));
41     else
42         sig_min_ext = sign(Y_old(end));
43     end
44     Y_old = Y_old-sig_min_ext*Y_min_ext;
45     %[Y_old(1) Y_old(end)]
46
47 %flip
48 if y_old(1)~=y_old(end)
49     % flip is needed
50     if ind_min_ext==1
```

```
51          X_old_c = X_old + (X_old(end)-X_old(1)+dxold);
52          X_old = [X_old, X_old_c];
53          %sizeXold = size(X_old)
54
55          X_new_c = X_new + (X_new(end)-X_new(1)+dxnew);
56          X_new = [X_new, X_new_c];
57          %sizeXnew = size(X_new)
58
59          Y_old = [Y_old; flipud(Y_old)];
60          %sizeYold = size(Y_old)
61      else
62          X_old_c = X_old + (X_old(1)-X_old(end)-dxold);
63          X_old = [X_old_c, X_old];
64          %sizeXold = size(X_old)
65
66          X_new_c = X_new + (X_new(1)-X_new(end)-dxnew);
67          X_new = [X_new_c, X_new];
68          %sizeXnew = size(X_new)
69
70          Y_old = [flipud(Y_old); Y_old];
71          %sizeYold = size(Y_old)
72      end
73  end
74
75  % if Y_old(1)~=Y_old(end)
76  %     if ind_min_ext==1
77  %         Y_old = [Y_old; Y_old(1)];
78  %         X_old = [X_old, X_old(end)+dxold];
79  %     else
80  %         Y_old = [Y_old(end); Y_old];
81  %         X_old = [X_old(1)-dxold, X_old];
82  %     end
```

```
% end
%S = @(xold,xnew) sinc( (pi/dx)*xnew - pi*(floor((xold-xold(1)
    )/dx)) );
%S = @(xshift,xnew) sinc( (pi/dx)*xnew - pi*xshift );
%[Xshift,Xnew] = meshgrid([0:N-1],X_new);
[Xnew,Xold] = ndgrid(X_new,X_old);
SS = sinc((Xnew-Xold)/dxold);
%[Xnewshift,Xoldshift] = ndgrid([0:length(X_new)-1],[0:length(
    X_old)-1]);
%SS = sinc(Xnewshift-Xoldshift);
%SSsize = size(SS)
%Yoldsize = size(Y_old)
Y_new = SS*Y_old;

%reshift
Y_new = Y_new+sig_min_ext*Y_min_ext;
% if Y_old(1)~=Y_old(end)
%     if ind_min_ext==1
%         Y_new = Y_new(1:end-1);
%     else
%         Y_new = Y_new(2:end);
%     end
% end
if ind_min_ext==1
    Y_new = Y_new(1:length(x_new));
else
    Y_new = Y_new(length(x_new)+1:end);
end
if rot_flag==1
    y_new = Y_new.';
else
    y_new = Y_new;
```

```
113 end
114 return
```

Appendix O

Pseudospectral Fourier Discrtization

```
function [x,t,u1,u2,u3] = twri_solver(c,s,a,eta,u0,L,Nx,T,Nt)
% pseudo-spectral code for the 3WRI
%
% c = [c1,c2] is the array of the speeds
% s = [s1,s2,s3] is the array of the signs
% a = [a1,a2] is the array of the amplitudes
% eta = [eta1,eta2] is the array of the frequencies
%
% u0 is the initial condition, which has to be provided as Nx-by-3 array,
% with the first column being the values of u1 at t=0, the second column
% being the values of u2 at t=0, and the third column being the values of
% u3 at t=0
%
% [-L:dx:L-dx] is the range of integration, where dx=2*L/Nx and Nx is the
% number of spatial nodes
%
```

```
% T is the time range of the integration, including Nt time points
%
% x is the vector of the nodes
% t is the time vector
% u1, u2, u3 is the solution in the form of three Nx-by-3 arrays


% %%%%%%%%%%%%%%%%%%%%%%%%%%%%%%%%%%%%%%%%%%%%%%%%%%%%%%%%%%%%%%%%%%%%%%%%%%%%%%%
% setting global variables
% %%%%%%%%%%%%%%%%%%%%%%%%%%%%%%%%%%%%%%%%%%%%%%%%%%%%%%%%%%%%%%%%%%%%%%%%%%%%%%%
global time_start tout

% ridefines the final time as a global variable
tout = T;

% %%%%%%%%%%%%%%%%%%%%%%%%%%%%%%%%%%%%%%%%%%%%%%%%%%%%%%%%%%%%%%%%%%%%%%%%%%%%%%%
% computational grid in Fourier space
% %%%%%%%%%%%%%%%%%%%%%%%%%%%%%%%%%%%%%%%%%%%%%%%%%%%%%%%%%%%%%%%%%%%%%%%%%%%%%%%

% setup grid
dx = 2*L/Nx;
x = [-L:dx:L-dx];
```

```

% fourier wavenumbers
dk = pi/L;
k = fftshift([-Nx/2:(Nx/2)-1]*dk);
k = k.'; %k2 = k.^2;

% %%%%%%%%%%%%%%%%%%%%%%%%%%%%%%%%%%%%%%%%%%%%%%%%%%%%%%%%%%%%%%%%%%%%%%%%%%%%%%
% parameters
% %%%%%%%%%%%%%%%%%%%%%%%%%%%%%%%%%%%%%%%%%%%%%%%%%%%%%%%%%%%%%%%%%%%%%%%%%%%%%%

% Given speeds, signs, amplitudes and frequencies, reconstruct the
% parameters in the equation and in the plane wave solution.
aq = a.^2;
r = (c(1)-c(2))/(eta(1)+eta(2));
nu1 = (eta(1)/c(1))+s(1)*s(3)*aq(2)*(c(2)/c(1))*r;
nu2 = (eta(2)/c(2))+s(2)*s(3)*aq(1)*(c(1)/c(2))*r;
nu3 = -(nu1+nu2);
omega = c(1)*nu1+c(2)*nu2;

% %%%%%%%%%%%%%%%%%%%%%%%%%%%%%%%%%%%%%%%%%%%%%%%%%%%%%%%%%%%%%%%%%%%%%%%%%%%%%%
% initial condition
% %%%%%%%%%%%%%%%%%%%%%%%%%%%%%%%%%%%%%%%%%%%%%%%%%%%%%%%%%%%%%%%%%%%%%%%%%%%%%%

U1 = u0(:,1);  U2 = u0(:,2); U3 = u0(:,3);
```

```
V1 = exp(1i*(nu1*x(:))).*U1;
V2 = exp(1i*(nu2*x(:))).*U2;
V3 = exp(1i*(nu3*x(:))).*U3;

V0 = [V1(:); V2(:); V3(:)];

%
    %%%%%%%%%%%%%%%%%%%%%%%%%%%%%%%%%%%%%%%%%%%%%%%%%%%%%%%%%%%%%%%%%%%%%%%%%%%
% parameters for the ODE solver
%
    %%%%%%%%%%%%%%%%%%%%%%%%%%%%%%%%%%%%%%%%%%%%%%%%%%%%%%%%%%%%%%%%%%%%%%%%%%%

% sets appropriate ODE solver options
opts = odeset('OutputFcn',@twri_output,...
              'Refine',1,...
              'Stats','on',...
              'RelTol',1e-9,'AbsTol',1e-6,...
              'MaxStep',1e-3,...
              'InitialStep',1e-9,...
              'NormControl','on');

%
    %%%%%%%%%%%%%%%%%%%%%%%%%%%%%%%%%%%%%%%%%%%%%%%%%%%%%%%%%%%%%%%%%%%%%%%%%%%
% integration
%
    %%%%%%%%%%%%%%%%%%%%%%%%%%%%%%%%%%%%%%%%%%%%%%%%%%%%%%%%%%%%%%%%%%%%%%%%%%%

% starts the clock
```

```
time_start = tic;
disp(['pseudo-spectral code for HF: calculation started'])

% performs the integration in time
dt = T/Nt;
[t,y] = ode45(@(tt,yy) twri_rhs(tt,yy,Nx,k,c,s,omega),[0:dt:T],V0,opts);

% %%%%%%%%%%%%%%%%%%%%%%%%%%%%%%%%%%%%%%%%%%%%%%%%%%%%%%%%%%%%%%%%%%%%%%%%%%%%%
% recovering output solution from integration
% %%%%%%%%%%%%%%%%%%%%%%%%%%%%%%%%%%%%%%%%%%%%%%%%%%%%%%%%%%%%%%%%%%%%%%%%%%%%%
v1 = y(:,1:Nx);
v2 = y(:,Nx+1:2*Nx);
v3 = y(:,2*Nx+1:3*Nx);
[MX,MT] = meshgrid(x,t);
u1 = exp(-1i*nu1*(MX-c(1)*MT)).*v1;
u2 = exp(-1i*nu2*(MX-c(2)*MT)).*v2;
u3 = exp(-1i*(nu3*MX+omega*MT)).*v3;
disp(['pseudo-spectral code for 3WRI: calculation completed'])

% computing the time elapsed since the beginning of the integration
total_time_elapsed = toc(time_start);
total_days = datenum([0 0 0 0 0 total_time_elapsed]);
time_left = datevec(total_days - floor(total_days));
disp(['total time taken for the integration = ',...
      int2str(floor(total_days)),'d ',...
      int2str(time_left(4)),'h ',...
```

```
    int2str(time_left(5)),'m ',...
    num2str(time_left(6)),'s'])
return

%
   %%%%%%%%%%%%%%%%%%%%%%%%%%%%%%%%%%%%%%%%%%%%%%%%%%%%%%%%%%%%%%%%%%%%%%%%
% twri_output function, called at each time step
%
   %%%%%%%%%%%%%%%%%%%%%%%%%%%%%%%%%%%%%%%%%%%%%%%%%%%%%%%%%%%%%%%%%%%%%%%%

function status = twri_output(tt,yy,flag)
global time_start tout
status = 0;
if (strcmp(flag,''))
    time_elapsed = toc(time_start);
    seconds_left = ((tout/tt(end))-1)*time_elapsed;
    days_left = datenum([0 0 0 0 0 seconds_left]);
    time_left = datevec(days_left - floor(days_left));
    disp(['3wri_solver: time = ',num2str(tt(end)) ,...
        '(',num2str(tout),') computation time left = ' ,...
        int2str(floor(days_left)),'d ' ,...
        int2str(time_left(4)),'h ' ,...
        int2str(time_left(5)),'m ' ,...
        num2str(time_left(6)),'s'])
end
return

%
   %%%%%%%%%%%%%%%%%%%%%%%%%%%%%%%%%%%%%%%%%%%%%%%%%%%%%%%%%%%%%%%%%%%%%%%%
```

```
% twri_rhs, the right-hand side of the 3WRI system
% %%%%%%%%%%%%%%%%%%%%%%%%%%%%%%%%%%%%%%%%%%%%%%%%%%%%%%%%%%%%%%%%%%%%%%%%%%%%%

function dvdt = twri_rhs(tt,vv,Nx,k,c,s,omega)
%sizevv = size(vv)
v = reshape(vv,Nx,3);
v1 = v(:,1); v2 = v(:,2); v3 = v(:,3);
v1c = conj(v1); v2c = conj(v2); v3c = conj(v3);
v1x = ifft(1i*k.*fft(v1));
v2x = ifft(1i*k.*fft(v2));
%v3x = ifft(k.*fft(v3));

v1t = -c(1)*v1x+c(2)*s(1)*v2c.*v3c;
v2t = -c(2)*v2x+c(1)*s(2)*v1c.*v3c;
v3t = 1i*omega*v3+(c(1)-c(2))*s(3)*v1c.*v2c;

dvdt = [v1t; v2t; v3t];
return
```

Appendix P

Numerical Integration

```
% %%%%%%%%%%%%%%%%%%%%%%%%%%%%%%%%%%%%%%%%%%%%%%%%%%%%%%%%%%%%%%%%%%%%%%%%%%
% Flags for saving figures and generating data
% %%%%%%%%%%%%%%%%%%%%%%%%%%%%%%%%%%%%%%%%%%%%%%%%%%%%%%%%%%%%%%%%%%%%%%%%%%
% Dataflag. If 'dataflag=0' no data is generated. If 'dataflag=1', data is
% generated.
dataflag = 0;
% Saveflag. If 'saveflag=0' no figure is saved. If 'saveflag=1', all
% figures are saved.
saveflag = 1;
% Extractionflag. If 'extractionflag=0' no interpolated plot is extracted.
% If 'extractionflag=1', an interpolated plot is extracted at the time and
% space specified.
extractionflag = 1;
```

```
% %%%%%%%%%%%%%%%%%%%%%%%%%%%%%%%%%%%%%%%%%%%%%%%%%%%%%%%%%%%%%%%%%%%%%%%%%%%
% Parameters for the plane wave and perturbation
% %%%%%%%%%%%%%%%%%%%%%%%%%%%%%%%%%%%%%%%%%%%%%%%%%%%%%%%%%%%%%%%%%%%%%%%%%%%
% if c1 = -c2, then use the following syntax:
% epsilon = 1e-3; % epsilon approaches zero
% [c,s,a] = twri_from_p([p1 p2 p3/epsilon epsilon])
% for some values p1, p2, p3
p = [0.2 0.3 -0.6 1];
[c, s, a] = twri_from_p(p);
spectrumtopology = [2 0 0 1 0]; % G SG B L TL
experiment_number = ['01']; % update with the experiment number, namely,
% specfy if this is the first, second, third, ... experiment with the same
% topology of the spectrum.

% do not modify eta
eta = [1,1];

% %%%%%%%%%%%%%%%%%%%%%%%%%%%%%%%%%%%%%%%%%%%%%%%%%%%%%%%%%%%%%%%%%%%%%%%%%%%
% Computational grid
% %%%%%%%%%%%%%%%%%%%%%%%%%%%%%%%%%%%%%%%%%%%%%%%%%%%%%%%%%%%%%%%%%%%%%%%%%%%
L = 20;
```

```
numx = 2^(10);%5*(2^(7));%2^(9)
dx = 2*L/numx; x = [-L:dx:L-dx];
xspan = [x(1) x(end)];

T = 120;
numt = 600;
tspan = [0 T];
dt = (tspan(2)-tspan(1))/numt;
t = [tspan(1):dt:tspan(2)];

%[XX,TT] = meshgrid(x,t);

% values of the subgrid from the zoom-in
xmin =0; xmax = 20;
tmin =100; tmax = 120;
if tmax>T; tmax=T; end
if xmax>L-dx; xmax=L-dx; end
if xmin<-L; xmin=-L; end

% value of the time and spatial range for extracting an
    interpolated plot
t_extraction = 120;
x_extraction_min = 0; x_extraction_max =20;
num_x_extraction = 1e4; % interpolation points
if t_extraction>T; t_extraction=T; end
if x_extraction_max>L-dx; x_extraction_max=L-dx; end
if x_extraction_min<-L; x_extraction_min=-L; end

%
    %%%%%%%%%%%%%%%%%%%%%%%%%%%%%%%%%%%%%%%%%%%%%%%%%%%%%%%%%%%%%%%%%%%%%%

% Perturbation
```

```
%%%%%%%%%%%%%%%%%%%%%%%%%%%%%%%%%%%%%%%%%%%%%%%%%%%%%%%%%%%%%%%%%%%%%%%%%%%%%%

% amplitude of the perturbation in each component
epsilon1 = 1e-3;
epsilon2 = 1e-3;
epsilon3 = 1e-3;

% Pertubration mode. If pert_mode=0, then localised perturbation. If
% pert_mode=1, then random pertubration.
pert_mode = 1;

if pert_mode==0
    pert = @(x) cos(pi*x/(2*L)).*exp(-(2*(x).^2));
elseif pert_mode==1
    %pert = @(x) 2*rand(size(x))-1;
    numnod = numx/8; dnod = (2*L-dx)/numnod;
    pert = @(x) sincinterpr([0,0,0,0,0, 2*rand([1,numnod-9])-1, 0,0,0,0,0],[x(1):dnod:x(end)],x).';
end

%%%%%%%%%%%%%%%%%%%%%%%%%%%%%%%%%%%%%%%%%%%%%%%%%%%%%%%%%%%%%%%%%%%%%%%%%%%%%%
% Plane wave solution
%%%%%%%%%%%%%%%%%%%%%%%%%%%%%%%%%%%%%%%%%%%%%%%%%%%%%%%%%%%%%%%%%%%%%%%%%%%%%%
% p1 = (cq(1)*alphaq(1)*s(1)+cq(2)*alphaq(2)*s(2))/(s(1)*s(2)*s(3));
```

```
% p2 = (cq(1)*alphaq(1)*s(1)-cq(2)*alphaq(2)*s(2))/(s(1)*s(2)*s(3));
% p3 = (c(1)-c(2))/(c(1)+c(2));

aq = a.^2;
r = (c(1)-c(2))/(eta(1)+eta(2));
nu1 = (eta(1)/c(1))+s(1)*s(3)*aq(2)*(c(2)/c(1))*r;
nu2 = (eta(2)/c(2))+s(2)*s(3)*aq(1)*(c(1)/c(2))*r;
nu3 = -(nu1+nu2);
eta3 = -(eta(1)+eta(2));
%omega = c(1)*nu1+c(2)*nu2;

u1ex = @(x,t) a(1)*exp(1i*(eta(1)*t-nu1*x));
u2ex = @(x,t) a(2)*exp(1i*(eta(2)*t-nu2*x));
u3ex = @(x,t) 1i*s(3)*a(1)*a(2)*r*exp(1i*(eta3*t-nu3*x));

U10 = u1ex(x,0)+epsilon1*pert(x).*exp(1i*(-nu1*x));
U20 = u2ex(x,0)+epsilon2*pert(x).*exp(1i*(-nu2*x));
U30 = u3ex(x,0)+1i*epsilon3*pert(x).*exp(1i*(-nu3*x));

U0 = [U10(:) U20(:) U30(:)];

% %%%%%%%%%%%%%%%%%%%%%%%%%%%%%%%%%%%%%%%%%%%%%%%%%%%%%%%%%%%%%%%%%%%%%%%%%%%%%%%%
% Numerical integration
% %%%%%%%%%%%%%%%%%%%%%%%%%%%%%%%%%%%%%%%%%%%%%%%%%%%%%%%%%%%%%%%%%%%%%%%%%%%%%%%%

if dataflag == 1
    [xx,tt,u1,u2,u3] = twri_solver(c,s,a,eta,U0,L,numx,T,numt);
```

```
114 end
115
116 %disp(['p1 = ',num2str(p1)])
117 %disp(['p2 = ',num2str(p2)])
118 %disp(['p3 = ',num2str(p3)])
119
120 reu1min = floor(10*min(min(real(u1))))/10; reu1max = ceil(10*
        max(max(real(u1))))/10; reu1ticks = linspace(reu1min,
        reu1max,5);
121 imu1min = floor(10*min(min(imag(u1))))/10; imu1max = ceil(10*
        max(max(imag(u1))))/10; imu1ticks = linspace(imu1min,
        imu1max,5);
122 absu1min = floor(10*min(min(abs(u1))))/10; absu1max = ceil(10*
        max(max(abs(u1))))/10; absu1ticks = linspace(absu1min,
        absu1max,5);
123 reu2min = floor(10*min(min(real(u2))))/10; reu2max = ceil(10*
        max(max(real(u2))))/10; reu2ticks = linspace(reu2min,
        reu2max,5);
124 imu2min = floor(10*min(min(imag(u2))))/10; imu2max = ceil(10*
        max(max(imag(u2))))/10; imu2ticks = linspace(imu2min,
        imu2max,5);
125 absu2min = floor(10*min(min(abs(u2))))/10; absu2max = ceil(10*
        max(max(abs(u2))))/10; absu2ticks = linspace(absu2min,
        absu2max,5);
126 reu3min = floor(10*min(min(real(u3))))/10; reu3max = ceil(10*
        max(max(real(u3))))/10; reu3ticks = linspace(reu3min,
        reu3max,5);
127 imu3min = floor(10*min(min(imag(u3))))/10; imu3max = ceil(10*
        max(max(imag(u3))))/10; imu3ticks = linspace(imu3min,
        imu3max,5);
128 absu3min = floor(10*min(min(abs(u3))))/10; absu3max = ceil(10*
        max(max(abs(u3))))/10; absu3ticks = linspace(absu3min,
```

```
absu3max,5);

%
%%%%%%%%%%%%%%%%%%%%%%%%%%%%%%%%%%%%%%%%%%%%%%%%%%%%%%%%%%%%%%%%%%%%%%%%%%%%%%%%%%%%%%%%%%%%
% Exact solution
%
%%%%%%%%%%%%%%%%%%%%%%%%%%%%%%%%%%%%%%%%%%%%%%%%%%%%%%%%%%%%%%%%%%%%%%%%%%%%%%%%%%%%%%%%%%%%

[XX,TT] = meshgrid(xx,tt);
U1 = u1ex(XX,TT); U2 = u2ex(XX,TT); U3 = u3ex(XX,TT);

reU1min = floor(10*min(min(real(U1))))/10; reU1max = ceil(10*max(max(real(U1))))/10; reU1ticks = linspace(reU1min,reU1max,5);
imU1min = floor(10*min(min(imag(U1))))/10; imU1max = ceil(10*max(max(imag(U1))))/10; imU1ticks = linspace(imU1min,imU1max,5);
absU1min = floor(10*min(min(abs(U1))))/10; absU1max = ceil(10*max(max(abs(U1))))/10; absU1ticks = linspace(absU1min,absU1max,5);
reU2min = floor(10*min(min(real(U2))))/10; reU2max = ceil(10*max(max(real(U2))))/10; reU2ticks = linspace(reU2min,reU2max,5);
imU2min = floor(10*min(min(imag(U2))))/10; imU2max = ceil(10*max(max(imag(U2))))/10; imU2ticks = linspace(imU2min,imU2max,5);
absU2min = floor(10*min(min(abs(U2))))/10; absU2max = ceil(10*max(max(abs(U2))))/10; absU2ticks = linspace(absU2min,absU2max,5);
```

```
reU3min = floor(10*min(min(real(U3))))/10; reU3max = ceil(10*max(max(real(U3))))/10; reU3ticks = linspace(reU3min,reU3max,5);
imU3min = floor(10*min(min(imag(U3))))/10; imU3max = ceil(10*max(max(imag(U3))))/10; imU3ticks = linspace(imU3min,imU3max,5);
absU3min = floor(10*min(min(abs(U3))))/10; absU3max = ceil(10*max(max(abs(U3))))/10; absU3ticks = linspace(absU3min,absU3max,5);

% %%%%%%%%%%%%%%%%%%%%%%%%%%%%%%%%%%%%%%%%%%%%%%%%%%%%%%%%%%%%%%%%%%%%%%%%%%%%%%%%%%%%%%%%%%%%
% Parameters
% %%%%%%%%%%%%%%%%%%%%%%%%%%%%%%%%%%%%%%%%%%%%%%%%%%%%%%%%%%%%%%%%%%%%%%%%%%%%%%%%%%%%%%%%%%%%

disp([' '])
disp(['%%%%%%%%%%%%%%%%%%%%%%%%%%%%%%%%%%%%%%%%%%%%%%%%%%%%%%%%%%%%%%%%%%%%%%%%%%%%%%%%'])
disp(['parameters: p1=',num2str(p(1)),', p2=',num2str(p(2)),', p3=',num2str(p(3)),', p4=',num2str(p(4))]);
disp(['velocities: c1=',num2str(c(1)),', c2=',num2str(c(2))])
disp(['signs: s1=',int2str(s(1)),', s2=',int2str(s(2)),', s3=',int2str(s(3))])
disp(['amplitudes: a1=',num2str(a(1)),', a2=',num2str(a(2))])
disp([' '])

% %%%%%%%%%%%%%%%%%%%%%%%%%%%%%%%%%%%%%%%%%%%%%%%%%%%%%%%%%%%%%%%%%%%%%%%%%%%%%%%%%%%%%%%%%%%%
```

```
% Differences
% %%%%%%%%%%%%%%%%%%%%%%%%%%%%%%%%%%%%%%%%%%%%%%%%%%%%%%%%%%%%%%%%%%%%%%%%%%%%%%%%%%%%
disp(['%%%%%%%%%%%%%%%%%%%%%%%%%%%%%%%%%%%%%%%%%%%%%%%%%%%%%%%%%%%%%%%%%%%%%%%%%%%%%%%%%'])
if pert_mode==0
    disp(['localised pertubration: ',char(pert)])
elseif pert_mode==1
    disp(['random perturbation: ', char(pert)])
end
initrelerru1 = 100*max(max(abs(U1(1,:)-u1(1,:))))/max(max(abs(U1(1,:))));
initrelerru2 = 100*max(max(abs(U2(1,:)-u2(1,:))))/max(max(abs(U2(1,:))));
initrelerru3 = 100*max(max(abs(U3(1,:)-u3(1,:))))/max(max(abs(U3(1,:))));
maxrelerru1 = 100*max(max(abs(U1-u1)))/max(max(abs(U1)));
maxrelerru2 = 100*max(max(abs(U2-u2)))/max(max(abs(U2)));
maxrelerru3 = 100*max(max(abs(U3-u3)))/max(max(abs(U3)));
disp(['deviation from unperturbed solution']);
disp(['U1>> initial: ',num2str(initrelerru1),'% --- maximum: ',num2str(maxrelerru1),'%'])
disp(['U2>> initial: ',num2str(initrelerru2),'% --- maximum: ',num2str(maxrelerru2),'%'])
disp(['U3>> initial: ',num2str(initrelerru3),'% --- maximum: ',num2str(maxrelerru3),'%'])
disp([' '])

% %%%%%%%%%%%%%%%%%%%%%%%%%%%%%%%%%%%%%%%%%%%%%%%%%%%%%%%%%%%%%%%%%%%%%%%%%%%%%%%%%%%%
```

```
% Extracting a subplot (zoom-in) in the region [xmin xmax tmin tmax]
% %%%%%%%%%%%%%%%%%%%%%%%%%%%%%%%%%%%%%%%%%%%%%%%%%%%%%%%%%%%%%%%%%%%%%%%%%%%%%%%%%%%%%%%%%%%%%%%%%%%%%%%%%%%%%%%%%%%%%%%%%%%%%%%%%%%%%%%%%%%%%%%%%%%%%%%
[Nr, Nc] = size(XX);
YY = (XX>=xmin)&(XX<=xmax)&(TT>=tmin)&(TT<=tmax);
colind = ceil(find(YY)/Nr);
rowind = find(YY)-(colind-1)*Nr;
colind = unique(colind);
rowind = unique(rowind);
sX = XX(rowind,colind);
sT = TT(rowind,colind);
su1 = u1(rowind,colind);
su2 = u2(rowind,colind);
su3 = u3(rowind,colind);

% %%%%%%%%%%%%%%%%%%%%%%%%%%%%%%%%%%%%%%%%%%%%%%%%%%%%%%%%%%%%%%%%%%%%%%%%%%%%%%%%%%%%%%%%%%%%%%%%%%%%%%%%%%%%%%%%%%%%%%%%%%%%%%%%%%%%%%%%%%%%%%%%%%%%%%%
% Extracting a subplot at a given specific time in a given spatial range
% with interpolation of the result for high-definition plotting
% %%%%%%%%%%%%%%%%%%%%%%%%%%%%%%%%%%%%%%%%%%%%%%%%%%%%%%%%%%%%%%%%%%%%%%%%%%%%%%%%%%%%%%%%%%%%%%%%%%%%%%%%%%%%%%%%%%%%%%%%%%%%%%%%%%%%%%%%%%%%%%%%%%%%%%%

if extractionflag==1
    dxinterp = (x_extraction_max-x_extraction_min)/num_x_extraction;
```

```
    x_interp = x_extraction_min:dxinterp:x_extraction_max;
    [~,ind_extraction] = min(abs(t-t_extraction));
    t_extraction_eff = t(ind_extraction);

    x_extraction = xx;
    u1_extraction = u1(ind_extraction,:);
    u2_extraction = u2(ind_extraction,:);
    u3_extraction = u3(ind_extraction,:);
    %size_u1_extraction = size(u1_extraction)
    %size_x_extraction = size(x_extraction)
    x_extraction_range = (x_extraction>=x_extraction_min)&(x_extraction<=x_extraction_max);
    x_extraction = x_extraction(x_extraction_range);
    u1_extraction = u1_extraction(x_extraction_range);
    u2_extraction = u2_extraction(x_extraction_range);
    u3_extraction = u3_extraction(x_extraction_range);
    %size_u1_extraction = size(u1_extraction)
    %size_x_extraction = size(x_extraction)
    u1_interp = sincinterpr(u1_extraction,x_extraction,x_interp);
    u2_interp = sincinterpr(u2_extraction,x_extraction,x_interp);
    u3_interp = sincinterpr(u3_extraction,x_extraction,x_interp);
end

% %%%%%%%%%%%%%%%%%%%%%%%%%%%%%%%%%%%%%%%%%%%%%%%%%%%%%%%%%%%%%%%%%%%%%%%%%%
% General plotting parameters
% %%%%%%%%%%%%%%%%%%%%%%%%%%%%%%%%%%%%%%%%%%%%%%%%%%%%%%%%%%%%%%%%%%%%%%%%%%
```

```
%% load colormaps
% load('redblue')
% load('blueredyellow')
% load('blueredblue')
% load('redbluered')
% load('redbluered2')

% options for plotting
linwdth = 1.5; % Line Width
fnsztl = 16; % Font Size for Plot Titles
fnwgtl = 'bold'; % Font Weight for Plot Titles
fnszlb = 14; % Font Size for Plot Axis Labels
fnwglb = 'bold'; % Font Weight for Plot Axis Labels
fnsztk = 14; % Font Size for Plot Ticks
fnwgtk = 'normal'; % Font Weight for Plot Ticks
fnszcb = 14; % Font Size color bar
fnwgcb = 'normal'; % Font Weight color bar
fnnmcb = 'Serif'; % Font Name color bar

%
    %%%%%%%%%%%%%%%%%%%%%%%%%%%%%%%%%%%%%%%%%%%%%%%%%%%%%%%%%%%%%%%%%%%%%%%%%%%%%%%%
% Plotting the output
%
    %%%%%%%%%%%%%%%%%%%%%%%%%%%%%%%%%%%%%%%%%%%%%%%%%%%%%%%%%%%%%%%%%%%%%%%%%%%%%%%%

hf1 = figure(1);
clf
% colormap(jet) % use this map as an alternative colormap
```

```
253 fig1a = subplot(2,3,1);
254     pcolor(xx,tt,abs(u1))
255     xlabel('\boldmath${x}$','interpreter','Latex','fontsize',
            fnszlb,'fontweight',fnwglb)
256     ylabel('\boldmath${t}$','interpreter','Latex','fontsize',
            fnszlb,'fontweight',fnwglb)
257     title('\boldmath$${|u_{1}|}$ (numerical)','interpreter','
            Latex','fontsize',fnsztl,'fontweight',fnwgtl)
258     colormap(fig1a,jet)
259     shading flat
260     axis([-L L tspan(1) tspan(2)])
261     ax = gca;
262     ax.FontSize = fnsztk;
263     ax.FontWeight = fnwgtk;
264     ax.TickLabelInterpreter = 'latex';
265     caxis([absu1min absu1max]);
266     hBarhf1a = colorbar('location','southoutside','xtick',
            absu1ticks);
267     labelshf1a = {absu1min:(absu1max-absu1min)/4:absu1max};
268     set(hBarhf1a,'XTickLabel',labelshf1a,'fontsize',fnszcb,'
            fontweight',fnwgcb,'fontname',fnnmcb);
269 hf1b = subplot(2,3,2);
270     pcolor(xx,tt,abs(u2))
271     xlabel('\boldmath${x}$','interpreter','Latex','fontsize',
            fnszlb,'fontweight',fnwglb)
272     ylabel('\boldmath${t}$','interpreter','Latex','fontsize',
            fnszlb,'fontweight',fnwglb)
273     title('\boldmath$${|u_{2}|}$ (numerical)','interpreter','
            Latex','fontsize',fnsztl,'fontweight',fnwgtl)
274     colormap(hf1b,jet)
275     shading flat
276     axis([-L L tspan(1) tspan(2)])
```

```
277     ax = gca;
278     ax.FontSize = fnsztk;
279     ax.FontWeight = fnwgtk;
280     ax.TickLabelInterpreter = 'latex';
281     caxis([absu2min absu2max]);
282     hBarhf1b = colorbar('location','southoutside','xtick',
            absu2ticks);
283     labelshf1b = {absu2min:(absu2max-absu2min)/4:absu2max};
284     set(hBarhf1b,'XTickLabel',labelshf1b,'fontsize',fnszcb,'
            fontweight',fnwgcb,'fontname',fnnmcb);
285 fig1c = subplot(2,3,3);
286     pcolor(xx,tt,abs(u3))
287     xlabel('\boldmath${x}$','interpreter','Latex','fontsize',
            fnszlb,'fontweight',fnwglb)
288     ylabel('\boldmath${t}$','interpreter','Latex','fontsize',
            fnszlb,'fontweight',fnwglb)
289     title('\boldmath${|u_{3}|}$ (numerical)','interpreter','
            Latex','fontsize',fnsztl,'fontweight',fnwgtl)
290     colormap(fig1c,jet)
291     shading flat
292     axis([-L L tspan(1) tspan(2)])
293     ax = gca;
294     ax.FontSize = fnsztk;
295     ax.FontWeight = fnwgtk;
296     ax.TickLabelInterpreter = 'latex';
297     caxis([absu3min absu3max]);
298     hBarhf1c = colorbar('location','southoutside','xtick',
            absu3ticks);
299     labelshf1c = {absu3min:(absu3max-absu3min)/4:absu3max};
300     set(hBarhf1c,'XTickLabel',labelshf1c,'fontsize',fnszcb,'
            fontweight',fnwgcb,'fontname',fnnmcb);
301 fig1d = subplot(2,3,4);
```

```
302     pcolor(sX,sT,abs(su1))
303     xlabel('\boldmath${x}$','interpreter','Latex','fontsize',
            fnszlb,'fontweight',fnwglb)
304     ylabel('\boldmath${t}$','interpreter','Latex','fontsize',
            fnszlb,'fontweight',fnwglb)
305     title('\boldmath${|u_{1}|}$ (numerical)','interpreter','
            Latex','fontsize',fnsztl,'fontweight',fnwgtl)
306     colormap(fig1d,jet)
307     shading flat
308     axis([xmin xmax tmin tmax])
309     ax = gca;
310     ax.FontSize = fnsztk;
311     ax.FontWeight = fnwgtk;
312     ax.TickLabelInterpreter = 'latex';
313     caxis([absu1min absu1max]);
314     hBarhf1d = colorbar('location','southoutside','xtick',
            absu1ticks);
315     labelshf1d = {absu1min:(absu1max-absu1min)/4:absu1max};
316     set(hBarhf1d,'XTickLabel',labelshf1d,'fontsize',fnszcb,'
            fontweight',fnwgcb,'fontname',fnnmcb);
317 fig1e = subplot(2,3,5);
318     pcolor(sX,sT,abs(su2))
319     xlabel('\boldmath${x}$','interpreter','Latex','fontsize',
            fnszlb,'fontweight',fnwglb)
320     ylabel('\boldmath${t}$','interpreter','Latex','fontsize',
            fnszlb,'fontweight',fnwglb)
321     title('\boldmath${|u_{2}|}$ (numerical)','interpreter','
            Latex','fontsize',fnsztl,'fontweight',fnwgtl)
322     colormap(fig1e,jet)
323     shading flat
324     axis([xmin xmax tmin tmax])
325     ax = gca;
```

```
326     ax.FontSize = fnsztk;
327     ax.FontWeight = fnwgtk;
328     ax.TickLabelInterpreter = 'latex';
329     caxis([absu2min absu2max]);
330     hBarhf1e = colorbar('location','southoutside','xtick',
            absu2ticks);
331     labelshf1e = {absu2min:(absu2max-absu2min)/4:absu2max};
332     set(hBarhf1e,'XTickLabel',labelshf1e,'fontsize',fnszcb,'
            fontweight',fnwgcb,'fontname',fnnmcb);
333 fig1f = subplot(2,3,6);
334     pcolor(sX,sT,abs(su3))
335     xlabel('\boldmath${x}$','interpreter','Latex','fontsize',
            fnszlb,'fontweight',fnwglb)
336     ylabel('\boldmath${t}$','interpreter','Latex','fontsize',
            fnszlb,'fontweight',fnwglb)
337     title('\boldmath$${|u_{3}|}$ (numerical)','interpreter','
            Latex','fontsize',fnsztl,'fontweight',fnwgtl)
338     colormap(fig1f,jet)
339     shading flat
340     axis([xmin xmax tmin tmax])
341     ax = gca;
342     ax.FontSize = fnsztk;
343     ax.FontWeight = fnwgtk;
344     ax.TickLabelInterpreter = 'latex';
345     caxis([absu3min absu3max]);
346     hBarhf1f = colorbar('location','southoutside','xtick',
            absu3ticks);
347     labelshf1f = {absu3min:(absu3max-absu3min)/4:absu3max};
348     set(hBarhf1f,'XTickLabel',labelshf1f,'fontsize',fnszcb,'
            fontweight',fnwgcb,'fontname',fnnmcb);
349 fig = gcf;
350 fig.PaperPositionMode = 'auto';
```

```
fig_pos = fig.PaperPosition;
fig.PaperSize = [fig_pos(3) fig_pos(4)];

%
    %%%%%%%%%%%%%%%%%%%%%%%%%%%%%%%%%%%%%%%%%%%%%%%%%%%%%%%%%%%%%%%%%%%%%%%%%%%%%%

hf2 = figure(2);
clf
jtn = 5;
for jt = 1:jtn
    ind = floor(numt*jt/(jtn-1)+1-numt/(jtn-1));
    subplot(jtn,3,3*(jt-1)+1)
        plot(xx,abs(U1(ind,:)),'b')
        hold on
        plot(xx,abs(u1(ind,:)),'r')
        hold off
        xlabel('\boldmath${x}$','interpreter','Latex','
            fontsize',fnszlb,'fontweight',fnwglb)
        ylabel('\boldmath${|u_{1}|}$','interpreter','Latex','
            fontsize',fnszlb,'fontweight',fnwglb)
        title(['t=',num2str(tt(ind)),', (ex/b, num/r)'],'
            interpreter','Latex','fontsize',fnsztl,'fontweight'
            ,fnwgtl)
       %axis([-L L absu1min absu1max])
        axis tight
    subplot(jtn,3,3*(jt-1)+2)
        plot(xx,abs(U2(ind,:)),'b')
        hold on
        plot(xx,abs(u2(ind,:)),'r')
        hold off
```

```
        xlabel('\boldmath${x}$','interpreter','Latex','fontsize',fnszlb,'fontweight',fnwglb)
        ylabel('\boldmath${|u_{2}|}$','interpreter','Latex','fontsize',fnszlb,'fontweight',fnwglb)
        title(['t=',num2str(tt(ind)),', (ex/b, num/r)'],'interpreter','Latex','fontsize',fnsztl,'fontweight',fnwgtl)
        %axis([-L L absu2min absu2max])
        axis tight
    subplot(jtn,3,3*(jt-1)+3)
        plot(xx,abs(U3(ind,:)),'b')
        hold on
        plot(xx,abs(u3(ind,:)),'r')
        hold off
        xlabel('\boldmath${x}$','interpreter','Latex','fontsize',fnszlb,'fontweight',fnwglb)
        ylabel('\boldmath${|u_{3}|}$','interpreter','Latex','fontsize',fnszlb,'fontweight',fnwglb)
        title(['t=',num2str(tt(ind)),', (ex/b, num/r)'],'interpreter','Latex','fontsize',fnsztl,'fontweight',fnwgtl)
        %axis([-L L absu3min absu3max])
        axis tight
end
fig = gcf;
fig.PaperPositionMode = 'auto';
fig_pos = fig.PaperPosition;
fig.PaperSize = [fig_pos(3) fig_pos(4)];

%%%%%%%%%%%%%%%%%%%%%%%%%%%%%%%%%%%%%%%%%%%%%%%%%%%%%%%%%%%%%%%%%%%%%%%%%%
```

```
398
399 if extractionflag==1
400     hf3 = figure(3);
401     clf
402     subplot(3,1,1)
403         hold on
404         plot(x_extraction,abs(u1_extraction),'r.')
405          plot(x_interp,abs(u1_interp),'b')
406         hold off
407         xlabel('\boldmath${x}$','interpreter','Latex','
                fontsize',fnszlb,'fontweight',fnwglb)
408         ylabel('\boldmath${|u_{1}|}$','interpreter','Latex','
                fontsize',fnszlb,'fontweight',fnwglb)
409         title(['t=',num2str(t_extraction_eff),', (num/r,
                interp/b)'],'interpreter','Latex','fontsize',fnsztl
                ,'fontweight',fnwgtl)
410         axis tight
411     subplot(3,1,2)
412         hold on
413         plot(x_extraction,abs(u2_extraction),'r.')
414         plot(x_interp,abs(u2_interp),'b')
415         hold off
416         xlabel('\boldmath${x}$','interpreter','Latex','
                fontsize',fnszlb,'fontweight',fnwglb)
417         ylabel('\boldmath${|u_{2}|}$','interpreter','Latex','
                fontsize',fnszlb,'fontweight',fnwglb)
418         title(['t=',num2str(t_extraction_eff),', (num/r,
                interp/b)'],'interpreter','Latex','fontsize',fnsztl
                ,'fontweight',fnwgtl)
419         axis tight
420     subplot(3,1,3)
421         hold on
```

```
        plot(x_extraction,abs(u3_extraction),'r.')
        plot(x_interp,abs(u3_interp),'b')
        hold off
        xlabel('\boldmath${x}$','interpreter','Latex','fontsize',fnszlb,'fontweight',fnwglb)
        ylabel('\boldmath${|u_{3}|}$','interpreter','Latex','fontsize',fnszlb,'fontweight',fnwglb)
        title(['t=',num2str(t_extraction_eff),', (num/r,interp/b)'],'interpreter','Latex','fontsize',fnsztl,'fontweight',fnwgtl)
        axis tight
    fig = gcf;
    fig.PaperPositionMode = 'auto';
    fig_pos = fig.PaperPosition;
    fig.PaperSize = [fig_pos(3) fig_pos(4)];
end

%%%%%%%%%%%%%%%%%%%%%%%%%%%%%%%%%%%%%%%%%%%%%%%%%%%%%%%%%%%%%%%%%%%%%%%%%%%%%%%%%%%%%%
% Saving the figures
%%%%%%%%%%%%%%%%%%%%%%%%%%%%%%%%%%%%%%%%%%%%%%%%%%%%%%%%%%%%%%%%%%%%%%%%%%%%%%%%%%%%%%

if saveflag==1

    if pert_mode==0
        pert_tag = ['localised'];
    elseif pert_mode==1
        pert_tag = ['random'];
    end
```

```
446     file_name = ['twri_planewave_',...
447         int2str(spectrumtopology(1)),'G_',...
448         int2str(spectrumtopology(2)),'SG_',...
449         int2str(spectrumtopology(3)),'B_',...
450         int2str(spectrumtopology(4)),'L_',...
451         int2str(spectrumtopology(5)),'TL_',...
452         pert_tag,'_','exp_',experiment_number];
453
454     fig1a = figure(4);
455     clf
456     pcolor(xx,tt,abs(u1))
457     xlabel('\boldmath${x}$','interpreter','Latex','fontsize',
            fnszlb,'fontweight',fnwglb)
458     ylabel('\boldmath${t}$','interpreter','Latex','fontsize',
            fnszlb,'fontweight',fnwglb)
459     %title('\boldmath${|u_{1}|}$ (numerical)','interpreter','
            Latex','fontsize',fnsztl,'fontweight',fnwgtl)
460     colormap(fig1a,jet)
461     shading flat
462     axis([-L L tspan(1) tspan(2)])
463     ax = gca;
464     ax.FontSize = fnsztk;
465     ax.FontWeight = fnwgtk;
466     ax.TickLabelInterpreter = 'latex';
467     caxis([absu1min absu1max]);
468     hBarhf1a = colorbar('location','southoutside','xtick',
            absu1ticks);
469     labelshf1a = {absu1min:(absu1max-absu1min)/4:absu1max};
470     set(hBarhf1a,'XTickLabel',labelshf1a,'fontsize',fnszcb,'
            fontweight',fnwgcb,'fontname',fnnmcb);
471     fig = gcf;
472     fig.PaperPositionMode = 'auto';
```

```
473     fig_pos = fig.PaperPosition;
474     fig.PaperSize = [fig_pos(3) fig_pos(4)];
475
476     fig1b = figure(5);
477     clf
478     pcolor(xx,tt,abs(u2))
479     xlabel('\boldmath${x}$','interpreter','Latex','fontsize',
            fnszlb,'fontweight',fnwglb)
480     ylabel('\boldmath${t}$','interpreter','Latex','fontsize',
            fnszlb,'fontweight',fnwglb)
481     %title('\boldmath$${|u_{2}|}$ (numerical)','interpreter','
            Latex','fontsize',fnsztl,'fontweight',fnwgtl)
482     colormap(fig1b,jet)
483     shading flat
484     axis([-L L tspan(1) tspan(2)])
485     ax = gca;
486     ax.FontSize = fnsztk;
487     ax.FontWeight = fnwgtk;
488     ax.TickLabelInterpreter = 'latex';
489     caxis([absu2min absu2max]);
490     hBarhf1b = colorbar('location','southoutside','xtick',
            absu2ticks);
491     labelshf1b = {absu2min:(absu2max-absu2min)/4:absu2max};
492     set(hBarhf1b,'XTickLabel',labelshf1b,'fontsize',fnszcb,'
            fontweight',fnwgcb,'fontname',fnnmcb);
493     fig = gcf;
494     fig.PaperPositionMode = 'auto';
495     fig_pos = fig.PaperPosition;
496     fig.PaperSize = [fig_pos(3) fig_pos(4)];
497
498     fig1c = figure(6);
499     clf
```

```
500     pcolor(xx,tt,abs(u3))
501     xlabel('\boldmath${x}$','interpreter','Latex','fontsize',
            fnszlb,'fontweight',fnwglb)
502     ylabel('\boldmath${t}$','interpreter','Latex','fontsize',
            fnszlb,'fontweight',fnwglb)
503     %title('\boldmath${|u_{3}|}$ (numerical)','interpreter','
            Latex','fontsize',fnsztl,'fontweight',fnwgtl)
504     colormap(fig1c,jet)
505     shading flat
506     axis([-L L tspan(1) tspan(2)])
507     ax = gca;
508     ax.FontSize = fnsztk;
509     ax.FontWeight = fnwgtk;
510     ax.TickLabelInterpreter = 'latex';
511     caxis([absu3min absu3max]);
512     hBarhf1c = colorbar('location','southoutside','xtick',
            absu3ticks);
513     labelshf1c = {absu3min:(absu3max-absu3min)/4:absu3max};
514     set(hBarhf1c,'XTickLabel',labelshf1c,'fontsize',fnszcb,'
            fontweight',fnwgcb,'fontname',fnnmcb);
515     fig = gcf;
516     fig.PaperPositionMode = 'auto';
517     fig_pos = fig.PaperPosition;
518     fig.PaperSize = [fig_pos(3) fig_pos(4)];
519
520     fig1d = figure(7);
521     clf
522     pcolor(sX,sT,abs(su1))
523     xlabel('\boldmath${x}$','interpreter','Latex','fontsize',
            fnszlb,'fontweight',fnwglb)
524     ylabel('\boldmath${t}$','interpreter','Latex','fontsize',
            fnszlb,'fontweight',fnwglb)
```

```
525     %title('\boldmath${|u_{1}|}$ (numerical)','interpreter','
            Latex','fontsize',fnsztl,'fontweight',fnwgtl)
526     colormap(fig1d,jet)
527     shading flat
528     axis([xmin xmax tmin tmax])
529     ax = gca;
530     ax.FontSize = fnsztk;
531     ax.FontWeight = fnwgtk;
532     ax.TickLabelInterpreter = 'latex';
533     caxis([absu1min absu1max]);
534     hBarhf1d = colorbar('location','southoutside','xtick',
            absu1ticks);
535     labelshf1d = {absu1min:(absu1max-absu1min)/4:absu1max};
536     set(hBarhf1d,'XTickLabel',labelshf1d,'fontsize',fnszcb,'
            fontweight',fnwgcb,'fontname',fnnmcb);
537     fig = gcf;
538     fig.PaperPositionMode = 'auto';
539     fig_pos = fig.PaperPosition;
540     fig.PaperSize = [fig_pos(3) fig_pos(4)];
541
542     fig1e = figure(8);
543     clf
544     pcolor(sX,sT,abs(su2))
545     xlabel('\boldmath${x}$','interpreter','Latex','fontsize',
            fnszlb,'fontweight',fnwglb)
546     ylabel('\boldmath${t}$','interpreter','Latex','fontsize',
            fnszlb,'fontweight',fnwglb)
547     %title('\boldmath${|u_{2}|}$ (numerical)','interpreter','
            Latex','fontsize',fnsztl,'fontweight',fnwgtl)
548     colormap(fig1e,jet)
549     shading flat
550     axis([xmin xmax tmin tmax])
```

```
551     ax = gca;
552     ax.FontSize = fnsztk;
553     ax.FontWeight = fnwgtk;
554     ax.TickLabelInterpreter = 'latex';
555     caxis([absu2min absu2max]);
556     hBarhf1e = colorbar('location','southoutside','xtick',
            absu2ticks);
557     labelshf1e = {absu2min:(absu2max-absu2min)/4:absu2max};
558     set(hBarhf1e,'XTickLabel',labelshf1e,'fontsize',fnszcb,'
            fontweight',fnwgcb,'fontname',fnnmcb);
559     fig = gcf;
560     fig.PaperPositionMode = 'auto';
561     fig_pos = fig.PaperPosition;
562     fig.PaperSize = [fig_pos(3) fig_pos(4)];
563
564     fig1f = figure(9);
565     clf
566     pcolor(sX,sT,abs(su3))
567     xlabel('\boldmath${x}$','interpreter','Latex','fontsize',
            fnszlb,'fontweight',fnwglb)
568     ylabel('\boldmath${t}$','interpreter','Latex','fontsize',
            fnszlb,'fontweight',fnwglb)
569     %title('\boldmath$${|u_{3}|}$ (numerical)','interpreter','
            Latex','fontsize',fnsztl,'fontweight',fnwgtl)
570     colormap(fig1f,jet)
571     shading flat
572     axis([xmin xmax tmin tmax])
573     ax = gca;
574     ax.FontSize = fnsztk;
575     ax.FontWeight = fnwgtk;
576     ax.TickLabelInterpreter = 'latex';
577     caxis([absu3min absu3max]);
```

```
578     hBarhf1f = colorbar('location','southoutside','xtick',
            absu3ticks);
579     labelshf1f = {absu3min:(absu3max-absu3min)/4:absu3max};
580     set(hBarhf1f,'XTickLabel',labelshf1f,'fontsize',fnszcb,'
            fontweight',fnwgcb,'fontname',fnnmcb);
581     fig = gcf;
582     fig.PaperPositionMode = 'auto';
583     fig_pos = fig.PaperPosition;
584     fig.PaperSize = [fig_pos(3) fig_pos(4)];
585
586     fig3a = figure(10);
587     clf
588     hold on
589     plot(x_extraction,abs(u1_extraction),'r.')
590      plot(x_interp,abs(u1_interp),'b')
591     hold off
592     xlabel('\boldmath${x}$','interpreter','Latex','fontsize',
            fnszlb,'fontweight',fnwglb)
593     ylabel('\boldmath${|u_{1}|}$','interpreter','Latex','
            fontsize',fnszlb,'fontweight',fnwglb)
594    %title(['t=',num2str(t_extraction_eff),', (num/r, interp/b
            )'],'interpreter','Latex','fontsize',fnsztl,'fontweight
            ',fnwgtl)
595     axis tight
596     fig = gcf;
597     fig.PaperPositionMode = 'auto';
598     fig_pos = fig.PaperPosition;
599     fig.PaperSize = [fig_pos(3) fig_pos(4)];
600
601     fig3b = figure(11);
602     clf
603     hold on
```

```
604     plot(x_extraction,abs(u2_extraction),'r.')
605     plot(x_interp,abs(u2_interp),'b')
606     hold off
607     xlabel('\boldmath${x}$','interpreter','Latex','fontsize',
            fnszlb,'fontweight',fnwglb)
608     ylabel('\boldmath${|u_{2}|}$','interpreter','Latex','
            fontsize',fnszlb,'fontweight',fnwglb)
609     %title(['t=',num2str(t_extraction_eff),', (num/r, interp/b
            )'],'interpreter','Latex','fontsize',fnsztl,'fontweight
            ',fnwgtl)
610     axis tight
611     fig = gcf;
612     fig.PaperPositionMode = 'auto';
613     fig_pos = fig.PaperPosition;
614     fig.PaperSize = [fig_pos(3) fig_pos(4)];
615
616     fig3c = figure(12);
617     clf
618     hold on
619     plot(x_extraction,abs(u3_extraction),'r.')
620     plot(x_interp,abs(u3_interp),'b')
621     hold off
622     xlabel('\boldmath${x}$','interpreter','Latex','fontsize',
            fnszlb,'fontweight',fnwglb)
623     ylabel('\boldmath${|u_{3}|}$','interpreter','Latex','
            fontsize',fnszlb,'fontweight',fnwglb)
624     %title(['t=',num2str(t_extraction_eff),', (num/r, interp/b
            )'],'interpreter','Latex','fontsize',fnsztl,'fontweight
            ',fnwgtl)
625     axis tight
626     fig = gcf;
627     fig.PaperPositionMode = 'auto';
```

```
628     fig_pos = fig.PaperPosition;
629     fig.PaperSize = [fig_pos(3) fig_pos(4)];
630
631
632     print(fig1a,[pwd '/Figures/' file_name '_u1.jpeg'],'-djpeg
            ')
633     print(fig1b,[pwd '/Figures/' file_name '_u2.jpeg'],'-djpeg
            ')
634     print(fig1c,[pwd '/Figures/' file_name '_u3.jpeg'],'-djpeg
            ')
635     print(fig1d,[pwd '/Figures/' file_name '_u1_zoom.jpeg'],'-
            djpeg')
636     print(fig1e,[pwd '/Figures/' file_name '_u2_zoom.jpeg'],'-
            djpeg')
637     print(fig1f,[pwd '/Figures/' file_name '_u3_zoom.jpeg'],'-
            djpeg')
638     print(fig3a,[pwd '/Figures/' file_name '_u1_(t_',num2str(
            t_extraction),').jpeg'],'-djpeg')
639     print(fig3b,[pwd '/Figures/' file_name '_u2_(t_',num2str(
            t_extraction),').jpeg'],'-djpeg')
640     print(fig3c,[pwd '/Figures/' file_name '_u3_(t_',num2str(
            t_extraction),').jpeg'],'-djpeg')
641
642     print(fig1a,[pwd '/Figures/' file_name '_u1.eps'],'-depsc'
            ,'-tiff','-r600')
643     print(fig1b,[pwd '/Figures/' file_name '_u2.eps'],'-depsc'
            ,'-tiff','-r600')
644     print(fig1c,[pwd '/Figures/' file_name '_u3.eps'],'-depsc'
            ,'-tiff','-r600')
645     print(fig1d,[pwd '/Figures/' file_name '_u1_zoom.eps'],'-
            depsc','-tiff','-r600')
```

```
646     print(fig1e,[pwd '/Figures/' file_name '_u2_zoom.eps'],'-
            depsc','-tiff','-r600')
647     print(fig1f,[pwd '/Figures/' file_name '_u3_zoom.eps'],'-
            depsc','-tiff','-r600')
648     print(fig3a,[pwd '/Figures/' file_name '_u1_(t_',num2str(
            t_extraction),').eps'],'-depsc','-tiff','-r600')
649     print(fig3b,[pwd '/Figures/' file_name '_u2_(t_',num2str(
            t_extraction),').eps'],'-depsc','-tiff','-r600')
650     print(fig3c,[pwd '/Figures/' file_name '_u3_(t_',num2str(
            t_extraction),').eps'],'-depsc','-tiff','-r600')
651
652     print(fig1a,[pwd '/Figures/' file_name '_u1.pdf'],'-dpdf',
            '-r600') %-painters
653     print(fig1b,[pwd '/Figures/' file_name '_u2.pdf'],'-dpdf',
            '-r600')
654     print(fig1c,[pwd '/Figures/' file_name '_u3.pdf'],'-dpdf',
            '-r600')
655     print(fig1d,[pwd '/Figures/' file_name '_u1_zoom.pdf'],'-
            dpdf','-r600')
656     print(fig1e,[pwd '/Figures/' file_name '_u2_zoom.pdf'],'-
            dpdf','-r600')
657     print(fig1f,[pwd '/Figures/' file_name '_u3_zoom.pdf'],'-
            dpdf','-r600')
658     print(fig3a,[pwd '/Figures/' file_name '_u1_(t_',num2str(
            t_extraction),').pdf'],'-dpdf','-r600')
659     print(fig3b,[pwd '/Figures/' file_name '_u2_(t_',num2str(
            t_extraction),').pdf'],'-dpdf','-r600')
660     print(fig3c,[pwd '/Figures/' file_name '_u3_(t_',num2str(
            t_extraction),').pdf'],'-dpdf','-r600')
661
662 end
```

Bibliography

[1] Lord Kelvin (W. Thompson), "Hydrokinetic solutions and observations", The London, Edinburgh, and Dublin Philosophical Magazine and Journal of Science, Issue 281, Volume 42, pp 362-377, 1871.

[2] H. von Helmholtz, "Über discontinuierliche Flüssigkeits-Bewegungen (On the discontinuous movements of fluids)", Monatsberichte der Königlichen Preussische Akademie der Wissenschaften zu Berlin, Volume 23, pp 215-228, 1868.

[3] P. G. Drazin, "Introduction to Hydrodynamic Stability", Cambridge texts in Applied Mathematics, 2002.

[4] R. D. Richtmyer, "Taylor instability in a shock acceleration of compressible fluids", Communications on Pure and Applied Mathematics, Volume 13, pp 297-319, May 1960.

[5] E. E. Meshkov, "Instability of the interface of two Gases Accelerated by Shock Waves", Soviet Fluid Dynamics, Volume 4, pp 101-104, 1969.

[6] M. Brouillette, "The Richtmyer-Meshkov Instability", Annu. Rev. Fluid Mech., Volume 34, pp 445-468, 2002.

[7] D. R. Williams, T. Török, P. Démouilin, L. van Driel-Gesztelyi, B. Kliem, "Eruption of a kink-unstable in NOAA active region 10696", The Astrophysical Journal, Volume 628, pp L162-L166, 1 August 2005.

[8] A. K. Srivastava, R. Erdélyi, D. Tripathi, V. Fedun, N. C. Joshi, P. Kayshap, "Observational Evidence of Sausage-Pinch Instability in Solar Corona by SDO/AIA", The Astrophysical Journal Letters, Issue2, Volume 765, pp L42-L49, 10 March 2013.

[9] V. E. Zakharov, "Modulation Instability: The beginning", Physica D Nonlinear Phenomena, Issue 5, Volume 238, pp 540-548, March 2009.

[10] L. I.Zagryadskaya, L. A. Ostrovskii, "Observed self-influence of modulated waves in a nonlinear line", Radiophysics and Quantum Electronics, Issue 6, Volume 11, pp 548-550, June 1928.

[11] K. Tai, A. Hasegawa, A. Tomita, "Observation of modulation instability in optical fibres", Phys. Rev. Lett., Issue 2, Volume 56, p 135, 13 January 1986.

[12] A. Hasegawa, "Stimulated Modulational Instabilities of Plasma Waves", Phys. Rev. A, Volume 1, p 1746, 1 June 1970.

[13] T. B. Benjamin, J. E. Feir, "The disintegration of wave trains on deep water", Part 1. Theory, J. Fliud Mech. Volume27, pp 417-430, 1967.

[14] T. B.Benjamin, "Instability of periodic wave trains in nonlinear dispersive system", Proc. Roy. Soc. A., Issue 1456, Volume 299, pp 59-75, 13 June 1967.

[15] T. Dauxois, M. Peyrard, "Physics of Solitons", Cambridge University Press, 2006.

[16] A. Degasperis, S. Lombardo, "Integrability in Action: Solitons, Instability and Rogue Waves", Rogue and Shock Waves in Nonlinear Dispersive Media, Lecture Notes in Physics book series, Volume 926, pp 23-53, 20 September 2016.

[17] G. B. Whitham, "Linear and Nonlinear Waves", John Wiley & Sons Inc., 1999.

[18] A. C. Scott, F. Y. F. Chu, David W. McLaughlin, "The Soliton: A New Concept in Applied Science", Proceeding of the IEEE, Issue 10, Volume 61, pp 1443-1483, October 1973.

[19] N. Karjanto, "Mathematical Aspects of Extreme Water Waves", PhD Thesis, 1 December 2006.

[20] D. F. Griffiths, "Classification of PDEs", Springer, 25 September 2015.

[21] M. J. Lighhtill, "Contribution to the theory of waves in non-linear dispersive systems", J. Inst. Math. Appl., Volume 1, pp 269-306, 1965.

[22] Sir G. Stokes, "On the Theory of Oscillatory Waves", Transactions of the Cambridge Philosophical Society, Vol. 8, p 441, 1 March 1847.

[23] P. Müller, C. Garrett, A. Osborne, "Rogue Waves", Oceanography, Issue 3, Volume 18, p 47, September 2005.

[24] B. Kibler, A. Chabchoub, A. Gelash, N. Akhmediev, V. E. Zakharov, "Superregular Breathers in Optics and Hydrodynamics: Omnipresent Modulation Instability beyond Simple Periodicity", Physical Review X, Volume 5, p 041026, 13 November 2005.

[25] V. E. Zakharov, A. A. Gelash, "Nonlinear Stage of Modulation Instability", Physical Review Letters, 2 August 2013.

[26] M. Ablowitz, H. Segur, "Solitons and the Inverse Scattering Transform", SIAM, Philadelphia, 1981.

[27] N. Asano, Y. Kato, "Algebraic and Spectral Methods for Nonlinear Wave Equations", Longman Scientific & Technical, Pitman monographs and surveys in pure and applied mathematics, Volume 49, 1990.

[28] M. Ablowitz, P. Clarkson, "Solitons Nonlinear Evolution Equations and Inverse Scattering", Cambridge University Press, 1991.

[29] V. E. Zakharov, A. B. Shabat, "Exact theory of two-dimensional of self-focusing and one-dimensional self-modulation of waves in nonlinear media", Institute of Hydrodynamics, Siberian Division, U.S.S.R. Academy of Sciences, Zh. Esker. Teor. Fiz., Volume 61, pp 118-134, July 1971.

[30] M. J. Ablowitz, D. J. Kaup, A. C. Newell, H. Segur, "The inverse scattering transform - Fourier analysis for nonlinear problems", Stud. Appl. Math. Volume 15, pp 249-315, 1974.

[31] C. Gardner, G. Green, M. Kruskal, R. Miura, "Method for Solving the Korteweg-de Vries Equation", Phys. Rev. Lett., Volume 19, p. 1095, 6 November 1967.

[32] E. A. Kuznetson, A. V. Mikhailov, "Stability of stationary waves in nonlinear dispersive media", Institute of Automation and Electrometry, Siberian Division, USSR Academy of Sciences, Zh. Esker. Thor. Fiz., Volume 67, pp 1717-1727, November 1974.

[33] A. B. Shabat, "On the Korteweg-de Vries equation", Institute of Automation and Electrometry, Siberian Branch, Academy of Sciences of the USSR, Novosibirsk, Dokl. Akad. Nauk SSSR, Volume 211, p 1311, 1973.

[34] E. A. Kuznetsov, "Solitons in a parametrically unstable plasma", Institute of Automation and Electrometry, Siberian Branch, Academy of Sciences of the USSR, Novosibirsk, Dokl. Akad. Nauk SSSR, Volume 236, pp 575-577, September 1977.

[35] E. A. Kuznetsov, M. D. Spector, G. E. Fal'kovich, "On the stability of nonlinear waves in integrable models", Institute of Automation and Electrometry, Sib. Br. USSR Ac. Sci., Novosibirsk 90, p 630090, USSR, 16 October 1982.

[36] G. Biondini, G. Kovacic, "Inverse scattering transform for the focusing nonlinear Schrödinger equation with nonzero boundary conditions", J. Math. Phys., Volume 55, p 031506, 2014.

[37] G. Biondini, E. Fagerstrom, "The integrable nature of modulational instability", SIAM J. Appl. Math., Issue 1, Volume 75, pp 136-163, 2015.

[38] G. Biondini, S. Li, D. Mantzavinos, S. Trillo, "Universal Behaviour of Modulationally Unstable Media", SIAM Review, Issue 4, Volume 60, pp. 888-908, 12 October 2017.

[39] D. S. Agafontsev, V. E. Zakharov, "Integrable turbulence and formation of rogue waves", Nonlinearity, Volume 28, pp. 2791-2821, 2015.

[40] E. R. Tracy, H. H. Chen, "Non-linear self-modulation: An exactly solvable model", Phys. Rev. A37, pp 815-839, 1988.

[41] P. G. Grinevich, P. M. Santini, "The finite-gap method and the periodic NLS Cauchy problem of anomalous waves for a finite number of unstable modes", Russian Mathematical Surveys, Issue 2, Volume 74, 2019.

[42] P. G. Grinevich, P. M. Santini, "The finite gap method and the analytic description of the exact rogue wave recurrence in the periodic NLS Cauchy problem. 1", Nonlinearity, Issue11, Volume 31, 18 October 2018.

[43] P. G. Grinevich, P. M. Santini, "The exact rogue wave recurrence in the NLS periodic setting via matched asymptotic expansions, for 1 and 2 unstable modes", Physics Letters A, Issue 14, Volume 382, pp 973-979, 12 April 2018.

[44] M. J. Ablowitz, D. J. Kaup, A. C. Newell, H. Segur, "The inverse scattering transform-Fourier analysis for nonlinear problems", Stud. Appl. Math., Volume 53, pp 249-315, 1974.

[45] M. G. Forest, J. E. Lee, "Geometry and modulation theory for the periodic nonlinear Schrödinger equation. Oscillation theory, computation, and methods of compensated compactness", IMA Vol. Math. Appl., Volume 2, pp 35-69, 1986.

[46] D. W. McLaughin, E. A. II Overman, "Whiskered tori for integrable PDEs: chaotic behaviour in integrable PDEs", Surveys in Applied Mathematics, New York: Plenum, Volume 1, pp 83-203, 1995.

[47] P. D. Lax, "Integrals of nonlinear equations of evolution and solitary waves", Comm. on Pure and Appl. Math., Volume 21, p 467, 1968.

[48] A. Calini, S. F. Keith, S. Lafortune, "Squared eigenfunctions and linear stability properties of losed vortex filaments", Nonlinearity, Issue 12, Volume 24, 15 November 2011.

[49] S. D. Griffiths, R. H. J. Grimshaw, K. R. Khusnutdinova, "Modulational instability of two pair of counter-propagating waves and energy in a two-component system", Physica D:Nonlinear Phenomena, Issue 1, Volume 214, pp 1-24, 21 November 2005.

[50] K. R. Khusnutdinova, "Coupled Klein-Gordon equations and energy exchange in two-component system", Eur.Phys. J. Special Topics, Volume 147, pp 45-72, 2007.

[51] S. D. Griffiths, R. H. J. Grimshaw, K. R. Khusnutdinova, "The influence of modulation instability on energy exchange in coupled sine-Gordon equations", Theoretical and Mathematical Physics, Issue 1, Volume 137, pp 1448-1458, October 2003.

[52] M.G. Forest, O. C. Wright, "Un integrable model for stable:unstable wave coupling phenomena", Elsevier, Physica D:Nonlinear Phenomena, Volume 178, pp 173-189, 2003.

[53] V. E. Zakharov, S. V. Manakov, "Resonant interaction of wave packets in nonlinear media", Pis'ma Zh. Eksp. Teor. Fiz., Volume 18, p 413, 1973.

[54] A. V. Buryak, P. Di Trapani, D. V. Skryabin, S. Trillo, "Optical solitons due to quadratic nonlinearities: from basic physics to futuristic applications", Physics Reports, Volume 370, pp 63-235, 2002.

[55] R. J. Buckingham, R. M. Jenkins, P. D. Miller, "Semiclassical soliton ensembles for the three-wave resonant interaction equations", Communications in Mathematical Physics, Volume 354, p 1059, September 2016.

[56] M. Conforti, F. Baronio, A. Degasperis, "Modulation Instability of dark solitons in three wave resonant interaction", Physica D, Volume 240, pp 1362-1369, 20 May 2011.

[57] D. J. Kaup, A. Reiman, A. Bers, "Space-time evolution of nonlinear three-wave interactions. I. Interaction in a homogeneous medium", Reviews of Modern Physics, Issue 2, Volume 51, pp 275-310, April 1979.

[58] D. J. Kaup, 'The Three-Wave Interaction-A Nondispersive Phenomenon", Studies in Applied Mathematics, Volume 55, pp 9-44, 1976.

[59] M. J. Ablowitz, J. Kaup, A. C. Newell, "Coherent pulse propagation, a dispersive, irreversible phenomenon", Journal of Mathematical Physics, Volume 15, p 1852, 2003.

[60] B. Coppi, M. N. Rosenbluth, R. N. Sudan, "Nonlinear Interaction of Positive and Negative Energy Modes in Rarefield Plasmas (I)", Annals of Physics, Volume 55, pp 207-247, 1969.

[61] M. N. Rosenbluth, B. Coppi, R. N. Sudan, "Nonlinear Interactions of Positive and Negative Energy Modes In Rarefied Plasmas (II)", Annals of Physics, Volume 55, pp 248-270, 1969.

[62] D. J. Kaup, "Integrable systems and squared eigenfunctions", Theoretical and Mathematical Physics, Volume 159, pp 806-818, 2009.

[63] D. J. Kaup, Robert A. Van Gorder, "The inverse scattering transform and squared eigenfunctions for the nondegenerate 3×3 operator and its soliton structure", IOPscience, Issue 5, Volume 26, 2010.

[64] A. Degasperis, S. Lombardo, M. Sommacal, "Integrability and Linear Stability of Nonlinear Waves", Journal of Nonlinear Science, Issue 4, Volume 28, pp 1251-1291, 2018.

[65] C.B. Garcia and T.Y. Li, "On the numbers of solutions to polynomial systems of equations", SIAM J. Numer. Anal., Issue 4 Volume 17, pp. 540-546, 1980.

[66] T. P. Horikis, "Rogue Waves: Extreme Waves of Water and Light", J. Appl. Computat. Math., Issue 1, Volume 3, 2014.

[67] S. H. Strogatz, "Nonlinear Dynamics and Chaos", Perseus Books, 1994.

[68] D. H. Sattinger, V. D. Zurkowski, "Gauge theory of Bäcklund transformations", Physica D, Volume 26, pp 225-250, 1987.

[69] A. Calini, C. M. Schober, "Dynamical criteria for rogue waves in nonlinear Schrödinger models", IOP Science, Issue 12, Volume 25, 2 November 2012.

[70] A. Calini, C. M. Schober, "Numerical investigation of stability of breather-type solutions of the nonlinear Schrödinger equation", Nat. Hazards Earth Syst. Sci., Volume 14, pp 1431-1440, 2014.

[71] M. G. Forest, D. W. McLaughlin, D. J. Muraki, O. C. Wright, "Nonfocusing Instabilities in Coupled, Integrable Nonlinear Schrödinger pdes", J. Nonlinear Sci., Volume 10, p 291, 2000.

[72] F. Baronio, M. Conforti, A. Degasperis, S. Lombardo, M. Onorato, S. Wabnitz, "Vector Rogue Waves and Baseband Modulation Instability in the Defocusing Regime", Physical Review Letters, PRL 113, p 034101, 2014.

[73] F. Baronio, S. Chen, P. Grelu, S. Wabnitz, M. Conforti, "Baseband modulation instability as the origin of rogue waves", Phys. Rev. A, Volume 91, p 033804, 4 March 2015.

[74] H. N. Chan, K. W. Chow, "Rogue Wave Modes for the Coupled Nonlinear Schrödinger System with Three Components: A Computational Study", Applied Sciences, MDPI, Volume 7, p 559, 29 May 2017.

[75] A. Degasperis, S. Lombardo, "Rational Solitons of wave resonant-interaction models", Physical Review E, Volume 88, p 052914, 2013.

[76] A. Degasperis, S. Lombardo, "Multicomponent integrable wave equations I. Darboux-Dressing Transformation", Journal of Physics A: Mathematical and Theoretical, Issue 5, Volume 40, 17 January 2007.

[77] A. Degasperis, S. Lombardo, "Multicomponent integrable wave equations II. Soliton solutions", J. Phys. A: Math. Theor., Volume 42, p 385206, 2009.

[78] H. Segur, "Lecture 13: Triad (or 3-wave) resonances", https://www.whoi.edu/fileserver.do?id=136505&pt=10&p=85713, 22 June 2009.

[79] H. Segur, "Lecture 20: The explosive instability due to 3-wave or 4-wave mixing.", https://www.whoi.edu/fileserver.do?id=136644&pt=10&p=85713, 26 June 2009.

[80] M. Funakoshi, M. Oikawa, "The Resonant Interaction between a Long Internal Gravity Wave and a Surface Gravity Wave Packet", Journal of the Physical Society of Japan, Issue 6, Volume 52, pp 1982-1995, June 1983.

[81] D. J. Benney, "Significant Interactions Between Small and Large Scale Surface Waves", Studies in Applied Mathematics, Issue2, Volume 55, 1976.

[82] A. Degasperis, S. Lombardo, "Exact solutions of the 3-wave resonant interaction equation", Physica D, Volume 214, pp 157-168, 2006.

[83] A. Degasperis, "The Three-Wave Resonant Interaction Equations: Spectral and Numerical Methods", Letters in Mathematical Physics, Issue 1-3, Volume 96, pp 367-403, 2011.

[84] "What is Integrability?", Editors: Zakharov, Vladimir E. (Ed.), Springer Series in Nonlinear Dynamics, 1991.

[85] G. Darboux, "Leçons sur la théorie général des surfaces" , Gauthier-Villars, 1992.

[86] V.B. Matveev, M.A. Salle, "Darboux transformations and solitons" , Springer, 1991.

[87] G. Zhang, Z. Yan, "Multi-rational and semi-rational solitons and interactions for the nonlocal coupled nonlinear Schrödinger equations", EPL (Europhysics Letters), Issue6, Volume 118, 28 August 2017.

[88] K. Nashikawa, "Parametric excitation of coupled waves I. General Formulation", Journal of the Physical Society of Japan, Issue 4, Volume 24, April 1968.

[89] K. Hasselman, "A criterion for nonlinear wave stability", J. Fluid Mech., Volume 30, part 4, pp 737-739, 3 July 1967.

[90] K. Hasselmann, "Feynman Diagrams and Interaction Rules of Wave-Wave Scattering Processes", Reviews of Geophysics, Issue1, Volume 4, pp 1-32, February 1966.

[91] M. Onorato, D. Proment, A. Toffoli, "Freak waves in crossing seas", Eur. Phys. J. Special Topics, Volume 185, pp 45-55, 2010.

[92] A. Chabchoub, N. P. Hoffmann, Akhmediev N, Rogue Wave Observation in a Water Wave Tank, Phys. Rev. Lett., Volume 106, p 204502, 2011.

[93] H. Bailung, S. K. Sharma, Y. Nakamura, "Observation of Peregrine Solitons in a Multicomponent Plasma with Negative Ions", Phys. Rev. Lett., Volume 107, p 255005, 2011.

[94] L. Stenflo, P. K. Shukla, "Nonlinear acoustic-gravity waves", J. Plasma Phys. Volume 75, p 841, 2009.

[95] A. N. Ganshin, V. B. Efimov, G. V. Kolmakov, L. P. Mezhov-Deglin, P. V. E. McClintock, "Observation of an Inverse Energy Cascade in Developed Acoustic Turbulence in Superfluid Helium", Phys. Rev. Lett., Volume 101, p 065303, 2008.

[96] Y. V. Bludov, V. V. Konotop, N. Akhmediev, "Matter rogue waves", Phys. Rev. A, Volume 80, p 033610, 2009.

[97] M. Shats, H. Punzmann, H. Xia, "Capillary Rogue Waves", Phys. Rev. Lett., Volume 104, p 104503, 2010.

[98] R. Y. Chiao, E. Garmire, C. H. Townes, "Self-Trapping of Optical Beams", Pys. Rev. Lett., Volume 14, p 1056, 21 June 1965.

[99] P. L. Kelley, "Self-focusing of optical beams", Phys. Rev. Lett., Volume 15, pp 1005-1008, 1965.

[100] V. I. Talanov, "Self Focusing of Wave Beans in Nonlinear Media", Scientific Research Radio Physics, 6 July 1965.

[101] M. J. Ablowitz, "Nonlinear dispersive waves. Asymptotic analysis and solitons", Cambridge University Press, pp 152-156, 2011.

[102] P. Miller, "Lecture Notes", University of Michigan, 2015.

[103] V. E. Zakharov, "Stability of periodic waves of finite amplitude on the surface of a deep fluid", Zh. Prikl. Mekh. i Tekhn. Fiz, Volume 9, pp 86-94, Transl. J. Appl. Mech. and Tech. Phys., Volume 9, pp 190-194, 1968.

[104] J. Vanneste, "Explosive resonant interaction of baroclinic Rossby waves and stability of multilayer quasi-geostrophic flow", J. Fluid Mech., Volume 291, pp 83-107, 25 May 1995.

[105] J. Vanneste, "Wave interactions", Lecture Notes, University of Edinburgh.

[106] D. J. Benney, A. C. Newell, "The Propagation of Nonlinear Wave Envelopes", Studies in Applied Mathematics, Issue 1-4, Volume 46, pp 133-139, April 1967.

[107] J. M. Manley, H. E. Rowe, "Some General Properties of Nonlinear Elements-Part I. General Energy Relations", Proc. IRE, Volume 44, pp 904-913, 1956.

[108] Y. B. Band, "Light and Matter: Electromagnetism, Optics, Spectroscopy and Lasers", Wiley-Blackwell, 2006.

[109] G. New, "Introduction to Nonlinear Optics", Cambridge University Press, 2011.

[110] J. Rauch, ' "Hyperbolic Partial Differential Equations and Geometric Optics", Graduate Studies in Mathematics, American Mathematical Society, 2012.

[111] A. Bers, D. J. Kaup, A. H. Reiman, "Nonlinear Interactions of Three Wave Packets in a Homogeneous Medium", Phys. Rev. Lett., Volume 37, p 182, 1976.

[112] A. Reiman, "Space-time evolution of nonlinear three-wave interactions. II. Interaction in an inhomogeneous medium",Reviews of modern physics, Volume 51, pp 311-330, 1979.

[113] F. Baronio, M. Conforti, C. De Angelis, "Velocity-locked solitary waves in quadratic media", Phys, Rev. Lett, Volume 104, p 113902 , 2010.

[114] A. Degasperis, M. Conforti, F. Baronio, S. Wabnitz, "Effects of nonlinear wave coupling: accelerated solitons", The European Physical Journal Special Topics, Issue 1, Volume 147, pp 233-252, 2007.

[115] M. Conforti, F. Baronio, A. Degasperis, S. Wabnitz, "Inelastic Scattering and Interactions of Three-Wave Resonant Parametric Solitons", Phys. Rev. E, Volume 74, p 065602, 2006.

[116] A. Degasperis, M. Conforti, F. Baronio, S. Wabnitz, "Stable Control of Pulse Speed in Parametric Three-Wave Solitons", Phys. Rev. Lett., Volume 97, p 093901, 2006.

[117] E. L. Rees, "Graphical Discussion of the Roots of a Quartic Equation", The American Mathematical Monthly, Issue 2, Volume 29, pp 51-55, 1922.

[118] F. Baronio, M. Conforti, A. Degasperis, S. Lombardo, "Rogue waves emerging from the resonant interaction of three waves", Phys. Rev. Lett., Volume 111, p 114101, 2013.

[119] R. J. Marks II, "Introduction to Shannon Sampling and Interpolation Theory", Springer-Verlag, 1991.

[120] "ROGUE WAVES: Impact on ships and offshore structures", DNV GL STRATEGIC RESEARCH & INNOVATION, May 2015.

[121] N. Karjanto, E. van Groesen, "Derivation of the NLS Breather Solutions Using displaced Phase-Amplitude Variables", Proceedings of SEAMS-GMU Conference 2007, Applied Mathematics, 2007.

[122] S. P. Sheu, "Bäcklund transformations and homoclinic solutions for the nonlinear Schrödinger system", PhD Thesis, 1992.